

---

# **BEYOND BORN-OPPENHEIMER**

## Conical Intersections and Electronic Nonadiabatic Coupling Terms

---

**MICHAEL BAER**

Soreq Nuclear Research Center  
Yavne, Israel

The Fritz–Haber Research Center for Molecular Dynamics  
The Hebrew University of Jerusalem, Jerusalem, Israel



A JOHN WILEY & SONS, INC., PUBLICATION

Copyright © 2006 by John Wiley & Sons, Inc. All rights reserved.

Published by John Wiley & Sons, Inc., Hoboken, New Jersey  
Published simultaneously in Canada

No part of this publication may be reproduced, stored in a retrieval system, or transmitted in any form or by any means, electronic, mechanical, photocopying, recording, scanning, or otherwise, except as permitted under Section 107 or 108 of the 1976 United States Copyright Act, without either the prior written permission of the Publisher, or authorization through payment of the appropriate per-copy fee to the Copyright Clearance Center, Inc., 222 Rosewood Drive, Danvers, MA 01923, 978-750-8400, fax 978-750-4470, or on the web at [www.copyright.com](http://www.copyright.com). Requests to the Publisher for permission should be addressed to the Permissions Department, John Wiley & Sons, Inc., 111 River Street, Hoboken, NJ 07030, 201-748-6011, fax 201-748-6008, or online at <http://www.wiley.com/go/permission>.

**Limit of Liability/Disclaimer of Warranty:** While the publisher and author have used their best efforts in preparing this book, they make no representations or warranties with respect to the accuracy or completeness of the contents of this book and specifically disclaim any implied warranties of merchantability or fitness for a particular purpose. No warranty may be created or extended by sales representatives or written sales materials. The advice and strategies contained herein may not be suitable for your situation. You should consult with a professional where appropriate. Neither the publisher nor author shall be liable for any loss of profit or any other commercial damages, including but not limited to special, incidental, consequential, or other damages.

For general information on our other products and services or for technical support, please contact our Customer Care Department within the United States at 877-762-2974, outside the United States at 317-572-3993 or fax 317-572-4002.

Wiley also publishes its books in a variety of electronic formats. Some content that appears in print may not be available in electronic formats. For more information about Wiley products, visit our web site at [www.wiley.com](http://www.wiley.com).

***Library of Congress Cataloging-in-Publication Data:***

Baer, M. (Michael)

Beyond Born–Oppenheimer : electronic nonadiabatic coupling terms and conical intersections / by Michael Baer.

p. cm.

Includes index.

ISBN-13 978-0-471-77891-2

ISBN-10 0-471-77891-5 (cloth)

1. Molecular dynamics—Quantum mechanics. 2. Born-Oppenheimer treatment.

3. Adiabatic and diabatic states. I. Title.

QD96.M65B34 2006

541'.28—dc22

2005021350

Printed in the United States of America

10 9 8 7 6 5 4 3 2 1

To my wife Mali (Malvine)

# CONTENTS

---

|  |             |
|--|-------------|
| <b>PREFACE</b>   | <b>xiii</b> |
| <b>ABBREVIATIONS</b>   | <b>xvii</b> |
| <b>1 MATHEMATICAL INTRODUCTION</b>                                     | <b>1</b>    |
| 1.1 Hilbert Space / 1  |             |
| 1.1.1 Eigenfunction and Electronic Nonadiabatic Coupling Term / 1      |             |
| 1.1.2 Abelian and Non-Abelian Curl Equations / 3                       |             |
| 1.1.3 Abelian and Non-Abelian Divergence Equations / 6                 |             |
| 1.2 Hilbert Subspace / 8   |             |
| 1.3 Vectorial First-Order Differential Equation and Line Integral / 11 |             |
| 1.3.1 Vectorial First-Order Differential Equation / 12                 |             |
| 1.3.1.1 <i>Study of Abelian Case</i> / 12                              |             |
| 1.3.1.2 <i>Study of Non-Abelian Case</i> / 13                          |             |
| 1.3.1.3 <i>Orthogonality</i> / 14                                      |             |
| 1.3.2 Integral Equation / 14   |             |
| 1.3.2.1 <i>Integral Equation along an Open Contour</i> / 15            |             |
| 1.3.2.2 <i>Integral Equation along a Closed Contour</i> / 16           |             |
| 1.3.3 Solution of Differential Vector Equation / 20                    |             |
| 1.4 Summary and Conclusions / 23                                       |             |
| Problem / 23   |             |
| References / 25  |             |

|   |           |
|---|-----------|
| <b>2 BORN–OPPENHEIMER APPROACH: DIABATIZATION AND TOPOLOGICAL MATRIX</b>                                    | <b>26</b> |
| 2.1 Time-Independent Treatment / 26   |           |
| 2.1.1 Adiabatic Representation / 26   |           |
| 2.1.2 Diabatic Representation / 28  |           |
| 2.1.3 Adiabatic-to-Diabatic Transformation / 30   |           |
| 2.1.3.1 <i>Transformation for Electronic Basis Sets</i> / 30  |           |
| 2.1.3.2 <i>Transformation for Nuclear Wavefunctions</i> / 33  |           |
| 2.1.3.3 <i>Implications Due to Adiabatic-to-Diabatic Transformation</i> / 34                                |           |
| 2.1.3.4 <i>Final Comments</i> / 38  |           |
| 2.2 Application of Complex Eigenfunctions / 39  |           |
| 2.2.1 Introducing Time-Independent Phase Factors / 39   |           |
| 2.2.1.1 <i>Adiabatic Schrödinger Equation</i> / 39  |           |
| 2.2.1.2 <i>Adiabatic-to-Diabatic Transformation</i> / 40  |           |
| 2.2.2 Introducing Time-Dependent Phase Factors / 41   |           |
| 2.3 Time-Dependent Treatment / 43   |           |
| 2.3.1 Time-Dependent Perturbative Approach / 43   |           |
| 2.3.2 Time-Dependent Nonperturbative Approach / 45  |           |
| 2.3.2.1 <i>Adiabatic Time-Dependent Electronic Basis Set</i> / 45   |           |
| 2.3.2.2 <i>Adiabatic Time-Dependent Nuclear Schrödinger Equation</i> / 46                                   |           |
| 2.3.2.3 <i>Time-Dependent Adiabatic-to-Diabatic Transformation</i> / 47                                     |           |
| 2.3.3 Summary / 49  |           |
| Problem / 50  |           |
| 2A Appendixes / 51  |           |
| 2A.1 Dressed Nonadiabatic Coupling Matrix $\tilde{\tau}$ / 51   |           |
| 2A.2 Analyticity of Adiabatic-to-Diabatic Transformation Matrix $\tilde{A}$ in Spacetime Configuration / 52 |           |
| References / 54   |           |
| <b>3 MODEL STUDIES</b>  | <b>58</b> |
| 3.1 Treatment of Analytical Models / 58   |           |
| 3.1.1 Two-State Systems / 59  |           |
| 3.1.1.1 <i>Adiabatic-to-Diabatic Transformation Matrix</i> / 59   |           |
| 3.1.1.2 <i>Topological (D) Matrix</i> / 60  |           |
| 3.1.1.3 <i>The Diabatic Potential Matrix</i> / 61   |           |

|         |   |
|---------|---|
| 3.1.2   | Three-State Systems / 62  |
| 3.1.2.1 | <i>Adiabatic-to-Diabatic Transformation Matrix</i> / 62                     |
| 3.1.2.2 | <i>Topological Matrix</i> / 63  |
| 3.1.3   | Four-State Systems / 64   |
| 3.1.3.1 | <i>Adiabatic-to-Diabatic Transformation Matrix</i> / 64                     |
| 3.1.3.2 | <i>Topological Matrix</i> / 65  |
| 3.1.4   | Comments Related to General Case / 66                                       |
| 3.2     | Study of $2 \times 2$ Diabatic Potential Matrix and Related Topics / 67     |
| 3.2.1   | Treatment of General Case / 67  |
| 3.2.2   | The Jahn–Teller Model / 70  |
| 3.2.3   | Elliptic Jahn–Teller Model / 72   |
| 3.2.4   | Distribution of Conical Intersections and Diabatic Potential Matrix / 73    |
| 3.3     | Adiabatic-to-Diabatic Transformation Matrix and Wigner Rotation Matrix / 75 |
| 3.3.1   | Wigner Rotation Matrices / 76   |
| 3.3.2   | Adiabatic-to-Diabatic Transformation Matrix and Wigner $d^j$ Matrix / 77    |
|         | Problem / 79  |
|         | References / 82   |

#### 4 STUDIES OF MOLECULAR SYSTEMS 84

|         |   |
|---------|---|
| 4.1     | Introductory Comments / 84  |
| 4.2     | Theoretical Background / 85   |
| 4.3     | Quantization of Nonadiabatic Coupling Matrix: Study of Ab Initio Molecular Systems / 87 |
| 4.3.1   | Two-State Quasiquantization / 87  |
| 4.3.1.1 | $\{H_2, H\}$ System / 87  |
| 4.3.1.2 | $\{H_2, O\}$ System / 91  |
| 4.3.1.3 | $\{C_2, H_2\}$ System / 92  |
| 4.3.2   | Multistate Quasiquantization / 96   |
| 4.3.2.1 | $\{H_2, H\}$ System / 96  |
| 4.3.2.2 | $\{C_2, H\}$ System / 99  |
|         | References / 102  |

#### 5 DEGENERACY POINTS AND BORN–OPPENHEIMER COUPLING TERMS AS POLES 105

|     |  |
|-----|--|
| 5.1 | Relation between Born–Oppenheimer Coupling Terms and Degeneracy Points / 105 |
|-----|--|

|         |  |
|---------|--|
| 5.2     | Construction of Hilbert Subspace / 108   |
| 5.3     | Sign Flips of Electronic Eigenfunctions / 109  |
| 5.3.1   | Two-State Hilbert Subspace / 109   |
| 5.3.2   | Three-State Hilbert Subspace / 110   |
| 5.3.3   | General Hilbert Subspace / 114   |
| 5.3.4   | Multidegeneracy Point / 120  |
| 5.3.4.1 | <i>General Approach</i> / 120  |
| 5.3.4.2 | <i>Model Studies</i> / 121   |
| 5.4     | Topological Spin / 122   |
| 5.5     | Extended Euler Matrix as a Model for Adiabatic-to-Diabatic Transformation Matrix / 125                                   |
| 5.5.1   | Introductory Comments / 125  |
| 5.5.2   | Two-Dimensional Case / 126   |
| 5.5.3   | Three-Dimensional Case / 127   |
| 5.5.4   | Multidimensional Case / 130  |
| 5.6     | Quantization of $\tau$ Matrix and its Relation to Size of Configuration Space: Mathieu Equation as a Case of Study / 131 |
| 5.6.1   | Mathieu Equation and Its Eigenfunctions / 131  |
| 5.6.2   | Nonadiabatic Coupling Matrix ( $\tau$ ) and Topological Matrix (D) / 133   |
|         | Problems / 134   |
|         | References / 136   |

## 6 MOLECULAR FIELD 139

|         |   |
|---------|---|
| 6.1     | Solenoid as a Model for the Seam / 139  |
| 6.2     | Two-State (Abelian) System / 141  |
| 6.2.1   | Nonadiabatic Coupling Term as a Vector Potential / 141                                  |
| 6.2.2   | Two-State Curl Equation / 143   |
| 6.2.3   | (Extended) Stokes Theorem / 144   |
| 6.2.4   | Application of Stokes Theorem for Several Two-State Conical Intersections / 146         |
| 6.2.5   | Application of Vector Algebra to Calculate the Field of a Two-State Hilbert Space / 147 |
| 6.2.6   | A Numerical Example: Study of {H <sub>2</sub> ,Na} System / 149                         |
| 6.2.7   | A Short Summary / 151   |
| 6.3     | Multistate Hilbert Subspace / 151   |
| 6.3.1   | Non-Abelian Stokes Theorem / 151  |
| 6.3.2   | The Curl–Divergence Equations / 154   |
| 6.3.2.1 | <i>Three-State Hilbert Subspace</i> / 155   |

|   |
|---|
| 6.3.2.2 <i>Derivation of Poisson Equations</i> / 157<br>6.3.2.3 <i>Strange Matrix Element and Gauge Transformation</i> / 159<br>6.4 A Numerical Study of {H <sub>2</sub> ,H} System / 160<br>6.4.1 Introductory Comments / 160<br>6.4.2 Introducing Fourier Expansion / 160<br>6.4.3 Introducing Boundary Conditions / 161<br>6.4.4 Numerical Results / 162<br>6.5 Multistate Hilbert Subspace: Breakup of Nonadiabatic Coupling Matrix / 162<br>6.6 Pseudomagnetic Field / 167<br>6.6.1 Quantization of Pseudomagnetic Field along the Seam / 168<br>6.6.2 Non-Abelian Magnetic Fields / 168<br>Problems / 168<br>References / 172 |
|---|

## **7 OPEN PHASE AND BERRY PHASE FOR MOLECULAR SYSTEMS** 175

|  |
|--|
| 7.1 Studies of Ab Initio Systems / 175<br>7.1.1 Introductory Comments / 175<br>7.1.2 Open Phase and Berry Phase for Singlevalued Eigenfunctions: Berry's Approach / 176<br>7.1.3 Open Phase and Berry Phase for Multivalued Eigenfunctions: Present Approach / 177<br>7.1.3.1 <i>Derivation of Time-Dependent Equation</i> / 177<br>7.1.3.2 <i>Treatment of Adiabatic Case</i> / 179<br>7.1.3.3 <i>Treatment of Nonadiabatic (General) Case</i> / 181<br>7.1.4 {H <sub>2</sub> ,H} System as a Case Study / 183<br>7.2 Phase–Modulus Relations for an External Cyclic Time-Dependent Field / 187<br>7.2.1 Derivation of Reciprocal Relations / 187<br>7.2.2 Mathieu Equation / 189<br>7.2.2.1 <i>Time-Dependent Schrödinger Equations</i> / 189<br>7.2.2.2 <i>Numerical Study of Topological Phase</i> / 191<br>7.2.3 Short Summary / 194<br>Problem / 194<br>References / 195 |
|--|

|  |            |
|--|------------|
| <b>8 EXTENDED BORN–OPPENHEIMER APPROXIMATIONS</b>  | <b>197</b> |
| 8.1 Introductory Comments / 197  |            |
| 8.2 Born–Oppenheimer Approximation as Applied to a Multistate Model System / 199   |            |
| 8.2.1 Extended Approximate Born–Oppenheimer Equation / 199   |            |
| 8.2.2 Gauge Invariance Condition for Approximate Born–Oppenheimer Equations / 201  |            |
| 8.3 Multistate Born–Oppenheimer Approximation: Energy Considerations to Reduce Dimensions of Diabatic Potential Matrix / 201 |            |
| 8.3.1 Introductory Comments / 201  |            |
| 8.3.2 Derivation of Reduced Diabatic Potential Matrix / 202  |            |
| 8.3.3 Application of Extended Euler Matrix: Introducing the <i>N</i> -State Adiabatic-to-Diabatic Transformation Angle / 206 |            |
| 8.3.3.1 <i>Introductory Comments / 206</i>   |            |
| 8.3.3.2 <i>Derivation of Adiabatic-to-Diabatic Transformation Angle / 206</i>  |            |
| 8.3.4 Two-State Diabatic Potential Energy Matrix / 210   |            |
| 8.3.4.1 <i>Derivation of Diabatic Potential Matrix / 210</i>   |            |
| 8.3.4.2 <i>A Numerical Study of <math>\Delta W</math> Matrix Elements / 211</i>  |            |
| 8.3.4.3 <i>A Different Approach: Helmholtz Decomposition / 214</i>   |            |
| 8.4 A Numerical Study of a Reactive (Exchange) Scattering Two-Coordinate Model / 214   |            |
| 8.4.1 Basic Equations / 214  |            |
| 8.4.2 A Two-Coordinate Reactive (Exchange) Model / 216   |            |
| 8.4.3 Numerical Results and Discussion / 217   |            |
| Problem / 220  |            |
| References / 221   |            |
| <b>9 A SUMMARY</b>   | <b>224</b> |
| <b>INDEX</b>   | <b>227</b> |

## PREFACE

---

The study of molecular systems is based on the Born–Oppenheimer theory, which distinguishes between rapidly moving electrons and slowly moving nuclei and therefore leads to the formation of the electronic (adiabatic) eigenstates and the corresponding *nonadiabatic coupling terms* (NACTs). The existence of the adiabatic states seems to be compatible with a wide range of experimental studies, from photochemical processes through photodissociation and unimolecular processes and finally to bimolecular interactions accompanied by exchange and/or charge transfer processes. Having available the adiabatic states, the dynamical treatment is frequently carried out applying the Born–Oppenheimer *approximation*, which assumes the existence of a single decoupled state, thus ignoring the NACTs that couple the various states. The justification for this approximation is in the fact that NACTs are proportional to the mass ratio, namely,  $(m_e/m_p)^{(1/2)}$  (where  $m_e$  and  $m_p$  are the masses of an electron and a proton, respectively), and therefore are expected to be about two orders of magnitude smaller than other characteristic magnitudes that appear in the nuclear Schrödinger equation. However, as more and more molecular systems are studied and the number of ab initio treatments increases, it is realized that this approximation holds, at most, for small regions in configuration space, but otherwise cannot be satisfied.

The main reason for this misfortune is the existence of molecular *degenerate* states, which in turn cause the NACTs not only to become infinitely large but also to dress as *poles*. Being poles, the NACTs become the source for numerous phenomena that are considered as topological effects and lead to several interesting issues, including the well-known *Longuet–Higgins/Berry* phase and the *open-path* phase, the less known *quantization* feature of the NACTs, the existence of *molecular fields*, and finally but not less interesting, *topological spin*. Since the potential energy surfaces are expected to behave linearly in the vicinity of these points, the degeneracy points are frequently

referred to as (points of) *conical intersection (cis)*, the potential energy surfaces may in fact behave parabolically, in the vicinity of a conical intersection, but we still refer to these points as *cis*.

Conical intersections are of most concern because, in contrast to what was believed until the 1990s, they are not rare. In fact, ab initio calculations indicate that molecular systems tend to form a *ci*, between every two *adjacent* states (and on many occasions more than one *ci*). This fact impacts the numerical study of any process connected with electronic transitions such as energy transfer, chemical reactions, and charge transfer. In other words, unlike in the case of the Born–Oppenheimer approximation, the *cis* cannot be ignored and the corresponding NACTs, which, because of their singularity and due to the formation of topological effects have to be approached analytically. This analytic approach, which finally leads to the rigorous elimination of the troublesome NACTs (and of the topological effects), is termed *diabatization* and is one of the more important issues discussed in this book.

The book is intended to serve the theoreticians interested in treating, quantum-mechanically, the issues mentioned in the title of the book. I want to emphasize that since the mathematics to be applied is somewhat different from the usual, I take the initiative of explaining the basic concepts by giving step-to-step derivations and using a simple mathematical language. For this purpose, I devote a special chapter (Chapter 1) to the mathematical aspects of the issues to be discussed in later chapters. But I go further than that: I present models of varying complexity to illuminate the meaning of the mathematical treatment and I discuss numerous ab initio systems to reveal the prediction ability of the theory that is derived. Consequently I hope that this book will contribute significantly to the understanding of the theory of electronic nonadiabatic processes.

While treating the NACTs we also discuss known issues such as the previously mentioned *topological* effects in molecular systems (see Chapter 7, which treats the Berry phase and related subjects) and some new issues such as *quantization* of the NACTs matrix (see Chapter 2) and the existence of a new type of a field, namely, the *molecular* field (see Chapter 6). In particular, I want to mention that while treating the time-dependent Schrödinger equation we encounter features related to the *special theory of relativity* without introducing them explicitly.

My own studies related to electronic nonadiabatic processes and the features of the NACTs themselves extend over two periods:

*The First Period: 1974–1980.* I became acquainted with the subject during a 4-month stay at the Max Planck Institut für Strömungsforschung in Göttingen in the year 1974 as a guest of its director, Professor J. P. Toennies. At that time I was interested in developing a quantum-mechanical method to compute S-matrix elements for *charge transfer* processes that take place during bimolecular (gas-phase) interactions. These processes were treated, with a limited success, employing the well known *trajectory surface hopping* method. During that visit I came across a publication, by Felix Smith, that discusses a transformation from the Born–Oppenheimer *adiabatic* framework to Lichten’s *diabatic*

framework. This transformation was later termed *adiabatic-to-diabatic transformation* (ADT). Since Smith's study was carried out for *atom–atom* systems I extended it to make it applicable to polyatomic systems and soon revealed the necessity of carrying out calculus along *contours*. It was not obvious to me what, in fact, is gained by applying ADT for atom–atom systems, as the *noncrossing rule* inhibits the formation of *singular* NACTs. However, since the NACTs in polyatomic systems may become singular, ADT eliminates these troublesome NACTs, thus enabling a smooth numerical treatment of the resulting nuclear Schrödinger equation. Although the infinitely large NACTs that appear in the adiabatic Schrödinger equation for *charge transfer* are of a different type (they become the Dirac  $\delta$  function), they still can be eliminated by the ADT as indeed was done, by my student Z. Top and myself, while studying the (charge transfer)  $H^+ + H_2 \rightarrow H + H_2^+$  reaction. It was because of this ADT that we could calculate, quantum-mechanically, as early as the 1970s, the relevant charge transfer probabilities for reduced dimensions. Ten years later these calculations were extended to three dimensions and successfully compared with the state-to-state differential cross sections of the abovementioned process as measured by Niedner–Schatterburg and Toennies.

*The Second Period: 1990–2005.* During the academic year 1989/90 I took a sabbatical leave in the Department of Chemistry at Iowa State University in Ames as a guest of Professor C. Y. Ng. During my stay there, I extended the charge transfer treatment to include spin–orbit coupling, and studied spin transitions coupled with the charge transfer process in the  $Ar + H_2^+ \leftrightarrow Ar^+ + H_2$  and  $(Ar + H_2^+; Ar^+ + H_2) \rightarrow ArH^+ + H$  reactions. A good agreement with Ng's detailed experiments was achieved. During that visit I familiarized myself with the Berry phase and wondered whether there is a connection between this phase (and likewise the Longuet–Higgins phase) and the ADT angle as discussed in our earlier studies. The answer to that question and the studies that succeeded it form a major part of the present book.

This book could not have been written if it were not for my collaborations with some members of our community and their support. In particular, I want to mention the following people, starting with two scientists from my own institute, the Soreq Nuclear Research Center in Yavne. The first is the late Yehiel Yelamed (Lehrer), a professor of mathematics, who in the early 1970s introduced me to calculus along *contours*; the second is Robert Englman, a professor of physics with whom I have collaborated for more than 10 years since the early 1990s. I would also like to thank Professors Ágnes Vibók and Gábor J. Halász from the University of Debrecen (Debrecen, Hungary); Professor Alexander M. Mebel, of the Florida International University in Miami; and the late Professor Gert D. Billing of the University of Copenhagen (Copenhagen, Denmark), who joined efforts with me at different stages during the period 1999–2005. Also, I thank Professors Donald J. Kouri (Houston, Texas) and David K. Hoffman (Ames, Iowa) who collaborated with me on the theory of time-dependent NACTs, during my 2002 stay at the University of Houston.

Next, I want to thank my younger colleagues: Drs. D. Charutz (Soreq, Israel), A. Yahalom (Tel Aviv, Israel), Z. R. Xu (Coimbra, Portugal), A. Alijah (Bielefeld, Germany), S. Adhikari (Guwahati, India), and in particular Dr. T. Vértesi (Debrecen, Hungary), who did his Ph.D. thesis on this subject (with Professor Vibók) and made important contributions. Finally I mention my son, Professor R. Baer of the Institute of Chemistry, The Hebrew University in Jerusalem, whom I want to thank for many fruitful discussions on the various aspects of the theory presented here and especially for his significant contribution while studying time-dependent NACTs.

Our collaborative research was supported by several science funding agencies and national academies: The U.S.–Israel Binational Science Foundation, The U.S. National Science Foundation, The R. A. Welch Foundation, The Alexander von Humboldt Stiftung, The Danish Research Training Council, Academia Sinica of Taiwan, and The Hungarian National Academy. I am indebted and grateful to all of them.

*Rehovot, Israel, 2005*

MICHAEL BAER

## ABBREVIATIONS

---

|           |   |
|-----------|---|
| ADT       | Adiabatic-to-diabatic transformation        |
| a.u.      | Atomic unit (0.529Å)                        |
| CASSCF    | Complete active-space self-consistent field |
| C-D       | Curl–divergence                             |
| <i>ci</i> | Conical intersection                        |
| l.h.s.    | Left-hand side                              |
| NACM      | Nonadiabatic coupling matrix                |
| NACT      | Nonadiabatic coupling term                  |
| OPP       | Open-path phase                             |
| PES       | Potential energy surface                    |
| POPP      | Principal open-path phase                   |
| r.h.s.    | Right-hand side                             |

# CHAPTER 1

---

## MATHEMATICAL INTRODUCTION

---

### 1.1 HILBERT SPACE

#### 1.1.1 Eigenfunction and Electronic Nonadiabatic Coupling Term

We consider a complete basis set of electronic eigenfunctions  $|\zeta_k(\mathbf{s}_e|\mathbf{s})\rangle$ ;  $k = 1, 2, \dots, N$ , which depend explicitly on the electronic coordinate  $\mathbf{s}_e$  and parametrically on the nuclear coordinate  $\mathbf{s}$ . The  $|\zeta_k(\mathbf{s}_e|\mathbf{s})\rangle$  functions are the eigenfunctions of the following electronic Hamiltonian  $\mathbf{H}_e(\mathbf{s}_e|\mathbf{s})$

$$(\mathbf{H}_e(\mathbf{s}_e|\mathbf{s}) - \mathbf{u}_k(\mathbf{s})) |\zeta_k(\mathbf{s}_e|\mathbf{s})\rangle = 0; \quad k = 1, \dots, N \quad (1.1)$$

where  $\mathbf{u}_k(\mathbf{s})$  are the electronic eigenvalues [which later are recognized as the adiabatic potential energy surfaces (PESs)].

The fact that the  $|\zeta_k(\mathbf{s}_e|\mathbf{s})\rangle$  functions form a complete set yields the resolution of the unity in the following way:

$$\mathbf{I} = \sum_{k=1}^N |\zeta_k(\mathbf{s}_e|\mathbf{s})\rangle \langle \zeta_k(\mathbf{s}_e|\mathbf{s})| \quad (1.2)$$

This equation (1.2) guarantees that an arbitrary function  $|\xi(\mathbf{s}_e|\mathbf{s})\rangle$  can be expressed in terms of a linear combination of the  $|\zeta_k(\mathbf{s}_e|\mathbf{s})\rangle$  functions with coefficients (which parametrically depend on the nuclear coordinates):

$$|\xi(\mathbf{s}_e|\mathbf{s})\rangle = \sum_{k=1}^N |\zeta_k(\mathbf{s}_e|\mathbf{s})\rangle \langle \zeta_k(\mathbf{s}_e|\mathbf{s})| \xi(\mathbf{s}_e|\mathbf{s})\rangle. \quad (1.3)$$

---

*Beyond Born–Oppenheimer: Conical Intersections and Electronic Nonadiabatic Coupling Terms*  
By Michael Baer. Copyright © 2006 John Wiley & Sons, Inc.

This expansion is known as Born–Oppenheimer expansion,<sup>1,2</sup> and the bracket notation, introduced by Dirac<sup>3</sup> and used throughout this book, implies integration over the electronic coordinates.

Next we form the following magnitude

$$\boldsymbol{\tau}_{jk} = \langle \zeta_j | \nabla \zeta_k \rangle; \quad k, j = \{1, 2, \dots, N\} \quad (1.4)$$

which is defined as the electronic nonadiabatic coupling term (NACT).<sup>1,2</sup> Here the grad operator is expressed in terms of the nuclear coordinate  $\mathbf{s}$

$$\nabla = \left\{ \frac{\partial}{\partial p}, \frac{\partial}{\partial q}, \dots \right\} \quad (1.5)$$

where  $p$  and  $q$  are two Cartesian (mass-scaled) coordinates. It is important to note that the elements  $\boldsymbol{\tau}_{jk}$  form a matrix  $\boldsymbol{\tau}$  with elements that are vectors.

With these definitions we form the Hilbert space defined at a given point  $\mathbf{s}$ , namely, the space that contains all the functions that solve Eq. (1.1) at a given point  $\mathbf{s}$ .<sup>4</sup> One of the more important tasks is to connect Hilbert spaces defined at different points, for instance, at  $\mathbf{s}$  and  $\mathbf{s} + \Delta\mathbf{s}$ . It can be shown that a connection is established through the NACTs<sup>5</sup>

$$|\zeta_k(\mathbf{s}_e|\mathbf{s} + \Delta\mathbf{s})\rangle = \sum_{j=1}^N (\delta_{kj} - \Delta\mathbf{s} \cdot \boldsymbol{\tau}_{kj}) |\zeta_j(\mathbf{s}_e|\mathbf{s})\rangle \quad (1.6)$$

where  $\delta_{jk}$  is the Krönecker delta function and the dot stands for a scalar product. Equation (1.6) is always fulfilled if the Hilbert spaces at point  $\mathbf{s}$  and at points close to it are of  $N$  dimensions (viz., contain  $N$  eigenfunctions). However, we show later that this relation holds, under certain conditions, also for a smaller group of states that is defined as a Hilbert subspace.

To prove Eq. (1.6) we consider the Taylor expansion for  $|\zeta_k(\mathbf{s}_e|\mathbf{s} + \Delta\mathbf{s})\rangle$ :

$$|\zeta_k(\mathbf{s}_e|\mathbf{s} + \Delta\mathbf{s})\rangle = |\zeta_k(\mathbf{s}_e|\mathbf{s})\rangle + \Delta\mathbf{s} \cdot |\nabla \zeta_k(\mathbf{s}_e|\mathbf{s})\rangle \quad (1.7)$$

Since the derivative  $|\nabla \zeta_k(\mathbf{s}_e|\mathbf{s})\rangle$  is also a function that belongs to the same Hilbert space, it can be presented in terms of the (electronic) basis set introduced earlier:

$$|\nabla \zeta_k(\mathbf{s}_e|\mathbf{s})\rangle = \sum_{j=1}^N \mathbf{Z}_{kj}(\mathbf{s}) |\zeta_j(\mathbf{s}_e|\mathbf{s})\rangle \quad (1.8)$$

Multiplying both sides by  $\langle \zeta_i(\mathbf{s}_e|\mathbf{s})|$  (which also implies integration over  $\mathbf{s}_e$ ) yields [see Eq. (1.4)]

$$\mathbf{Z}_{ki} = -\boldsymbol{\tau}_{ki}; \quad i, k = \{1, 2, \dots, N\} \quad (1.9)$$

Substituting Eqs. (1.8) and (1.9) in Eq. (1.7) yields Eq. (1.6). In what follows we consider only *real* eigenfunctions, for which it is easy to show that the diagonal elements of the  $\boldsymbol{\tau}$  matrix, namely,  $\tau_{jj}$ , are identically zero. As a result, Eq. (1.6) leads to an important relation known as the *parallel transport law*:<sup>6a</sup>

$$\langle \xi_k(\mathbf{s}_e|\mathbf{s}) | \xi_k(\mathbf{s}_e|\mathbf{s} + \Delta\mathbf{s}) \rangle = 1 + O(\Delta\mathbf{s}^2) \quad (1.10)$$

Equation (1.6) can also be written employing matrix notation

$$\xi(\mathbf{s}_e|\mathbf{s} + \Delta\mathbf{s}) = (\mathbf{I} - \Delta\mathbf{s} \cdot \boldsymbol{\tau})\xi(\mathbf{s}_e|\mathbf{s}) \quad (1.6')$$

where  $\mathbf{I}$  is the unity matrix.

### 1.1.2 Abelian and Non-Abelian Curl Equations

In what follows we distinguish between Abelian and non-Abelian magnitudes. Abelian magnitudes are usually vectors and therefore field operations act on them in the ordinary way as, for instance, in electrodynamics. As an example, we may consider the definition of the Curl equation, for a vector  $\boldsymbol{\tau}$  that is to be of the form

$$\mathbf{H} = \text{Curl } \boldsymbol{\tau} \quad (1.11)$$

where  $\mathbf{H}$  is also a vector. The Curl operator implies that the  $z$  component takes the form

$$\mathbf{H}_z = \frac{\partial \boldsymbol{\tau}_x}{\partial y} - \frac{\partial \boldsymbol{\tau}_y}{\partial x} \quad (1.12)$$

The situation changes significantly in case  $\boldsymbol{\tau}$  (and consequently also  $\mathbf{H}$ ) becomes a matrix (of vectors). This situation is known as the *non-Abelian case*,<sup>6b,7</sup> and as will be shown next, the fact that vectors are replaced by matrices of vectors affects relations known to exist between ordinary vector functions.

As an example we consider the *non-Abelian Curl* equation, which is sometimes also called the *extended Curl equation* (to avoid confusion with the *ordinary Abelian Curl equation*). This equation, as mentioned earlier, is written in a matrix form and for this purpose we introduce a few definitions:

Considering two (nuclear) Cartesian coordinates  $p$  and  $q$ , we define the following tensorial vector  $\mathbf{F}_{pq}$ :

$$\mathbf{F}_{pq} = \frac{\partial \boldsymbol{\tau}_p}{\partial q} - \frac{\partial \boldsymbol{\tau}_q}{\partial p} - [\boldsymbol{\tau}_p, \boldsymbol{\tau}_q] \quad (1.13)$$

where  $\tau_\lambda; \lambda = q, p$  are the  $\lambda$  components of  $\tau$ , defined as [see Eq. (1.4)]

$$\tau_{\lambda jk} = \left\langle \zeta_j \left| \frac{\partial}{\partial \lambda} \zeta_k \right. \right\rangle; \quad \{k, j = 1, \dots, N; \lambda = p, q\} \quad (1.14)$$

and  $[\tau_p, \tau_q]$  is the commutation relation between  $\tau_p$  and  $\tau_q$ . Equation (1.13) can be written in a more compact way

$$\mathbf{F} = \mathbf{H} - \mathbf{T} \quad (1.15)$$

where

$$\mathbf{H}_{pq} = \frac{\partial \tau_p}{\partial q} - \frac{\partial \tau_q}{\partial p} \Rightarrow \mathbf{H} = \text{Curl } \tau \quad (1.16)$$

and

$$\mathbf{T}_{pq} = [\tau_p, \tau_q] \Rightarrow \mathbf{T} = [\tau \times \tau] \quad (1.17)$$

$\mathbf{F}$  is the field tensor known also as the *Yang–Mills field*.<sup>6b,7–10</sup> Next we prove the following lemma.

**Lemma 1.1** For a Hilbert space,  $\mathbf{F}$  has to be identically zero:<sup>11,12</sup>

$$\mathbf{F} = \mathbf{0} \quad (1.18)$$

*Proof* We consider the  $p$ th and  $q$ th components of Eq. (1.16):

$$\left( \frac{\partial \tau_p}{\partial q} \right)_{jk} = \left\langle \frac{\partial \zeta_j}{\partial q} \left| \frac{\partial \zeta_k}{\partial p} \right. \right\rangle + \left\langle \zeta_j \left| \frac{\partial^2 \zeta_k}{\partial q \partial p} \right. \right\rangle \quad (1.19a)$$

$$\left( \frac{\partial \tau_q}{\partial p} \right)_{jk} = \left\langle \frac{\partial \zeta_j}{\partial p} \left| \frac{\partial \zeta_k}{\partial q} \right. \right\rangle + \left\langle \zeta_j \left| \frac{\partial^2 \zeta_k}{\partial p \partial q} \right. \right\rangle \quad (1.19b)$$

Subtracting Eq. (1.19b) from Eq. (1.19a) and assuming that the eigenfunctions are *analytic* functions with respect to the nuclear coordinates yields the following result:

$$(\mathbf{H}_{pq})_{jk} = \left( \frac{\partial}{\partial q} \tau_p - \frac{\partial}{\partial p} \tau_q \right)_{jk} = \left\langle \frac{\partial \zeta_j}{\partial q} \left| \frac{\partial \zeta_k}{\partial p} \right. \right\rangle - \left\langle \frac{\partial \zeta_j}{\partial p} \left| \frac{\partial \zeta_k}{\partial q} \right. \right\rangle \quad (1.20)$$

Next we consider the  $(j, k)$  element of the first term in Eq. (1.17):

$$(\tau_p \tau_q)_{jk} = \sum_{i=1}^N \left\langle \zeta_j \left| \frac{\partial \zeta_i}{\partial p} \right. \right\rangle \left\langle \zeta_i \left| \frac{\partial \zeta_k}{\partial q} \right. \right\rangle \quad (1.21)$$

and recall the following relation (that holds for real functions):

$$\left\langle \zeta_j \left| \frac{\partial \zeta_i}{\partial p} \right. \right\rangle = - \left\langle \frac{\partial \zeta_j}{\partial p} \left| \zeta_i \right. \right\rangle$$

Eq. (1.21) becomes

$$(\boldsymbol{\tau}_p \boldsymbol{\tau}_q)_{jk} = - \sum_{i=1}^N \left\langle \frac{\partial \zeta_j}{\partial p} \left| \zeta_i \right. \right\rangle \left\langle \zeta_i \left| \frac{\partial \zeta_k}{\partial q} \right. \right\rangle = - \left\langle \frac{\partial \zeta_j}{\partial p} \left| \sum_{i=1}^N \left( \left| \zeta_i \right\rangle \langle \zeta_i \right| \right) \right| \frac{\partial \zeta_k}{\partial q} \right\rangle$$

or, due to the resolution of the unity [see Eq. (I.2)], we finally get

$$(\boldsymbol{\tau}_p \boldsymbol{\tau}_q)_{jk} = - \left\langle \frac{\partial \zeta_j}{\partial p} \left| \frac{\partial \zeta_k}{\partial q} \right. \right\rangle \quad (1.22a)$$

A similar result is obtained for the second term in Eq. (1.17):

$$(\boldsymbol{\tau}_q \boldsymbol{\tau}_p)_{jk} = - \left\langle \frac{\partial \zeta_j}{\partial q} \left| \frac{\partial \zeta_k}{\partial p} \right. \right\rangle \quad (1.22b)$$

Subtracting Eq. (1.22b) from Eq. (1.22a) yields the following  $(jk)$  element of  $\mathbf{T}_{pq}$ :

$$(\mathbf{T}_{pq})_{jk} = (\boldsymbol{\tau}_p \boldsymbol{\tau}_q - \boldsymbol{\tau}_q \boldsymbol{\tau}_p)_{jk} = - \left( \left\langle \frac{\partial \zeta_j}{\partial p} \left| \frac{\partial \zeta_k}{\partial q} \right. \right\rangle - \left\langle \frac{\partial \zeta_j}{\partial q} \left| \frac{\partial \zeta_k}{\partial p} \right. \right\rangle \right) \quad (1.23)$$

Next, comparing Eqs. (1.23) and (1.20), it is readily noted that for any arbitrary components  $p$  and  $q$  we have

$$\mathbf{H}_{pq} = \mathbf{T}_{pq} \Rightarrow \mathbf{F}_{pq} = \mathbf{H}_{pq} - \mathbf{T}_{pq} = 0 \quad (1.24)$$

which implies that Eq. (1.18) is fulfilled for a complete Hilbert space.

As a final issue in this section we consider the two-state ( $N = 2$ ) case. In this case the matrix  $\mathbf{T}$  is identically zero so that Eq. (1.15) [see also Eq. (1.13)] becomes

$$\mathbf{F} = \mathbf{H} = \text{Curl } \boldsymbol{\tau} = \mathbf{0} \quad (1.25)$$

which, because of the following structure of the  $2 \times 2$   $\boldsymbol{\tau}$  matrix

$$\boldsymbol{\tau} = \begin{pmatrix} 0 & \tau_{12} \\ -\tau_{12} & 0 \end{pmatrix} \quad (1.26)$$

leads to the result that

$$\text{Curl } \boldsymbol{\tau}_{12} = \mathbf{0} \quad (1.27)$$

This result implies that for any pair of coordinates  $(p, q)$  we have (in case the Hilbert space is formed by two states)

$$\frac{\partial \tau_{p12}}{\partial q} - \frac{\partial \tau_{q12}}{\partial p} = 0 \quad (1.28)$$

which is the Abelian form of the Curl equation.

**Corollary 1.1** Equation (1.28) indicates that in case of two states ( $N = 2$ ) the non-Abelian case becomes Abelian.

We want to complete this section with two comments:

1. We emphasize the fact that all the derivations in this section apply as long as the electronic eigenfunctions are analytic functions at *every* point in the region of interest. In case certain eigenfunctions may not have first-order derivatives at some points in configuration space, for instance, at *conical intersections* (see Chapter 5), the respective derivative of the  $\tau$ -matrix elements are not defined at these points and therefore also the final outcome, namely, that  $\mathbf{F} = \mathbf{0}$  is unlikely to hold at these points.
2. The importance of the fact that  $\mathbf{F} = \mathbf{0}$  for Born–Oppenheimer systems and how it is related to other fields in physics is briefly discussed by Englman and Yahalom.<sup>9</sup>

### 1.1.3 Abelian and Non-Abelian Divergence Equations

To guarantee the connection between Hilbert spaces defined at relative remote points, specifically, where  $\Delta s$  is relatively large, one has to include in Eq. (1.6) terms that contain both higher powers of  $\tau_{kj}$  and higher-order derivatives of  $\tau_{kj}$ . In this respect we prove next the relation between the second-order NACTs  $\tau_{jk}^{(2)}$  defined as

$$\tau_{jk}^{(2)} = \langle \zeta_j | \nabla^2 \zeta_k \rangle; \quad k, j = \{1, 2, \dots, N\} \quad (1.29)$$

and the ordinary (first-order) one  $\tau_{kj}$  introduced in Eq. (1.4).

**Lemma 1.2** The second-order NACT  $\tau_{jk}^{(2)}$  can be presented in the form<sup>11–13</sup>

$$\tau_{jk}^{(2)} = \sum_{i=1}^N \tau_{ji} \tau_{ik} + \nabla \tau_{jk} \quad (1.30)$$

or in matrix notation

$$\boldsymbol{\tau}^{(2)} = \boldsymbol{\tau}^2 + \nabla \boldsymbol{\tau} \quad (1.31)$$

*Proof* To derive Eq. (1.30) we consider  $\nabla\tau_{jk}$ . Recalling Eq. (1.4), we get

$$\nabla\tau_{jk} = \nabla\langle\zeta_j|\nabla\zeta_k\rangle = \langle\nabla\zeta_j|\nabla\zeta_k\rangle + \langle\zeta_j|\nabla^2\zeta_k\rangle \quad (1.32)$$

To continue, we need to evaluate the first term on the right-hand side (r.h.s.) of this expression. For this purpose we employ the resolution of the unity given in Eq. (1.2)

$$\langle\nabla\zeta_j|\nabla\zeta_k\rangle = \langle\nabla\zeta_j|\left(\sum_{i=1}^N |\zeta_i\rangle\langle\zeta_i|\right)|\nabla\zeta_k\rangle = \sum_{i=1}^N \langle\nabla\zeta_j|\zeta_i\rangle\langle\zeta_i|\nabla\zeta_k\rangle = \sum_{i=1}^N \boldsymbol{\tau}_{ij}\cdot\boldsymbol{\tau}_{ik}$$

or, finally

$$\langle\nabla\zeta_j|\nabla\zeta_k\rangle = -\sum_{i=1}^N \boldsymbol{\tau}_{ji}\cdot\boldsymbol{\tau}_{ik} \quad (1.33)$$

Substituting Eq. (1.33) in Eq. (1.32) (and recalling the definitions given above) yields Eq. (1.30) [or Eq. (1.31)].

**Corollary 1.2** Equation (1.31) was originally derived for the purpose of presenting the adiabatic nuclear Schrödinger equation in a *complete* and efficient form that guarantees yielding significant physical insight (see Section 2.1.1). However, it also serves another purpose and thus will be written in a slightly different form:

$$\nabla\boldsymbol{\tau} = \boldsymbol{\tau}^{(2)} - \boldsymbol{\tau}^2 \quad (1.34)$$

This equation is recognized as the extended *divergence* (div) equation, which together with the extended *Curl* equation [see Eqs. (1.15)–(1.18)] forms the *Curl–Div* equations that the  $\boldsymbol{\tau}$  matrix has to fulfill. These two equations are reminiscent of the *Curl–Div* equations for the vector potential in electrodynamics.<sup>14,15</sup>

The two-state system is of special interest because in this case the non-Abelian situation becomes Abelian [i.e., the equations for the matrices become equations for the single (1,2) term]; thus, in case of the divergence equation, we have

$$\nabla\boldsymbol{\tau}_{12} = \boldsymbol{\tau}_{12}^{(2)} \quad (1.35)$$

(The two-state  $\boldsymbol{\tau}^2$  matrix produces only diagonal elements.) Equation (1.35) indicates that the divergence equation encountered in molecular physics is, in general, different from zero.

Equations (1.27) and (1.35) form the *Curl–Div* equations in case of a two-dimensional Hilbert space.

## 1.2 HILBERT SUBSPACE

Complete Hilbert spaces, in particular for realistic molecular systems, contain an infinite number of states; therefore, to be able to treat such systems numerically, we have to reveal the conditions or establish situations for which finite groups of states will behave as a quasi-complete Hilbert space. If such a group of states can be formed, we define it as a *Hilbert subspace*.

In the present study the breakup of the Hilbert space into Hilbert subspaces is dictated by the behavior of the previously introduced NACTs elements  $\tau_{jk}$ . It will be shown that the features that exist within a complete Hilbert space, for instance, the the Curl–Div equations and the *quantization* (to be discussed in Chapters 2 and 3), are *approximately* valid within the respective Hilbert subspace.<sup>1</sup>

In what follows we consider a group of  $N$  states, and for convenience we assume them to be the  $N$  lowest states. Next we assume the Hilbert space to break up into two groups: a finite group, designated as the  $P$  space, which contains  $N$  (lowest) states, and the complementary group, designated as the  $Q$  space, which contains the rest of the Hilbert space (its dimensions can be infinite). As already mentioned, the breakup of the Hilbert space is based on the following assumption:<sup>1</sup>

$$|\tau_{jk}| \cong O(\varepsilon) \quad \text{for } j \leq N; \quad k > N \quad (1.36)$$

Here  $\varepsilon$  is a relatively small number. Equation (1.36) indicates that the NACTs between  $P$  states and  $Q$  states are all assumed to be negligibly small. This implies that the  $\tau$  matrix has the following form:<sup>2</sup>

$$\tau = \begin{pmatrix} 0 & \tau_{12} & \tau_{13} & \tau_{1N} \\ -\tau_{12} & 0 & \tau_{23} & \tau_{2N} \\ -\tau_{13} & -\tau_{23} & 0 & \tau_{3N} \\ & & 0 & O(\varepsilon) \\ -\tau_{1N} & -\tau_{2N} & -\tau_{3N} & 0 \\ & & & 0 & \tau_{N+1N+2} & \tau_{N+1N+3} \\ & & & -\tau_{N+1N+2} & 0 & \tau_{N+2N+3} \\ & & & -\tau_{N+1N+3} & -\tau_{N+2N+3} & 0 \\ O(\varepsilon) & & & & & 0 \\ & & & & & 0 \\ & & & & & 0 \end{pmatrix} \quad (1.37)$$

(Comment: In Section 6.5 this assumption is proved to exist in given regions in configuration space.)

To continue, we define the following Feshbach projection operators,<sup>3,4</sup> namely,  $\mathbf{P}_N$ , the projection operator for the  $P$  space

$$\mathbf{P}_N = \sum_{j=1}^N |\zeta_j\rangle\langle\zeta_j| \quad (1.38a)$$

and  $\mathbf{Q}_N$ , the projection operator for the  $Q$  space

$$\mathbf{Q}_N = \mathbf{I} - \mathbf{P}_N \quad (1.38b)$$

Our aim is to use the Feshbach operators in order to show that both the extended Curl equation given in Eqs. (1.15)–(1.18) and the Div equation given in Eq. (1.34) are approximately fulfilled within this Hilbert subspace. Since the mathematical proof in both cases is similar, we present the proof just for the divergence equation. The proof for the extended Curl equation can be found in Refs. 5, 6, and 7.

Our starting point is, like before, Eq. (1.30) which, following a slight rearrangement based on Eq. (1.33), takes the form

$$\boldsymbol{\tau}_{jk}^{(2)} = -\langle \nabla \zeta_j | \nabla \zeta_k \rangle + \nabla \boldsymbol{\tau}_{jk} \quad (1.39)$$

It is important to realize that Eq. (1.39) is valid for any two states  $j$  and  $k$  and therefore also for those that fulfill  $j, k \leq N$ . In what follows we consider only states belonging to the subspace. The first term on the r.h.s. is treated further as

$$\langle \nabla \zeta_j | \nabla \zeta_k \rangle = \langle \nabla \zeta_j | \mathbf{P}_N + \mathbf{Q}_N | \nabla \zeta_k \rangle = \langle \nabla \zeta_j | \mathbf{P}_N | \nabla \zeta_k \rangle + \langle \nabla \zeta_j | \mathbf{Q}_N | \nabla \zeta_k \rangle \quad (1.40)$$

where the first of the two terms in Eq. (1.40) becomes

$$\langle \nabla \zeta_j | \mathbf{P}_N | \nabla \zeta_k \rangle = \sum_{i=1}^N \langle \nabla \zeta_j | \zeta_i \rangle \langle \zeta_i | \nabla \zeta_k \rangle = \sum_{i=1}^N (-\boldsymbol{\tau}_{ji}) \boldsymbol{\tau}_{ik} \quad (1.41a)$$

and the second

$$\langle \nabla \zeta_j | \mathbf{Q}_N | \nabla \zeta_k \rangle = \sum_{i>N} \langle \nabla \zeta_j | \zeta_i \rangle \langle \zeta_i | \nabla \zeta_k \rangle = \sum_{i>N} (-\boldsymbol{\tau}_{ji}) \boldsymbol{\tau}_{ik} \quad (1.41b)$$

Recalling Eq. (1.37), we note that the contribution due to Eq. (1.41b) is negligibly small (because both  $j, k \leq N$ ), and therefore Eq. (1.40) becomes

$$\langle \nabla \zeta_j | \nabla \zeta_k \rangle = \langle \nabla \zeta_j | \mathbf{P}_N | \nabla \zeta_k \rangle = - \sum_{i=1}^N (\boldsymbol{\tau}_N)_{ji} (\boldsymbol{\tau}_N)_{ik} \quad (1.42)$$

which yields the following result for Eq. (1.39)

$$(\boldsymbol{\tau}_N)_{jk}^{(2)} = \sum_{i=1}^N (\boldsymbol{\tau}_N)_{ji} (\boldsymbol{\tau}_N)_{ik} + \nabla (\boldsymbol{\tau}_N)_{jk} \quad (1.43)$$

Equation (1.43) is essentially identical to Eq. (1.30), which was derived for the complete Hilbert space. Equation (1.43) can now also be written as an equation between

the submatrices  $\boldsymbol{\tau}_N$ ,  $\nabla\boldsymbol{\tau}_N$ , and  $\boldsymbol{\tau}_N^{(2)}$

$$\boldsymbol{\tau}_N^{(2)} = \boldsymbol{\tau}_N^2 + \nabla\boldsymbol{\tau}_N \quad (1.44)$$

which is similar to Eq. (1.31). Writing Eq. (1.44) slightly differently, as

$$\nabla\boldsymbol{\tau}_N = \boldsymbol{\tau}_N^{(2)} - \boldsymbol{\tau}_N^2 \quad (1.45)$$

yields the corresponding divergence equation.

We reiterate that one can show, employing similar considerations, that the Curl equations in Eqs. (1.15)–(1.18) can be written in the same way for a Hilbert subspace but for the corresponding  $N \times N$  submatrices.

As the last subject on this issue, we would like to estimate the size of the error introduced by ignoring the contributions from the  $Q$  subspace. For this purpose we consider the Curl equation or, more specifically, the two components of the (unperturbed) vectorial  $\boldsymbol{\tau}$  matrix, namely, the matrices  $\boldsymbol{\tau}_q$  and  $\boldsymbol{\tau}_p$  with elements as presented in Eq. (1.14). Each of these matrices is now written [following the presentation in Eq. (1.37)] as follows:<sup>7</sup>

$$\boldsymbol{\tau}_x = \begin{pmatrix} \boldsymbol{\tau}_x^{(N)} & \boldsymbol{\tau}_x^{(N,L)} \\ \boldsymbol{\tau}_x^{(L,N)} & \boldsymbol{\tau}_x^{(L)} \end{pmatrix}; \quad x = q, p \quad (1.46)$$

Here  $\boldsymbol{\tau}_x^{(N)}$  and  $\boldsymbol{\tau}_x^{(L)}$ ;  $x = p, q$  are the diagonal submatrices that contain the dominant NACTs, whereas  $\boldsymbol{\tau}_x^{(N,L)}$  [and  $\boldsymbol{\tau}_x^{(L,N)}$ ];  $x = p, q$  are the two off-diagonal submatrices that couple the two diagonal ones and are assumed to contain weak coupling terms, all of the order  $O(\varepsilon)$ . Next, following Eq. (1.13), we introduce the components of the reduced tensorial vector  $\tilde{\mathbf{F}}_{pq}^{(N)}$ :

$$\tilde{\mathbf{F}}_{pq}^{(N)} = \frac{\partial \boldsymbol{\tau}_p^{(N)}}{\partial q} - \frac{\partial \boldsymbol{\tau}_q^{(N)}}{\partial p} - [\boldsymbol{\tau}_p^{(N)}, \boldsymbol{\tau}_q^{(N)}] \quad (1.47)$$

Recalling Eqs. (1.15)–(1.17), the  $N \times N$  upper diagonal block of  $\mathbf{F}$ , specifically,  $\mathbf{F}_{pq}^{(N)}$ , can be written in the form

$$\mathbf{F}_{pq}^{(N)} = \tilde{\mathbf{F}}_{pq}^{(N)} - \{\boldsymbol{\tau}_p^{(N,L)} \boldsymbol{\tau}_q^{(L,N)} - \boldsymbol{\tau}_q^{(N,L)} \boldsymbol{\tau}_p^{(L,N)}\} \quad (1.48)$$

but because of Eq. (1.18) we have  $\mathbf{F}_{pq}^{(N)} = \mathbf{0}$  and therefore we get for  $\tilde{\mathbf{F}}_{pq}^{(N)}$  the following result:

$$\tilde{\mathbf{F}}_{pq}^{(N)} = \{\boldsymbol{\tau}_p^{(N,L)} \boldsymbol{\tau}_q^{(L,N)} - \boldsymbol{\tau}_q^{(N,L)} \boldsymbol{\tau}_p^{(L,N)}\} \quad (1.47')$$

Since all four matrices  $\tau_x^{(N,L)}$  and  $\tau_x^{(L,N)}$ ;  $x = p, q$  contain elements of the order  $O(\varepsilon)$  (or smaller), the elements of the matrix on the r.h.s. of Eq. (1.48) are of the order  $O(\varepsilon^2)$ , which implies that the relevant elements of  $\mathbf{F}_{pq}^{(N)}$  are of the following order:

$$\tilde{\mathbf{F}}_{pq}^{(N)} = O(\varepsilon^2) \quad (1.49a)$$

In other words, the extended Curl equation within the Hilbert *subspace* is fulfilled up to  $O(\varepsilon^2)$ . A similar equation holds for the divergence (Div) equation

$$\nabla \tau_N - \tau_N^{(2)} + \tau_N^2 = O(\varepsilon^2) \quad (1.49b)$$

where  $\tau_N$  is identical to the previously defined  $\tau^{(N)}$ .

Because of these findings we do not distinguish any more between complete, usually infinite, Hilbert spaces and finite Hilbert subspaces. However, we do distinguish between groups of states that form a Hilbert subspace and those that do not form a Hilbert subspace.

### 1.3 VECTORIAL FIRST-ORDER DIFFERENTIAL EQUATION AND LINE INTEGRAL

In this section we consider various issues concerning the following first-order differential equation<sup>1,2</sup>

$$\nabla \Omega(\mathbf{s}) + \boldsymbol{\tau}(\mathbf{s})\Omega(\mathbf{s}) = \mathbf{0} \quad (1.50)$$

where  $\boldsymbol{\tau}$  is a vector–matrix and  $\Omega$  is a scalar–matrix and  $\mathbf{s}$  is a point in configuration space. Equation (1.50) was probably mentioned for the first time by Hobey and McLachlan<sup>3</sup> (although in the context of two states only). However, no attempts were made to study it. On the contrary, McMlachlan, in a follow-up publication,<sup>4</sup> termed them as “inconsistent” and concluded that they are relevant only when  $\mathbf{s}$  stands for a (single) Cartesian coordinate.

Equation (1.50) has to be integrated from a point  $\mathbf{s}_0$  to a point  $\mathbf{s}$ , and this integration is usually done by assuming a contour  $\Gamma$  that combines  $\mathbf{s}_0$  and  $\mathbf{s}$ . However, before doing that we devote the next few sections to investigating these equations with the aim of obtaining the conditions to be satisfied by  $\boldsymbol{\tau}$  in order to guarantee an analytic solution in a given region of configuration space (and if not analytic, then, at least, as close as possible to being analytic as will be discussed later). This investigation is carried out first by considering the differential equation as written above (Section 1.3.1) or its corresponding integral equation (Section 1.3.3). In order to simplify this study, we consider first the case where  $\boldsymbol{\tau}$  is an *ordinary* vector (the Abelian case) and then extend the treatment to the case where  $\boldsymbol{\tau}$  is a vector–matrix (the non-Abelian case).

### 1.3.1 Vectorial First-Order Differential Equation

#### 1.3.1.1 Study of Abelian Case

In this section  $\tau$  is a vector, namely,  $(\tau_x, \tau_y, \dots)$ , and consequently  $\Omega$  is a scalar function,  $f(x, y)$ . The study is carried out for any two components of  $\tau$  and therefore we consider the following two equations:

$$\frac{\partial}{\partial x} f(x, y) + \tau_x f(x, y) = 0 \quad (1.51a)$$

$$\frac{\partial}{\partial y} f(x, y) + \tau_y f(x, y) = 0 \quad (1.51b)$$

**Continuity and Differentiability** From the way the equations are presented, the function  $f(x, y)$  is differentiable to the first order with respect to both  $x$  and  $y$ . All other features depend on the analytic characteristics of the various components of  $\tau$ , in this case, the two functions  $\tau_x(x, y)$  and  $\tau_y(x, y)$ . Therefore, if they are differentiable with respect to  $x$  and  $y$ , then  $f(x, y)$  has second-order derivatives, namely,  $f_{xx}$ ,  $f_{xy}$ ,  $f_{yx}$ , and  $f_{yy}$ . For instance, Eq. (1.51a) guarantees the second derivative  $f_{xx}$  in the following way

$$f_{xx} = \frac{\partial^2 f}{\partial x^2} = -\frac{\partial \tau_x}{\partial x} f - \tau_x \frac{\partial f}{\partial x} = -\frac{\partial \tau_x}{\partial x} f + \tau_x^2 f \quad (1.52)$$

and in a similar way it guarantees the existence of  $f_{xy}$ . The same applies to Eq. (1.51b) and other equations.

**Analyticity** It is well known that a necessary condition, for a function defined in terms of several variables, to be analytic in a given region is having derivatives (with respect to all coordinates) to all orders. However, this condition is not sufficient. The missing feature is relations between the mixed derivatives of the same order such as  $f_{xy}$  and  $f_{yx}$  and all others. Thus the analyticity is guaranteed if and only if the order of differentiation does not affect the result; for instance, we demand that  $f_{xy} = f_{yx}$ , and so on. For this requirement to be fulfilled at a given point  $(x, y)$ , the two components of  $\tau$ , namely,  $\tau_x(x, y)$  and  $\tau_y(x, y)$ , cannot be arbitrary but have to be related to each other.

To find this relation, we differentiate Eq. (1.51a) with respect to  $y$

$$f_{yx} = \frac{\partial^2 f}{\partial y \partial x} = -\frac{\partial \tau_x}{\partial y} f - \tau_x \frac{\partial f}{\partial y} = -\frac{\partial \tau_x}{\partial y} f + \tau_x \tau_y f \quad (1.53a)$$

and Eq. (1.51b) with respect to  $x$ :

$$f_{xy} = \frac{\partial^2 f}{\partial x \partial y} = -\frac{\partial \tau_y}{\partial x} f - \tau_y \frac{\partial f}{\partial x} = -\frac{\partial \tau_y}{\partial x} f + \tau_y \tau_x f \quad (1.53b)$$

and subtract the first equation from the second so that we obtain

$$f_{xy} - f_{yx} = \left( \frac{\partial \tau_x}{\partial y} - \frac{\partial \tau_y}{\partial x} \right) f \quad (1.54)$$

Equation (1.54) implies that in order for  $f(x, y)$  to be an *analytic* function (viz., having  $f_{xy} = f_{yx}$ ),  $\tau_x$  and  $\tau_y$  have to fulfill the following relation:<sup>3</sup>

$$\frac{\partial \tau_x}{\partial y} - \frac{\partial \tau_y}{\partial x} = 0 \quad (1.55)$$

Although Eq. (1.55) can be interpreted as the  $z$  component of a Curl equation, in fact it applies for any number of pairs of coordinates. We recall that Eq. (1.55) is identical to Eq. (1.28), which was derived earlier for two electronic eigenfunctions that form a two-state Hilbert space.

### 1.3.1.2 Study of Non-Abelian Case

Next we extend the previous treatment to the case where  $\boldsymbol{\tau}$  is a *matrix* and concentrate again on its two components  $\tau_x$  and  $\tau_y$ . As before, the elements of  $\tau_x$  and  $\tau_y$  are assumed to be analytic functions of the coordinates, and we demand that  $\boldsymbol{\Omega}$  be analytic, which implies that  $\boldsymbol{\Omega}_{xy} = \boldsymbol{\Omega}_{yx}$ . As before, we consider two components of Eq. (1.50), namely<sup>1</sup>

$$\frac{\partial}{\partial x} \boldsymbol{\Omega}(x, y) + \boldsymbol{\tau}_x \boldsymbol{\Omega}(x, y) = \mathbf{0} \quad (1.56a)$$

$$\frac{\partial}{\partial y} \boldsymbol{\Omega}(x, y) + \boldsymbol{\tau}_y \boldsymbol{\Omega}(x, y) = \mathbf{0} \quad (1.56b)$$

and differentiate the first equation with respect to  $y$ , and the second with respect to  $x$  and subtract the results:

$$\frac{\partial^2 \boldsymbol{\Omega}(x, y)}{\partial y \partial x} - \frac{\partial^2 \boldsymbol{\Omega}(x, y)}{\partial x \partial y} = - \left[ \frac{\partial \boldsymbol{\tau}_x}{\partial y} - \frac{\partial \boldsymbol{\tau}_y}{\partial x} - (\boldsymbol{\tau}_x \boldsymbol{\tau}_y - \boldsymbol{\tau}_y \boldsymbol{\tau}_x) \right] \boldsymbol{\Omega}(x, y)$$

Thus, in contrast to the previous case, we see that in order to guarantee the analyticity of  $\boldsymbol{\Omega}$ , requiring that the corresponding component of the Curl equation be zero is not enough. In fact, what is required is that the following expression become zero:<sup>1</sup>

$$\frac{\partial \boldsymbol{\tau}_x}{\partial y} - \frac{\partial \boldsymbol{\tau}_y}{\partial x} - (\boldsymbol{\tau}_x \boldsymbol{\tau}_y - \boldsymbol{\tau}_y \boldsymbol{\tau}_x) = \mathbf{0} \quad (1.57)$$

This is the  $(x, y)$  component of the tensor equation given in Eq. (1.18):

$$\text{Curl} \boldsymbol{\tau} - [\boldsymbol{\tau} \times \boldsymbol{\tau}] = \mathbf{0} \quad (1.58)$$

It is seen that in order for the  $\tau$  matrix to yield, an analytic solution for Eq. (1.50) in a given region, it has to fulfill the extended Curl equation, a condition that only *certain* groups of electronic states may guarantee. In Section 1.1 we showed that these are the groups that form, in that region, a Hilbert space or, at least, a Hilbert subspace (and in this case the analyticity is fulfilled only approximately). It is important to emphasize that if Eq. (1.58) is not fulfilled, this implies not that Eq. (1.50) does not have a solution but that the solution is not analytic.

### 1.3.1.3 Orthogonality

This subject is related to the previous section because it is intimately associated with the first-order equation Eq. (I.50). However, because of its exceptional importance, it is treated in a separate section.

**Lemma 1.3** The matrix solution  $\Omega$  of Eq. (1.50) is an orthogonal matrix.

*Proof* To prove this lemma, we consider Eq. (1.50) and its complex conjugate

$$\nabla\Omega^\dagger(\mathbf{s}) - \Omega^\dagger(\mathbf{s})\tau(\mathbf{s}) = \mathbf{0} \quad (1.50')$$

where we recall that  $\tau(\mathbf{s})$  is an antisymmetric matrix. Next, multiplying Eq. (1.50) from the left by  $\Omega^\dagger$  and Eq. (1.50') from the right by  $\Omega$  and adding up the two equalities, we get

$$(\nabla\Omega^\dagger)\Omega + \Omega^\dagger\nabla\Omega = \nabla(\Omega^\dagger\Omega) = \mathbf{0} \Rightarrow \Omega^\dagger\Omega = \text{const} \quad (1.59)$$

or by choosing appropriate boundary conditions, we obtain the following:

$$\Omega^\dagger\Omega = \mathbf{I} \Rightarrow \Omega\Omega^\dagger = \mathbf{I} \quad (1.60)$$

The orthogonality relation in Eq. (1.60) can be maintained in any region as long as the  $\tau$ -matrix elements are analytic functions in that region. It is important to emphasize that the orthogonality condition exists even if the Curl equation [see Eq. (1.58)] in that region is not fulfilled.

### 1.3.2 Integral Equation

The *integral* equation approach, in contrast to the *differential* equation approach, supplies a more general view on what to expect from the solution in a given region. The differential approach concentrates on what happens at a given point and its close neighborhood, whereas the integral approach yields information related to a given region. In the forthcoming sections we derive the relevant integral equations first for the case that  $\tau(\mathbf{s})$  is a vector and then when it is a matrix.

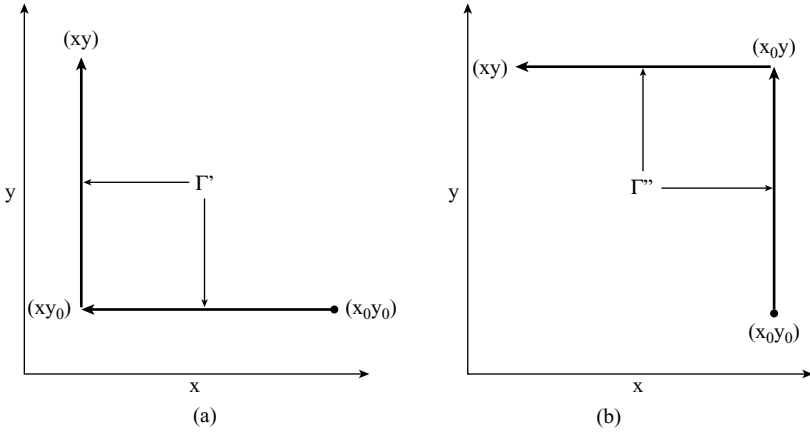


**Figure 1.1** Two rectangular paths  $\Gamma'$  and  $\Gamma''$  connecting the points  $(x_0, y_0)$  and  $(x, y)$  in the  $(x, y)$  plane.

### 1.3.2.1 Integral Equation along an Open Contour

We start by considering again Eqs. (1.50), where  $\tau(s)$  is an ordinary vector and  $\Omega(s)$  is a scalar function  $f(s)$ . In order to convert Eq. (1.50) into an integral equation that connects an initial point  $s_0$  with a final point  $s$ , we have also to assume a contour  $\Gamma$  that contains these two points and along which the integral equation has to be solved. Thus symbolically the relevant integral equation to be considered is<sup>1</sup>

$$f(s|\Gamma) = f(s_0) - \int_{s_0}^s d\mathbf{s} \cdot \tau(\mathbf{s}|\Gamma) f(\mathbf{s}|\Gamma) \quad (1.61)$$

In order to simplify our discussion, we assume a specific contour,  $\Gamma'$  (see Fig. 1.1(a)) made up of two straight lines as

$$\Gamma' \equiv \{(x_0, y_0) \rightarrow (x, y_0) \rightarrow (x, y)\} \quad (1.62a)$$

so that the relevant integral equation (1.61) becomes

$$f(x, y) = f(x_0, y_0) - \int_{x_0}^x dx' \tau_x(x', y_0) f(x', y_0) - \int_{y_0}^y dy' \tau_y(x, y') f(x, y') \quad (1.63a)$$

In order to verify that this expression is a solution, it has to be substituted in Eqs. (1.51) and examined accordingly. As an example, we consider Eq. (1.51a) and start by evaluating  $(\partial/\partial x)f(x, y)$ :

$$\frac{\partial f(x, y)}{\partial x} = -\tau_x(x, y_0) f(x, y_0) - \int_{y_0}^y dy' \left( \frac{\partial \tau_y(x, y')}{\partial x} f(x, y') + \tau_y(x, y') \frac{\partial f(x, y')}{\partial x} \right) \quad (1.64)$$

Next we assume that the Curl equation is fulfilled (at least) along  $\Gamma'$  so that we can replace  $(\partial/\partial x)\tau_y(x, y')$  in the first term under the integral sign by  $(\partial/\partial y')\tau_x(x, y')$  and then replace the resulting expression  $[(\partial/\partial y')\tau_x(x, y')]f(x, y')$  by

$$\frac{\partial \tau_x(x, y')}{\partial y'} f(x, y') = \frac{\partial[\tau_x(x, y')f(x, y')]}{\partial y'} - \tau_x(x, y') \frac{\partial f(x, y')}{\partial y'}$$

Carrying out both steps yields, for Eq. (1.64), the following result:

$$\frac{\partial f(x, y)}{\partial x} = -\tau_x(x, y)f(x, y) - \int_{y_0}^y dy' \left( -\tau_x(x, y') \frac{\partial f(x, y')}{\partial y'} + \tau_y(x, y') \frac{\partial f(x, y')}{\partial x} \right) \quad (1.64')$$

However, it can be seen that, due to Eqs. (1.51), the term under the integral sign is identically zero so that, in fact, Eq. (1.64') becomes identical to (1.51a). Thus the expression in (1.63a), indeed, satisfies Eq. (1.51).

In a similar way we can show that Eq. (1.63a) is also a solution of Eq. (1.51b). In fact, the derivation is straightforward and does not require even fulfillment of the Curl condition.

**Short Summary** We showed that Eq. (1.63a) satisfies Eqs. (1.51) if the Curl condition is satisfied for a given  $x$  value and for any  $y'$  value defined in the interval. However, if at a given point, say,  $P(x_z, y_z)$ , the Curl condition is not fulfilled, then an integral equation for a contour that contains  $P(x_z, y_z)$  cannot be formed. Still we are allowed to employ any other contour as long as it surrounds  $P(x_z, y_z)$ .

Having derived Eq. (1.61) for a function  $f(x, y)$ , where  $\tau$  is a vector, we are in a position to extend it for the case where  $\tau$  is a matrix (which causes  $\Omega$  to be a matrix as well):

$$\Omega(\mathbf{s}|\Gamma) = \Omega(\mathbf{s}_0) - \int_{s_0}^s d\mathbf{s} \cdot \boldsymbol{\tau}(\mathbf{s}|\Gamma) \Omega(\mathbf{s}|\Gamma) \quad (1.65)$$

We do not derive Eq. (1.65) as it is essentially similar to the derivation of Eq. (1.61). The only difference is that in this case we have to consider, in the appropriate instance, the extended Curl equation [see Eq. (1.58)] instead of Eq. (1.55).

### 1.3.2.2 Integral Equation along a Closed Contour

The equation to be treated in this case is of the form

$$f(\mathbf{s}_0|\Gamma) = f(\mathbf{s}_0) - \oint_{\Gamma} d\mathbf{s} \cdot \boldsymbol{\tau}(\mathbf{s}|\Gamma) f(\mathbf{s}|\Gamma) \quad (1.66)$$

Equation (1.66) does not look like an ordinary integral equation; rather, it appears to be more a result of an integration along a closed contour. In the present section we study the condition(s) for which the final value  $f(\mathbf{s}_0|\Gamma)$  differs from the initial value  $f(\mathbf{s}_0)$ . If the two are equal, this implies that the value of the integral along the closed contour is identically zero. In principle, the two values are expected to be the same, but as is shown next, this is not always the case. In what follows we continue to call Eq. (1.66) an integral equation because, after all, it is the equation used to calculate the value of  $f(\mathbf{s})$  at the endpoint:  $\mathbf{s} = \mathbf{s}_0$ .

The integral equation along a *closed* contour is best studied by considering two *open* contours with identical initial and final points<sup>2,5</sup> (see Fig. 1.1). For this purpose we consider the integral equation along a second contour (see Fig. (1.1(b))

$$\Gamma'' \equiv \{(x_0, y_0) \rightarrow (x_0, y) \rightarrow (x, y)\} \quad (1.62b)$$

so that the relevant integral equation is

$$f(x, y) = f(x_0, y_0) - \int_{y_0}^y dy \tau_y(x_0, y) f(x_0, y) - \int_{x_0}^x dx \tau_x(x, y) f(x, y) \quad (1.63b)$$

It is important to emphasize that Eqs. (1.63) are both legitimate solutions of Eq. (1.50) or, more specifically, of Eq. (1.51), at the point  $(x, y)$ , although the results as obtained by the two independent calculations may not be the same.

Having the two equations, Eqs. (1.63a) and (1.63b), we examine what happens at the point of contact  $(x, y) = (x_f, y_f)$ —the point where the two contours  $\Gamma'$  and  $\Gamma''$  cross and form the closed contour  $\Gamma$ , which can be symbolically written as

$$\Gamma = \Gamma' - \Gamma'' \quad (1.67)$$

At that point Eq. (1.63a) yields the value  $f(x_f, y_f|\Gamma')$  and Eq. (1.63b), the value  $f(x_f, y_f|\Gamma'')$ —the two values are not necessarily the same. Thus, if  $\Delta f(x_f, y_f|\Gamma)$  is defined as the difference

$$\Delta f(x_f, y_f|\Gamma') = f(x_f, y_f|\Gamma'') - f(x_f, y_f|\Gamma') \quad (1.67')$$

then, due to Eq. (1.67),  $\Delta f(x_f, y_f|\Gamma)$  is the value of the integral along the *closed* contour  $\Gamma$ . Therefore, if the two integral equations yield the same result at  $(x_f, y_f)$ , this implies that the value of the integral equation along the *closed* contour is zero. In what follows we designate the value of  $\Delta f(x_f, y_f|\Gamma)$  by  $\Delta f(\Gamma)$ .

In order to continue, we consider a situation where the initial point  $(x_0, y_0)$  and the final point  $(x_f, y_f)$  are close to each other, so that if  $x_f = x_0 + \Delta x$  and  $y_f = y_0 + \Delta y$ , then both  $\Delta x$  and  $\Delta y$ , are small enough to justify the approximations to be employed.

Thus  $\Gamma'$  is assumed to be the following open contour:

$$\Gamma' \equiv \{(x_0, y_0) \rightarrow (x_0 + \Delta x, y_0) \rightarrow (x_0 + \Delta x, y_0 + \Delta y)\} \quad (1.68a)$$

and, in the same way,  $\Gamma''$  is assumed to be

$$\Gamma'' \equiv \{(x_0, y_0) \rightarrow (x_0, y_0 + \Delta y) \rightarrow (x_0 + \Delta x, y_0 + \Delta y)\} \quad (1.68b)$$

Substitute Eqs. (1.63a) and (1.63b) in Eq. (1.67'), replace  $(x_f, y_f)$  by  $(x_0 + \Delta x, y_0 + \Delta y)$ , and perform the required algebraic changes leading to the result

$$\begin{aligned} \Delta f(\Gamma) = & \int_{x_0}^{x_0 + \Delta x} dx \{\tau_x(x, y_0) f(x, y_0) - \tau_x(x, y_0 + \Delta y) f(x, y + \Delta y)\} \\ & + \int_{y_0}^{y_0 + \Delta y} dy \{\tau_y(x_0, y) f(x_0, y) - \tau_y(x_0 + \Delta x, y) f(x_0 + \Delta x, y)\} \end{aligned}$$

which can be written (because  $\Delta x$  and  $\Delta y$  are small enough) as

$$\Delta f(\Gamma') = \Delta y \int_{x_0}^{x_0 + \Delta x} dx \frac{\partial(\tau_x(x, \tilde{y}) f(x, \tilde{y}))}{\partial y} + \Delta x \int_{y_0}^{y_0 + \Delta y} dy \frac{\partial(\tau_y(\tilde{x}, y) f(\tilde{x}, y))}{\partial x} \quad (1.69)$$

Next we replace each integral by a product between the relevant integrand (at some intermediate point) and the respective interval length so that Eq. (1.69) becomes

$$\Delta f(\Gamma) = \Delta y \Delta x \left[ \frac{\partial(\tau_x(\tilde{x}, \tilde{y}) f(\tilde{x}, \tilde{y}))}{\partial y} - \frac{\partial(\tau_y(\tilde{x}, \tilde{y}) f(\tilde{x}, \tilde{y}))}{\partial x} \right] \quad (1.70)$$

Recalling again Eqs. (1.51) and assuming that  $f(x, y)$  is a continuous function, Eq. (1.70) can be further simplified so that we finally have

$$\Delta f(\Gamma) = \Delta y \Delta x \left[ \frac{\partial \tau_x(x, y)}{\partial y} - \frac{\partial \tau_y(x, y)}{\partial x} \right] f(x, y) \quad (1.71)$$

or

$$\Delta f(\Gamma) = (\text{Curl } \boldsymbol{\tau})_{xy} f(x, y) \Delta x \Delta y \quad (1.72)$$

where  $(x, y)$  is some point in the interval  $x_0 \leq x \leq x_0 + \Delta x$  and  $y_0 \leq y \leq y_0 + \Delta y$  and  $\Delta x$  and  $\Delta y$  both  $\rightarrow 0$ .

It is readily noted that the value of  $\Delta f(x_0, y_0|\Gamma)$  depends solely on  $\text{Curl } \boldsymbol{\tau}$ . So, if  $\boldsymbol{\tau}$  fulfills Eq. (1.55), then the results as calculated along the two different *infinitesimal* contours are identical but differ if  $\text{Curl } \boldsymbol{\tau} \neq 0$ .

Although  $\Gamma'$  and  $\Gamma''$  are infinitesimal contours, this does not detract from the generality of the derivation. In case we are interested in a regular-size region that contains one such point [which causes  $\Delta f(x_f, y_f|\Gamma) \neq 0$ ], it has been shown (see Appendix C in Ref. 2) that any closed contour that surrounds this point can be presented as a sum of all the infinitesimal closed contours in the region surrounded by this regular-size contour, and therefore the conclusions regarding the value of the *closed-contour-integration* depends solely on what happens at this one point inside that region immaterial of the size of that region.

**Short Summary** If in a given region  $\text{Curl } \boldsymbol{\tau} = 0$  at *every* point in that region, the *integral* in Eq. (1.66), along any closed contour in that region, is equal to zero. If, in a given region,  $\text{Curl } \boldsymbol{\tau}$  is not defined at some points in the region (these points can be considered, at this stage, as *pathological* points), then the *integral* in Eq. (1.66) is zero as long as the closed contour does not surround any of these points. If, however, it surrounds one (or more) points of this kind, it becomes mathematically undefined (this problem and how it is related to Extended Stokes theorem is discussed further in Section 6.2.3).

Having studied Eq. (1.66), for a function  $f(x, y, \dots)$  where  $\boldsymbol{\tau}$  is a vector, we can now extend it for the case that both  $\boldsymbol{\tau}$  and  $\boldsymbol{\Omega}$  are matrices:

$$\boldsymbol{\Omega}(\mathbf{s}_0|\Gamma) = \boldsymbol{\Omega}(\mathbf{s}_0) - \oint_{\Gamma} ds \cdot \boldsymbol{\tau}(\mathbf{s}|\Gamma) \boldsymbol{\Omega}(\mathbf{s}|\Gamma) \quad (1.73)$$

The procedure that led to the analysis and the conclusions that ended with Eq. (1.72) applies also for the matrix equation in Eq. (1.73) with only one modification. The condition to be fulfilled in this case is now not by the  $\text{Curl } \boldsymbol{\tau}$  but by its extended non-Abelian version, namely, tensorial field  $\mathbf{F}$ . Thus, Eq. (1.72) has to be replaced in this case by<sup>5</sup>

$$\Delta \boldsymbol{\Omega}(\Gamma) = \Delta y \Delta x \mathbf{F}_{xy} \boldsymbol{\Omega}(x, y) \quad (1.74)$$

where both  $\Delta x$  and  $\Delta y \rightarrow 0$ .

We do not repeat the relevant derivation (it can be found in Ref. 5) but just present the following summary. If in a given region  $\mathbf{F} = 0$  at *every* point in that region the *integral* in Eq. (1.73), along any closed contour in that region, is equal to zero. If, in a given region,  $\mathbf{F}$  differs from zero at some points, then the closed line *integral*, in Eq. (1.73), is zero as long as the closed contour does not surround any of these points, but differs from zero when the contour surrounds one of these points. If, in a given region,  $\mathbf{F}$  is not well defined at some points, then any closed line *integral* that surrounds one of these points is mathematically undefined.

### 1.3.3 Solution of Differential Vector Equation

In this section we derive the solution of the differential equation for the *matrix*  $\Omega$  as given Eq. (1.50). Since we are considering matrices and not functions, the derivation is not straightforward. For instance, an expansion in terms of some power series is not likely to succeed because the product of two different matrices is not commutative (unless both are diagonal). This is the reason why the derivation has to be done in a different way, known as *propagation*.<sup>6–8</sup> Propagation is characterized by the fact that the value of the unknown function at one point is calculated by its value, at a nearby point employing an approximation based on finite differences. As mentioned earlier, in order to solve Eq. (1.50), we have to assign a contour  $\Gamma$  and solve the equations along this contour. Therefore the *propagation* has to be done along that contour.

As an example, we consider a planar case characterized by the coordinates  $(x, y)$  and show how to solve Eqs. (1.56). Defining a grid of  $L$  points along  $\Gamma$ , namely,  $\{P_0, P_1, \dots, P_n, \dots, P_L\}$ , where each point is defined as  $P_n = P_n(x_n, y_n)$  and  $P_0$  is the initial point for which is assigned an initial value in terms of the matrix  $\Omega(x_0, y_0)$ .

Assuming that we reached, by propagation, the point  $P_n$ , we show how to continue to the point  $P_{n+1}$ . This we do by carrying out two consecutive steps  $(x_n, y_n) \rightarrow (x_n + \Delta x, y_n)$  and then  $(x_n + \Delta x, y_n) \rightarrow (x_n + \Delta x, y_n + \Delta y)$  where  $\Delta x$  and  $\Delta y$  are both small enough. Next we consider a point  $(\tilde{x}_n, \tilde{y}_n)$  in the planar interval:

$$x_n \leq \tilde{x}_n \leq x_n + \Delta x \quad \text{and} \quad y_n \leq \tilde{y}_n \leq y_n + \Delta y \quad (1.75)$$

To carry out the first step, we employ the approximate equation [see Eq. (1.56a)]

$$\frac{\partial}{\partial x} \Omega(x, y) + \tau_x(\tilde{x}_n, \tilde{y}_n) \Omega(x, y) = \mathbf{0} \quad (1.76a)$$

where  $\tau_x(x, y)$  is replaced by  $\tau_x$  calculated at some intermediate point  $(\tilde{x}_n, \tilde{y}_n)$ , namely,  $\tau_x(x, y) \sim \tau_x(\tilde{x}_n, \tilde{y}_n)$ .

Next, we introduce the orthogonal matrix  $\mathbf{G}(x, y)$  and the corresponding *diagonal* matrix  $\mathbf{t}_x(x, y)$ , both defined through the relation

$$\mathbf{t}_x(\tilde{x}_n, \tilde{y}_n) = \mathbf{G}(\tilde{x}_n, \tilde{y}_n) \tau_x(\tilde{x}_n, \tilde{y}_n) \mathbf{G}^\dagger(\tilde{x}_n, \tilde{y}_n) \quad (1.77)$$

Here  $\mathbf{G}$  and  $\mathbf{t}_x$  contain, respectively, the eigenvectors and the eigenvalues of the  $\tau_x$  matrix. Multiplying Eq. (1.76a) from the left by  $\mathbf{G}(\tilde{x}_n, \tilde{y}_n)$  and from the right by  $\mathbf{G}^\dagger(\tilde{x}_n, \tilde{y}_n)$  and defining

$$\tilde{\Omega}(x, y) = \mathbf{G}(\tilde{x}_n, \tilde{y}_n) \Omega(x, y) \mathbf{G}^\dagger(\tilde{x}_n, \tilde{y}_n) \quad (1.78)$$

we get

$$\frac{\partial}{\partial x} \tilde{\Omega}(x, y) + \mathbf{t}_x(\tilde{x}_n, \tilde{y}_n) \tilde{\Omega}(x, y) = \mathbf{0} \quad (1.79)$$

Since  $\mathbf{t}_x$  is a diagonal (constant) matrix, the solution of Eq. (1.79) at  $x = x_{n+1}$  is straightforward:

$$\tilde{\Omega}(x_{n+1}, \tilde{y}_n) = \exp\{-\Delta x \mathbf{t}_x(\tilde{x}_n, \tilde{y}_n)\} \tilde{\Omega}(x_n, y_n) \quad (1.80)$$

To return to the original matrices  $\boldsymbol{\tau}_x$  and  $\boldsymbol{\Omega}$ , Eq. (1.80) is multiplied from the left and right by  $\mathbf{G}^\dagger(\tilde{x}_n, \tilde{y}_n)$  and  $\mathbf{G}(\tilde{x}_n, \tilde{y}_n)$ , respectively, and following other minor modifications, we get

$$\Omega(x_{n+1}, \tilde{y}_n) = \exp \left\{ - \int_{x_n}^{x_{n+1}} \boldsymbol{\tau}_x(x, \tilde{y}_n) dx \right\} \Omega(x_n, y_n) \quad (1.81)$$

To perform the second step, in the  $y$  direction, we employ Eq. (1.56b) and consider, as before, the approximate equation

$$\frac{\partial}{\partial y} \Omega(x, y) + \boldsymbol{\tau}_y(\tilde{x}_n, \tilde{y}_n) \Omega(x, y) = \mathbf{0} \quad (1.76b)$$

where  $\boldsymbol{\tau}_y(x, y)$  is replaced by  $\boldsymbol{\tau}_y$  calculated at some (other) intermediate point  $(\tilde{x}_n, \tilde{y}_n)$ , namely,  $\boldsymbol{\tau}_y(x, y) = \boldsymbol{\tau}_y(\tilde{x}_n, \tilde{y}_n)$ .

Continuing in the same manner as before [see Eq. (1.81)], we get

$$\Omega(x_{n+1}, y_{n+1}) = \exp \left\{ - \int_{y_n}^{y_{n+1}} \boldsymbol{\tau}_y(\tilde{x}_n, y) dy \right\} \Omega(x_{n+1}, \tilde{y}_n) \quad (1.82)$$

Substituting Eq. (1.81) in Eq. (1.82) and recalling the definition of the scalar product

$$\boldsymbol{\tau}(s) \cdot ds \sim \boldsymbol{\tau}_x(x, \tilde{y}_n) dx + \boldsymbol{\tau}_y(\tilde{x}_n, y) dy \quad (1.83)$$

where  $s \equiv (x, y)$ , we finally obtain

$$\Omega(s_{n+1}) = \exp \left\{ - \int_{s_n}^{s_{n+1}} \boldsymbol{\tau}(s) \cdot ds \right\} \Omega(s_n) \quad (1.84)$$

Equation (1.84) can be now be extended to any number of steps so that the final result is

$$\Omega(s|\Gamma) = \wp \exp \left\{ - \int_{s_0}^s \boldsymbol{\tau}(s'|\Gamma) \cdot ds' \right\} \Omega(s_0) \quad (1.85)$$

where  $\wp$  is the ordering operator that tells us to carry out the integration, in Eq. (1.85), in the following order  $\{P_0 \rightarrow P_1 \cdots \rightarrow P_n \rightarrow P_{n+1} \cdots \rightarrow P_L\}$  all this along the assigned contour  $\Gamma$ .

As a final subject in this section we derive the numerical representation of the solution in Eq. (1.85) for a given contour  $\Gamma$ . This is done according to the following recipe:

1. Divide  $\Gamma$  into  $L$  sections where the  $n$ th section is defined in terms of its two endpoints  $[\mathbf{s}_{n-1}, \mathbf{s}_n]$ .
2. Write the exponentiated integral as an ordered product of  $L$  exponentiated integrals, each related to one section:

$$\Omega(\mathbf{s}_L) = \left[ \prod_{n=1}^L \exp \left\{ - \int_{\mathbf{s}_{n-1}}^{\mathbf{s}_n} \boldsymbol{\tau}(\mathbf{s}') \cdot d\mathbf{s}' \right\} \right] \Omega(\mathbf{s}_0) \quad (1.86)$$

3. Approximate the integrals in each exponential by  $\boldsymbol{\tau}(\tilde{\mathbf{s}}_n) \Delta_n$ , where  $\tilde{\mathbf{s}}_n$  is some intermediate point and  $\Delta_n$  is defined as vectorial length  $\Delta_n = \mathbf{s}_n - \mathbf{s}_{n-1}$ , so that Eq. (1.86) becomes

$$\Omega(\mathbf{s}_L) = \left[ \prod_{n=1}^L \exp \{-\boldsymbol{\tau}(\tilde{\mathbf{s}}_n) \cdot \Delta_n\} \right] \Omega(\mathbf{s}_0) \quad (1.87)$$

4. Replace each exponential by

$$\exp(-\boldsymbol{\tau}(\tilde{\mathbf{s}}_n) \cdot \Delta_n) = \mathbf{G}(\tilde{\mathbf{s}}_n) \mathbf{E}(\tilde{\mathbf{s}}_n) \mathbf{G}^\dagger(\tilde{\mathbf{s}}_n) \quad (1.88)$$

where  $\mathbf{G}(\tilde{\mathbf{s}}_n)$  is a matrix that diagonalizes  $\boldsymbol{\tau}(\tilde{\mathbf{s}}_n)$ , namely

$$\boldsymbol{\tau}(\tilde{\mathbf{s}}_n) = \mathbf{G}(\tilde{\mathbf{s}}_n) \mathbf{t}(\tilde{\mathbf{s}}_n) \mathbf{G}^\dagger(\tilde{\mathbf{s}}_n) \quad (1.89)$$

[here  $\mathbf{t}(\tilde{\mathbf{s}}_n)$  is a diagonal matrix that contains the eigenvalues of  $\boldsymbol{\tau}(\tilde{\mathbf{s}}_n)$ ] and  $\mathbf{E}(\tilde{\mathbf{s}}_n)$  is given in the form

$$\mathbf{E}(\tilde{\mathbf{s}}_n) = \exp(-\mathbf{t}(\tilde{\mathbf{s}}_n) \cdot \Delta_n) \quad (1.90)$$

5. Substitute Eq. (1.88) in Eq. (1.87) so that

$$\Omega(\mathbf{s}_L) = \left\{ \prod_{n=1}^L [\mathbf{G}(\tilde{\mathbf{s}}_n) \mathbf{E}(\tilde{\mathbf{s}}_n) \mathbf{G}^\dagger(\tilde{\mathbf{s}}_n)] \right\} \Omega(\mathbf{s}_0) \quad (1.91)$$

This completes the numerical presentation of the solution to Eq. (1.50).

## 1.4 SUMMARY AND CONCLUSIONS

In Section 1.3 two approaches are presented to treat first-order differential equations as presented in Eq. (1.50): (1) by converting it into an integral equation as presented in Eq. (1.65) and (2) by employing the propagation technique and deriving an analytic expression as presented in Eq. (1.85). This expression is then “translated” into a numerical language as given in Eq. (1.91). The two approaches are expected to yield the same results. In this section we discuss to some extent results, for *closed* contours.

Equation (1.73) [see also (1.66)] is the integral equation for a closed contour, and we have shown that the value of the integral is zero when the contour  $\Gamma$  does not surround any of the points for which the tensorial field  $\mathbf{F}$  is not defined. In case it surrounds one or more points, the integral becomes undefined. The same is expected for the explicit closed contour that follows from Eq. (1.85):

$$\Omega(\mathbf{s}_0|\Gamma) = \wp \exp \left\{ - \oint_{\Gamma} \boldsymbol{\tau}(\mathbf{s}'|\Gamma) \cdot d\mathbf{s}' \right\} \Omega(\mathbf{s}_0) \quad (1.92)$$

Defining the abovementioned exponentiated closed-contour integral as  $\mathbf{D}(\Gamma)$

$$\mathbf{D}(\Gamma) = \wp \exp \left\{ - \oint_{\Gamma} \boldsymbol{\tau}(\mathbf{s}'|\Gamma) \cdot d\mathbf{s}' \right\} \quad (1.93)$$

we can state that the  $\mathbf{D}$  matrix is the unit matrix  $\mathbf{I}$  if the contour does not surround any of the *pathological* points.

The  $\mathbf{D}$  matrix can also be defined in terms of the line integral [see Eq. 1.73)] as follows

$$\mathbf{D}(\Gamma) = \mathbf{I} - \oint_{\Gamma} d\mathbf{s} \cdot \boldsymbol{\tau}(\mathbf{s}|\Gamma) \Omega(\mathbf{s}|\Gamma) \quad (1.94)$$

where  $\mathbf{I}$  is the unit matrix.

## PROBLEM

- 1.1** Consider a planar system described in terms of two polar coordinates  $\mathbf{s} = (\varphi, q)$  and the corresponding components of  $\boldsymbol{\tau}$ :  $\boldsymbol{\tau} = (\boldsymbol{\tau}_{\varphi}/q, \boldsymbol{\tau}_q)$ . Assume  $\boldsymbol{\tau}_q$  to be identically zero and  $\boldsymbol{\tau}_{\varphi}$  to be a  $2 \times 2$  matrix of the type

$$\boldsymbol{\tau}_{\varphi} = \begin{pmatrix} 0 & \frac{1}{2} \\ -\frac{1}{2} & 0 \end{pmatrix} \quad (1.95)$$

Employing Eq. (1.94) for a circular contour, prove that the corresponding two-state  $\mathbf{D}$  matrix takes the following form:

$$\mathbf{D} \begin{pmatrix} -1 & 0 \\ 0 & -1 \end{pmatrix} \quad (1.96)$$

*Solution* Our first step is to derive  $\Omega(\varphi, q)$ , and this is done using Eqs. (1.56) after transforming them to polar coordinates:

$$\frac{\partial}{\partial q} \Omega(\varphi, q) + \tau_q \Omega(qq) = \mathbf{0} \quad (1.97a)$$

$$\frac{1}{q} \left( \frac{\partial}{\partial \varphi} \Omega(\varphi, q) + \tau_\varphi \Omega(\varphi, q) \right) = \mathbf{0} \quad (1.97b)$$

Recalling that  $\tau_q$  is identically zero (and consequently  $q = q_0$ ) and  $\tau_\varphi$  is given in Eq. (1.95), we find that  $\Omega(\varphi, q = q_0)$  has to fulfill the following (matrix) first-order differential equation:

$$\frac{\partial}{\partial \varphi} \Omega(\varphi, q_0) + \begin{pmatrix} 0 & \frac{1}{2} \\ -\frac{1}{2} & 0 \end{pmatrix} \Omega(\varphi, q_0) = \mathbf{0} \quad (1.98)$$

To derive the solution of Eq. (1.98), we assume that

$$\Omega(\varphi, q_0) = \begin{pmatrix} \cos \gamma(\varphi) & \sin \gamma(\varphi) \\ -\sin \gamma(\varphi) & \cos \gamma(\varphi) \end{pmatrix} \quad (1.99)$$

Substituting Eq. (1.99) in Eq. (1.98) yields for  $\gamma(\varphi)$  the result  $\gamma(\varphi) = \varphi/2$ . Next, substituting Eq. (1.99) in Eq. (1.98), we get for  $\mathbf{D}(\Gamma) = \mathbf{D}(q_0)$

$$\mathbf{D}(q_0) = \mathbf{I} - \int_0^{2\pi} d\varphi \begin{pmatrix} 0 & \frac{1}{2} \\ -\frac{1}{2} & 0 \end{pmatrix} \begin{pmatrix} \cos(\varphi/2) & \sin(\varphi/2) \\ -\sin(\varphi/2) & \cos(\varphi/2) \end{pmatrix}$$

or following the integration

$$\mathbf{D}(q_0) = \mathbf{I} - 2\mathbf{I} = -\mathbf{I} \quad (1.100)$$

which is identical to Eq. (1.96).

## REFERENCES

### Section 1.1

1. M. Born and J. R. Oppenheimer, *Ann. Phys.* (Leipzig) **84**, 457 (1927).
2. M. Born and K. Huang, *Dynamical Theory of Crystal Lattices*, Oxford Univ. Press, New York, 1954, Chapter IV.
3. P. A. M. Dirac, *The Principles of Quantum Mechanics*, Oxford at the Clarendon Press, 1958, Chapter II.
4. A. Messiah, *Quantum Mechanics*, North Holland , Amsterdam, 1964, Vol. I, Section V.2.
5. R. Baer, *J. Chem. Phys.* **117**, 7405 (2002).
6. M. Guidry, *Gauge Field Theories, an Introduction with Application*, Wiley Science Paperback Series, New York, 1999: (a) Chapter 13; (b) Chapter 7.
7. M. E. Peskin and D. V. Schroeder, *An Introduction to Quantum Field Theory*, Perseus Books, Cambridge, MA, 1995, Section 15.2.
8. C. N. Yang and R. L. Mills, *Phys. Rev.* **96**, 191 (1954).
9. R. Englman and A. Yahalom, *Adv. Chem. Phys.* **124**, 197 (2003).
10. R. Baer, D. J. Kouri, M. Baer, and D. K. Hoffman, *J. Chem. Phys.* **119**, 6998 (2003).
11. M. Baer, *Chem. Phys. Lett.* **35**, 112 (1975).
12. M. Baer, *Phys. Rep.* **358**, 75 (2002).
13. W. D. Hobey and A. D. McLachlan, *J. Chem. Phys.* **33**, 1695 (1960).
14. J. D. Jackson, *Classical Electrodynamics*, 3rd ed., Wiley, 1998, Chapter 6.
15. L. Landau and E. Lifshitz, *The Classical Theory of Fields*, Addison-Wesley Press, Cambridge, MA, 1951, p. 47.

### Section 1.2

1. M. Baer, *Chem. Phys. Lett.* **322**, 520 (2000).
2. M. Baer, T. Vértesi, G. J. Halász, Á. Vibók, and S. Suhai, *Faraday Disc.* **127**, 337 (2004).
3. H. Feshbach, *Ann. Phys. (NY)* **5**, 357 (1958).
4. C. L. Shoemaker and R. E. Wyatt, *Adv. Quant. Chem.* **14**, 169 (1981).
5. M. Baer, *Phys. Rep.* **358**, 75 (2002).
6. M. Baer, *Adv. Chem. Phys.* **124**, 19 (2003).
7. M. Baer and R. Englman, *Chem. Phys. Lett.* **335**, 85 (2001).

### Section 1.3

1. M. Baer, *Chem. Phys. Lett.* **35**, 112 (1975).
2. M. Baer, *Phys. Rep.* **358**, 75 (2002).
3. W. D. Hobey and A. D. McLachlan, *J. Chem. Phys.* **33**, 1695 (1960).
4. A. D. McLachlan, *Molec. Phys.* **4**, 417 (1961).
5. M. Baer, *Chem. Phys.* **259**, 123 (2000) (see Appendix B).
6. M. Baer, *Molec. Phys.* **40**, 1011 (1980).
7. T. Pacher, L. S. Cederbaum, and H. Köppel, *Adv. Chem. Phys.* **84**, 293 (1993).
8. M. Baer, *J. Phys. Chem. A*, **104**, 3181 (2000).

# CHAPTER 2

---

## BORN–OPPENHEIMER APPROACH: DIABATIZATION AND TOPOLOGICAL MATRIX

---

### 2.1 TIME-INDEPENDENT TREATMENT

#### 2.1.1 Adiabatic Representation

The Hamiltonian  $\mathbf{H}$  that governs the motion of the nuclei and the electrons is usually written in the following form

$$\mathbf{H}(\mathbf{s}_e, \mathbf{s}) = \mathbf{T}_n(\mathbf{s}) + \mathbf{H}_e(\mathbf{s}_e|\mathbf{s}) \quad (2.1)$$

where  $\mathbf{T}_n(\mathbf{s})$  is the nuclear kinetic energy and  $\mathbf{H}_e(\mathbf{s}_e|\mathbf{s})$  is the electronic Hamiltonian, which also contains the nuclear Coulomb interactions and depends parametrically on the nuclei coordinates.

The Schrödinger equation to be considered is of the form

$$(\mathbf{H} - E) |\Psi(\mathbf{s}_e, \mathbf{s})\rangle = 0 \quad (2.2)$$

where  $E$  is the total energy and  $|\Psi(\mathbf{s}_e, \mathbf{s})\rangle$  is the complete wavefunction that describes the motion of both the electrons and the nuclei. Next we employ the Born–Oppenheimer expansion<sup>1–3</sup>

$$|\Psi(\mathbf{s}_e, \mathbf{s})\rangle = \sum_{j=1}^N |\zeta_j(\mathbf{s}_e|\mathbf{s})\rangle \psi_j(\mathbf{s}) \quad (2.3)$$

where the  $\psi_j(\mathbf{s}), j = 1, \dots, N$  are the nuclear-coordinate-dependent coefficients (recognized later as the nuclear wavefunctions) and  $|\zeta_j(\mathbf{s}_e|\mathbf{s})\rangle; j = 1, \dots, N$  are the

---

*Beyond Born–Oppenheimer: Conical Intersections and Electronic Nonadiabatic Coupling Terms*  
By Michael Baer. Copyright © 2006 John Wiley & Sons, Inc.

electronic (adiabatic) eigenfunctions of the electronic Hamiltonian introduced above:

$$(\mathbf{H}_e(\mathbf{s}_e|\mathbf{s}) - u_j(\mathbf{s})) |\zeta_j(\mathbf{s}_e|\mathbf{s})\rangle = 0; \quad j = 1, \dots, N \quad (2.4)$$

Here  $u_j(\mathbf{s})$ ,  $j = 1, \dots, N$  are the electronic eigenvalues. In this treatment we assume that the Hilbert space is of dimension  $N$ . Substituting Eq. (2.3) in Eq. (2.2), multiplying it from the left by  $\langle \zeta_k(\mathbf{s}_e|\mathbf{s}) |$ , and integrating over the electronic coordinates while recalling Eqs. (2.1) and (2.4) yields the following set of coupled equations:

$$\sum_{j=1}^N \langle \zeta_k | \mathbf{T}_n \psi_j(\mathbf{s}) | \zeta_j \rangle + (u_k(\mathbf{s}) - E) \psi_k(\mathbf{s}) = 0; \quad k = 1, \dots, N \quad (2.5)$$

Next, we recall that the kinetic operator  $\mathbf{T}_n$  can be written (in terms of mass-scaled coordinates) as

$$\mathbf{T}_n = -\frac{\hbar^2}{2m} \nabla^2 \quad (2.6)$$

where  $m$  is the mass of the system and  $\nabla$  is the gradient (vector) operator expressed in terms of mass-scaled coordinates. Substituting Eq. (2.6) in Eq. (2.5) and, performing the corresponding differentiations with respect to the nuclear coordinates and the integrations with respect to the electronic coordinates yield the more explicit form of the Born–Oppenheimer system of coupled equations:<sup>4</sup>

$$-\frac{\hbar^2}{2m} \nabla^2 \psi_k + (u_k - E) \psi_k - \frac{\hbar^2}{2m} \sum_{j=1}^N (2\boldsymbol{\tau}_{kj} \cdot \nabla + \boldsymbol{\tau}_{kj}^{(2)}) \psi_j = 0; \quad k = 1, \dots, N \quad (2.7)$$

where  $\boldsymbol{\tau}$  is the (first-order) nonadiabatic coupling (vector) matrix with the elements

$$\boldsymbol{\tau}_{jk} = \langle \zeta_j | \nabla \zeta_k \rangle \quad (2.8a)$$

(see Section 1.1) and  $\boldsymbol{\tau}^{(2)}$  is the nonadiabatic (scalar) matrix of the second order with the elements

$$\boldsymbol{\tau}_{jk}^{(2)} = \langle \zeta_j | \nabla^2 \zeta_k \rangle \quad (2.8b)$$

For a system of real electronic wavefunctions  $\boldsymbol{\tau}$  is an antisymmetric matrix.

Equation (2.7) can also be written in a matrix form as follows<sup>5</sup>

$$-\frac{\hbar^2}{2m} \nabla^2 \Psi + (\mathbf{u} - E) \Psi - \frac{\hbar^2}{2m} (2\boldsymbol{\tau} \cdot \nabla + \boldsymbol{\tau}^{(2)}) \Psi = \mathbf{0} \quad (2.9)$$

where the dot designates the scalar product,  $\Psi(\mathbf{s})$  is a column vector that contains the abovementioned nuclear functions  $\{\psi_j(\mathbf{s}), j = 1, \dots, N\}$ , and  $\mathbf{u}$  is a diagonal matrix that contains the adiabatic potentials. This equation is valid for any group of states.

In Section 1.1 it is proved that when the group of states forms a Hilbert space (or even a Hilbert subspace—see Section 1.2) so that the  $\tau$  matrix fulfills the *divergence* condition (see Section 1.1.3), then  $\tau^{(2)}$  can be presented in terms of  $\tau$  as follows:<sup>5–7</sup>

$$\tau^{(2)} = \tau^2 + \nabla\tau \quad (2.10)$$

Substituting Eq. (2.10) in Eq. (2.9) yields

$$-\frac{\hbar^2}{2m}\nabla^2\Psi + \left(\mathbf{u} - \frac{\hbar^2}{2m}\tau^2 - E\right)\Psi - \frac{\hbar^2}{2m}(2\tau \cdot \nabla + \nabla\tau)\Psi = \mathbf{0} \quad (2.11)$$

This equation (2.11) can also be written in a more compact way:<sup>8,9</sup>

$$-\frac{\hbar^2}{2m}(\nabla + \tau)^2\Psi + (\mathbf{u} - E)\Psi = \mathbf{0} \quad (2.12)$$

This is the nuclear Schrödinger equation within the adiabatic framework for a group of states that forms a Hilbert space. In this sense Eq. (2.12) differs from Eq. (2.9), which is valid for any group of states.

### 2.1.2 Diabatic Representation

Our starting equation is Eq. (2.3) with one difference, namely, we replace  $|\zeta_j(\mathbf{s}_e|\mathbf{s})\rangle$  by  $|\tilde{\zeta}_j(\mathbf{s}_e|\mathbf{s}_0)\rangle$ ;  $j = 1, \dots, L$  where  $\mathbf{s}_0$  is a set of nuclear coordinates for a *fixed* point in configuration space. Thus, instead of the expansion in Eq. (2.3)  $|\tilde{\Psi}(\mathbf{s}_e, \mathbf{s})\rangle$  is presented in a slightly different form:<sup>4,10–14</sup>

$$|\tilde{\Psi}(\mathbf{s}_e, \mathbf{s})\rangle = \sum_{j=1}^L |\tilde{\zeta}_j(\mathbf{s}_e|\mathbf{s}_0)\rangle \tilde{\psi}_j(\mathbf{s}) \quad (2.13)$$

Here  $\tilde{\psi}_j(\mathbf{s})$ , the corresponding nuclear coefficient, stands for  $\tilde{\psi}_j(\mathbf{s}|\mathbf{s}_0)$ , which depends parametrically on  $\mathbf{s}_0$  and  $|\tilde{\zeta}_j(\mathbf{s}_e|\mathbf{s}_0)\rangle$  in exactly the same way that  $|\zeta_j(\mathbf{s}_e|\mathbf{s})\rangle$  is an eigenfunction of a similar Hamiltonian

$$(\mathbf{H}_e(\mathbf{s}_e|\mathbf{s}_0) - u_j(\mathbf{s}_0))|\tilde{\zeta}_j(\mathbf{s}_e|\mathbf{s}_0)\rangle = 0 \quad (2.14)$$

where  $u_j(\mathbf{s}_0)$ ,  $j = 1, \dots, L$  are the corresponding electronic eigenvalues as calculated for this (fixed) set of nuclear coordinates. Substituting Eqs. (2.13) and (2.14) in Eq. (2.2), recalling that the coordinates  $\mathbf{s}_0$  are not variables, yields the following expression:

$$\sum_{j=1}^L |\tilde{\zeta}_j(\mathbf{s}_e|\mathbf{s}_0)\rangle (\mathbf{T}_n - E)\tilde{\psi}_j(\mathbf{s}) + \sum_{j=1}^L \tilde{\psi}_j(\mathbf{s})\mathbf{H}_e(\mathbf{s}_e|\mathbf{s})|\tilde{\zeta}_j(\mathbf{s}_e|\mathbf{s}_0)\rangle = 0 \quad (2.15)$$

Here  $\mathbf{T}_n$  ( $= \mathbf{T}_n(\mathbf{s})$ ) is as given in Eq. (2.6). Multiplying Eq. (2.15) by  $\langle \zeta_k(\mathbf{s}_e|\mathbf{s}) |$  and integrating over the electronic coordinates yield the following result

$$\left( -\frac{1}{2m} \nabla^2 - E \right) \tilde{\psi}_k(\mathbf{s}) + \sum_{j=1}^L \mathbf{V}_{kj}(\mathbf{s}|\mathbf{s}_0) \tilde{\psi}_j(\mathbf{s}) = 0 \quad (2.16)$$

where  $\mathbf{V}_{kj}(\mathbf{s}|\mathbf{s}_0)$  is the  $(k,j)$  diabatic matrix element given in the following form:

$$\mathbf{V}_{kj}(\mathbf{s}|\mathbf{s}_0) = \langle \zeta_k(\mathbf{s}_e|\mathbf{s}_0) | \mathbf{H}_e(\mathbf{s}_e|\mathbf{s}) | \zeta_j(\mathbf{s}_e|\mathbf{s}_0) \rangle \quad (2.17)$$

Next, recalling that  $\mathbf{H}_e(\mathbf{s}_e|\mathbf{s})$  operator is given as the sum of the electronic kinetic energy operator  $\mathbf{T}_e(\mathbf{s}_e)$  and the potential energy operator  $U(\mathbf{s}_e|\mathbf{s})$ , we have

$$\mathbf{H}_e(\mathbf{s}_e|\mathbf{s}) = \mathbf{T}_e(\mathbf{s}_e) + \mathbf{U}(\mathbf{s}_e|\mathbf{s}) \quad (2.18a)$$

Here  $U(\mathbf{s}_e|\mathbf{s})$  is the Coulomb field, which governs the motion of the electrons and we include also Coulomb interactions due to the fixed, nuclei. A similar expression holds also for  $\mathbf{H}_e(\mathbf{s}_e|\mathbf{s}_0)$ :

$$\mathbf{H}_e(\mathbf{s}_e|\mathbf{s}_0) = \mathbf{T}_e(\mathbf{s}_e) + \mathbf{U}(\mathbf{s}_e|\mathbf{s}_0) \quad (2.18b)$$

Since the kinetic energy operator of the electrons does not depend on the nuclear coordinates,  $\mathbf{H}_e(\mathbf{s}_e|\mathbf{s})$  can be written in the following way:

$$\mathbf{H}_e(\mathbf{s}_e|\mathbf{s}) = \mathbf{H}_e(\mathbf{s}_e|\mathbf{s}_0) + (\mathbf{U}(\mathbf{s}_e|\mathbf{s}) - \mathbf{U}(\mathbf{s}_e|\mathbf{s}_0)) \quad (2.19)$$

Having this relation, we are capable of presenting more explicitly the expression  $\mathbf{V}_{jk}(\mathbf{s}|\mathbf{s}_0)$  given in Eq. (2.17):

$$\mathbf{V}_{jk}(\mathbf{s}|\mathbf{s}_0) = \mathbf{v}_{jk}(\mathbf{s}|\mathbf{s}_0) + \delta_{jk} \mathbf{u}_j(\mathbf{s}_0) \quad (2.20)$$

where

$$\mathbf{v}_{jk}(\mathbf{s}|\mathbf{s}_0) = \langle \zeta_j(\mathbf{s}_e|\mathbf{s}_0) | (\mathbf{U}(\mathbf{s}_e|\mathbf{s}) - \mathbf{U}(\mathbf{s}_e|\mathbf{s}_0)) | \zeta_k(\mathbf{s}_e|\mathbf{s}_0) \rangle \quad (2.21)$$

Equation (2.16) can be also written in matrix form:

$$-\frac{\hbar^2}{2m} \nabla^2 \tilde{\Psi} + (\mathbf{V} - E) \tilde{\Psi} = \mathbf{0} \quad (2.22)$$

Here  $\tilde{\Psi}(\mathbf{s})$  is a column vector that contains the nuclear functions  $\tilde{\psi}_j(\mathbf{s})$ ;  $j = 1, \dots, L$  and  $\mathbf{V}(\mathbf{s}|\mathbf{s}_0)$  is the *diabatic* potential matrix, which, in contrast to  $u(\mathbf{s})$  in Eq. (2.12), is a full matrix.

Equation (2.22) is the Schrödinger equation within the diabatic representation.

### 2.1.3 Adiabatic-to-Diabatic Transformation

Having adiabatic and diabatic frameworks with the two different Schrödinger equations, the obvious question is: Under what conditions will the two equations yield similar results? In general, the two approaches are expected to yield similar results because the two frameworks are connected by an orthogonal (unitary) transformation. However, it is shown that the two frameworks *cannot always* be connected through an orthogonal transformation.<sup>15,16</sup> In other words, such a transformation can be formed only if certain conditions are fulfilled. Essentially there are two ways to derive this transformation. One is by considering the relevant electronic basis sets, namely,  $\zeta(\mathbf{s}_e|\mathbf{s})$  and  $\zeta(\mathbf{s}_e|\mathbf{s}_0)$  and the other, by considering the two nuclear functions  $\Psi(\mathbf{s})$  and  $\tilde{\Psi}(\mathbf{s}|\mathbf{s}_0)$  in Eqs. (2.12) and (2.22), respectively.

#### 2.1.3.1 Transformation for Electronic Basis Sets

The derivation via the electronic basis sets is essentially in the spirit of *quantum chemistry*, and we start with it by assuming that the two electronic basis sets are connected as follows<sup>5,6</sup>

$$\zeta(\mathbf{s}_e|\mathbf{s}) = \tilde{\mathbf{A}}(\mathbf{s}|\mathbf{s}_0)\zeta(\mathbf{s}_e|\mathbf{s}_0) \quad (2.23)$$

where  $\tilde{\mathbf{A}}(\mathbf{s}|\mathbf{s}_0)$  is the matrix to be determined. It is important to emphasize that writing Eq. (2.23) in this way implies that  $\zeta(\mathbf{s}_e|\mathbf{s}_0)$  contains the *diabatic* basis set and  $\zeta(\mathbf{s}_e|\mathbf{s})$ , for  $\mathbf{s} \neq \mathbf{s}_0$ , contains the *adiabatic* one (although both are legitimate eigenfunctions of the same Hamiltonian but are calculated at two different points in configuration space). To continue along these lines, we refer the reader to Eq. (1.6), where we mentioned that in case the group of  $N$  states forms a *Hilbert space* and  $\Delta\mathbf{s}$  is small enough, the following relation holds:<sup>18</sup>

$$|\zeta_k(\mathbf{s}_e|\mathbf{s} + \Delta\mathbf{s})\rangle = \sum_{j=1}^N (\delta_{kj} - \Delta\mathbf{s} \cdot \boldsymbol{\tau}_{kj}(\mathbf{s})) |\zeta_j(\mathbf{s}_e|\mathbf{s})\rangle \quad (2.24)$$

This relation holds, approximately, also for a Hilbert subspace of the type discussed in Section 1.2. Equation (2.24) can be converted into a set of first-order differential equations for the  $\zeta_j(\mathbf{s}_e|\mathbf{s})$  eigenfunctions:

$$\nabla |\zeta_k(\mathbf{s}_e|\mathbf{s})\rangle = - \sum_{j=1}^N \boldsymbol{\tau}_{kj}(\mathbf{s}) |\zeta_j(\mathbf{s}_e|\mathbf{s})\rangle; \quad k = 1, \dots, N \quad (2.25)$$

or in matrix form:

$$\nabla \zeta(\mathbf{s}_e|\mathbf{s}) + \boldsymbol{\tau}(\mathbf{s}) \zeta(\mathbf{s}_e|\mathbf{s}) = \mathbf{0} \quad (2.26)$$

In order to calculate  $\zeta(\mathbf{s}_e|\mathbf{s})$  at a given point  $\mathbf{s}$  for an initial value  $\zeta(\mathbf{s}_e|\mathbf{s}_0)$ , we have to assume a contour  $\Gamma$  that connects  $\mathbf{s}$  and  $\mathbf{s}_0$  and then solve Eq. (2.26) along this contour. One way to see it more explicitly is to convert Eq. (2.26) into an integral

equation

$$\zeta(\mathbf{s}_e|\mathbf{s}) = \zeta(\mathbf{s}_e|\mathbf{s}_0) - \int_{\mathbf{s}_0}^{\mathbf{s}} d\mathbf{s} \cdot \boldsymbol{\tau}(\mathbf{s}) \zeta(\mathbf{s}_e|\mathbf{s}) \quad (2.27)$$

where the integration is done along the given contour.

Equations (2.26) also has an explicit solution given in the form [see derivation in Section 1.3.3 and the final result in Eq. (1.85)]<sup>15–18</sup>

$$\zeta(\mathbf{s}_e|\mathbf{s}|\mathbf{s}_0) = \wp \exp \left( - \int_{\mathbf{s}_0}^{\mathbf{s}} d\mathbf{s} \cdot \boldsymbol{\tau}(\mathbf{s}) \right) \zeta(\mathbf{s}_e|\mathbf{s}_0) \quad (2.28)$$

where, again, the integration is done along  $\Gamma$  and we replaced  $\zeta(\mathbf{s}_e|\mathbf{s})$  by  $\zeta(\mathbf{s}_e|\mathbf{s}|\mathbf{s}_0)$  to emphasize the fact that the calculation is started at  $\mathbf{s} = \mathbf{s}_0$ . This exponentiated integration has to be carried out in a given order and therefore the symbol  $\wp$  [see more in a sentence following Eq. (1.85)]. Comparing Eqs. (2.28) and (2.23), we get a similar representation for the  $\tilde{\mathbf{A}}$  matrix:

$$\tilde{\mathbf{A}}(\mathbf{s}|\mathbf{s}_0|\Gamma) = \wp \exp \left( - \int_{\mathbf{s}_0}^{\mathbf{s}} d\mathbf{s} \cdot \boldsymbol{\tau}(\mathbf{s}|\Gamma) \right) \quad (2.29)$$

where  $\tilde{\mathbf{A}}(\mathbf{s}|\mathbf{s}_0|\Gamma)$  replaces  $\tilde{\mathbf{A}}(\mathbf{s}|\mathbf{s}_0)$  to emphasize the fact that the calculations are done along the given contour  $\Gamma$ . Although solving Eq. (2.29) numerically seems to be straightforward, it may in fact contain inherent complications since the exponentiated *line integral* with an arbitrary  $\boldsymbol{\tau}$  matrix is not guaranteed to yield a single-valued  $\tilde{\mathbf{A}}$  matrix (although one may wonder whether a single-valued  $\tilde{\mathbf{A}}$  matrix is really required). This exponentiated *line integral* is used to solve Eq. (2.28) and here, as a result of possible internal inconsistency, the difficulties are more apparent because the  $\boldsymbol{\tau}$ -matrix elements are formed by eigenfunctions that we now intend to derive. Since the eigenfunctions can be determined up to a phase factor (which may depend on the *nuclear* coordinates), the whole approach is self-consistent *if and only if* the  $\boldsymbol{\tau}$  matrix produces, up to phase factors, the *same* (initial) eigenfunctions. In order to reveal the conditions for this situation to occur, we extend the integration in Eq. (2.28) to a *closed* contour,  $\Gamma$ . In this way the integration that yields the  $\tilde{\mathbf{A}}$  matrix returns to the initial point and we expect to obtain the initial set of eigenfunctions  $\zeta(\mathbf{s}_e|\mathbf{s}_0)$ . The set of functions,  $\zeta(\mathbf{s}_e|\mathbf{s}_0|\mathbf{s}_0)$ , that results from this calculation is given as

$$\zeta(\mathbf{s}_e|\mathbf{s}_0|\mathbf{s}_0) = \wp \left[ \exp \left( - \oint_{\Gamma} d\mathbf{s} \cdot \boldsymbol{\tau}(\mathbf{s}|\Gamma) \right) \right] \zeta(\mathbf{s}_e|\mathbf{s}_0) \quad (2.30)$$

In order for the theory to be self-consistent, the original set of electronic eigenfunctions  $\zeta(\mathbf{s}_e|\mathbf{s}_0)$  and the newly formed  $\zeta(\mathbf{s}_e|\mathbf{s}_0|\mathbf{s}_0)$  have to be the same up to a phase factor, namely

$$\zeta_j(\mathbf{s}_e|\mathbf{s}_0|\mathbf{s}_0) = \exp(i\vartheta_j(\Gamma)) \zeta_j(\mathbf{s}_e|\mathbf{s}_0); \quad j = 1, \dots, N \quad (2.31)$$

where  $\vartheta_j; j = \{1, N\}$  are real phases. Returning to Eq. (2.29) and introducing a new matrix  $\mathbf{D}(\Gamma)$  calculated for the *closed* contour  $\Gamma^{14,19,20}$  [see also Eq. (1.93)], namely

$$\mathbf{D}(\Gamma) = \tilde{\mathbf{A}}(\mathbf{s}_0|\mathbf{s}_0|\Gamma) = \wp \exp \left( - \oint_{\Gamma} \mathbf{d}\mathbf{s} \cdot \boldsymbol{\tau}(\mathbf{s}|\Gamma) \right) \quad (2.32)$$

we ascertain that the  $\mathbf{D}$  matrix elements have to be of the form

$$\mathbf{D}_{jk}(\Gamma) = \delta_{jk} \exp(i\vartheta_j(\Gamma)); \quad j, k = \{1, N\} \quad (2.33)$$

In case of real eigenfunctions, the phases,  $\vartheta_j(\Gamma)$  are multiples of  $\pi$  so that the diagonal elements of the  $\mathbf{D}$  matrix are  $\pm 1^{14-16,19,20}$

Equation (2.31) can be also be written as

$$\zeta_j(\mathbf{s}_e|\mathbf{s}_0|\mathbf{s}_0) = \mathbf{D}_{jj}(\Gamma) \zeta_j(\mathbf{s}_e|\mathbf{s}_0); \quad j = \{1, N\} \quad (2.31')$$

which explicitly shows that in case of real eigenfunctions we have  $\zeta_j(\mathbf{s}_e|\mathbf{s}_0|\mathbf{s}_0) = \pm \zeta_j(\mathbf{s}_e|\mathbf{s}_0); j = \{1, N\}$ .

**Short Summary** We showed that the two *adiabatic* electronic basis sets calculated at two different points are related by an orthogonal transformation matrix  $\tilde{\mathbf{A}}(\mathbf{s}|\Gamma)$  presented explicitly in Eq. (2.29). To satisfy self-consistency, it has to have, for any (closed) contour  $\Gamma$  in the region, the feature presented in Eq. (2.33).

Next we review results derived in Chapter 1. In Section 1.3.2.2 we considered a group of states that form a Hilbert subspace in a given region but at some *isolated* points the corresponding tensorial field  $\mathbf{F}$  is not well defined. In such a case, the following equation for  $\zeta(\mathbf{s}_e|\mathbf{s}_0|\Gamma)$

$$\zeta(\mathbf{s}_e|\mathbf{s}_0|\Gamma) = \zeta(\mathbf{s}_e|\mathbf{s}_0) - \oint_{\Gamma} \mathbf{d}\mathbf{s} \cdot \boldsymbol{\tau}(\mathbf{s}|\Gamma) \zeta(\mathbf{s}_e|\mathbf{s}|\Gamma) \quad (2.34)$$

[which is the closed-contour extension of Eq. (2.27)] does not necessarily produce the *initial* set of functions  $\zeta(\mathbf{s}_e|\mathbf{s}_0)$ . The contrary is also true, namely, as long as a contour  $\Gamma$  does not surround any of these *pathological* points, the closed line integral is zero and the two functions  $\zeta(\mathbf{s}_e|\mathbf{s}_0)$  and  $\zeta(\mathbf{s}_e|\mathbf{s}_0|\Gamma)$  are identical. This means that the electronic manifold is singlevalued and therefore implies that the exponentiated line integral as given in Eq. (2.32) is the unit matrix, namely, that the diagonal elements of the  $\mathbf{D}$  matrix are *all* equal to +1.

For the situation where the contour surrounds the abovementioned *pathological* points, the mathematical approach presented in Section 1.3.2.2 is not conclusive. However, it is conclusive according to the theory presented here. It implies that even in the case where the contour surrounds such points, the two sets  $\zeta(\mathbf{s}_e|\mathbf{s}_0)$  and  $\zeta(\mathbf{s}_e|\mathbf{s}_0|\Gamma)$  [as given in Eq. (2.30)] are related. As can be seen from Eq. (2.31), they are not necessarily identical but differ at most by phase factors. This possibility is guaranteed because the Curl equation [i.e., Eq. (1.18) or (1.49a), in case of a Hilbert

subspace] guarantees the solution given in Eq. (2.28) as long as the (open) contour avoids the *problematical* points.

In case of real eigenfunctions the phase factors become  $\pm 1$ , which means that some (or all) of the  $\zeta(\mathbf{s}_e|\mathbf{s}_0)$  functions flip their sign as a result of tracing the closed contour  $\Gamma$ . From Eq. (2.31') it is noted that the functions that flip their sign are those that are *multiplied* by the negative diagonal element of the matrix  $\mathbf{D}$ . Therefore, if the  $\mathbf{D}$  matrix contains  $K$  elements that are  $-1$ , then the  $K$  corresponding eigenfunctions flip their sign.

Before closing this section, I mention that the two-state case deserves special consideration because of its utmost importance. The two-state case is treated in detail in Section 3.1.1.

### 2.1.3.2 Transformation for Nuclear Wavefunctions

The fact that the two nuclear Schrödinger equations, presented in Eqs. (2.12) and (2.22), are expected to yield the same solution implies that both equations carry with them the same amount of information and therefore are related through an orthogonal transformation matrix. In order to derive this transformation matrix, we start with the adiabatic Schrödinger equation, eliminate the  $\tau$ -matrix elements, and form the relevant diabatic Schrödinger equation. Later on, we show that the newly formed *diabatic* Schrödinger equation and the one presented in Eq. (2.22) are identical.

We start by replacing, in Eq. (2.12), the column vector  $\Psi$  by another column vector  $\Phi$  where the two are related as follows:<sup>5–8</sup>

$$\Psi = \mathbf{A}\Phi \quad (2.35)$$

Here  $\mathbf{A}$  is a matrix of the coordinates to be determined by the requirement that the  $\tau$  matrix in Eq. (2.12) will not appear in the Schrödinger equation for  $\Phi$ . To achieve that, we evaluate the following expression

$$\begin{aligned} (\nabla + \tau)^2 \mathbf{A}\Phi &= (\nabla + \tau)(\nabla + \tau)\mathbf{A}\Phi \\ &= (\nabla + \tau)(\mathbf{A}\nabla\Phi + (\nabla\mathbf{A})\Phi + \tau\mathbf{A}\Phi) \\ &= 2(\nabla\mathbf{A}) \cdot \nabla\Phi + \mathbf{A}\nabla^2\Phi + (\nabla^2\mathbf{A})\Phi \\ &\quad + (\nabla\tau)\mathbf{A}\Phi + 2\tau(\nabla\mathbf{A}) + 2\tau\mathbf{A}(\nabla\Phi) + \tau^2\mathbf{A}\Phi \end{aligned}$$

which can be arranged to become

$$\therefore \mathbf{A}\nabla^2\Phi + 2(\nabla\mathbf{A} + \tau\mathbf{A}) \cdot \nabla\Phi + \{(\tau + \nabla) \cdot (\nabla\mathbf{A} + \tau\mathbf{A})\}\Phi \quad (2.36)$$

where the grad operator, in the third term, does not act beyond the curled parentheses (curly braces) { }. Now, choosing  $\mathbf{A}$  to be a solution of the following equation

$$\nabla\mathbf{A} + \tau\mathbf{A} = \mathbf{0} \quad (2.37)$$

Eq. (2.36) becomes

$$(\nabla + \tau)^2 \mathbf{A} \Phi = \mathbf{A} \nabla^2 \Phi \quad (2.36')$$

Substituting Eqs. (2.35) and (2.36') in Eq. (2.12), we have

$$-\frac{\hbar^2}{2m} \mathbf{A} \nabla^2 \Phi + (\mathbf{u} - E) \mathbf{A} \Phi = \mathbf{0} \quad (2.12')$$

In Section 1.3.1.3 we proved that the solution of Eq. (2.37) has to be an orthogonal matrix. Therefore multiplying Eq. (2.12') by  $\mathbf{A}^\dagger$ —the complex conjugate matrix of  $\mathbf{A}$ —we get

$$-\frac{\hbar^2}{2m} \nabla^2 \Phi + (\mathbf{W} - E) \Phi = \mathbf{0} \quad (2.38)$$

where  $\mathbf{W}$  is given in the form

$$\mathbf{W} = \mathbf{A}^\dagger \mathbf{u} \mathbf{A} \quad (2.39)$$

Equation (2.38) is the nuclear *adiabatic* Schrödinger equation, and  $\mathbf{W}$  is the corresponding *adiabatic* potential.

In Section (1.3.3) we proved that the solution of (2.37) is given in the following form [see Eq. (1.85)]:<sup>17</sup>

$$\mathbf{A}(\mathbf{s}|\Gamma) = \varphi \exp \left\{ - \int_{\mathbf{s}_0}^{\mathbf{s}} \boldsymbol{\tau}(\mathbf{s}'|\Gamma) \cdot d\mathbf{s}' \right\} \mathbf{A}(\mathbf{s}_0) \quad (2.40)$$

Comparing Eq. (2.40) with Eq. (2.29), it is noted that  $\mathbf{A}(\mathbf{s}|\Gamma)$  and  $\tilde{\mathbf{A}}(\mathbf{s}|\Gamma)$  are, up to a constant orthogonal transformation, identical. Therefore from now on we refer to both as the “ $\mathbf{A}$  matrix.”

**Short Summary** We showed that the orthogonal transformation matrix  $\mathbf{A}(\mathbf{s}|\Gamma)$  that connects two *adiabatic* basis sets,  $\zeta(\mathbf{s}_e|\mathbf{s}|\Gamma)$  and  $\zeta(\mathbf{s}_e|\mathbf{s}_0)$ , defined at two different points  $\mathbf{s}$  and  $\mathbf{s}_0$ , also eliminates, step by step along the same contour, the electronic nonadiabatic coupling matrix (NACM)  $\boldsymbol{\tau}$ , from the *adiabatic* Schrödinger equation and in this way forms a *diabatic* Schrödinger equation.

The fact that these two transformations are carried out by the same matrix leads to several interesting consequences to be discussed next.

### 2.1.3.3 Implications Due to Adiabatic-to-Diabatic Transformation

In this section we discuss four corollaries that are directly related to the findings of the previous sections.

**Corollary 2.1 Singlevaluedness of the Diabatic Potential Matrix  $\mathbf{W}$**  The potential matrix  $\mathbf{W}$  [see Eq. (2.39)] has to be singlevalued because the Schrödinger equation in Eq. (2.38) cannot be solved unless  $\mathbf{W}$  is singlevalued.

From Eq. (2.39) we note that  $\mathbf{W}$  is singlevalued (in a given region) if the matrix  $\mathbf{A}$  is singlevalued in that region [the eigenvalues  $u_j(\mathbf{s})$ ;  $j = \{1, N\}$  that form the  $\mathbf{u}$  matrix are singlevalued by construction]. However, in Section 1.3.2.2 we showed that the singlevaluedness of the  $\mathbf{A}$  matrix (where it was labeled as  $\Omega$ ) is in general not guaranteed unless the tensor  $\mathbf{F}$  is identically zero in the region of interest. In what follows we derive the *necessary* condition for  $\mathbf{W}$  to be singlevalued, and during this derivation that it becomes clear that, in fact, the singlevaluedness of the  $\mathbf{A}$  matrix is not required.

The proof<sup>19–20</sup> is carried out for a region in configuration space for which the relevant electronic manifold forms a Hilbert *subspace*.

We consider a closed contour  $\Gamma$  defined in terms of a continuous parameter  $\lambda$  so that the starting point  $\mathbf{s}_0$  of the contour is at  $\lambda = 0$ . Next,  $\beta$  is defined as the value attained by  $\lambda$  once the contour completes a full cycle and returns to its starting point. For instance, in case of a circle,  $\lambda$  is an angle and  $\beta = 2\pi$ .

Given a closed contour  $\Gamma$  and a point  $\mathbf{s}_0$  located on it, we calculate both  $\mathbf{A}(\lambda)$  and  $\mathbf{W}(\lambda)$  starting at  $\lambda = 0$  ( $\mathbf{s} = \mathbf{s}_0$ ) and continue until we reach  $\lambda = \beta$ . To reveal the necessary condition, we assume that at  $\mathbf{s}_0$  the calculated diabatic potential matrix  $\mathbf{W}(\lambda = \beta)$  and the initial one— $\mathbf{W}(\lambda = 0)$ —are identical, specifically

$$\mathbf{W}(\lambda = 0) = \mathbf{W}(\lambda = \beta) \quad (2.41)$$

and derive the condition for that to happen. Following Eq. (2.39), this requirement implies that for any arbitrary point  $\mathbf{s}_0$  (on the contour) we have

$$\mathbf{A}^\dagger(0)\mathbf{u}(0)\mathbf{A}(0) = \mathbf{A}^\dagger(\beta|\Gamma)\mathbf{u}(\beta)\mathbf{A}(\beta|\Gamma) \quad (2.42)$$

Next, we introduce the matrix  $\mathbf{B}(\Gamma)$  defined as

$$\mathbf{B}(\Gamma) = \mathbf{A}(\beta|\Gamma)\mathbf{A}^\dagger(0) \quad (2.43)$$

which, following Eq. (2.43), connects  $\mathbf{u}(\beta)$  with  $\mathbf{u}(0)$ :

$$\mathbf{u}(\beta) = \mathbf{B}(\Gamma)\mathbf{u}(0)\mathbf{B}^\dagger(\Gamma) \quad (2.44)$$

The  $\mathbf{B}$  matrix is, by definition, a unitary matrix (it is a product of two unitary matrices) but other than that is not known and therefore will be derived next.

We recall that the adiabatic potential matrix  $\mathbf{u}(\mathbf{s})$  is uniquely defined at each point in configuration space and therefore  $\mathbf{u}(0) \equiv \mathbf{u}(\beta)$ . Consequently Eq. (2.44) implies that the two matrices  $\mathbf{B}(\Gamma)$  and  $\mathbf{u}(\beta)$  commute:

$$[\mathbf{B}(\Gamma), \mathbf{u}(\beta)] = \mathbf{0} \quad (2.45)$$

Since any two matrices that commute have to be diagonal, this implies that  $\mathbf{B}(\Gamma)$  is diagonal. Recalling that  $\mathbf{B}(\Gamma)$  is also unitary implies that

$$\mathbf{B}_{jk}(\Gamma) = \delta_{jk} \exp(i\vartheta_k(\Gamma)) \quad (2.46)$$

In other words,  $\mathbf{B}(\Gamma)$  is a diagonal matrix that contains in its diagonal real phase factors.

Returning to Eq. (2.43), we observe that the  $\mathbf{B}$  matrix transforms the  $\mathbf{A}$  matrix from its initial value at  $\lambda = 0$  to its final value at  $\lambda = \beta$  while tracing a *closed* contour,  $\Gamma$ :

$$\mathbf{A}(\beta|\Gamma) = \mathbf{B}(\Gamma)\mathbf{A}(0) \quad (2.47)$$

To obtain a more explicit expression for  $\mathbf{B}(\Gamma)$ , we consider Eq. (1.92) for the case that  $\Omega(\mathbf{s}) \equiv \mathbf{A}(\mathbf{s})$  and for a closed contour starting at the point  $\mathbf{s} = \mathbf{s}_0$ :

$$\mathbf{A}(\mathbf{s}_0|\Gamma) = \mathbf{A}(\beta|\Gamma) = \wp \exp\left(-\oint_{\Gamma} d\mathbf{s} \cdot \boldsymbol{\tau}\right) \mathbf{A}(\mathbf{s}_0) \quad (2.48)$$

Comparing Eqs. (2.48) and (2.47) and recalling the meaning of  $\lambda = 0$ , we obtain:

$$\mathbf{B}(\Gamma) = \wp \exp\left(-\oint_{\Gamma} d\mathbf{s} \cdot \boldsymbol{\tau}(\mathbf{s})\right) \quad (2.49)$$

where  $\mathbf{B}$  is contour-dependent but does not depend on any specific point located on that contour (see a detailed study on this subject in Ref. 21). Recalling Eq. (2.32), it is clearly noted that  $\mathbf{B}(\Gamma) \equiv \mathbf{D}(\Gamma)$  introduced earlier to guarantee fundamental features related to the electronic manifold that forms the Hilbert *subspace*.

**Short Summary** We established that the *necessary* condition for the  $\mathbf{A}$  matrix to yield a *singlevalued* diabatic potential as given in Eq. (2.40) is that the  $\mathbf{B}$  matrix, defined in Eq. (2.49), be diagonal and contain phase factors with real phases (because the  $\mathbf{B}$  matrix, just like the  $\mathbf{A}$  matrix, is unitary). Since we consider only real electronic eigenfunctions, these phase factors are  $\pm 1$ . It is important to emphasize that for this to happen, the  $\mathbf{A}$  matrix is not necessarily singlevalued because the  $\mathbf{B}$  matrix, as was just proved, is not necessarily a *unit* matrix.

We showed that the  $\mathbf{B}$  matrix is *identical* to the  $\mathbf{D}$  matrix, and therefore we refer, from now on, to both as the  $\mathbf{D}$  matrix. As already mentioned earlier that the  $\mathbf{D}$  matrix depends only on the closed contour  $\Gamma$ , which is a geometric magnitude, and therefore we frequently refer to the  $\mathbf{D}$  matrix as the *topological* matrix. As will be discussed later, the magnitude that characterizes the  $\mathbf{D}$  matrix most is the number of  $(-1)$ s along its diagonal. We define this number as  $K$  and term it the *topological* number.

(Comment: Because of the close relation between the  $\mathbf{D}$  matrix and the  $\boldsymbol{\tau}$  matrix as given in Eq. (2.49) and because the  $\mathbf{D}$  matrix has to be diagonal in case of a Hilbert space, we suggest that the corresponding  $\boldsymbol{\tau}$  matrix will be termed *quantized*.<sup>19–20</sup> The

*quantization* is well recognized in case of a two-state Hilbert space as discussed in Section 3.1.1.2.

**Corollary 2.2 Uniqueness of the Diabatic Potential Matrices** Earlier we discussed two different diabatic potential energy matrices: (1) one matrix— $\mathbf{V}(\mathbf{s})$ , presented in Eq. (2.17)—is derived in terms of a single basis set attached to a *fixed* point in configuration space and therefore is formed directly in the diabatic framework; (2) the second matrix— $\mathbf{W}(\mathbf{s})$ , presented in Eq. (2.39)—is formed by a more involved process that starts with an *adiabatic* potential matrix but then, through an orthogonal transformation, becomes a diabatic potential matrix. In what follows we show that the two matrices are identical.<sup>15–16</sup>

We start with Eq. (2.17) and replace the  $\zeta(\mathbf{s}_e|\mathbf{s}_0)$  set, which serves, for the present treatment, as the diabatic basis set by the corresponding adiabatic basis set—the  $\zeta(\mathbf{s}_e|\mathbf{s})$  set—employing Eq. (2.23) [and Eq. (2.28)]. Thus

$$\zeta(\mathbf{s}_e|\mathbf{s}_0) = \mathbf{A}^\dagger(\mathbf{s}|\mathbf{s}_0|\Gamma)\{\zeta(\mathbf{s}_e|\mathbf{s})\} \quad (2.50)$$

where we slightly changed the notation [replacing  $\zeta(\mathbf{s}_e|\mathbf{s}|\mathbf{s}_0)$  by  $\zeta(\mathbf{s}_e|\mathbf{s})$ ]. Substituting Eq. (2.50) in Eq. (2.17) and considering one particular matrix element  $V_{ij}(\mathbf{s}|\mathbf{s}_0)$ , we get

$$\mathbf{V}_{ij}(\mathbf{s}|\mathbf{s}_0) = \sum_{k=1}^N \sum_{k'=1}^N \mathbf{A}_{ki}^*(\mathbf{s}|\mathbf{s}_0|\Gamma) \langle \zeta_k(\mathbf{s}_e|\mathbf{s}) | \mathbf{H}_e(\mathbf{s}_e|\mathbf{s}) | \zeta_{k'}(\mathbf{s}_e|\mathbf{s}) \rangle \mathbf{A}_{k'j}(\mathbf{s}|\mathbf{s}_0|\Gamma) \quad (2.51)$$

Next, recalling that the  $\zeta_k(\mathbf{s}_e|\mathbf{s})$ ;  $k = \{1, N\}$  are the eigenfunctions of  $\mathbf{H}_e(\mathbf{s}_e|\mathbf{s})$  [see Eq. (2.4)], we obtain

$$\mathbf{V}_{ij}(\mathbf{s}|\Gamma) = \sum_{k=1}^N \mathbf{A}_{ki}^*(\mathbf{s}|\Gamma) \mathbf{u}_{kk}(\mathbf{s}) \mathbf{A}_{kj}(\mathbf{s}|\Gamma) \quad (2.52)$$

or

$$\mathbf{V} = \mathbf{A}^\dagger \mathbf{u} \mathbf{A} \quad (2.53)$$

Comparing Eq. (2.53) with Eq. (2.39), it is seen that the two potential matrices, namely,  $\mathbf{V}$  and  $\mathbf{W}$ , are identical.

**Corollary 2.3 Uniqueness of the Total Wavefunction  $\Psi(\mathbf{s}_e, \mathbf{s})$**  The total wavefunction  $\Psi(\mathbf{s}_e, \mathbf{s})$  is presented in Eq. (2.3) in terms of the adiabatic electronic eigenfunction  $\zeta(\mathbf{s}_e|\mathbf{s})$  and the corresponding nuclear functions  $\Psi(\mathbf{s})$ :

$$\Psi(\mathbf{s}_e, \mathbf{s}) = \zeta^T(\mathbf{s}_e|\mathbf{s}) \Psi(\mathbf{s}) \quad (2.54a)$$

A similar representation for total wavefunction  $\tilde{\Psi}(\mathbf{s}_e, \mathbf{s})$  is given in terms the diabatic functions  $\zeta(\mathbf{s}_e|\mathbf{s}_0)$  and the corresponding nuclear functions  $\tilde{\Psi}(\mathbf{s})$  [see Eq. (2.13)]:

$$\tilde{\Psi}(\mathbf{s}_e, \mathbf{s}) = \zeta^T(\mathbf{s}_e|\mathbf{s}_0) \tilde{\Psi}(\mathbf{s}) \quad (2.54b)$$

We show that the two wavefunctions  $\Psi(s_e, s)$  and  $\tilde{\Psi}(s_e, s)$  are identical. To do that, we have to treat the relations between the electronic and the nuclear wavefunctions separately.

Whereas the relation between the two electronic basis sets is presented explicitly in Eq. (2.50), the relation between the two nuclear wavefunctions deserves more attention. We start by reminding the reader that the two nuclear *diabatic* wavefunctions  $\tilde{\Psi}(s)$  and  $\Phi(s)$  are solutions of the same (diabatic) Schrödinger equation, namely, Eqs. (2.22) and (2.38) (recalling that the two potential matrices  $\mathbf{V}$  and  $\mathbf{W}$  are identical), and therefore, when solved for the same boundary conditions, are identical. Next, it was shown that the *adiabatic* function  $\Psi(s)$  is related to  $\Phi(s)$  by the orthogonal transformation as given in Eq. (2.35). This implies that the same relation holds between  $\Psi(s)$  and  $\tilde{\Psi}(s)$ , thus

$$\Psi(s) = \mathbf{A}(s)\tilde{\Psi}(s) \quad (2.55)$$

where we remember that  $\tilde{\mathbf{A}} \equiv \mathbf{A}$ . Substituting Eqs. (2.55) and (2.50) in Eq. (2.54a) (with the obvious slight changes) yields Eq. (2.54b).

To conclude this derivation, we state that treatment of the Schrödinger equation, whether it is done in the adiabatic or the diabatic framework, yields the same solution. In other words, the transformation from the adiabatic to the diabatic frameworks (or vice versa) discussed above does not affect the solution of this equation.

Since  $\mathbf{A}$  is the (orthogonal) transformation matrix that connects the two frameworks, it will be termed the *adiabatic-to-diabatic transformation matrix* and recognized by its acronym as the ADT matrix.

#### 2.1.3.4 Final Comments

It is now well accepted that in order to calculate spectroscopic and scattering cross sections, one has to solve the diabatic Schrödinger equation. In many studies the method employed to reach the diabatic framework follows the procedure as discussed in Section 2.1.3.2<sup>22–43</sup> (sometimes termed the *dynamic approach*). However, there are also numerous approaches that circumvent the use of the NACTs.<sup>44–62</sup>

One of the more popular approaches is based on the *smoothness* of diabatic states as a function of nuclear coordinates. Assuming smooth diabatic states, Macias and Riera<sup>44,45</sup> apply such an approach to certain operators in the vicinity of the avoided crossing region assuming their corresponding diabatic presentation to be smooth as well. This approach was extended and generalized by Kryachko by introducing what he calls an *equation of motion*.<sup>46,47</sup> Werner and Meyer applied this approach to LiF assuming a *smooth* electronic dipole moment operator.<sup>48</sup> Petrongolo et al.,<sup>49,50</sup> while studying the NH<sub>2</sub> and NO<sub>2</sub> systems, considered for the first system the quadrupole moment and, for the second, one of the dipole moments. This approach has so far been applied only for two-state systems. Its extension to a multistate system does not seem to be obvious and so far has not been tried. A somewhat different approach was suggested by Rebentrost and others<sup>51,52</sup> according to which the so-called ADT angle or also the *mixing* angle (to be properly introduced in the next chapter) is replaced by an angle that the open-shell orbital forms with the intermolecular axis. Similar

approaches were suggested by Romero et al.,<sup>53</sup> Sidis,<sup>54</sup> Domcke and stock,<sup>55</sup> Schinke and colleagues<sup>56,57</sup> and Dobbyn and Knowles.<sup>58</sup> A different approach is employed by Pacher et al.<sup>59,60</sup> that is based on block diagonalization leading to the Lorentz gauge. In all cases reported so far the calculated ADT angles exhibit a reasonable functional form. Since this approach assumes a diabatic behavior at some parts in the region of interest, its application may encounter difficulties if applied within a region of numerous conical intersections (see next chapter). A different approach is suggested by Sevryuk et al.,<sup>61</sup> namely, an approach based on the postadiabatic representation developed by Klar and Fano.<sup>62</sup> According to this approach, the diabatic framework is reached by a series of transformations.

A different approach to treat the ADT matrix directly is given by due to Ryb and Baer.<sup>63</sup> They suggest presenting the ADT matrix as a product of overlap matrices:

$$\mathbf{A}(q_i \rightarrow q_f) = \lim_{N \rightarrow \infty} O_{N,N-1} O_{N-1,N-2} \dots O_{2,1}$$

where  $q_1 = q_i$  is the initial point and  $q_N = q_f$  is the final point of a given contour. The matrix  $O_{n+1,n}$  is defined by

$$[O_{n+1,n}]_{ij} \equiv \langle \zeta_j(q_{n+1}) | \zeta_j(q_n) \rangle$$

where  $\zeta_j(q_n)$  is the  $j$ th adiabatic (electronic) wavefunction at point  $q_n$ .

## 2.2 APPLICATION OF COMPLEX EIGENFUNCTIONS

### 2.2.1 Introducing Time-Independent Phase Factors

#### 2.2.1.1 Adiabatic Schrödinger Equation

In the previous section we presented the Born–Openheimer treatment employing real eigenfunctions. Here we extend this treatment and show that employing a complex basis set may affect the adiabatic Schrödinger equation but not the final (diabatic) Schrödinger equation, which follows applying the corresponding ADT.

In what follows we continue to refer to  $\zeta_j(\mathbf{s}_e|\mathbf{s})$ ,  $j = \{1, N\}$  as real eigenfunctions but multiply them by a phase factor (with a real phase) to make them complex:

$$\tilde{\zeta}_j(\mathbf{s}_e|\mathbf{s}) = \exp(i\vartheta_j(\mathbf{s}))\zeta_j(\mathbf{s}_e|\mathbf{s}) \quad (2.56)$$

To continue, we introduce the diagonal matrix  $\omega(\mathbf{s})$

$$\omega_{jk}(\mathbf{s}) = \delta_{jk} \exp(i\vartheta_j(\mathbf{s})) \quad (2.57)$$

so that the column vector  $|\tilde{\zeta}(\mathbf{s}_e|\mathbf{s})\rangle$  can be written as

$$|\tilde{\zeta}(\mathbf{s}_e|\mathbf{s})\rangle = \omega(\mathbf{s})|\zeta(\mathbf{s}_e|\mathbf{s})\rangle \quad (2.56')$$

It is important to realize that the  $\tilde{\zeta}(s_e|s)$  functions, just like the real  $\zeta(s_e|s)$  functions, are eigenfunctions of the electronic Hamiltonian in Eq. (2.4).

Having these definitions, we next introduce the corresponding nonadiabatic coupling matrix (NACM) elements,  $\tilde{\tau}_{jk}(s)$

$$\tilde{\tau}_{jk} = \langle \tilde{\zeta}_j | \nabla \tilde{\zeta}_k \rangle \quad (2.58)$$

or employing Eq. (2.56) yields

$$\tilde{\tau}_{jk} = \exp(-i\theta_j) \langle \zeta_j | \nabla \zeta_k \rangle \exp(i\theta_k) + i\delta_{jk} \nabla \theta_k \quad (2.59)$$

It can be shown that  $\tilde{\tau}(s)$  and  $\tau(s)$  are related in the following way

$$\tilde{\tau}(s) = \omega^\dagger(s) \tau(s) \omega(s) + i \nabla \Theta(s) \quad (2.60)$$

where  $\Theta(s)$  is a diagonal matrix that contains the attached phases. In the same way we introduce the second-order NACM  $\tilde{\tau}^{(2)}(s)$ :

$$\tilde{\tau}^{(2)}(s) = \omega^\dagger(s) (\tau^{(2)}(s) + 2i\tau(s)\nabla\Theta(s)) \omega(s) + i\nabla^2\Theta(s) - \nabla\Theta(s)^2 \quad (2.61)$$

where the  $\tau^{(2)}(s)$  matrix elements are as given in Eq. (2.8b). Continuing as in Section 2.1.1, we get the corresponding adiabatic nuclear Schrödinger equation:

$$-\frac{\hbar^2}{2m} (\nabla + \tilde{\tau})^2 \Psi + (\mathbf{u} - E) \Psi = \mathbf{0} \quad (2.62)$$

### 2.2.1.2 Adiabatic-to-Diabatic Transformation

Next we perform the ADT, namely

$$\Psi = \tilde{\mathbf{A}} \tilde{\Phi} \quad (2.35')$$

and it can be shown that if  $\tilde{\mathbf{A}}$  is chosen to be the solution of the following equation

$$\nabla \tilde{\mathbf{A}} + \tilde{\tau} \tilde{\mathbf{A}} = \mathbf{0} \quad (2.63)$$

then the corresponding diabatic Schrödinger equation becomes similar to the one presented in Eq. (2.38) with the potential  $\tilde{\mathbf{W}}$  given in the following form [similar to Eq. (2.39)]:

$$\tilde{\mathbf{W}} = \tilde{\mathbf{A}}^\dagger \mathbf{u} \tilde{\mathbf{A}} \quad (2.64)$$

Next, substituting Eq. (2.60) in Eq. (2.63) and recalling that the  $\mathbf{A}$  matrix fulfills Eq. (2.37), it can be seen that  $\tilde{\mathbf{A}}$  and  $\mathbf{A}$  are related as follows:

$$\tilde{\mathbf{A}}(s) = \omega^\dagger(s) \mathbf{A}(s) \quad (2.65)$$

Finally, substituting Eq. (2.65) in Eq. (2.64) yields the diabatic potential presented in terms of the real  $\mathbf{A}$  matrix [see Eq. (2.39)]:

$$\mathbf{W}(\mathbf{s}) \equiv \tilde{\mathbf{W}}(\mathbf{s}) \quad (2.66)$$

**Summary** Equation (2.60) is reminiscent of a gauge transformation in the theory of electromagnetic fields for time-independent phases<sup>1</sup>

$$\boldsymbol{\tau}(\mathbf{s}) \rightarrow \boldsymbol{\tau}(\mathbf{s}) + \nabla\theta(\mathbf{s}) \quad (2.67)$$

where  $\theta(\mathbf{s})$  is an arbitrary potential function of the coordinates. It is well known that such transformations do not affect the magnetic field, or, in other words that the magnetic field is *invariant* under this (gauge) transformation. However, we do not consider magnetic fields but diabatic potentials, and therefore the above mentioned gauge invariance is observed with respect to the diabatic potential. Attaching a phase factor to the (real) eigenfunctions of an electronic Hamiltonian [see Eq. (2.56)] forms the gauge transformation given in Eq. (2.60) [and is similar to the one in Eq. (2.67)]. This transformation is shown not to affect the final *diabatic* potential [see Eq. (2.66)]. In other words, the *diabatic* Schrödinger equation is gauge-invariant under the transformation in Eq. (2.56).

## 2.2.2 Introducing Time-Dependent Phase Factors

The starting point is the time-dependent Schrödinger equation for the full wavefunction  $\Psi$  of the electrons and the nuclei

$$i\hbar \frac{\partial \Psi}{\partial t} = \left( -\frac{\hbar^2}{2m} \nabla^2 + \mathbf{H}_e \right) \Psi \quad (2.68)$$

where  $\mathbf{H}_e$  is the electronic (time-independent) Hamiltonian and we continue, as usual, employing the Born–Oppenheimer expansion for the total wavefunction  $\Psi$  written in the form

$$\Psi(\mathbf{s}_e, \mathbf{s}, t) = \zeta^T(\mathbf{s}_e | \mathbf{s}, t) \psi(\mathbf{s}, t) \quad (2.69)$$

Here  $\zeta^T(\mathbf{s}_e | \mathbf{s}, t)$  is a row vector [in contrast to  $\zeta(\mathbf{s}_e | \mathbf{s}, t)$ , which is a column vector] and  $\psi(\mathbf{s}, t)$  the corresponding column vector. Since  $\mathbf{H}_e$  is time-*independent*, the electronic basis set functions  $\zeta_j(\mathbf{s}_e | \mathbf{s}, t); j = \{1, N\}$  are the eigenfunctions of the time-*independent* electronic Hamiltonian [see Eq. (2.4)]. To introduce the time dependence, the eigenfunctions are multiplied by time-dependent phase factors [see Eqs. (2.56) and (2.57)]

$$\zeta(\mathbf{s}_e | \mathbf{s}, t) = \omega(\mathbf{s}, t) \zeta^{(0)}(\mathbf{s}_e | \mathbf{s}) \quad (2.70)$$

where the  $\zeta_j^{(0)}(\mathbf{s}_e|\mathbf{s})$  values are the *real* eigenfunctions of  $\mathbf{H}_e(\mathbf{s}_e|\mathbf{s})$  and  $\omega(\mathbf{s}, t)$  is a diagonal matrix that contains the phase factors [see Eq. (2.57)]. The extension as in Eq. (2.70) does not affect the orthonormalization of the eigenfunctions.

Continuing the derivation as in Section 2.2.1 leads to a similar (but not exactly the same) expression for the corresponding adiabatic Schrödinger equation, namely

$$i\hbar \frac{\partial \Psi(\mathbf{s}, t)}{\partial t} = -\frac{\hbar^2}{2m} (\nabla + \tilde{\tau}(\mathbf{s}, t))^2 \Psi(\mathbf{s}, t) + \tilde{\mathbf{u}}(\mathbf{s}, t) \Psi(\mathbf{s}, t) \quad (2.71)$$

where  $\tilde{\tau}(\mathbf{s}, t)$  is the “dressed” NACM given in the form [see Eq. (2.60)]<sup>2</sup>

$$\tilde{\tau}(\mathbf{s}, t) = \boldsymbol{\omega}^\dagger(\mathbf{s}, t) \boldsymbol{\tau}(\mathbf{s}) \boldsymbol{\omega}(\mathbf{s}, t) + i \nabla \Theta(\mathbf{s}, t) \quad (2.72)$$

and  $\tilde{\mathbf{u}}(\mathbf{s}, t)$  is an “extended” potential given as:<sup>2</sup>

$$\tilde{\mathbf{u}}(\mathbf{s}, t) = \mathbf{u}(\mathbf{s}) - \hbar \frac{\partial \Theta(\mathbf{s}, t)}{\partial t} \quad (2.73)$$

Here  $\Theta(\mathbf{s}, t)$  is a diagonal matrix that contains the phases themselves, and similarly  $\nabla \Theta(\mathbf{s}, t)$  and  $\partial \Theta(\mathbf{s}, t)/\partial t$  are diagonal matrices that contain the corresponding space and time derivatives of  $\Theta(\mathbf{s}, t)$ .

The only change caused by the fact that the phases are now time-dependent (in contrast to those described in Section 2.2.1) is the additional potential  $\hbar(\partial \Theta(\mathbf{s}, t)/\partial t)$ , which affects  $\mathbf{u}(\mathbf{s})$  and leads to  $\tilde{\mathbf{u}}(\mathbf{s}, t)$ .

The rest of the derivation is similar to the one given in the previous section. Moreover, it can be shown that here, too, the *adiabatic* potential matrix is invariant with respect to the gauge transformation presented in Eqs. (2.72) and (2.73).

We would like to refer to one special type of phase, namely, any phase that is proportional to time  $t$ :

$$\Theta(\mathbf{s}, t) = \Theta_0(\mathbf{s})t \quad (2.74)$$

Substituting Eq. (2.74) in Eq. (2.73) leaves  $\tilde{\mathbf{u}}(\mathbf{s})$  time-independent:

$$\tilde{\mathbf{u}}(\mathbf{s}) = \mathbf{u}(\mathbf{s}) - \hbar \Theta_0(\mathbf{s}) \quad (2.75)$$

So far  $\Theta_0(\mathbf{s})$  is arbitrary; however, assuming it to be equal to  $\mathbf{u}(\mathbf{s})/\hbar$  leads to a particular interesting Schrödinger equation [see Eq. (2.71)], namely

$$i\hbar \frac{\partial \Psi(\mathbf{s}, t)}{\partial t} = -\frac{\hbar^2}{2m} (\nabla + \tilde{\tau}(\mathbf{s}, t))^2 \Psi(\mathbf{s}, t) \quad (2.76)$$

where

$$\tilde{\tau}(\mathbf{s}, t) = \boldsymbol{\omega}^\dagger(\mathbf{s}, t) \boldsymbol{\tau}(\mathbf{s}) \boldsymbol{\omega}(\mathbf{s}, t) + (i/\hbar)t \nabla \mathbf{u}(\mathbf{s}) \quad (2.77)$$

This result is somewhat unexpected for two reasons:

1. We encounter a nuclear Schrödinger equation that does not contain a potential and is completely dominated by the (dressed) NACM.
2. As is noted from Eq. (2.77), the potential matrix is not really missing but becomes, as a result of this particular gauge transformation, part of the extended NACM.

Equations (2.72) and (2.73) are the gauge transformations for the NACM and the potential matrix, again reminiscent of the gauge transformation within the theory of electromagnetism<sup>1</sup>

$$\begin{aligned}\mathbf{A}(\mathbf{s}, t) &\rightarrow \mathbf{A}(\mathbf{s}, t) + \nabla\theta(\mathbf{s}, t) \\ \phi(\mathbf{s}, t) &\rightarrow \phi(\mathbf{s}, t) + \frac{1}{c} \frac{\partial\theta(\mathbf{s}, t)}{\partial t}\end{aligned}\quad (2.78)$$

where  $\mathbf{A}(\mathbf{s}, t)$  is the electromagnetic vector potential (not to be confused with the ADT matrix) and  $\phi(\mathbf{s}, t)$  is the *electric* potential. It is noted that, because of the time-dependent phases, the similarity between the two types of gauge transformations is enhanced. We not only clearly note that the molecular NACM is similar to the vector potential  $\mathbf{A}(\mathbf{s}, t)$  in electromagnetism—a fact known for quite some time<sup>3–8</sup>—but also show here a new connection between the two frameworks, namely, the similarity between molecular adiabatic potential energy surfaces  $\mathbf{u}(\mathbf{s})$  and the electric potentials  $\phi(\mathbf{s}, t)$ .

The diabatization process of Eq. (2.71) is similar to the one presented in Section 2.2.1.2 and will not be presented here.

## 2.3 TIME-DEPENDENT TREATMENT

### 2.3.1 Time-Dependent Perturbative Approach

The starting point is the time-dependent Schrödinger equation for the total wavefunction,  $\Psi(\mathbf{s}_e, \mathbf{s}, t)$  given in Eq. (2.68), where the electronic Hamiltonian  $\mathbf{H}_e$  is time-dependent for  $t \geq 0$ , specifically,  $\mathbf{H}_e = \mathbf{H}_e(\mathbf{s}_e|\mathbf{s}, t)$ . In what follows we employ an electronic basis set that is time-independent and therefore contains the eigenfunctions of  $\mathbf{H}_e(\mathbf{s}_e|\mathbf{s}, t)$  for  $t \leq 0$ . Consequently  $\Psi(\mathbf{s}_e, \mathbf{s}, t)$  is assumed to be of the form<sup>1</sup>

$$\Psi(\mathbf{s}_e, \mathbf{s}, t) = \zeta^T(\mathbf{s}_e|\mathbf{s})\psi(\mathbf{s}, t) \quad (2.79)$$

Substituting Eq. (2.79) in Eq. (2.68) yields the following time-dependent equation for the nuclear wavefunctions

$$i\hbar\zeta^T(\mathbf{s}_e|\mathbf{s})\frac{\partial\psi(\mathbf{s}, t)}{\partial t} = -\frac{\hbar^2}{2m}\nabla^2(\zeta^T(\mathbf{s}_e|\mathbf{s})\psi(\mathbf{s}, t)) + \mathbf{H}_e(\mathbf{s}_e|\mathbf{s}, t)\zeta^T(\mathbf{s}_e|\mathbf{s})\psi(\mathbf{s}, t) \quad (2.80)$$

or

$$i\hbar\zeta^T \frac{\partial\psi}{\partial t} = -\frac{\hbar^2}{2m} (\zeta^T \nabla^2 \psi + \nabla^2 \zeta^T \psi + 2\nabla \zeta^T \nabla \psi) + \mathbf{H}_e \zeta^T \psi \quad (2.81)$$

Multiplying Eq. (2.81) (from the left-hand side) by  $\zeta(\mathbf{s}_e|\mathbf{s})$  and integrating over the electronic coordinates [which entails multiplying Eq. (2.81), each time, by one of the time-independent eigenfunctions and integrating over  $\mathbf{s}_e$ ], we obtain the (adiabatic) time-dependent equation for the nuclear wavefunctions

$$i\hbar \frac{\partial\psi}{\partial t} = -\frac{\hbar^2}{2m} (\nabla + \boldsymbol{\tau})^2 \psi + \tilde{\mathbf{H}}_e \psi \quad (2.82)$$

where  $\boldsymbol{\tau}$  is the usual (time-independent) NACM but  $\tilde{\mathbf{H}}_e$  is the time-dependent potential matrix defined as follows:

$$\tilde{\mathbf{H}}_{ejk}(\mathbf{s}, t) = \langle \zeta_j(\mathbf{s}_e|\mathbf{s}) | \mathbf{H}_e(\mathbf{s}_e|\mathbf{s}, t) | \zeta_k(\mathbf{s}_e|\mathbf{s}) \rangle \quad (2.83)$$

It is important to mention that  $\tilde{\mathbf{H}}_e$ , for  $t \leq 0$ , is a diagonal matrix that is identical to the adiabatic potential matrix  $\mathbf{u}$  introduced in Eq. (2.4) but becomes nondiagonal for  $t > 0$ .

The next step is to perform the ADT in order to eliminate the  $\boldsymbol{\tau}$  matrix which is done in a way similar to that performed within the time-independent framework, namely, replacing  $\Psi$  by  $\mathbf{A}\Phi$  and performing the required algebra [see also Eqs. (2.36) and (2.37)]. This derivation yields the following time-dependent nuclear Schrödinger equation

$$i\hbar \frac{\partial\Phi}{\partial t} = -\frac{\hbar^2}{2m} \nabla^2 \Phi + \mathbf{W}_e(\mathbf{s}, t) \Phi \quad (2.84)$$

where the diabatic potential  $\mathbf{W}_e$  is similar to  $\mathbf{W}$  in Eq. (2.39) but defined with respect to  $\tilde{\mathbf{H}}_e$ , given in Eq. (2.83):

$$\mathbf{W}_e = \mathbf{A}^\dagger \tilde{\mathbf{H}}_e \mathbf{A} \quad (2.85)$$

As for the  $\mathbf{A}$  matrix, this is, as usual, the solution of Eq. (2.37). Since the electronic basis set is time-independent, the same rule applies to the  $\boldsymbol{\tau}$  matrix as well as to the  $\mathbf{A}$  matrix so that the time dependence of the diabatic potential  $\mathbf{W}_e$  follows solely from  $\tilde{\mathbf{H}}_e$ .

At this stage we call the reader's attention to the following difficulty. We note that the number of coupled (nuclear) Schrödinger equations to be solved is equal to the number of electronic eigenstates, designated as  $L$ , employed in the derivation of  $\tilde{\mathbf{H}}_e$  (and therefore also in the derivation of  $\mathbf{W}_e$ ). However if  $N$  is the size of the relevant Hilbert subspace (viz., the size of a group of states that forms the Hilbert subspace), then  $L$  has to be identical to  $N$  because otherwise *multivalued* diabatic potentials would be expected from Eq. (2.85).

### 2.3.2 Time-Dependent Nonperturbative Approach

#### 2.3.2.1 Adiabatic Time-Dependent Electronic Basis Set

In this section is assumed that the electronic basis set,  $\zeta(\mathbf{s}_e|\mathbf{s}, t)$ , is time-dependent so that the total wavefunction is written as in Eq. (2.69). At this stage we remind the reader that, as in the time-independent case, the size of the Hilbert space is  $N$ , which implies that  $N$  electronic eigenfunctions of the type  $\zeta_j(\mathbf{s}_e|\mathbf{s}, t)$ ;  $j = \{1, N\}$  form the Hilbert subspace. As is well known, these functions fulfill the time-dependent eigenvalue equation:<sup>2</sup>

$$i\hbar \frac{\partial}{\partial t} \zeta^T(\mathbf{s}_e|\mathbf{s}, t) = \zeta^T(\mathbf{s}_e|\mathbf{s}, t) \mathbf{H}_e(\mathbf{s}_e|\mathbf{s}, t) \quad (2.86)$$

This way of writing The time-dependent eigenvalue equation is written this way only for convenience and implies that each eigenfunction fulfills the following equation:<sup>2</sup>

$$i\hbar \frac{\partial}{\partial t} |\zeta_j(\mathbf{s}_e|\mathbf{s}, t)\rangle = \mathbf{H}_e(\mathbf{s}_e|\mathbf{s}, t) |\zeta_j(\mathbf{s}_e|\mathbf{s}, t)\rangle; j = \{1, N\} \quad (2.87)$$

In order to proceed, we have to be somewhat more specific on the electronic Hamiltonian. In what follows we assume that  $\mathbf{H}_e$  is independent of time as long as  $t \leq 0$ . Consequently, for  $t \leq 0$ , the  $j$ th eigenfunction  $\zeta_j(\mathbf{s}_e|\mathbf{s}, t)$  assumes the form<sup>1,3</sup>

$$\zeta_j(\mathbf{s}_e|\mathbf{s}, t) = \zeta_{j0}(\mathbf{s}_e|\mathbf{s}) \exp((-i/\hbar)\mathbf{u}_j(\mathbf{s})t) \quad (2.88)$$

where the substitution of Eq. (2.88) in Eq. (2.87) leads to the  $j$ th time-independent eigenvalue equation for  $\zeta_{j0}(\mathbf{s}_e|\mathbf{s})$ :

$$(\mathbf{H}_e(\mathbf{s}_e|\mathbf{s}, t=0) - \mathbf{u}_j(\mathbf{s})) \zeta_{j0}(\mathbf{s}_e|\mathbf{s}) = 0 \quad (2.89)$$

To solve Eq. (2.87) subject to the initial condition presented in Eq. (2.88),  $\zeta_j(\mathbf{s}_e|\mathbf{s}, t)$  is expanded in terms of  $L$  eigenfunctions of  $\mathbf{H}_e$  as calculated at  $t = 0$ . Thus

$$|\zeta_j(\mathbf{s}_e|\mathbf{s}, t)\rangle = \sum_{k=1}^L |\zeta_{k0}(\mathbf{s}_e|\mathbf{s})\rangle \omega_{kj}(\mathbf{s}, t); j = 1, \dots, N \quad (2.90)$$

where the  $\omega(\mathbf{s}, t)$  is a rectangular matrix of dimensions  $L \times N$  that contains the expansion coefficients. It is important to realize that  $L$  can be made arbitrarily large and the only constraints on  $L$  is that  $L \geq N$ . Substituting Eq. (2.90) in Eq. (2.87) and continuing in the usual way yields the differential equation for  $\omega(\mathbf{s}, t)$

$$i\hbar \frac{\partial \omega(\mathbf{s}, t)}{\partial t} = \tilde{\mathbf{H}}_e(\mathbf{s}, t) \omega(\mathbf{s}, t) \quad (2.91)$$

where  $\tilde{\mathbf{H}}_e$  is a square matrix of dimension  $L \times L$  and its elements are given in the following form:

$$\tilde{\mathbf{H}}_e(\mathbf{s}, t)_{kj} = \langle \zeta_{k0}(\mathbf{s}_e|\mathbf{s}) | \tilde{\mathbf{H}}_e(\mathbf{s}, t) | \zeta_{j0}(\mathbf{s}_e|\mathbf{s}) \rangle; \quad 0 \leq k \leq L, 0 \leq j \leq L \quad (2.92)$$

The solution of Eq. (2.91) is given in the form

$$\omega(\mathbf{s}, t) = \wp \exp \left\{ -\frac{i}{\hbar} \int_{-\infty}^t dt' \cdot \tilde{\mathbf{H}}_e(\mathbf{s}, t') \right\} \mathbf{I}^{(r)} \quad (2.93)$$

where  $\wp$  is now a time-ordering operator and  $\mathbf{I}^{(r)}$  is a rectangular unit matrix of dimension  $L \times N$  (where  $r$  denotes “rectangular”). It can be seen that for  $t \leq 0$  the matrix  $\omega(\mathbf{s}, t)$  becomes

$$\omega_{jk}(\mathbf{s}, t \leq 0) = \exp(i u_j(\mathbf{s}) t) \delta_{jk} \quad (2.94)$$

Next we prove that  $\omega(\mathbf{s}, t)$  is a unitary matrix and for this purpose we consider Eq. (2.91) and form the equation for its complex conjugate  $\omega^\dagger(\mathbf{s}, t)$

$$-i\hbar \frac{\partial \omega^\dagger(\mathbf{s}, t)}{\partial t} = \omega^\dagger \tilde{\mathbf{H}}_e(\mathbf{s}, t) \quad (2.95)$$

where  $\omega^\dagger(\mathbf{s}, t)$  is a rectangular matrix of dimension  $N \times L$ . Multiplying Eq. (2.91) from the left-hand side by  $\omega^\dagger(\mathbf{s}, t)$  and Eq. (2.95) from the right-side by  $\omega(\mathbf{s}, t)$  and subtracting the first equation from the second one yields

$$i\hbar \frac{\partial (\omega^\dagger \omega)}{\partial t} = 0 \Rightarrow \omega^\dagger \omega = \text{const} \quad (2.96)$$

Next, recalling Eq. (2.94), it is easy to see that for any time  $t$  we have

$$\omega^\dagger(\mathbf{s}, t) \omega(\mathbf{s}, t) = \mathbf{I}^{(s)} \quad (2.97)$$

where  $\mathbf{I}^{(s)}$  is a square matrix of dimension  $N \times N$  (where  $s$  denotes “square”). Thus, we proved that  $\omega(\mathbf{s}, t)$  is a unitary matrix with respect to its short dimension (i.e.,  $N$ ).

### 2.3.2.2 Adiabatic Time-Dependent Nuclear Schrödinger Equation

Substituting Eqs. (2.69) and (2.86) in Eq. (2.68) yields (after a few algebraic rearrangements) the following time-dependent equation for the nuclear wavefunctions:

$$i\hbar \zeta^T(\mathbf{s}_e|\mathbf{s}, t) \frac{\partial \psi(\mathbf{s}, t)}{\partial t} = -\frac{\hbar^2}{2m} \nabla^2 (\zeta^T(\mathbf{s}_e|\mathbf{s}, t) \psi(\mathbf{s}, t)) \quad (2.98)$$

The interesting feature related to this equation is the fact that it is entirely dominated by the nuclear kinetic operator.

Evaluating the r.h.s., one obtains

$$i\hbar \zeta^T \frac{\partial \psi}{\partial t} = -\frac{\hbar^2}{2m} \{ \zeta^T \nabla^2 \psi + 2\nabla \zeta^T \nabla \psi + (\nabla^2 \zeta^T) \psi \} \quad (2.99)$$

Multiplying Eq. (2.98) (from the left side) by  $\zeta^\dagger(\mathbf{s}_e|\mathbf{s}, t)$  and integrating over the electronic coordinates, we obtain (see Appendix 2A.1):

$$i\hbar \frac{\partial \psi}{\partial t} = -\frac{\hbar^2}{2m} (\nabla + \tilde{\tau})^2 \psi \quad (2.100)$$

where  $\tilde{\tau}$  is a *time-dependent, dressed*, NACM of dimension  $N \times N$  given in the form

$$\tilde{\tau} = \omega^\dagger \tau \omega + \omega^\dagger \nabla \omega \quad (2.101)$$

Here  $\tau$  is the NACM (dimension  $L \times L$ ) defined in terms the time-*independent* basis set  $\zeta_0(\mathbf{s}_e|\mathbf{s})$  [see Eq. (2.8a)].

Equation (2.100), the general adiabatic time-dependent nuclear Schrödinger equation, is somewhat unexpected because it lacks the potential matrix. A similar expression is encountered in the simplified version of the present treatment when we attached time-dependent phase factors to the electronic eigenfunctions [see discussion in Section 2.2.2 and in particular Eq. (2.76)].

### 2.3.2.3 Time-Dependent Adiabatic-to-Diabatic Transformation

To carry out the ADT for Eq. (2.100), we follow the procedure given for the time-independent case in Section 2.1.3.2, but to distinguish this case from the previous one, we label the ADT matrix as  $\tilde{\mathbf{A}}$ . Substituting Eq. (2.35) in Eq. (2.100) yields the following expression:

$$i\hbar \tilde{\mathbf{A}} \frac{\partial \Phi}{\partial t} = -\frac{\hbar^2}{2m} [\tilde{\mathbf{A}} \nabla^2 + 2(\mathbf{G}\tilde{\mathbf{A}}) \nabla + (\mathbf{G}^2 \tilde{\mathbf{A}})] \Phi - i\hbar \frac{\partial \tilde{\mathbf{A}}}{\partial t} \Phi \quad (2.102)$$

Here  $\mathbf{G}$  is an operator that acts only on  $\tilde{\mathbf{A}}$  and is given in the form

$$\mathbf{G} = \nabla + \tilde{\tau} \quad (2.103)$$

To continue, we add and subtract an undetermined matrix  $\tau_t$  multiplied by  $\tilde{\mathbf{A}}\Phi$ , so that Eq. (2.102) becomes

$$i\hbar \tilde{\mathbf{A}} \frac{\partial \Phi}{\partial t} = -\frac{\hbar^2}{2m} [\tilde{\mathbf{A}} \nabla^2 + 2(\mathbf{G}\tilde{\mathbf{A}}) \nabla + (\mathbf{G}^2 \tilde{\mathbf{A}})] \Phi - (\mathbf{G}_t - \tau_t) \tilde{\mathbf{A}} \Phi \quad (2.104)$$

where  $\mathbf{G}_t$  is an operator that acts on  $\tilde{\mathbf{A}}$  only and is defined as

$$\mathbf{G}_t = i\hbar \frac{\partial}{\partial t} + \tau_t \quad (2.105)$$

The *four*-dimensional vector  $(\mathbf{G}, \mathbf{G}_t)$  is also known by the term *covariant derivative*.<sup>4</sup> The  $\tilde{\mathbf{A}}$  matrix is chosen as a simultaneous solution of the spatial (component) equation

$$\mathbf{G}\tilde{\mathbf{A}} = \mathbf{0} \quad (2.106a)$$

and the (time) equation

$$\mathbf{G}_t \tilde{\mathbf{A}} = \mathbf{0} \quad (2.106b)$$

Once derived, we demand that the matrix,  $\tilde{\mathbf{A}}$ , is an analytic function at every point in a given *four-dimensional* configuration spacetime. This means that each element of the  $\tilde{\mathbf{A}}$  matrix has to be differentiable to any order with respect to all the spatial coordinates and with respect to time. In addition, analyticity requires fulfillment of the following two conditions:

1. The results of two consecutive differentiations of the  $\tilde{\mathbf{A}}$  matrix with respect to two spatial coordinates,  $p$  and  $q$ , should not depend on the order of differentiation. This requirement can be shown to lead to the extended Curl equation similar to the one discussed in Chapter 1 [see Eqs. (1.13)–(1.18)] but where  $\tau$  is replaced by, its time-dependent counterpart,  $\tilde{\tau}$  [see Eq. (2.101)].
2. The results of two consecutive differentiations of the  $\tilde{\mathbf{A}}$  matrix, one with respect to *time* and the other with respect to any spatial coordinate  $p$ , should not depend on the order of differentiation. This requirement implies

$$\frac{\partial}{\partial t} (\nabla \tilde{\mathbf{A}}) - \nabla \left( \frac{\partial}{\partial t} \tilde{\mathbf{A}} \right) = \mathbf{0} \quad (2.107)$$

In Appendix 2A.2 we prove that the condition for the equality in Eq. (2.107) to hold is that the  $\tau_t$  matrix [introduced earlier, in Eqs. (2.104) and (2.105), but not yet determined] has to be

$$\tau_t \equiv \tilde{\mathbf{H}}_e = \boldsymbol{\omega}^\dagger \tilde{\mathbf{H}}_e \boldsymbol{\omega} \quad (2.108)$$

With this result, the first-order differential equations to be fulfilled by  $\tilde{\mathbf{A}}$  are [see Eqs. (2.106)]

$$\nabla \tilde{\mathbf{A}} + \tilde{\tau} \tilde{\mathbf{A}} = \mathbf{0} \quad (2.109a)$$

$$i\hbar \frac{\partial \tilde{\mathbf{A}}}{\partial t} + \tilde{\mathbf{H}}_e \tilde{\mathbf{A}} = \mathbf{0} \quad (2.109b)$$

which can be written in terms of a *four* component vector equation

$$\tilde{\mathbf{G}} \tilde{\mathbf{A}} = \mathbf{0} \quad (2.110)$$

where  $\tilde{\mathbf{G}}$  is the *covariant derivative* given in the form

$$\tilde{\mathbf{G}} = \tilde{\nabla} + \tilde{\tilde{\tau}} \quad (2.111)$$

Here  $\tilde{\nabla}$  is a *four*-component grad operator and

$$\tilde{\nabla} = \left\{ \frac{\partial}{\partial q_1}, \frac{\partial}{\partial q_2}, \dots, \frac{\partial}{\partial q_n}, i\hbar \frac{\partial}{\partial t} \right\} \quad (2.112)$$

and, similarly  $\tilde{\tau}$  is recognized as a *four*-component vector–matrix

$$\tilde{\tau} = \{\tilde{\tau}_{q_1}, \tilde{\tau}_{q_2}, \dots, \tilde{\tau}_{q_n}, \tilde{\mathbf{H}}_e\} \quad (2.113)$$

where  $\tilde{\mathbf{H}}_e$  is the time component of  $\tilde{\tau}$ . It is important to mention that in our case we do not have necessarily *four* components but in general  $(n + 1)$  components.

The corresponding *four*-component non-Abelian Curl equation, which guarantees the existence of an analytic solution for Eq. (2.110), takes the form

$$\frac{\partial}{\partial \mu'} \tilde{\tau}_\mu - \frac{\partial}{\partial \mu} \tilde{\tau}_{\mu'} - [\tilde{\tau}_\mu, \tilde{\tau}_{\mu'}] = \mathbf{0}; \quad \{\mu, \mu' = p, q, t/(i\hbar)\} \quad (2.114)$$

where  $\tilde{\tau}_t$ , is the time component of  $\tilde{\tau}$ , namely,  $\tilde{\tau}_t \equiv \tilde{\mathbf{H}}_e$ .

It can be shown that the  $\tilde{\mathbf{A}}$  matrix that solves Eq. (2.110) is a unitary matrix and as a result the diabatic Schrödinger equation takes the simplified form [see Eq. (2.104)]

$$i\hbar \frac{\partial \Phi}{\partial t} = \left( -\frac{\hbar^2}{2m} \nabla^2 + \tilde{\mathbf{W}}_e \right) \Phi \quad (2.115)$$

where  $\tilde{\mathbf{W}}_e$  is the ‘recovered’ potential matrix:

$$\tilde{\mathbf{W}}_e = \tilde{\mathbf{A}}^\dagger \tilde{\mathbf{H}}_e \tilde{\mathbf{A}} \quad (2.116)$$

The potential matrix  $\tilde{\mathbf{W}}_e$  is similar, in some respects, to  $\mathbf{W}_e$  in Eq. (2.39) because at time  $t \leq 0$  the matrix  $\tilde{\mathbf{H}}_e$  [and also the matrix  $\tilde{\mathbf{H}}_e$ ; see Eq. (2.92)] is a diagonal matrix that contains the adiabatic (ab initio) potentials. However, at  $t > 0$ ,  $\tilde{\mathbf{H}}_e$  and  $\tilde{\mathbf{H}}_e$  become nondiagonal and in general differ from each other. Consequently  $\tilde{\mathbf{W}}_e$  differs from  $\mathbf{W}_e$ .

(Comment: In all the derivations made in this chapter the matrices  $\mathbf{G}$ ,  $\mathbf{G}_t$ ,  $\tilde{\mathbf{A}}$ ,  $\tilde{\tau}$ ,  $\tilde{\mathbf{H}}_e$ ,  $\tilde{\mathbf{W}}_e$ ,  $\tilde{\tau}$  and  $\tilde{\mathbf{G}}$  are all square matrices of dimensions  $N \times N$ .)

### 2.3.3 Summary

In Sections 2.3.1 and 2.3.2 two different diabatization schemes are presented for a molecular system affected by a time-dependent perturbation. We termed the first, the simplified version, the *perurbative approach* and the second, more general one, the *nonperturbative approach*. In both treatments we end up with a unitary ADT matrix (reminiscent of the one encountered in the time-independent framework) calculated by solving a (vectorial) first-order differential equation along contours.

The main difference between the two approaches is as follows. Within the first approach we employ a time-*independent* electronic basis set so that the ADT matrix is time-*independent* and the resulting diabatic PES matrix is similar to the one encountered for a time-*independent* interaction. Within the second approach we apply a time-*dependent* electronic basis set so that we end up with a time-*dependent* ADT matrix that leads to a somewhat more complicated diabatic potential energy matrix.

There is no doubt that on the face of it the first approach, because of its simplified ADT, should be preferred. However, this version may have its disadvantages, due to two contradictory requirements:

1. For a correct ADT matrix, one has to apply a Hilbert subspace that contains  $N$  states (which results in a system of  $N$  nuclear Schrödinger equations to be solved).
2. Given a TD interaction, one may need  $L$  (TID) electronic eigenfunctions to present it reliably at all time (where  $L$  can be much larger than  $N$ ).

With the first approach  $N$  and  $L$  have to be the same, and if  $L$  is very large, for instance, as the result of an intense external field, one has to solve a large number ( $=L$ ) of nuclear Schrödinger equations. With the second approach the two numbers  $N$  and  $L$  are *independent*, namely the number of Schrödinger equations to be solved is, as before,  $N$ , but this approach allows applying a (much) larger electronic basis set to represent the perturbation. It is true that within this process one encounters rectangular (as opposed to square) matrices, but the theory, as presented here, overcomes this obstacle in a reliable, coherent, and consistent way. Thus the final outcome is a set of  $N$  (not  $L$ ) nuclear Schrödinger equations just as in the previous case, and the inconvenience encountered with the second approach is mainly in constructing the diabatic potential matrix but not in solving the nuclear Schrödinger equations.

[Comment: In Problem 2.1 we show that for  $L = N$  the nonperturbative nuclear Hamiltonian given in Eqs. (2.115) and (2.116) reduces to the perturbative one given in Eqs. (2.84) and (2.85).]

One of the more interesting results that follows from the time-dependent approach is the dressed NACM,  $\tilde{\tau}$ , as given in Eq. (2.101) and the interesting new nuclear Schrödinger equation presented in Eq. (2.100), namely, an equation that lacks a potential and is governed by the extended NACM only. Similar expressions were derived in Section 2.2.2 [see Eq. (2.76)] where time-dependent phase factors are employed to form time-dependent eigenfunctions.

Another interesting result is the way the Curl condition extends in case of a time-dependent Hamiltonian [see Eq. (2.114)]. We note that the extension is of the kind expected from a relativistic theory, although relativistic arguments are not explicitly mentioned in this context.

As a final issue in this section, we mention that the ability to treat time-dependent Born–Oppenheimer systems is crucial because of the intensive studies of shaped and specially designed laser pulses to control molecular processes.<sup>5–12</sup>

## PROBLEM

- 2.1** Show that for  $L = N$  (where  $L$  is the size of the perturbation and  $N$  the size of the Hilbert subspace) the final Schrödinger equation for the nonperturbative case in Eqs (2.115) and (2.116) reduces to the perturbative one given in Eqs. (2.84) and (2.85).

*Solution* We start by considering Eqs. (2.109) and assuming that  $\tilde{\mathbf{A}}$  can be written in the form

$$\tilde{\mathbf{A}} = \boldsymbol{\omega}^\dagger \mathbf{B} \quad (2.117)$$

where  $\mathbf{B}$  is still unknown and  $\boldsymbol{\omega}$  is given in Eq. (2.93). This product is well defined as all three matrices  $\tilde{\mathbf{A}}$ ,  $\boldsymbol{\omega}$ , and  $\mathbf{B}$  are square matrices. Substituting Eq. (2.117) in Eq. (2.109a) and recalling the definition of  $\tilde{\tau}$  [see Eq. (2.101)], we note, following a few algebraic operations, that  $\mathbf{B}$  is a solution of the following first-order vectorial equation:

$$\nabla \mathbf{B} + \boldsymbol{\tau} \mathbf{B} = 0 \quad (2.118)$$

In other words,  $\mathbf{B}$  is the ADT matrix  $\mathbf{A}$  [see Eq. (2.37)], which among other things, implies that  $\mathbf{B}$  is time-*independent*. Next we check to what extent Eq. (2.109b) is satisfied. Substituting Eq. (2.117) in Eq. (2.109b) and recalling Eq. (2.108) yields the first-order equation for  $\boldsymbol{\omega}$  as given in Eq. (2.91). Summarizing our findings so far, we may say that in the case in which  $L = N$ , the matrix  $\tilde{\mathbf{A}}$ , as expressed in Eq. (2.117), yields the relevant solution for Eqs. (2.109). To conclude the proof, we consider Eq. (2.116). Substituting Eq. (2.117) in Eq. (2.116) and recalling again Eq. (2.108), we get the diabatic potential matrix for the perturbative case as presented in Eq. (2.85).

## 2A APPENDIXES

### 2A.1 Dressed Nonadiabatic Coupling Matrix $\tilde{\tau}$

Our starting point is Eq. (2.100):

$$i\hbar \zeta^T \frac{\partial \psi}{\partial t} = -\frac{\hbar^2}{2m} \{ \zeta^T \nabla^2 \psi + 2\nabla \zeta^T \cdot \nabla \psi + (\nabla^2 \zeta^T) \psi \} \quad (2A.1)$$

Employing Eq. (2.90), we replace  $\zeta^T(\mathbf{s}_e|\mathbf{s}, t)$  by  $\zeta^T(\mathbf{s}_e|\mathbf{s}, t=0)\boldsymbol{\omega}(\mathbf{s}, t)$  where we recall that (1) the group of functions  $\zeta(\mathbf{s}_e|\mathbf{s}, t=0)$  forms an orthogonal set of eigenfunctions and (2) the matrix  $\boldsymbol{\omega}(\mathbf{s}, t)$  is a unitary matrix. Thus we get

$$\begin{aligned} i\hbar \zeta^T(\mathbf{s}_e|\mathbf{s}, t=0)\boldsymbol{\omega}(\mathbf{s}, t) \frac{\partial \psi}{\partial t} &= -\frac{\hbar^2}{2m} \{ \zeta^T(\mathbf{s}_e|\mathbf{s}, t=0)\boldsymbol{\omega}(\mathbf{s}, t) \nabla^2 \psi \\ &+ 2\nabla(\zeta^T(\mathbf{s}_e|\mathbf{s}, t=0)\boldsymbol{\omega}(\mathbf{s}, t)) \cdot \nabla \psi + \nabla^2(\zeta^T(\mathbf{s}_e|\mathbf{s}, t=0)\boldsymbol{\omega}(\mathbf{s}, t)) \psi \} \end{aligned} \quad (2A.2)$$

Next, multiplying Eq. (2A.2) from the left side by  $\boldsymbol{\omega}(\mathbf{s}, t)\zeta(\mathbf{s}_e|\mathbf{s}, t=0)$  and integrating over the electronic coordinates yields the following equation:

$$\begin{aligned} i\hbar \frac{\partial \psi}{\partial t} &= -\frac{\hbar^2}{2m} \{ \nabla^2 \psi + 2\boldsymbol{\omega}^\dagger(\boldsymbol{\tau}\boldsymbol{\omega} + \nabla \boldsymbol{\omega}) \cdot \nabla \psi \\ &+ \boldsymbol{\omega}^\dagger(\boldsymbol{\tau}^{(2)}\boldsymbol{\omega} + 2\boldsymbol{\tau} \cdot \nabla + \nabla^2 \boldsymbol{\omega}) \psi \} \end{aligned} \quad (2A.3)$$

where  $\omega$  replaces  $\omega(s, t)$ ,  $\tau$  is the time-independent NACM introduced in Eq. (2.8a), and  $\tau^{(2)}$  is the time-independent NACM of the second order introduced in Eq. (2.8b). Replacing  $\tau^{(2)}$  (see Eq. (2.10)), we get

$$\begin{aligned} i\hbar \frac{\partial \psi}{\partial t} = & -\frac{\hbar^2}{2m} \{ \nabla^2 \psi + 2\omega^\dagger (\tau \omega + \nabla \omega) \cdot \nabla \psi \\ & + \omega^\dagger (\tau^2 \omega + \nabla \tau \omega + 2\tau \cdot \nabla \omega + \nabla^2 \omega) \psi \} \end{aligned} \quad (2A.4)$$

We now turn to Eq. (2.100) (and also Eq. (2.101))

$$i\hbar \frac{\partial \psi}{\partial t} = -\frac{\hbar^2}{2m} \{ \nabla^2 \psi + 2\tilde{\tau} \cdot \nabla \psi + (\nabla \tilde{\tau} + \tilde{\tau}^2) \psi \} \quad (2A.5)$$

and intend to prove that it is identical to Eq. (2A.4). Recalling Eq. (2.101), we note that what is left to prove is that the coefficients of  $\psi$  in Eqs. (2A.4) and (2A.5), namely

$$\nabla \tilde{\tau} + \tilde{\tau}^2 \quad \text{and} \quad \omega^\dagger (\tau^2 \omega + \nabla \tau \omega + 2\tau \cdot \nabla \omega + \nabla^2 \omega) \quad (2A.6)$$

are equal. For this sake we evaluate the first expression of Eq. (2A.6) and employ Eq. (2.101):

$$\begin{aligned} \nabla \tilde{\tau} + \tilde{\tau}^2 = & \nabla (\omega^\dagger \tau \omega + \omega^\dagger \nabla \omega) \\ & + (\omega^\dagger \tau \omega + \omega^\dagger \nabla \omega) (\omega^\dagger \tau \omega + \omega^\dagger \nabla \omega) \end{aligned} \quad (2A.7)$$

It is seen that the main obstacle for the expression of the r.h.s. of Eq. (2A.7) and the second expression in Eq. (2A.6) to become equal is the fact that in Eq. (2A.7) we encounter terms that contain  $\nabla \omega^\dagger$ , which is missing in the second expression of Eq. (2A.6). To overcome this difficulty, we recall that  $\omega$  is a unitary matrix [see Eq. (2.96)]. Consequently

$$\nabla (\omega^\dagger \omega) = (\nabla \omega^\dagger) \omega + \omega^\dagger \nabla \omega = 0 \quad (2A.8)$$

which allows us to express  $\nabla \omega^\dagger$  as follows:

$$\nabla \omega^\dagger = -\omega^\dagger (\nabla \omega) \omega^\dagger \quad (2A.9)$$

Evaluating the r.h.s. in Eq. (2A.7) and employing Eq. (2A.9) for the relevant expressions finally yields the verification that Eqs. (2A.4) and (2A.5) are equal.

## 2A.2 Analyticity of Adiabatic-to-Diabatic Transformation Matrix $\tilde{\mathbf{A}}$ in Timespace Configuration

In this section of the appendix we intend to derive the matrix  $\tau_t$  [introduced in Eqs. (2.104) and (2.105)], which will yield an analytic  $\tilde{\mathbf{A}}$  matrix in the configuration

timespace that (besides being differentiable with respect to all coordinates) has to satisfy the following condition [see Eq. (2.107)]:

$$i\hbar \frac{\partial}{\partial t} (\nabla \tilde{\mathbf{A}}) - \nabla \left( i\hbar \frac{\partial}{\partial t} \tilde{\mathbf{A}} \right) = \mathbf{0} \quad (2A.10)$$

From Eqs. (2.106) we can see that  $\tilde{\mathbf{A}}$  has to fulfill two first-order differential equations:

$$\nabla \tilde{\mathbf{A}} + \tilde{\tau} \tilde{\mathbf{A}} = \mathbf{0} \quad (2A.11)$$

$$i\hbar \frac{\partial \tilde{\mathbf{A}}}{\partial t} + \tau_t \tilde{\mathbf{A}} = \mathbf{0} \quad (2A.12)$$

Activating the grad operator on Eq. (2A.12), differentiating Eq. (2A.11) with respect to time  $t$  [and multiplying it by  $(i\hbar)$ ], subtracting the second from the first, and assuming Eq. (2A.10), we obtain the following expression that *has to be fulfilled*:

$$i\hbar \frac{\partial \tilde{\tau}}{\partial t} \tilde{\mathbf{A}} + \tilde{\tau} i\hbar \frac{\partial \tilde{\mathbf{A}}}{\partial t} - (\nabla \tau_t) \tilde{\mathbf{A}} - \tau_t \nabla \tilde{\mathbf{A}} = \mathbf{0} \quad (2A.13)$$

Replacing the various derivates of  $\tilde{\mathbf{A}}$ , employing Eqs. (2A.11) and (2A.12) yields

$$\left( i\hbar \frac{\partial \tilde{\tau}}{\partial t} - \tilde{\tau} \tau_t - \nabla \tau_t + \tau_t \tilde{\tau} \right) \tilde{\mathbf{A}} = \mathbf{0}$$

or since  $\tilde{\mathbf{A}}$  fulfills Eq. (2A.11), it is a unitary matrix and therefore the expression

$$i\hbar \frac{\partial \tilde{\tau}}{\partial t} - \tilde{\tau} \tau_t - \nabla \tau_t + \tau_t \tilde{\tau} = \mathbf{0} \quad (2A.14)$$

has to be fulfilled.

Employing Eq. (2.101), we evaluate the first term in Eq. (2A.14), namely

$$i\hbar \frac{\partial \tilde{\tau}}{\partial t} = i\hbar \left( \frac{\partial \omega^\dagger}{\partial t} \tau \omega + \omega^\dagger \tau \frac{\partial \omega}{\partial t} + \frac{\partial \omega^\dagger}{\partial t} \nabla \omega + \omega^\dagger \nabla \left( \frac{\partial \omega}{\partial t} \right) \right)$$

where we recall that by definition the  $\tau$  matrix is *time-independent*, and then continue by replacing the various time derivatives employing Eq. (2.91) so that we get

$$i\hbar \frac{\partial \tilde{\tau}}{\partial t} = -\omega^\dagger \tilde{\mathbf{H}}_e \tau \omega + \omega^\dagger \tau \tilde{\mathbf{H}}_e \omega + \omega^\dagger (\nabla \tilde{\mathbf{H}}_e) \omega \quad (2A.15)$$

The next step is to evaluate the expression  $\nabla(\omega \tilde{\mathbf{H}}_e \omega^\dagger)$  while recalling the unitarity of  $\omega$  [see Eq. (2.96)]. The unitarity leads to the relation

$$\nabla \omega^\dagger = -\omega^\dagger (\nabla \omega) \omega^\dagger$$

so that  $\nabla(\omega \tilde{\mathbf{H}}_e \omega^\dagger)$  becomes

$$\nabla(\omega^\dagger \tilde{\mathbf{H}}_e \omega) = -\omega^\dagger (\nabla \omega) \omega^\dagger \tilde{\mathbf{H}}_e \omega + \omega^\dagger (\nabla \tilde{\mathbf{H}}_e) \omega + \omega^\dagger \tilde{\mathbf{H}}_e \nabla \omega \quad (2A.16)$$

This expression is used to replace, in Eq. (2A.15), the term  $\omega (\nabla \tilde{\mathbf{H}}_e) \omega^\dagger$  so that Eq. (2A.15) becomes

$$\begin{aligned} i\hbar \frac{\partial \tilde{\boldsymbol{\tau}}}{\partial t} = & -\omega^\dagger \tilde{\mathbf{H}}_e \boldsymbol{\tau} \omega + \omega^\dagger \boldsymbol{\tau} \tilde{\mathbf{H}}_e \omega + \nabla \tilde{\mathbf{H}}_e \\ & + \omega^\dagger (\nabla \omega) \omega^\dagger \tilde{\mathbf{H}}_e \omega - \omega^\dagger \tilde{\mathbf{H}}_e \nabla \omega \end{aligned} \quad (2A.17)$$

To continue, we first introduce a new definition, namely,  $\tilde{\tilde{\mathbf{H}}}_e$ :

$$\tilde{\tilde{\mathbf{H}}}_e = \omega \tilde{\mathbf{H}}_e \omega^\dagger \quad (2A.18)$$

We then substitute Eqs. (2A.17) and (2A.18) in Eq. (2A.14) so that, by following a few algebraic rearrangement, we get

$$-\tilde{\tilde{\mathbf{H}}}_e \tilde{\boldsymbol{\tau}} + \tilde{\boldsymbol{\tau}} \tilde{\tilde{\mathbf{H}}}_e + \nabla \tilde{\tilde{\mathbf{H}}}_e - \tilde{\boldsymbol{\tau}} \boldsymbol{\tau}_t - \nabla \boldsymbol{\tau}_t + \boldsymbol{\tau}_t \tilde{\boldsymbol{\tau}} = \mathbf{0} \quad (2A.19)$$

We note that this expression becomes identically zero when  $\boldsymbol{\tau}_t \equiv \tilde{\tilde{\mathbf{H}}}_e$ .

## REFERENCES

### Section 2.1

1. M. Born and J. R. Oppenheimer, *Ann. Phys. (Leipzig)* **84**, 457 (1927).
2. M. Born, *Festschrift Goett. Nach. Math. Phys.* **K1**, 1 (1951).
3. M. Born and K. Huang, *Dynamical Theory of Crystal Lattices*, Oxford Univ. Press, New York, 1954, Chapter IV.
4. H. C. Longuet-Higgins, *Adv. Spectrosc.* **2**, 429 (1961).
5. M. Baer, *Chem. Phys. Lett.* **35**, 112 (1975).
6. W. D. Hobey and A. D. McLachlan, *J. Chem. Phys.* **33**, 1695 (1960).
7. M. Baer, in *Theory of Chemical Reaction Dynamics*, M. Baer, ed., CRC Press, Boca Raton, FL, 1985, Vol. II, Chapter 4.
8. F. T. Smith, *Phys. Rev.* **179**, 111 (1969).
9. T. Pacher, L. S. Cederbaum, and H. Köppel, *Adv. Chem. Phys.* **84**, 293 (1993).
10. W. Moffitt and A. D. Liehr, *Phys. Rev.* **106**, 1195 (1956).
11. A. D. McLachlan, *Molec. Phys.* **4**, 417 (1961).
12. W. Lichten, *Phys. Rev.* **131**, 229 (1963); *ibid.* **164**, 131 (1967).
13. C. J. Ballhausen and A. E. Hansen, *Ann. Rev. Phys. Chem.* **23**, 15 (1972).

14. M. Baer, *Phys. Rep.* **358**, 75 (2002).
15. M. Baer, T. Vértesi, G. J. Halász, Á Vibók, and S. Suhai, *Faraday Disc.* **127**, 337 (2004).
16. M. Baer, T. Vértesi, G. J. Halász, and Á Vibók, *J. Phys. Chem. A* **108**, 9134 (2004).
17. M. Baer, *Molec. Phys.* **40**, 1011 (1980).
18. R. Baer, *J. Chem. Phys.* **117**, 7405 (2002).
19. M. Baer and A. Alijah, *Chem. Phys. Lett.* **319**, 489 (2000).
20. M. Baer, S. H. Lin, A. Alijah, S. Adhikari, and G. D. Billing, *Phys. Rev. A* **62**, 032506-1 (2000).
21. G. J. Halász, Á Vibók, S. Suhai, and M. Baer, *J. Chem. Phys.* **122**, 134109-1 (2005).
22. P. McGuire and J. C. Bellum, *J. Chem. Phys.* **71**, 1975 (1979).
23. P. Halvick and D. G. Truhlar, *J. Chem. Phys.* **96**, 2895 (1992).
24. G. J. Tawa, S. L. Mielke, D. G. Truhlar, and D. W. Schwenke, *J. Chem. Phys.* **100**, 5751 (1994).
25. T. Suzuki, H. Katayanagi, S. Nanbu, and M. Aoyagi, *J. Chem. Phys.* **109**, 5778 (1998).
26. L.-C. Wang, *Chem. Phys.* **237**, 305 (1998).
27. M. Chajjia and R. D. Levine, *Phys. Chem. Chem. Phys.* **1**, 1205 (1999).
28. S. Adhikari and G. D. Billing, *J. Chem. Phys.* **111**, 40 (1999).
29. A. Alijah and E. E. Nikitin, *Molec. Phys.* **96**, 1399 (1999).
30. H. Köppel, *Faraday Disc.* **127**, 35 (2004).
31. T. Takayanagi, Y. Kurasaki, and A. Ichihara, *J. Chem. Phys.* **112**, 2615 (2000).
32. C. Shin and S. Shin, *J. Chem. Phys.* **113**, 6528 (2000).
33. T. Takayanagi and Y. Kurasaki, *J. Chem. Phys.* **113**, 7158 (2000).
34. G. Troisi and G. Orlandi, *J. Chem. Phys.* **118**, 5356 (2003).
35. A. Kuppermann and R. Abrol, *Adv. Chem. Phys.* **124**, 283 (2002).
36. R. Abrol and A. Kuppermann, *J. Chem. Phys.* **116**, 1035 (2002).
37. X. Chapuisat, A. Nauts, and D. Dehareug-Dao, *Chem. Phys. Lett.* **95**, 139 (1983).
38. D. Hehareug-Dao, X. Chapuisat, J. C. Lorquet, C. Galloy, and G. Raseev, *J. Chem. Phys.* **78**, 1246 (1983).
39. P. Barragan, L. F. Errea, A. Macias, L. Mendez, I. Rabadan, A. Riera, J. M. Lucas, and A. Aguilar, *J. Chem. Phys.* **121**, 11629 (2004).
40. H. J. Werner, B. Follmeg, and M. H. Alexander, *J. Chem. Phys.* **91**, 5425 (1989).
41. R. G. Sadygov and D. R. Yarkony, *J. Chem. Phys.* **109**, 20 (1998).
42. T. G. Heil, S. E. Butler, and A. Dalgarno, *Phys. Rev. A* **23**, 1100 (1981).
43. A. Thiel and H. Köppel, *J. Chem. Phys.* **110**, 9371 (1999).
44. A. Macias and A. Riera, *J. Phys. B* **11**, L489 (1978).
45. A. Macias and A. Riera, *Int. J. Quant. Chem.* **17**, 181 (1980).
46. E. S. Kryachko, *J. Phys. Chem. A* **103**, 4368 (1999).
47. E. S. Kryachko, *Adv. Quant. Chem.* **44**, 119 (2003).
48. H. J. Werner and W. Meyer, *J. Chem. Phys.* **74**, 5802 (1981).
49. C. Petrongolo, G. Hirsch, and R. Buenker, *Molec. Phys.*, **70**, 825 (1990).

50. C. Petrongolo, G. Hirsch, and R. Buenker, *Molec. Phys.* **70**, 835 (1990).
51. F. Rebentrost and W. A. Lester, *J. Chem. Phys.* **64**, 3879 (1976).
52. F. Rebentrost, in *Theoretical Chemistry: Advances and Perspectives*, D. Henderson and H. Eyring, eds., Academic Press, 1981, Vol. II, p. 32.
53. T. Romero, A. Aguilar, and F. X. Gadea, *J. Chem. Phys.* **110**, 6219 (1999).
54. V. Sidis, *Adv. Chem. Phys.* **82**, 73 (1992).
55. W. Domcke and G. Stock, *Adv. Chem. Phys.* **100**, 1 (1997).
56. C. C. Marston, K. Weide, R. Schinke, and H. U. Suter, *J. Chem. Phys.* **98**, 4718 (1993).
57. B. Heumann, K. Weide, R. Duren, and R. Schinke, *J. Chem. Phys.* **98**, 5508 (1993).
58. A. J. Dobbyn and P. J. Knowles, *Molec. Phys.* **110**, 91 (1997).
59. T. Pacher, L. S. Cederbaum, and H. Köppel, *Adv. Chem. Phys.* **84**, 293 (1993).
60. T. Pacher, L. S. Cederbaum, and H. Köppel, *J. Chem. Phys.* **89**, 7367 (1988).
61. M. B. Sevryuk, L. Y. Rusin, S. Cavalli, and V. Aquilanti, *J. Phys. Chem. A* **108**, 8731 (2004).
62. H. Klar and U. Fano, *Phys. Rev. Lett.* **37**, 1132 (1976).
63. I. Ryb and R. Baer, *J. Chem. Phys.* **121**, 10370 (2004).

## Section 2.2

1. J. D. Jackson, *Classical Electrodynamics*, 2nd ed., Wiley, New York, 1998, Chapter 6.
2. R. Baer, private communication.
3. Y. Aharonov, E. Ben-Reuven, S. Popescu, and D. Rohrlich, *Nucl. Phys. B* **350**, 818 (1991).
4. T. Pacher, L. S. Cederbaum, and H. Köppel, *Adv. Chem. Phys.* **84**, 293 (1993).
5. M. Baer, *Chem. Phys. Lett.* **349**, 84 (2001).
6. R. Englman and A. Yahalom, *Acta Univ. Debreceniensis (Series Physica et Chimica)* **34–35**, 283 (2002).
7. M. Baer, *Adv. Chem. Phys.* **124**, 39 (2002).
8. T. Vértesi, Á. Vibók, G. J. Halász, and M. Baer, *J. Chem. Phys.* **121**, 4000 (2004).

## Section 2.3

1. M. Baer, *J. Phys. Chem.* **107**, 4724 (2003).
2. P. A. M. Dirac, *The Principles of Quantum Mechanics*, Clarendon Press, Oxford, 1958. Section 27.
3. R. Baer, D. J. Kouri, M. Baer, and D. K. Hoffman, *J. Chem. Phys.* **119**, 6988 (2003).
4. M. E. Peskin and D. V. Schroeder, *An Introduction to Quantum Field Theory*, Preseus Books, Cambridge, MA, 1995, p. 78.
5. D. J. Tannor and S. A. Rice, *J. Chem. Phys.* **83**, 5013 (1985).
6. P. Brumer and M. Shapiro, *Chem. Phys. Lett.* **126**, 541 (1986).
7. S. Shi and H. Rabitz, *J. Chem. Phys.* **92**, 364 (1990).
8. D. Hammerich, R. Kosloff, and M. A. Ratner, *J. Chem. Phys.* **97**, 6410 (1992).

9. R. Baer and R. Kosloff, *J. Phys. Chem. A* **99**, 2534 (1995).
10. D. Barash, A. E. Orel, and R. Baer, *Phys. Rev. A* **61**, 3402 (2000).
11. P. Brumer and M. Shapiro, *Coherent Control of Atomic and Molecular Processes*, Wiley, New York, 2003.
12. G. Balint-Kurti, F. R. Mambay, Q. Ren, M. Artamonov, T.-S. Ho, and H. Rabitz, *J. Chem. Phys.* **122**, 084110 (2005).

# CHAPTER 3

---

## MODEL STUDIES

---

In this chapter we discuss a few interesting cases that are expected to extend our knowledge regarding the material presented in Chapters 1 and 2. In Section 3.1 we concentrate on a certain type of model for the  $\tau$  matrix related to Hilbert spaces of various dimensions. In Section 3.2 we discuss mainly the two-state *diabatic* potential matrix elements and their ability to form NACTs with interesting features. In Section 3.3 we show to what extent certain types of ADT matrices are related to Wigner's rotation matrices.

### 3.1 TREATMENT OF ANALYTICAL MODELS

The issues to be discussed are the ADT matrix,  $\mathbf{A}(\mathbf{s}|\Gamma)$  ( $\equiv \tilde{\mathbf{A}}(\mathbf{s}|\Gamma)$ ) as presented in Eq. (2.29) and the topological matrix  $\mathbf{D}(\Gamma)$  as presented in Eq. (2.32) [see also Eq. (2.33)]. For this purpose we consider  $\tau$  matrices presented as a product of a real function (vector)  $\lambda(\mathbf{s})$  that depends on the (nuclear) coordinates and a constant (real) matrix  $\mathbf{g}$  of the required dimension:<sup>1–3</sup>

$$\tau(\mathbf{s}) = \mathbf{g}\lambda(\mathbf{s}) \quad (3.1)$$

The main advantage in having this presentation for the  $\tau$  matrix is the fact that all the derivations can be carried out analytically.

### 3.1.1 Two-State Systems

#### 3.1.1.1 Adiabatic-to-Diabatic Transformation Matrix

The two-state model is in fact *not* a model at all—it is the general case per se. The reason is that the most *general*  $2 \times 2$   $\tau$  matrix is written in the following form:

$$\boldsymbol{\tau}(\mathbf{s}) = \begin{pmatrix} 0 & \tau_{12}(\mathbf{s}) \\ -\tau_{12}(\mathbf{s}) & 0 \end{pmatrix} \quad (3.2)$$

In other words, the general,  $2 \times 2$ ,  $\tau$  matrix contains only one single nonzero (vectorial) term,  $\tau_{12}$ . It is seen that the  $\mathbf{g}$  matrix in this case is

$$\mathbf{g} = \begin{pmatrix} 0 & 1 \\ -1 & 0 \end{pmatrix} \quad (3.3)$$

and therefore  $\lambda(\mathbf{s}) \equiv \tau_{12}(\mathbf{s})$ .

Our task is to derive the corresponding ADT matrix  $\mathbf{A}$ , and this is done in two ways:

1. Since  $\mathbf{A}$  has to be a real *orthogonal* matrix of dimension  $2 \times 2$ , it can be presented in the form

$$\mathbf{A}(\mathbf{s}) = \begin{pmatrix} \cos \gamma(\mathbf{s}) & \sin \gamma(\mathbf{s}) \\ -\sin \gamma(\mathbf{s}) & \cos \gamma(\mathbf{s}) \end{pmatrix} \quad (3.4)$$

where  $\gamma(\mathbf{s})$  is the angle to be determined. Substituting Eq. (3.4) in Eq. (1.50) yields the first-order differential equation for  $\gamma(\mathbf{s})$  in the form

$$\nabla \gamma(\mathbf{s}) + \tau_{12}(\mathbf{s}) = \mathbf{0} \quad (3.5a)$$

or

$$\nabla \gamma(\mathbf{s}) + \lambda(\mathbf{s}) = \mathbf{0} \quad (3.5b)$$

which has to be solved along a given contour  $\Gamma$ . The solution is

$$\gamma(\mathbf{s}|\mathbf{s}_0|\Gamma) = - \int_{\mathbf{s}_0}^{\mathbf{s}} d\mathbf{s} \cdot \lambda(\mathbf{s}|\Gamma) \quad (3.6)$$

where we assumed that  $\gamma(\mathbf{s}_0) \equiv 0$ . In what follows  $\gamma(\mathbf{s})$  is defined as the *adiabatic-to-diabatic transformation* (ADT) angle.

2. We employ the general solution of the differential equation as given in Eq. (1.85) [see also Eq. (1.91)]. For this purpose we have to derive the matrix  $\mathbf{G}$  that diagonalizes the  $\mathbf{g}$  matrix given in (3.3):

$$\mathbf{G} = \frac{1}{\sqrt{2}} \begin{pmatrix} 1 & 1 \\ i & -i \end{pmatrix} \quad (3.7)$$

The corresponding (two) eigenvalues are  $t_{1,2}(\mathbf{s}) = \pm i$ . Recalling that in the present case the matrix  $\mathbf{G}$  is a constant matrix, the expression in Eq. (1.91) simplifies to become

$$\mathbf{A}(\mathbf{s}) = \mathbf{G}\mathbf{E}(\mathbf{s})\mathbf{G}^\dagger \quad (3.8)$$

where the two diagonal elements of the  $\mathbf{E}$  matrix are

$$E_{1,2}(\mathbf{s}) = \exp \left( \pm i \int_{\mathbf{s}_0}^{\mathbf{s}} \boldsymbol{\lambda}(\mathbf{s}') \cdot d\mathbf{s}' \right) \quad (3.9)$$

Performing the two matrix multiplications in Eq. (3.8) yields  $\mathbf{A}(\mathbf{s}) \equiv \mathbf{A}(\gamma(\mathbf{s}))$  as given in Eq. (3.4), where  $\gamma(\mathbf{s})$  is as defined in Eq. (3.6).

### 3.1.1.2 Topological ( $\mathbf{D}$ ) Matrix

Closing the contour in Eq. (3.6) yields the angle  $\alpha(\Gamma)$

$$\gamma(\mathbf{s}_0 | \mathbf{s}_0 | \Gamma) = \alpha(\Gamma) = \oint_{\Gamma} d\mathbf{s} \cdot \boldsymbol{\lambda}(\mathbf{s} | \Gamma) \quad (3.10)$$

which, on replacing  $\gamma(\mathbf{s})$  by  $\alpha(\Gamma)$  in Eq. (3.4) yields the corresponding  $\mathbf{D}$  matrix:

$$\mathbf{D}(\Gamma) = \begin{pmatrix} \cos \alpha(\Gamma) & \sin \alpha(\Gamma) \\ -\sin \alpha(\Gamma) & \cos \alpha(\Gamma) \end{pmatrix} \quad (3.11)$$

However, according to Eq. (2.33) the  $\mathbf{D}$  matrix has to be diagonal, and this enforces  $\alpha(\Gamma)$  [see Eq. (3.10)] to be an integer multiple of  $\pi$ . Thus

$$\alpha(\Gamma) = \oint_{\Gamma} d\mathbf{s} \cdot \boldsymbol{\lambda}(\mathbf{s}) = n\pi \quad (3.12)$$

where  $n$  is an integer. In case  $n$  is an even number, Eq. (3.12) is essentially the Bohr–Sommerfeld quantization condition for the (spatial) angular momentum of the electron in a given closed system.<sup>4</sup> But in our case  $n$  is also allowed to be an odd number; in particular,  $n$  may become 1. In this case the quantization condition is more reminiscent of the spin of the electron (this subject is discussed further in Section (5.4)).

It is noted that if  $n$  is an odd integer, the diagonal of the  $\mathbf{D}$  matrix contains two  $(-1)$ s, which means that the two (diagonal) elements of the ADT matrix that at the initial point are equal to  $(+1)$  become, following the integration along the closed contour  $\Gamma$ , equal to  $(-1)$ . Recalling Eq. (2.31'), this change of sign implies that the two electronic eigenfunctions  $\zeta_j(\mathbf{s}_e|\mathbf{s}); j = 1, 2$ , flip their signs while tracing this particular closed contour  $\Gamma$ . In other words, starting at  $\mathbf{s} = \mathbf{s}_0$  with the values  $\zeta_j(\mathbf{s}_e|\mathbf{s}_0); j = 1, 2$ , the corresponding  $\zeta_j(\mathbf{s}_e|\mathbf{s})$  function becomes  $(-\zeta_j(\mathbf{s}_e|\mathbf{s}_0))$  after returning to the initial point.

In case the value of  $n$  [in Eq. (3.12)] is an even integer, the diagonal of the  $\mathbf{D}$  matrix contains two  $(+1)$ s, which implies that in this case none of the elements of the ADT matrix flip sign at the endpoint of  $\Gamma$ . Recalling, again, Eq. (2.30), this situation implies that the abovementioned  $\zeta(\mathbf{s}_e|\mathbf{s})$  manifold traces the closed contour and returns to its original value; namely,  $\zeta(\mathbf{s}_e|\mathbf{s} = \mathbf{s}_0|\Gamma)$  functions are unchanged.

The two possible outcomes for the  $\mathbf{D}$  matrix imply that in general we encounter two kinds of contours. In case the  $\mathbf{D}$  matrix is not the unit matrix, this implies that within the region surrounded by the contour there is at least one point where the function  $\tau(\mathbf{s})$  is not defined and therefore the eigenfunctions are multivalued in that region. In case the  $\mathbf{D}$  matrix is the unit matrix, the situation is not clear because the eigenfunctions may or may not be singlevalued in such a case. In case there are no problematic points in the region surrounded by the contour, the eigenfunctions are singlevalued in that particular region. However, in case there is an even number of such points, the eigenfunctions are multivalued although  $n$  is even. The discussion related to these issues is extended in Sections 5.3.1 and 5.3.3.

In principle we could have a situation where one of the diagonal elements is  $(+1)$  and one  $(-1)$ , but from the structure of the  $\mathbf{D}$  matrix one can see that this case can never occur.

### 3.1.1.3 The Diabatic Potential Matrix

The final issue in this section is the diabatic potential matrix  $\mathbf{W}$  as given by Eq. (2.39). Employing the  $\mathbf{A}$  matrix in Eq. (3.4) and recalling that  $\mathbf{u}$  is a  $2 \times 2$  diagonal matrix, we get the following elements for  $\mathbf{W}$ :

$$\begin{aligned} W_{11}(\mathbf{s}) &= \cos^2 \gamma(\mathbf{s}) u_1 + \sin^2 \gamma(\mathbf{s}) u_2 \\ W_{22}(\mathbf{s}) &= \sin^2 \gamma(\mathbf{s}) u_1 + \cos^2 \gamma(\mathbf{s}) u_2 \\ W_{12}(\mathbf{s}) &= \cos \gamma(\mathbf{s}) \sin \gamma(\mathbf{s}) (u_1 - u_2) \end{aligned} \quad (3.13)$$

In Corollary 2.1 it was proved that in order for the  $\mathbf{W}$  matrix to be singlevalued, the  $\mathbf{D}$  matrix has to be diagonal. In the previous section we showed that in order for this matrix to be diagonal, the value of  $\gamma(\mathbf{s})$  for a closed contour [when it becomes  $\alpha(\Gamma)$ ] has to be an integer multiple of  $\pi$  [see Eq. (3.12)]. Indeed, from Eq. (3.13) it can be seen immediately that the three matrix elements  $W_{ij}(\mathbf{s}); i, j = 1, 2$  at the initial point and at the endpoint (which is identical to the initial point) are equal if and only if this angle  $\alpha(\Gamma)$  ( $\equiv \gamma(\mathbf{s}_0|\mathbf{s}_0)$ ) is an integer multiple  $\pi$ .

**Short Summary** The fact that the NACT of the two-state system is quantized in a given region in configuration space guarantees that the  $2 \times 2$  diabatic potential matrix is *singlevalued* in this region.

### 3.1.2 Three-State Systems

#### 3.1.2.1 Adiabatic-to-Diabatic Transformation Matrix

The relevant  $3 \times 3$   $\mathbf{g}$  matrix is given in the form<sup>1-3</sup>

$$\mathbf{g} = \begin{pmatrix} 0 & 1 & 0 \\ -1 & 0 & \eta \\ 0 & -\eta & 0 \end{pmatrix} \quad (3.14)$$

where  $\eta$  is a parameter. The eigenvalues of the  $\mathbf{g}$  matrix are

$$t_{1,2} = \pm i\omega, \quad t_3 = 0; \quad \omega = \sqrt{1 + \eta^2} \quad (3.15)$$

and the corresponding matrix,  $\mathbf{G}$ , that diagonalizes it is

$$\mathbf{G} = \frac{1}{\omega\sqrt{2}} \begin{pmatrix} 1 & 1 & \eta\sqrt{2} \\ i\omega & -i\omega & 0 \\ -\eta & -\eta & \sqrt{2} \end{pmatrix} \quad (3.16)$$

Recalling Eq. (3.8), where the corresponding three diagonal elements of the  $\mathbf{E}$  matrix are

$$E_{1,2}(\mathbf{s}) = \exp(\pm i\omega\gamma(\mathbf{s})); \quad E_3(\mathbf{s}) = 1 \quad (3.17)$$

we get for  $\mathbf{A}$  the following matrix

$$\mathbf{A}(\mathbf{s}) = \omega^{-2} \begin{pmatrix} \eta^2 + C(\mathbf{s}) & \omega S(\mathbf{s}) & \eta(1 - C(\mathbf{s})) \\ \omega S(\mathbf{s}) & \omega^2 C(\mathbf{s}) & -\eta\omega S(\mathbf{s}) \\ \eta(1 - C(\mathbf{s})) & \eta\omega S(\mathbf{s}) & 1 + \eta^2 C(\mathbf{s}) \end{pmatrix} \quad (3.18)$$

where

$$C(\mathbf{s}) = \cos(\omega\gamma(\mathbf{s})); \quad S(\mathbf{s}) = \sin(\omega\gamma(\mathbf{s})) \quad (3.19)$$

and  $\gamma(\mathbf{s})$  is as given in Eq. (3.6).

### 3.1.2.2 Topological Matrix

Having the  $\mathbf{A}$  matrix, we can present the corresponding topological  $\mathbf{D}$  matrix

$$\mathbf{D}(\Gamma) = \omega^{-2} \begin{pmatrix} \eta^2 + C(\Gamma) & \omega S(\Gamma) & \eta(1 - C(\Gamma)) \\ \omega S(\Gamma) & \omega^2 C(\Gamma) & -\eta \omega S(\Gamma) \\ \eta(1 - C(\Gamma)) & \eta \omega S(\Gamma) & 1 + \eta^2 C(\Gamma) \end{pmatrix} \quad (3.20)$$

where

$$C(\Gamma) = \cos(\omega\alpha(\Gamma)); \quad S(\Gamma) = \sin(\omega\alpha(\Gamma)) \quad (3.21)$$

and  $\alpha(\Gamma)$  is as given in Eq. (3.10). We recall that the  $\mathbf{D}$  matrix has to be diagonal and in order for that to happen,  $\alpha(\Gamma)$  has to fulfill the condition

$$\omega\alpha(\Gamma) = \sqrt{1 + \eta^2}\alpha(\Gamma) = 2\pi n \Rightarrow \alpha(\Gamma) = 2\pi n/\omega \quad (3.22)$$

where  $n$  is an integer. Once this condition is fulfilled, it is noted that the  $\mathbf{D}$  matrix becomes a *unit* matrix because all three diagonal matrix elements are equal to +1.

In case  $\lambda(s)$  is chosen in such a way that it fulfills the equation

$$\alpha(\Gamma) = \oint_{\Gamma} ds \cdot \lambda(s) = \pi \quad (3.23)$$

we find that the condition to be fulfilled by  $\eta$  is

$$\eta = \sqrt{4n^2 - 1} \quad (3.24)$$

where, as we recall,  $n$  is an integer.

**Short Summary** For this particular type of  $3 \times 3$   $\tau$  matrix, the quantization takes place if and only if  $\eta$  and  $\lambda(s)$  fulfill the condition given in Eq. (3.22). It is interesting to mention that the resulting  $\mathbf{D}$  matrix is always a *unit* matrix that yields information regarding the way the three states are coupled. This type of coupling is discussed in Section 5.3.4.

### 3.1.3 Four-State Systems

#### 3.1.3.1 Adiabatic-to-Diabatic Transformation Matrix

The relevant  $4 \times 4$   $\mathbf{g}$  matrix in this case takes the form<sup>3</sup>

$$\mathbf{g} = \begin{pmatrix} 0 & 1 & 0 & 0 \\ -1 & 0 & \eta & 0 \\ 0 & -\eta & 0 & \sigma \\ 0 & 0 & -\sigma & 0 \end{pmatrix} \quad (3.25)$$

where  $\eta$  and  $\sigma$  are the two relevant parameters. The matrix  $\mathbf{G}$  that diagonalizes  $\mathbf{g}$  is

$$\mathbf{G} = \frac{1}{\sqrt{2}} \begin{pmatrix} i\lambda_q & i\lambda_q & -i\lambda_p & -i\lambda_p \\ p\lambda_q & -p\lambda_q & -q\lambda_p & q\lambda_p \\ i\lambda_p & i\lambda_p & i\lambda_q & i\lambda_q \\ q\lambda_p & -q\lambda_p & p\lambda_q & -p\lambda_q \end{pmatrix} \quad (3.26)$$

where  $\lambda_p$  and  $\lambda_q$  are constants given in the form

$$\lambda_p = \sqrt{\frac{p^2 - 1}{p^2 - q^2}}; \quad \lambda_q = \sqrt{\frac{1 - q^2}{p^2 - q^2}} \quad (3.27)$$

Here  $p$  and  $q$  are defined as

$$\begin{aligned} p &= \frac{1}{\sqrt{2}} \left( \omega^2 + \sqrt{\omega^4 - 4\sigma^2} \right)^{1/2} \\ q &= \frac{1}{\sqrt{2}} \left( \omega^2 - \sqrt{\omega^4 - 4\sigma^2} \right)^{1/2} \end{aligned} \quad (3.28)$$

with  $\omega$  given as

$$\omega = \sqrt{(1 + \eta^2 + \sigma^2)} \quad (3.29)$$

The corresponding four eigenvalues of  $\mathbf{g}$  are

$$t_{1,2} = \pm ip, \quad t_{3,4} = \pm iq \quad (3.30)$$

Employing Eq. (3.8) where the corresponding four *diagonal* elements of the  $\mathbf{E}$  matrix are

$$\begin{aligned} E_{1,2}(\mathbf{s}) &= \exp(\pm ip\gamma(\mathbf{s})) \\ E_{3,4}(\mathbf{s}) &= \exp(\pm iq\gamma(\mathbf{s})) \end{aligned} \quad (3.30')$$

we find the following expressions for the 16 **A**-matrix elements

$$\begin{aligned}
 \mathbf{A}_{11}(\mathbf{s}) &= \lambda_q^2 C_p + \lambda_p^2 C_q; & \mathbf{A}_{12}(\mathbf{s}) &= p \lambda_q^2 S_p + q \lambda_p^2 S_q \\
 \mathbf{A}_{13}(\mathbf{s}) &= \lambda_p \lambda_q (-C_p + C_q); & \mathbf{A}_{14}(\mathbf{s}) &= \lambda_p \lambda_q (-q S_p + p S_q) \\
 \mathbf{A}_{22}(\mathbf{s}) &= p^2 \lambda_q^2 C_p + q^2 \lambda_p^2 C_q; & \mathbf{A}_{23}(\mathbf{s}) &= \lambda_p \lambda_q (p S_p - q S_q) \\
 \mathbf{A}_{24}(\mathbf{s}) &= p q \lambda_p \lambda_q (C_p - C_q); & \mathbf{A}_{33}(\mathbf{s}) &= (\lambda_p^2 C_p + \lambda_q^2 C_q) \\
 \mathbf{A}_{34}(\mathbf{s}) &= -(q \lambda_p^2 S_p + p \lambda_q^2 S_q); & \mathbf{A}_{44}(\mathbf{s}) &= q^2 \lambda_p^2 C_p + p^2 \lambda_q^2 C_q \\
 \mathbf{A}_{21}(\mathbf{s}) &= -\mathbf{A}_{12}(\mathbf{s}); & \mathbf{A}_{31}(\mathbf{s}) &= \mathbf{A}_{13}(\mathbf{s}); & \mathbf{A}_{32}(\mathbf{s}) &= -\mathbf{A}_{23}(\mathbf{s}) \\
 \mathbf{A}_{41}(\mathbf{s}) &= -\mathbf{A}_{14}(\mathbf{s}); & \mathbf{A}_{42}(\mathbf{s}) &= \mathbf{A}_{24}(\mathbf{s}); & \mathbf{A}_{43}(\mathbf{s}) &= -\mathbf{A}_{34}(\mathbf{s})
 \end{aligned} \tag{3.31}$$

where

$$C_p = C_p(\mathbf{s}) = \cos(p\gamma(\mathbf{s})); \quad S_p = S_p(\mathbf{s}) = \sin(p\gamma(\mathbf{s})) \tag{3.32}$$

and similar expressions for  $C_q$  and  $S_q$ . The angle  $\gamma(\mathbf{s})$  is presented in Eq. (3.6).

### 3.1.3.2 Topological Matrix

As will be seen next, the four-state case is not just another case in this series because we encounter here more interesting laws of quantization.

We do not present the corresponding topological **D** matrix as it is identical to the **A** matrix given in Eq. (3.31) with the relevant  $C_p$ ,  $S_p$ ,  $C_q$ , and  $S_q$  functions having slightly different expressions, namely

$$\begin{aligned}
 C_p &= C_p(\Gamma) = \cos(p\alpha(\Gamma)); & S_p &= S_p(\Gamma) = \sin(p\alpha(\Gamma)) \\
 C_q &= C_q(\Gamma) = \cos(q\alpha(\Gamma)); & S_q &= S_q(\Gamma) = \sin(q\alpha(\Gamma))
 \end{aligned} \tag{3.33}$$

where  $\alpha(\Gamma)$  is as given in (3.10). Next are discussed the conditions for which the relevant **D** matrix becomes diagonal. This happens if and only if  $p$  and  $q$  fulfill the following relations

$$p\alpha = p \oint_{\Gamma} \mathbf{ds} \cdot \boldsymbol{\lambda}(\mathbf{s}) = 2\pi n \tag{3.34a}$$

$$q\alpha = q \oint_{\Gamma} \mathbf{ds} \cdot \boldsymbol{\lambda}(\mathbf{s}) = 2\pi \ell \tag{3.34b}$$

where  $n$  and  $\ell$ , defined in the range  $n, \ell \geq 0$ , are allowed to be either integers or half-integers but  $m (= n - \ell)$  can attain only *integer* values. Since  $p > q$  see [Eq. (3.28)] this implies that  $n > \ell$  and therefore  $m > 0$ . Again choosing  $\boldsymbol{\lambda}(\mathbf{s})$  to fulfill Eq. (3.23) yields  $(p, q) = (2n, 2\ell)$  for  $p$  and  $q$ .

The difference between the case where  $n$  and  $\ell$  are integers and the case where both are half-integers is as follows. Examining the expressions for the elements of the **D** matrix we note that in the first case all diagonal elements of **D** are (+1), so that **D** is, in fact, the unit matrix. In the second case it can be seen that all four diagonal

elements are  $(-1)$ , so that the  $\mathbf{D}$  matrix is the unit matrix multiplied by  $(-1)$ . These two situations are addressed later in Section 5.3.3 [see in particular Eq. (5.21c)].

Since  $p$  and  $q$  are directly related to the NACTs  $\eta$  and  $\sigma$  [see Eqs. (3.28) and (3.29)], the two conditions in Eqs. (3.34) imply, again, “quantization” conditions for the values of the  $\tau$ -matrix elements, namely, for  $\eta$  and  $\sigma$ , once  $\lambda(\mathbf{s})$  (or  $\alpha$ ) is given.

It is interesting to note that this is the first time in the present framework that quantization is formed by *two* quantum numbers. This case is reminiscent of the two quantum numbers that characterize, for instance, the hydrogen atom.

**Short Summary** In this special  $4 \times 4$   $\tau$  matrix the quantization takes place if and only if  $\eta$ ,  $\sigma$ , and  $\lambda(\mathbf{s})$  fulfill the condition given in Eq. (3.34). It is interesting to mention that the resulting  $\mathbf{D}$  matrix is always either the unit matrix or the unit matrix multiplied by  $(-1)$ . These two possibilities yield information regarding the way the four states are coupled with each other as is discussed in Section 5.3.3.

### 3.1.4 Comments Related to General Case

In Sections 3.1.1–3.1.3 we treat a particular group of  $\tau$  matrices (constructed for corresponding Hilbert spaces) as presented in Eq. (3.1), where  $g$  is a constant anti-symmetric matrix and  $\lambda(\mathbf{s})$  is a vector. The general theory demands that the matrix  $\mathbf{D}$  as presented in Eq. (2.33) be diagonal and that, as such, it contain  $(\pm 1)$ s in its diagonal. In the three examples that were just discussed, we found that the corresponding  $\mathbf{D}$  matrix contains either  $(+1)$ s or  $(-1)$ s in its diagonal but never a mixture of the two. In other words, the  $\mathbf{D}$  matrix for this type of model can be represented in the following way

$$\mathbf{D}(\Gamma) = (-1)^k \mathbf{I} \quad (3.35)$$

where  $k$  is either even or odd and  $\mathbf{I}$  is the unit matrix. Indeed, for the two-state case  $k$  was found to be either odd or even, for the three-state case it was found to be only *even*, and for the four-state case it was found, again, to be either odd or even. Assuming that this pattern continues (viz., the various  $\mathbf{D}$  matrices have a fix sign throughout their diagonal), the following conclusions can be drawn:

1. In case the dimension of  $\tau$  is an odd number, the  $\mathbf{D}$  matrix is always the unit matrix. The reason is that an odd antisymmetric matrix has, at least, one eigenvalue that is zero. The matrix  $\tau$  is such a matrix, and therefore it can be shown that the  $\mathbf{D}$  matrix has to have at least one diagonal term that is  $+1$ . Since all the diagonal terms are expected to have identical signs, this implies that the  $\mathbf{D}$  matrix has to be the unit matrix and therefore  $k$ , in Eq. (3.35), is an even number
2. In case the dimension of the  $\tau$  matrix is an even number, no restrictions are known to exist for the signs of the  $\mathbf{D}$ -matrix elements, which implies that  $\mathbf{D}$  is either  $\mathbf{I}$  or  $(-\mathbf{I})$ .
3. These two facts, based on our findings in Sections 3.1.1–3.1.3, imply that in case of an odd dimension, “quantization” is characterized by integers only [see Eq. (3.22)]

but in case of an even dimension it is characterized either by integers or half-integers [see Eqs. (3.12) and (3.34)].

## 3.2 STUDY OF $2 \times 2$ DIABATIC POTENTIAL MATRIX AND RELATED TOPICS

### 3.2.1 Treatment of General Case

The models to be discussed in this section are  $2 \times 2$  *diabatic* potential matrices of the following type:

$$\tilde{\mathbf{V}}(\mathbf{s}) = \begin{pmatrix} v_1(\mathbf{s}) & v(\mathbf{s}) \\ v(\mathbf{s}) & v_2(\mathbf{s}) \end{pmatrix} \quad (3.36)$$

These matrices have to be symmetric in order to guarantee unitarity of the  $\mathbf{S}$  matrix needed for the calculation of scattering and spectroscopic cross sections.<sup>1</sup> In order to simplify the forthcoming algebra, we introduce two new variables:

$$\begin{aligned} \tilde{v}(\mathbf{s}) &= \frac{1}{2} (v_1(\mathbf{s}) + v_2(\mathbf{s})) \\ w(\mathbf{s}) &= \frac{1}{2} (v_1(\mathbf{s}) - v_2(\mathbf{s})) \end{aligned} \quad (3.37)$$

The potential matrix  $\tilde{\mathbf{V}}(\mathbf{s})$  is written in the form

$$\tilde{\mathbf{V}}(\mathbf{s}) = \mathbf{V}_d(\mathbf{s}) + \mathbf{V}(\mathbf{s}) \quad (3.38)$$

where  $\mathbf{V}_d(\mathbf{s})$  is a diagonal matrix of the form  $\tilde{v}(\mathbf{s}) \mathbf{I}$  ( $\mathbf{I}$  is the unit matrix) and  $\mathbf{V}(\mathbf{s})$  is the resulting (diabatic) matrix

$$\mathbf{V}(\mathbf{s}) = \begin{pmatrix} w(\mathbf{s}) & v(\mathbf{s}) \\ v(\mathbf{s}) & -w(\mathbf{s}) \end{pmatrix} \quad (3.39)$$

which is the main issue of the present section.

We consider Eq. (2.17) and rewrite the general element of the *diabatic* potential matrix:

$$\tilde{\mathbf{V}}_{jk}(\mathbf{s} | \mathbf{s}_0) = \langle \zeta_j(\mathbf{s}_e | \mathbf{s}_0) | \mathbf{H}_c(\mathbf{s}_e | \mathbf{s}) | \zeta_k(\mathbf{s}_e | \mathbf{s}_0) \rangle \quad (3.40)$$

Next, following Eq. (2.23), we rewrite it in a somewhat modified way:

$$\zeta(\mathbf{s}_e | \mathbf{s}_0) = \mathbf{A}^\dagger(\mathbf{s}) \zeta(\mathbf{s}_e | \mathbf{s}) \quad (3.41)$$

Substituting Eq. (3.41) in Eq. (3.40) and recalling that  $\zeta(\mathbf{s}_e|\mathbf{s})$  contains the eigenfunctions of  $\mathbf{H}_e(\mathbf{s}_e|\mathbf{s})$ , we get for  $\tilde{\mathbf{V}}(\mathbf{s})$  the following outcome:

$$\tilde{\mathbf{V}} = \mathbf{A}^\dagger \mathbf{u} \mathbf{A} \quad (3.42)$$

Here  $\mathbf{u}(\mathbf{s})$  is a *diagonal* matrix that contains the *adiabatic* potentials, and Eq. (3.42) implies that  $\mathbf{A}(\mathbf{s})$  diagonalizes  $\tilde{\mathbf{V}}(\mathbf{s})$  and consequently also diagonalizes  $\mathbf{V}(\mathbf{s})$  [introduced in Eqs. 3.38 and (3.39)] because

$$\mathbf{u} - \mathbf{V}_d = \tilde{\mathbf{u}} = \mathbf{A}^\dagger \mathbf{V} \mathbf{A} \quad (3.43)$$

Here  $\tilde{\mathbf{u}}(\mathbf{s})$ , just like  $\mathbf{u}(\mathbf{s})$ , is a diagonal matrix. Since  $\mathbf{A}(\mathbf{s})$  is an orthogonal matrix, it can be written as in Eq. (3.4). Following Eq. (3.41), the two electronic eigenfunctions ( $|\zeta_1(\mathbf{s})\rangle, |\zeta_2(\mathbf{s})\rangle$ ) can be presented in terms of their initial values as follows:

$$\begin{pmatrix} |\zeta_1(\mathbf{s})\rangle \\ |\zeta_2(\mathbf{s})\rangle \end{pmatrix} = \begin{pmatrix} \cos \beta(\mathbf{s}) & \sin \beta(\mathbf{s}) \\ -\sin \beta(\mathbf{s}) & \cos \beta(\mathbf{s}) \end{pmatrix} \begin{pmatrix} |\zeta_1(\mathbf{s}_0)\rangle \\ |\zeta_2(\mathbf{s}_0)\rangle \end{pmatrix} \quad (3.44)$$

Here the notation  $\gamma(\mathbf{s})$  is replaced by  $\beta(\mathbf{s})$  to emphasize the fact that in Eq. (3.44) is encountered the *mixing* angle, which follows from diagonalizing the diabatic potential matrix  $\mathbf{V}(\mathbf{s})$  and not the ADT angle, which is computed employing a line integral [see Eqs. (3.5) and Eq. (3.6)]. Because it is the *mixing* angle,  $\beta(\mathbf{s})$  is given in the following form [see Eq. (3.39)]:<sup>2–5</sup>

$$\beta(\mathbf{s}) = \frac{1}{2} \tan^{-1} \left( \frac{v(\mathbf{s})}{w(\mathbf{s})} \right) \quad (3.45)$$

**Lemma 3.1** The *mixing* angle  $\beta(\mathbf{s})$  is identical, up to an additive constant, to the *ADT* angle  $\gamma(\mathbf{s})$ .

*Proof* To prove this lemma, we consider the corresponding NACT,  $\tau_{12}(\mathbf{s})$ :

$$\tau_{12} = \langle \zeta_1 | \nabla \zeta_2 \rangle \quad (3.46)$$

Substituting ( $|\zeta_1(\mathbf{s})\rangle, |\zeta_2(\mathbf{s})\rangle$ ) as given by Eq. (3.44) in Eq. (3.46) yields as a result the first-order differential equation for  $\beta(\mathbf{s})$ :<sup>2,3</sup>

$$\tau_{12}(\mathbf{s}) = -\nabla \beta(\mathbf{s}) \quad (3.47)$$

Comparison of Eq. (3.47) with Eq. (3.5a) shows that the two angles,  $\beta(\mathbf{s})$  and  $\gamma(\mathbf{s})$ , fulfill identical first-order differential equations which proves the lemma.

Since the two angles differ at most by an additive constant (which is of a minor physical significance), we do not distinguish anymore between the two angles. Both are termed *ADT angles*.

In what follows the subscript (12) is deleted from  $\tau_{12}(\mathbf{s})$ .

**Corollary 3.1** Combining Eqs. (3.45) and (3.47) yields the connection between the diabatic potentials  $v(\mathbf{s})$  and  $w(\mathbf{s})$  and the corresponding NACT,  $\tau(\mathbf{s})$ :<sup>6,7</sup>

$$\tau(\mathbf{s}) = -\frac{1}{2} \frac{1}{1 + (v(\mathbf{s})/w(\mathbf{s}))^2} \nabla(v(\mathbf{s})/w(\mathbf{s})) \quad (3.48)$$

The fact that the ADT angle and the mixing angles are identical introduces one additional result, which is expressed in terms of the following lemma.

**Lemma 3.2** The NACT,  $\tau(\mathbf{s})$ , formed by a diabatic potential is always *quantized*.

*Proof* To prove this lemma, we consider Eq. (3.45), from which it is seen that for any point  $\mathbf{s} = \mathbf{s}_p$  along the contour  $\Gamma$  we have the following relation:

$$\tan(2\beta(\mathbf{s}_p)) = \frac{v(\mathbf{s}_p)}{w(\mathbf{s}_p)} \quad (3.49)$$

Consider now the initial point  $\mathbf{s} = \mathbf{s}_i$  of a closed contour  $\Gamma$  and the final point  $\mathbf{s} = \mathbf{s}_f$  of this contour. Equation (3.49) is fulfilled for both points, but since  $\Gamma$  is a closed contour, we have that  $\mathbf{s} = \mathbf{s}_i$  and  $\mathbf{s} = \mathbf{s}_f$  are the same points (in configuration space) and consequently the mixing angle  $\beta$  calculated at the beginning of the contour and the one calculated at the end of the contour are related as

$$\beta(\mathbf{s}_f) = \beta(\mathbf{s}_i) + n\pi \quad (3.50)$$

where  $n$  is an (unspecified) integer. Equation (3.50) implies that the NACT  $\tau(\mathbf{s})$ , presented in Eq. (3.48) is always *quantized* [see Eq. (3.12)].

A numerical example for a calculation of the  $n$  value in Eq. (3.50) is given in Ref. 3.

As a final task, we check whether  $\tau(\mathbf{s})$  as presented in Eq. (3.48) fulfills the Curl equation. For this purpose we assume that  $\mathbf{s} \equiv (x, y)$  and we examine the expression [see Eq. (1.28)]

$$\frac{\partial \tau_x(x, y)}{\partial y} - \frac{\partial \tau_y(x, y)}{\partial x} = 0 \quad (1.28')$$

where

$$\tau_p(\mathbf{s}) = -\frac{1}{2} \frac{1}{1 + (v(\mathbf{s})/w(\mathbf{s}))^2} \frac{\partial(v(\mathbf{s})/w(\mathbf{s}))}{\partial p}; \quad p = x, y \quad (3.48')$$

Defining  $f(x, y) = v(x, y)/w(x, y)$ , it can be shown that:

$$\begin{aligned} \frac{\partial \tau_x(x, y)}{\partial y} &= (1 + f^2)^{-2} (2ff_x f_y - f_{yx}) \\ \frac{\partial \tau_y(x, y)}{\partial x} &= (1 + f^2)^{-2} (2ff_y f_x - f_{xy}) \end{aligned} \quad (3.51)$$

As is noted, the two expressions are identical if and only if  $f_{xv} = f_{yx}$ . Since this equality is fulfilled for all potentials  $v(x,y)$  and  $w(x,y)$  that are analytic functions of  $x$  and  $y$ , the Curl condition in Eq. (1.28) is fulfilled for such (diabatic) potentials.

### 3.2.2 The Jahn–Teller Model

The Jahn–Teller model is the better known diabatic potential. It is simple enough to be treated analytically and sufficiently general to have physical relevance.<sup>9–13</sup> Within this model we consider a planar case characterized by either general Cartesian coordinates  $(x,y)$  or their corresponding polar coordinates  $(q,\varphi)$ :

$$x = q \cos \varphi \quad \text{and} \quad y = q \sin \varphi \quad (3.52)$$

The Jahn–Teller model concentrates on a region around point  $P(0,0)$ , where the two diabatic potentials,  $u(x,y)$  and  $v(x,y)$  [see Eq. (3.39)], become zero:

$$w(x = 0, y = 0) = 0; \quad v(x = 0, y = 0) = 0 \quad (3.53)$$

The basic assumption of the Jahn–Teller model is that in the close vicinity of this point the diabatic potential  $\mathbf{V}(\mathbf{s})$  is linear and takes the form

$$\mathbf{V}(x,y) = k \begin{pmatrix} y & x \\ x & -y \end{pmatrix} \quad (3.54)$$

where  $k$  is a given constant. The two eigenvalues of  $\mathbf{V}(x,y)$  ( $\equiv V(q,\varphi)$ ) are

$$u_1 = kq \quad \text{and} \quad u_2 = -kq \quad (3.55)$$

and they are valid for any value of  $\varphi$  in the range:  $0 \leq \varphi \leq 2\pi$ . Since  $u_1$  and  $u_2$  are the adiabatic potential energy surfaces, it can be easily seen that each potential has a cone shape—one cone inverted with respect to the other—and have one common point at the origin (see Fig. 3.1). This situation is known as the *conical intersection*,<sup>11–13</sup> and we refer to the point of intersection as the *ci point* or simply as the *ci*. The *ci* points were also mentioned in Section 1.1.2, where we referred to them as points at which the relevant eigenfunction is not analytic.

The rest of this section concentrates on the polar components of the NACTs, namely, the radial component,  $\tau_q(\varphi,q)$  and the angular one,  $\tau_\varphi(\varphi,q)/q$ , where both  $\tau_p(\varphi,q)$ ;  $p = q, \varphi$  are defined as

$$\tau_p = \left\langle \xi_1 \left| \frac{\partial}{\partial p} \xi_2 \right. \right\rangle; \quad p = q, \varphi \quad (3.56)$$

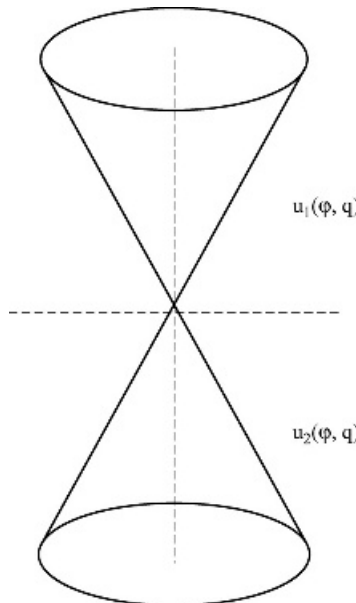


**Figure 3.1** The two interacting cones describing the Jahn–Teller model.

In case of the diabatic potentials, the two polar components  $\tau_p(\varphi, q); p = q, \varphi$  [which are similar to the Cartesian ones given in Eq. (3.48')] are

$$\tau_p(\varphi, q) = -\frac{1}{2(1 + (v/w)^2)} \frac{\partial(v/w)}{\partial p}; \quad p = q, \varphi \quad (3.48'')$$

Next, employing Eq. (3.48), we derive the polar NACT components for the Jahn–Teller model. Since  $w(x, y) = y$  and  $v(x, y) = x$ , we get the following result for  $v(x, y)/w(x, y)$  [see Eq. (3.52)];

$$v(\varphi, q)/w(\varphi, q) = \tan\varphi \quad (3.57)$$

Substituting Eq. (3.57) in Eq. (3.48) yields the two required components of  $\tau(\varphi, q)$ :

$$\tau_\varphi(\varphi, q) = -\frac{1}{2}; \quad \tau_q(\varphi, q) = 0 \quad (3.58)$$

Having these components, we are in a position to calculate the  $n$  value introduced in Eq. (3.50) for the Jahn–Teller model. Substituting Eq. (3.58) [viz.,  $\tau_\varphi(\varphi, q)/q = 1/(2q)$ ] in Eq. (3.12) and assuming the contour to be a circle (which implies that the tangential component of the infinitesimal vector  $ds$  is  $q d\varphi$ ), for  $\alpha(\Gamma) (\equiv \alpha(q))$  we get the result of  $\pi$ , namely,  $n = 1$ .

### 3.2.3 Elliptic Jahn–Teller Model

The *elliptic* Jahn–Teller model is defined in terms of<sup>6</sup>

$$w(\varphi, q)(=y) = q \cos \varphi \quad \text{and} \quad v(\varphi, q)(=bx) = b(q)q \sin \varphi \quad (3.59)$$

Consequently  $v(q, \varphi)/w(q, \varphi)$  becomes

$$v(\varphi, q)/w(\varphi, q) = b(q) \tan \varphi \quad (3.60)$$

Substituting Eq. (3.60) in Eq. (3.48'') yields the following expressions for the two components of  $\tau(\varphi, q)$ :

$$\tau_\varphi(\varphi, q) = -\frac{1}{2} \frac{b(q)}{\cos^2 \varphi + b(q)^2 \sin^2 \varphi} \quad (3.61a)$$

$$\tau_q(\varphi, q) = -\frac{1}{4} \frac{b(q)}{\cos^2 \varphi + b(q)^2 \sin^2 \varphi} \frac{db(q)}{dq} \quad (3.61b)$$

It is noted that  $\tau_q(\varphi, q)$  becomes zero if the parameter  $b$  does not depend on  $q$  and the circular Jahn–Teller model is obtained for  $b = 1$ .

Figure 3.2 presents three curves describing the angular NACT,  $\tau_\varphi(\varphi)$ , related to the elliptic model [see Eq. (3.61a)], as calculated for three different  $b$  values, namely,  $b = 2, 4, 6$ . It is noted that the curves have a double-hump structure. The humps are of equal size and increase as  $b$  increases. It is also noted that as  $b \rightarrow 1$ , the elliptic model converges to the Jahn–Teller model.

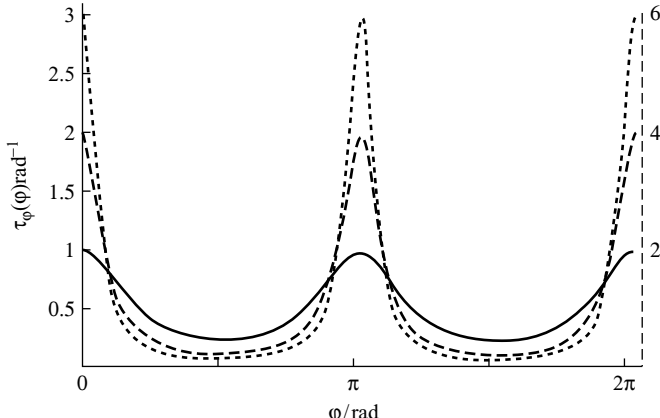


**Figure 3.2** The angular NACT,  $\tau_\varphi(\varphi)$ , as calculated for the *elliptic* Jahn–Teller model, for three  $b$  values [i.e.,  $b = 2, 4, 6$ ; see Eq. (3.61a)]. The  $b$  values are listed on the r.h.s. of the figure.

### 3.2.4 Distribution of Conical Intersections and Diabatic Potential Matrix

The fact that the two-state NACT,  $\tau(q,\varphi)$ , can be presented in terms of the diabatic potentials  $w(q,\varphi)$  and  $v(q,\varphi)$  [see Eq. (3.48)] opens up the possibility of studying the  $ci$  distribution, in a given region of configuration space, within the diabatic framework (i.e., without using the NACTs explicitly).

In Section 3.2.1 we proved that any  $(2 \times 2)$  diabatic potential matrix forms NACTs that satisfy the *quantization* condition. This implies that for the case where the contour  $\Gamma$  is a circle, Eq. (3.12) takes the form

$$\alpha(q) = \int_0^{2\pi} \tau_\varphi(q,\varphi) d\varphi = n\pi \quad (3.62)$$

where  $\tau_\varphi(\varphi,q)$  is as given in Eq. (3.48'') but the integer  $n$  is unknown. The present section is devoted to the determination of  $n$  for a given pair of potentials  $(v(q,\varphi), w(q,\varphi))$ . For this purpose we employ Eq. (3.48'') and break up the  $\varphi$  interval  $[0, 2\pi]$  into  $N$  subintervals  $[\varphi_{j-1}, \varphi_j]$  so that the integration along the angular  $[0, 2\pi]$  interval is presented in terms of a sum of integrals along adjacent segments:

$$\int_0^{2\pi} \tau_\varphi d\varphi = \sum_{j=1}^{j=N} \int_{\varphi_{j-1}}^{\varphi_j} \tau_\varphi d\varphi = \frac{1}{2} \sum_{j=1}^{j=N} \int_{\varphi_{j-1}}^{\varphi_j} \frac{1}{1 + (v/w)^2} \frac{\partial(v/w)}{\partial\varphi} d\varphi \quad (3.63)$$

The gridpoints  $\{\varphi_j\}$   $j = 0, 1, \dots, N$  possess the following features:

1. The starting point  $\varphi_0$  (which is also the final point of the closed contour) is chosen so that  $w(\varphi_0) \neq 0$ . For reasons of convenience it is preferred to choose  $\varphi_0$  in such a way that  $v(\varphi_0) = 0$ .
2. All other gridpoints are chosen so that either  $w(\varphi_j) = 0$  or  $v(\varphi_j) = 0$ . No other gridpoints are assumed.

In what follows the gridpoints  $\{\varphi_j\}$  for which  $v(\varphi_j) = 0$  are labeled as “ $z$  points” [these are the *zeros* of the function  $v(\varphi_j)/w(\varphi_j)$ ] and the gridpoints  $\{\varphi_j\}$  for which  $w(\varphi_j) = 0$  are labeled as “ $p$  points” [these are the *poles* of the function  $v(\varphi_j)/w(\varphi_j)$ ].

To continue we change the variable of integration in each integral in Eq. (3.63) so that we get

$$\int_0^{2\pi} \tau_\varphi d\varphi = \frac{1}{2} \sum_{j=1}^{j=N} \left( \pm \int_{f_{j-1}}^{f_j} \frac{1}{1 + f^2} df \right) \quad (3.64)$$

where the various  $f_j$  terms, defined as  $f_j = v(\varphi_j)/w(\varphi_j) = f(\varphi_j)$ , are either 0 or  $\infty$ . First let us consider the case of a single term for which  $f_{j-1} = 0$  and  $f_j = \infty$ :

$$\frac{1}{2} \int_0^\infty \frac{1}{1+f^2} df = \frac{1}{2} \tan^{-1} f \Big|_0^\infty = \frac{1}{2}\pi \quad (3.65)$$

Next we consider two successive intervals, the  $j$  and the  $(j+1)$  intervals defined by the three consecutive  $\varphi_j$  points:  $(z,p,z)$ . These gridpoints translate into the three consecutive  $f_j$  points  $\{0,\infty,0\}$ . Therefore, adding up the results due to two successive intervals yields

$$\begin{aligned} \int_{\varphi_{j-1}}^{\varphi_j} \tau_\varphi d\varphi + \int_{\varphi_j}^{\varphi_{j+1}} \tau_\varphi d\varphi &= \pm \left( \frac{1}{2} \int_0^\infty \frac{1}{1+f^2} df + \frac{1}{2} \int_\infty^0 \frac{1}{1+f^2} df \right) \\ &= \pm \left( \frac{\pi}{2} - \left( \frac{-\pi}{2} \right) \right) = \pm\pi \end{aligned} \quad (3.66)$$

The plus (minus) sign in front of the parentheses in Eq. (3.66) stands for the case where  $(v/u)$  is positive (negative) in the range  $[\varphi_{j-1}, \varphi_{j+1}]$ .

It is important to comment that for a given series of  $p-z$  points two (or more) successive points may be of the same kind, namely, either  $p-p$  or  $z-z$  points. Two such successive points produce an integral [of the kind given in Eq. (3.65)] with identical upper and lower limits, and therefore their value is zero.

The final result for the integral in Eq. (3.64) can be written as

$$\int_0^{\varphi_N} \tau_\varphi(q, \varphi) d\varphi = \int_0^{2\pi} \tau_\varphi(q, \varphi) d\varphi = \pm \frac{1}{2} m\pi \quad (3.67)$$

Here  $m$  is an integer (or zero) that stands for the number of  $zp$  pairs along the interval  $\{0, 2\pi\}$  and fulfills the condition  $m \leq M$  where  $M$  is the number of  $p$  points. However, the quantization condition [see Eq. (3.12)] requires that  $m$  be an even number (or zero). It is guaranteed to be zero if between any two consecutive  $z$  points we have an even number of  $p$  points. In case of a single  $ci$   $m$  has to be at least 2, which implies that in order for the (diabatic) potentials in Eq. (3.39) to yield a  $ci$  both  $w(q, \varphi)$  and  $v(q, \varphi)$  have to flip their signs (one after the other) at least twice along any closed contour that surrounds the  $ci$ . In other words, the four points have to be arranged in the sequence  $\{z, p, z, p\}$ .

[Comment: The roles of  $w(q, \varphi)$  and  $v(q, \varphi)$  can be reversed; namely, all points that are defined as *poles* can be defined as *zeros* and vice versa so that the same  $m$  value is expected in Eq. (3.67).]

In the applications one has to carry out the following steps:

1. Choose a point in the region of interest that is the center for the circular contours.
2. Select a set of radii  $q$  in the range  $q = [q_{\min}, q_{\max}]$ .
3. Find along each circle the zeros of  $u(q, \varphi)$  and  $v(q, \varphi)$  and arrange them in a (mixed) series according to their  $\varphi$  values.
4. *Delete* all two (or more) successive zeros of  $v(q, \varphi)$  and/or two (or more) successive zeros of  $u(q, \varphi)$ .
5. Count the remaining  $zp$  pairs to determine the number  $m$ .

The result of this procedure has to be a  $zp$  sequence of the kind  $\{z, p, z, p, \dots, z, p, \dots, z, p, z, p\}$ . Assuming that  $m$  is the number of  $zp$  pairs in this sequence, then the value of the line integral in Eq. (3.67) is equal to  $m \frac{1}{2}\pi$ , and because of the quantization rule  $m$  has to be an even number. It is important to note two facts:

1. Having  $m = 0$  does not necessarily imply that the region surrounded by the closed contour does not contain any *cis*. It may imply that it contains an even number of *cis* where half of them are *positive cis* and the other half are *negative cis* so that that their net contribution is zero.
2. The number  $m$  may vary from one closed contour to another but not necessarily uniformly (e.g., not always in an increasing order just because the region surrounded by the contour becomes larger).

As an example, we consider again the elliptic Jahn–Teller model discussed in Section 3.2.3. For this model we have

$$f(q, \varphi) = v(\varphi, q)/w(\varphi, q) = b(q) \tan \varphi \quad (3.60')$$

It is noted that the  $z$  points are at  $\varphi = 0, \pi, 2\pi$  and the  $p$  points, at  $\varphi = \pi/2, 3\pi/2$ . This means that we encounter the following  $(zp, zp)$  series; thus  $m = 2$ . Consequently the relevant contour surrounds one *ci* (a similar situation is encountered for the regular Jahn–Teller model). An exercise for studying a model with nine *cis* is presented at the end of this chapter (see Section 3.4 and Problem 3.1).

Before closing our discussion of this subject, we mention two earlier studies on this issue: (1) study<sup>14</sup> of the function  $\tan^{-1}(2f(\varphi))$  as a function  $\varphi$  for a specific case and (2) study<sup>15</sup> of a similar idea applied for a general case.

### 3.3 ADIABATIC-TO-DIABATIC TRANSFORMATION MATRIX AND WIGNER ROTATION MATRIX

The ADT matrix, as it is presented in Eq. (2.29), is somewhat reminiscent of the Wigner rotation matrix.<sup>1</sup> In order to see that, we first present a few well-known

features related to the definition of ordinary angular momentum operators (we follow the presentation by Rose<sup>2</sup>) and the corresponding rotation matrices and then return to discuss the similarities between the ADT matrix and the relevant Wigner rotational matrix.

### 3.3.1 Wigner Rotation Matrices

The ordinary angular rotation operator  $\mathbf{D}(\mathbf{k},\varphi)$  in the limit  $\varphi \rightarrow 0$  is written as

$$\mathbf{D}(\mathbf{k},\varphi) = \exp(-i\mathbf{S}(\mathbf{k},\varphi)) \quad (3.68)$$

where  $\mathbf{k}$  is a unit vector in the direction of the axis of rotation,  $\varphi$  is the angle of rotation, and  $\mathbf{S}(\mathbf{k},\varphi)$  is an operator that has to fulfill the condition  $\mathbf{S}(\mathbf{k},\varphi) \rightarrow 0$  for  $\varphi \rightarrow 0$  to guarantee that in this situation (i.e., when  $\varphi \rightarrow 0$ )  $\mathbf{D}(\mathbf{k},\varphi) \rightarrow I$ . Moreover, since  $\mathbf{D}(\mathbf{k},\varphi)$  has to be unitary, the operator  $\mathbf{S}(\mathbf{k},\varphi)$  has to be Hermitian (to guarantee real eigenvalues). Next it is shown that  $\mathbf{S}(\mathbf{k},\varphi)$  is related to the total angular momentum operator  $\mathbf{J}$  in the following way:<sup>4</sup>

$$\mathbf{S}(\mathbf{k},\varphi) = (\mathbf{k} \cdot \mathbf{J})\varphi \quad (3.69)$$

where the dot stands for scalar product. Substituting Eq. (3.69) in Eq. (3.68) yields the following expression for  $\mathbf{D}(\mathbf{k},\varphi)$ :

$$\mathbf{D}(\mathbf{k},\varphi) = \exp(-i(\mathbf{k} \cdot \mathbf{J})\varphi) \quad (3.68')$$

It has to be emphasized that in this framework  $\mathbf{J}$  is the angular momentum operator in the ordinary coordinates space (i.e., configuration space) and  $\varphi$  is a (differential) ordinary angular polar coordinate.

Next the Euler angles are employed for deriving the outcome due to a general rotation of a system of coordinates.<sup>3</sup> It can be shown that  $\mathbf{D}(\mathbf{k},\varphi)$  is, accordingly, presented as<sup>4</sup>

$$\mathbf{D}(\mathbf{k},\varphi) = e^{-i\alpha J_z} e^{-i\beta J_y} e^{-i\gamma J_z} \quad (3.70)$$

where  $\mathbf{J}_y$  and  $\mathbf{J}_z$  respectively are the  $y$  and the  $z$  components of  $\mathbf{J}$  and  $\alpha$ ,  $\beta$ , and  $\gamma$  are the corresponding three Euler angles. The explicit matrix elements of the rotation operator  $\mathbf{D}$  are given in the form<sup>1</sup>

$$\mathbf{D}_{m'm}^j(\varphi) = \langle jm' | \mathbf{R}(\mathbf{k}, \varphi) | jm \rangle = e^{-i(m'\alpha + m\gamma)} \mathbf{d}_{m'm}^j(\beta) \quad (3.71)$$

where  $m$  and  $m'$  are the components of  $\mathbf{J}$  along the  $\mathbf{J}_z$  and  $\mathbf{J}_{z'}$  axes, respectively,  $|jm\rangle$  is an eigenfunction of the Hamiltonian  $\mathbf{J}^2$  and  $\mathbf{J}_z$ , and  $\mathbf{d}_{m'm}^j(\beta(\varphi))$  is the  $y$  component

of the rotation matrix presented in the form:<sup>1</sup>

$$\mathbf{d}^j_{m'm}(\beta(\varphi)) = \langle jm' | e^{-i\beta(\varphi)\mathbf{J}_y} | jm \rangle \quad (3.72)$$

Here the  $\mathbf{d}^j$  matrix is termed *Wigner's matrix*, and it is for this matrix that we intend to show a close relationship with a certain class of ADT matrices.

### 3.3.2 Adiabatic-to-Diabatic Transformation Matrix and Wigner $\mathbf{d}^j$ Matrix

The simplest way to reveal the relationship between Wigner's  $\mathbf{d}^j$  matrix and the  $\mathbf{A}$  matrix is to consider the two matrices  $\mathbf{J}_y$  and the  $\tau$  that form  $\mathbf{d}^j$  and  $\mathbf{A}$ , respectively [see Eq. (2.29)].<sup>5,6</sup>

We start by considering the elements of the  $\mathbf{J}_y$  matrix. Employing Eqs. (2.18) and (2.28) of Ref. 2, it can be shown that  $\mathbf{J}_y$  is a tridiagonal imaginary Hermitian matrix with the following elements:

$$\begin{aligned} \langle jm | \mathbf{J}_y | jm + k \rangle &= \delta_{1k} \frac{1}{2i} \sqrt{(j+m+1)(j-m)} \\ \langle jm + k | \mathbf{J}_y | jm \rangle &= -\delta_{1k} \frac{1}{2i} \sqrt{(j-m+1)(j+m)} \end{aligned} \quad (3.73)$$

To see the similarity between the  $\mathbf{J}_y$  and the  $\tau$  matrix elements, we replace  $\mathbf{J}_y$  by  $\tilde{\mathbf{J}}_y$ , defined as

$$\tilde{\mathbf{J}}_y = -i\mathbf{J}_y \quad (3.74)$$

where  $\tilde{\mathbf{J}}_y$  is a real antisymmetric tridiagonal matrix. Having this real matrix, Wigner's  $\mathbf{d}^j$  matrix takes the form

$$\mathbf{d}^j(\beta(\varphi)) = \exp(-\tilde{\mathbf{J}}_y \beta(\varphi)) \quad (3.75)$$

which for a certain group of  $\tau$  matrices becomes similar to the ADT matrix  $\mathbf{A}$ . In fact, employing the  $\tau$  matrix for the models given in Eq. (3.1), where the  $\mathbf{g}$  matrix contains only *tridiagonal* elements [see Eqs. (3.2), (3.14), and (3.25)], enhances the similarity between the two types of matrices. Combining Eq. (2.29), Eq. (3.1), and (a modified version of) Eq. (3.6) yields the following expression for the  $\mathbf{A}$  matrix to be discussed:

$$\mathbf{A}(\varphi|\Gamma) = \exp(\mathbf{g}\gamma(\varphi|\Gamma)) \quad (3.76)$$

In Eq. (3.76) we assumed that the closed contour  $\Gamma$  is a circle, and consequently the vectorial variable  $\mathbf{s}$  becomes the scalar angular coordinate,  $\varphi$  defined along the interval  $\{0, 2\pi\}$ . In this way, both  $\gamma(\varphi|\Gamma)$  and  $\beta(\varphi)$  are defined in terms of the same independent angle  $\varphi$  and both relate to the same contour.

It is important to emphasize that the similarity between  $\mathbf{d}^1$  and  $\mathbf{A}$  is expected to be enhanced by the fact that both  $\tilde{\mathbf{J}}_y$  and  $\mathbf{g}$  fulfill similar *quantization* conditions.

In the following list we describe explicitly (our) two-state case (see Section 3.1.1), which in Wigner's notation is the case for which  $j = \frac{1}{2}$ , our three-state case (see Section 3.1.2), which in Wigner's notation is the case for which  $j = 1$ , and our four-state case (see Section 3.1.3), which in Wigner's notation is the case for which  $j = \frac{3}{2}$ :

1. For the two-state case (i.e.,  $j = \frac{1}{2}$ ) the condition for the two matrices to become identical is that  $\gamma(\varphi) \equiv (\frac{1}{2})\beta(\varphi)$ .
2. For the three-state case (i.e.,  $j = 1$ ) the condition for the two matrices to become identical is that  $\gamma(\varphi) \equiv (1/\sqrt{2})\beta(\varphi)$ . This relation yields, the following numerical values for the various parameters:  $\eta = 1$  [see Eq. (3.14)];  $\omega = \sqrt{2}$  [see Eq. (3.22)];  $\alpha = \sqrt{2}\pi$  [see Eq. (3.22)]. We emphasize that  $n$  in Eq. (3.22) has to be (an integer), and we assumed it to be 1. Substituting the values of these parameters in Eq. (3.18) yields the corresponding  $\mathbf{d}^1(\beta(\varphi))$  matrix given in the form:

$$\mathbf{d}^1(\beta) = \frac{1}{2} \begin{pmatrix} 1 + C(\beta) & \sqrt{2}S(\beta) & 1 - C(\beta) \\ \sqrt{2}S(\beta) & 2C(\beta) & -\sqrt{2}S(\beta) \\ 1 - C(\beta) & \sqrt{2}S(\beta) & 1 + C(\beta) \end{pmatrix} \quad (3.77)$$

where  $C(\beta) = \cos \beta$  and  $S(\beta) = \sin \beta$ .

3. For the four-state case (i.e.,  $j = \frac{3}{2}$ ) the condition for the two matrices to become identical is that  $\gamma(\varphi) \equiv \sqrt{3/4}\beta(\varphi)$ . This relation yields, the following numerical values for the various parameters:  $\eta = \sqrt{\frac{4}{3}}$  and  $\sigma = 1$  [see Eq. (3.25)];  $\omega = \sqrt{\frac{10}{3}}$  [see Eq. (3.29)];  $p = \sqrt{3}$  and  $q = 1/\sqrt{3}$  [see Eq. (3.28)];  $\alpha = \pi\sqrt{3}$  [see Eq. (3.34)]. It is important to emphasize that Eqs. (3.34) are employed for the case  $n = \frac{3}{2}$  and  $\ell = \frac{1}{2}$ .

Substituting the values of these parameters in Eq. (3.31) yields the corresponding  $\mathbf{d}^{3/2}(\beta(\varphi))$  matrix given in the form

$$\mathbf{d}^{3/2}(\beta) = \begin{pmatrix} C^3 & -\sqrt{3}C^2S & -\sqrt{3}S^2C & S^3 \\ \sqrt{3}C^2S & C(1 - 3S^2) & -S(1 - 3C^2) & -\sqrt{3}S^2C \\ -\sqrt{3}S^2C & S(1 - 3C^2) & C(1 - 3S^2) & -\sqrt{3}C^2S \\ -S^3 & -\sqrt{3}S^2C & \sqrt{3}C^2S & C^3 \end{pmatrix} \quad (3.78)$$

where  $C = \cos(\beta/2)$  and  $S = \sin(\beta/2)$ .

The main issue to realize is that the original  $y$  component of the total angular momentum operator  $\mathbf{J}$  is a special case of the quantized  $\mathbf{g}$  matrix. It is a special case because the elements of  $\tilde{\mathbf{J}}_y$  have well-defined values whereas the quantization laws as

established for the product  $\mathbf{g}\alpha(\Gamma)$  still leave freedom in choosing  $\gamma(\varphi)$ . Thus different choices of  $\gamma(\varphi)$  will lead to different types of  $\mathbf{d}^i(\beta)$  matrices.

## PROBLEM

- 3.1** Given the diabatic potential in Eq. (3.39), study the  $zp$  points (see Section (3.2.4)) for the following model

$$\begin{aligned} v(x,y) &= \sin(x) \\ w(x,y) &= \sin(y) \end{aligned} \quad (3.79)$$

and derive the values of the various line integrals along three different circles with three different radii  $q$ : (a)  $q < \pi$ ; (b)  $\pi < q < \sqrt{2}\pi$ ; (c)  $q > \sqrt{2}\pi$ .

*Solution* Having the potentials in Eq. (3.79), we note that all the points defined as

$$(x,y) = (\pm j\pi, \pm k\pi) \quad (3.80)$$

where  $j$  and  $k$  are integers (or zero) are  $ci$  points because at these points both  $v(x,y)$  and  $w(x,y)$  become identically zero (see Ref. 1 in Section 3.4).

Figure 3.3 shows nine  $cis$ , three circles, with radii  $q = 0.6\pi$ ,  $1.2\pi$ , and  $1.8\pi$ , that surround part or all of them, as well as three (horizontal) lines, namely,  $x = -\pi, 0, \pi$ , and three vertical lines, namely,  $y = -\pi, 0, \pi$ . Following Eqs. (3.79) and (3.80), we have a  $ci$  at each intersection between a horizontal  $x$  line and a vertical  $y$  line (thus, nine  $cis$  altogether). As for the  $zp$  points, the intersection between a circle and any horizontal  $x$  line forms a  $z$  point, and the intersection between a circle and any vertical  $y$  line forms a  $p$  point.

Next, we consider, the  $ci$  distribution in regions surrounded by three circles:

- (a) The *inner circle*, drawn for a radius  $q = 0.6\pi$ . We note that only the  $x = 0$  line and the  $y = 0$  lines cross it (twice) and that these crossings form the  $\{z,p,z,p\}$  sequence. In other words, we have here two  $zp$  pairs; thus  $m = 2$  and therefore the value of the integral in Eq. (3.67) is  $\pi$ . This fact implies that in the region surrounded by the inner circle is located one  $ci$  (or, eventually, an *odd* number of  $cis$  points). In fact, we see that we encounter one  $ci$  only.
- (b) The *intermediate circle*, drawn for a radius  $q = 1.2\pi$ . This circle is crossed (twice) by the three horizontal lines, namely,  $x = -\pi, 0, \pi$ , and by the three vertical lines,  $y = -\pi, 0, \pi$ . These intersection points form the following sequence of  $zp$  points:  $\{z,p,z,p,z,p,z,p,z,p\}$ —thus six pairs of  $zp$  points that yield the value  $m = 6$ . As a result line integral in Eq. (3.67) becomes  $3\pi$ , implying that in the region surrounded by this circle are located either three  $cis$  (with *identical* signs) or a larger number of  $cis$  where some of

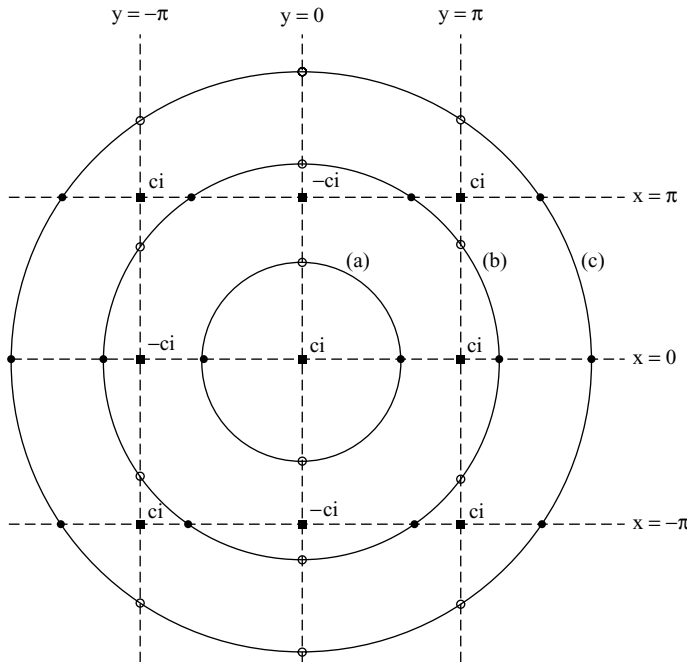


**Figure 3.3** The distribution of *cis* as obtained for the model system given in Eq. (3.81). Shown are *ci* points, the horizontal lines  $x = (\pi, 0, -\pi)$ , the vertical lines  $y = (\pi, 0, -\pi)$ , the three concentric circles *a*, *b* and *c* with radii  $q = 0.6\pi$ ,  $1.2\pi$ ,  $1.8\pi$ , respectively), and the *z* and *p* points (which are the crossing points between circles and the previously mentioned straight lines). Along the inner circle are located two *z* points and two *p* points and along the intermediate and the outer circles are located six *z* points and six *p* points. Note that the internal distribution of the *z* and *p* points in both circles is different. [Key: ■ positions of *ci* points; ○ crossing points between the circles and  $u = 0$  lines (forming *z* points); ● crossing points between the circles and  $v = 0$  lines (forming *p* points).]

them are with an opposite sign. In fact, we encounter five *cis*; four of them have identical signs, and one of them (the central one) possesses an opposite sign.

- (c) The *outer circle*, drawn for  $q = 1.8\pi$ , which is crossed by the same six previous lines, but at different points and therefore a different sequence of *zp* points is formed, namely,  $\{z, z, p, p, p, z, z, z, p, p, p, z\}$ . Since each pair of the same kind (i.e., *zz* or *pp*) cancel each other, we delete all these pairs so that we are left with the following sequence of points:  $(p, z, p, z)$ . In other words, the initial large series of *zp* points shrinks to become two pairs or  $m = 2$ , which implies that the value of the integral in Eq. (3.67) is now again,  $\pi$ , although we have a distribution that contains nine *cis*. The interpretation of this outcome is that in this enlarged region we find five *cis* with one sign and four with an opposite sign.

As a final issue in this exercise, we refer to direct calculation of the line integral in Eq. (3.67) where  $\tau_\varphi(\varphi|q)$  is given in the form

$$\tau_\varphi(x,y) = \frac{1}{2} \frac{y \cos x \sin y + x \sin x \cos y}{\sin^2 x + \sin^2 y} \quad (3.81)$$

In deriving Eq. (3.79) we used the fact that  $x = q \cos \varphi$  and  $y = q \sin \varphi$  and applied the relation

$$\tau_\varphi(x,y) = \tau_x(x,y) \frac{dx}{d\varphi} + \tau_y(x,y) \frac{dy}{d\varphi} \quad (3.82)$$

where  $\tau_x$  and  $\tau_y$  are calculated employing Eq. (3.48').

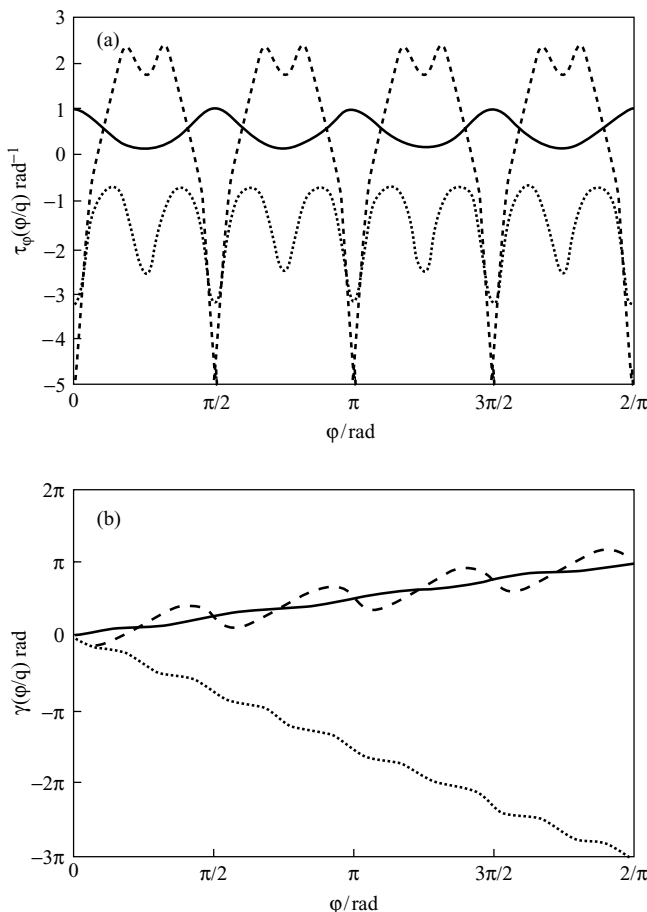


**Figure 3.4** The angular NACT,  $\tau_\varphi(\varphi|q)$ , and the ADT angle  $\gamma(\varphi|q)$ , both as functions of  $\varphi$  calculated along circles with radii  $q = 0.6\pi, 1.2\pi, 1.8\pi$ . (Key: —  $q = 0.6\pi$ ; ---  $q = 1.2\pi$ ; ....  $q = 1.8\pi$ ).

The calculations were done for the abovementioned three  $q$  values:  $q = 0.6\pi$ ,  $1.2\pi$ , and  $1.8\pi$ . Figures 3.4a and 3.4b present, respectively, the  $\tau_\varphi(\varphi|q)$  and  $\gamma(\varphi|q)$  values calculated, as a function of  $\varphi$  (see Eq. (4.3)), for the three  $q$  values. The values of  $\gamma(\varphi = 2\pi|q)$ , which represent the results of the line integral in Eq. (3.67) or the value  $\alpha(q)$  in Eq. (3.12), are  $\pi$ ,  $-3\pi$ , and  $\pi$ , respectively, just like the ones we obtained by applying the *zp* sequence approach.

This issue is discussed in the article by Vértesi et al.<sup>1</sup>

## REFERENCES

### Section 3.1

1. M. Baer and A. Alijah, *Chem. Phys. Lett.* **319**, 489 (2000).
2. M. Baer, *Chem. Phys.* **259**, 123 (2000).
3. M. Baer, *Phys. Rep.* **358**, 75 (2002).
4. D. Bohm, *Quantum Theory*, Dover Publications, New York, 1989, p. 41.

### Section 3.2

1. M. S. Child, *Molecular Collision Theory*, Academic Press, London, 1974, Section 6.2.
2. F. T. Smith, *Phys. Rev.* **179**, 111 (1969).
3. Z. R. Xu, M. Baer, and A. J. C. Varandas, *J. Chem. Phys.* **112**, 2746 (2000).
4. E. S. Kryachko, *Adv. Quant. Chem.* **44**, 119 (2003).
5. H. Köppel, *Faraday Disc.* **127**, 35 (2004).
6. M. Baer, A. M. Mebel, and R. Englman, *Chem. Phys. Lett.* **354**, 243 (2002).
7. T. Vértesi, Á Vibók, G. J. Halász, and M. Baer, *J. Chem. Phys.* **120**, 2565 (2004).
8. H. A. Jahn and E. Teller, *Proc. Roy. Soc. Lond. A* **161**, 220 (1937).
9. E. Teller, *J. Phys. Chem.* **41**, 109 (1937).
10. E. Teller, *Isr. J. Chem.* **7**, 227 (1969).
11. R. Englman, *The Jahn-Teller Effect in Molecules and Crystals*, Wiley-Interscience, New York, 1972.
12. I. B. Bersuker and V. Z. Polinger, *Vibronic Interactions in Molecules and Crystals*, Springer, New York, 1989.
13. I. B. Bersuker, *Chem. Rev.* **101**, 1067 (2001).
14. D. Yarkony, *J. Chem. Phys.* **100**, 18612 (1996).
15. R. Englman, A. Yahalom, M. Baer, and A. M. Mebel, *Int. J. Quant. Chem.* **92**, 135 (2003).

### Section 3.3

1. E. P. Wigner, *Gruppentheorie*, Friedrich Vieweg, Braunschweig, 1931.
2. M. E. Rose, *Elementary Theory of Angular Momentum*, Wiley, 1957.
3. H. Goldstein, *Classical Mechanics*, Addison-Wesley, Cambridge, MA, 1960, p. 107.

4. A. Messiah, *Quantum Mechanics*, North-Holland, Amsterdam, 1970, Vol. II, Chapter XIII.III.
5. M. Baer, *Chem. Phys. Lett.* **347**, 149 (2001).
6. M. Baer, in *Low-Lying Potential Energy Surfaces*, M. R. Hoffmann and K. G. Dyall, eds., ACS (American Chemical Society) Symposium Series 828, Washington, DC, 2002, p. 361.
7. J. Avery, M. Baer, and D. G. Billing, *Molec. Phys.* **100**, 1011 (2002).

### Section 3.4

1. T. Vértesi et al., *J. Chem. Phys.* **120**, 2565 (2004).

# CHAPTER 4

---

## STUDIES OF MOLECULAR SYSTEMS

---

### 4.1 INTRODUCTORY COMMENTS

The main issue to be discussed in this chapter is related to NACTs. The NACTs were appropriately introduced in Chapter 1 and discussed further in Chapter 2. Here we concentrate on their spatial distribution as obtained from ab initio treatments. Another concept that is frequently mentioned in this chapter is the conical intersection (*ci*). Although *cis* (or points of *cis*) were introduced in Section 3.2.2 their main features are presented and analyzed only in Chapter 5. Still, the fact that *cis* and NACTs are closely connected makes it impossible to refer to the one without mentioning the other. At this stage we emphasize that *ci* points are points at which two (adiabatic) electronic states become degenerate, and they are considered as the *sources* for forming NACTs. Therefore while studying the NACTs we concentrate on regions surrounding the various *ci* points.

Probably one of the most significant results of the theory so far is establishing the *quantization* of the NACM for a group of states<sup>1–4</sup> that forms a Hilbert space (or the approximate *quantization* for a group of states the forms a Hilbert subspace). This concept is introduced in Section 2.1.3.3. (see Corollary 2.1), is discussed extensively in Chapter 3 for simple models and is further established, in the present chapter, for realistic molecular systems. Another aspect of the theory, of similar importance, is the (approximate) fulfillment of the Curl equation (see Section 1.1.2) for a Hilbert subspace. However, this issue is discussed, later, in Chapter 6.

To study the NACTs, we consider a plane that contains three atoms (A,B,C). It is important to realize that there exists only one plane that contains these three atoms

(although the plane itself is, in general, not fixed but may flip and tumble in space). Still, for our purposes it suffices to consider only the body-fixed system of coordinates, where a point in configuration space is described in terms of three coordinates. However, in order to simplify the search for the positions of the *cis*, we break up the three-dimensional configuration space and present it as a series of two-dimensional spaces that are chosen to be a series of *parallel* planes. In what follows we distinguish between the various planes as follows. Each plane is formed while fixing the interatomic distance  $R$  between two (out of the three) atoms, for instance, atoms B and C (so that  $R = R_{BC}$ ) and leaving atom A (the third atom) to move freely on that plane. Atom A is used as a probe to examine the values of the different NACTs,  $\tau_{jk}(\mathbf{s})$ , at the various points  $\mathbf{s}$  belonging to the (planar) region of interest. It is important to mention that in order to obtain the NACTs for the three-dimensional configuration space the values of  $R_{BC}$  are varied in some order and in this way to reveal all the *cis* of the given molecular system. Doing it this way, it can be shown that the *cis* on the various planes are connected by continuous finite or infinite *lines* known by the term *seams*.

So far we mentioned triatom systems only. In fact, we also present results for a tetraatomic system. There the search is done by fixing the positions of three atoms and leaving, again, one atom to probe the NACTs. Since we limit our discussion to configurations where all four atoms form a plane, the free, *test* atom is assumed to move on that same plane as well. This system is discussed further in Section 4.3.1.3.

## 4.2 THEORETICAL BACKGROUND

The concept of *quantization* (without referring to it as such) was revealed a short time after the Born–Oppenheimer treatment. While considering triatomic radicals for which the ground electronic state in the collinear configuration is the doubly degenerate  $\Pi$  state, Renner presented a model, to study the spectroscopy of such molecules, which is based on an angular NACT that couples the two nondegenerate states formed by the (slightly) shifted central atom from the collinear arrangement.<sup>1,2</sup> The NACT is formed by the rotational motion of the central atom along a circular contour that surrounds the axis formed by the two (fixed) external atoms. The Renner model leads to two electronic states described in terms of the two electronic wavefunctions  $|\zeta_j(\mathbf{s}_e|\mathbf{s})\rangle$ ;  $j = 1, 2$  that satisfy the following relations<sup>2</sup>

$$\left| \frac{\partial}{\partial \varphi} \zeta_1 \right\rangle = -i\hbar m |\zeta_2\rangle; \quad \left\langle \frac{\partial}{\partial \varphi} \zeta_2 \right| = i\hbar m \langle \zeta_1 | \quad (4.1)$$

where  $m$  is an *integer*. These relations yield a quantized NACT, namely,  $\tau_{\varphi 12} = m$  [see Eq. (1.4)], and a typical example is the NH<sub>2</sub> molecule.<sup>2</sup> A different situation is encountered for the H + H<sub>2</sub> system, which, employing either perturbation theory<sup>3</sup> or ab initio treatment,<sup>4</sup> also leads to a quantized (angular) NACT, namely,  $\tau_{\varphi 12} = \frac{1}{2}$ , characterized by a half-integer.

It is important to mention that these studies are limited to an infinitely small (i.e.,  $\varepsilon$ -size) region surrounding the degeneracy axis, in the first (Renner) case, or the *ci* point in the second. They resulted from successful applications of perturbation

theory but were not considered as general features related to molecular systems, and therefore the concept of *quantization* was not used in this context. The contribution of the present author and his collaborators to this issue is in extending the *quantization* concept to *substantial* regions of configuration space and this first by discussing it theoretically (see Section 2.1.3.1) and then by supporting it by numerical calculations (as will be presented below). In this way the quantization is an inherent feature of Born–Oppenheimer systems and applies to a group of  $N$  states that, in a given region of configuration space, forms a Hilbert subspace (as introduced in Section 1.2).<sup>5–9</sup>

(Comment: Here we briefly mention that the *Renner–Teller model*, as it is now termed,<sup>2,10</sup> will not be discussed any further as this subject is beyond the scope of the present book.)

Some confusion is created when quantization is connected with diabatization—a process required if quantum-mechanical nonadiabatic calculations are to be carried out (see Chapter 2). It was established (in Section 2.1.3.3 and in numerous publications) that diabatization in a given region can be carried out *if and only if* the NACM is *quantized* (the quantization process is usually applied to the matrix as a whole and not to a particular element). Thus quantization also, has a very important practical aspect, and it is this aspect that is usually ignored. In other words, there exists the belief that one is capable of diabatizing, for instance, a two-state system without the topological phase  $\alpha(q)$  to be a multiple of  $\pi$  [a requirement closely related to Eq. (4.2)]. In Section 3.1.3.3 it is explained, why the NACT element [in this case the (1,2) matrix element] for a two-state system has to be *quantized* in order to guarantee the *singlevaluedness* of the diabatic potentials  $W_{jk}$ ;  $j,k = 1,2$ .

In Section 1.2 we discussed the subject of Hilbert subspace and the possibility of the  $\tau$  matrix to breaking up into finite (diagonal) submatrices that are only weakly coupled to each other. It is this breakup that enables the (quasi)quantization of finite blocks of the  $\tau$  matrix. Therefore part of the numerical study is devoted also to this subject.

The numerical study to be presented next emphasizes the two aspects of this issue; On one hand we show, numerically, that *quantization* of the two-state systems can take place at relatively large regions of configuration space (and therefore for beyond the region covered, e.g., by *perturbation theory*) and on the other hand show that in those cases that *two-state* quantization breaks down a *three-state* quantization takes over, and so on.

The theory is based on calculus performed along contours in configuration space as discussed in Chapter 1. We remind the reader that our approach concentrates on planes, and therefore the contours (in these planes) can be described in terms of two coordinates ( $x,y$ ) or ( $q,\varphi$ ). The magnitudes of interest in the two-states case are the ADT angle as given in Eq. (3.6), and in case of more than two states, the ADT matrix given in Eq. (2.29). In both cases the integration is carried out for the tangential component of the required  $\tau$ -matrix elements. In case of circular contours, the tangential components become the angular components, namely,  $(1/q)\tau_{\varphi jk}$ , where  $\tau_{\varphi jk}$  is defined as follows:

$$\tau_{\varphi jk}(\varphi|q) = \left\langle \zeta_j(s_e|\varphi|q) \left| \frac{\partial}{\partial \varphi} \zeta_k(s_e|\varphi|q) \right. \right\rangle \quad (4.2)$$

Thus, the ADT angle  $\gamma(\varphi|q)$  related to the states  $j$  and  $j + 1$  (the ADT angle is defined only with respect to two adjacent states) is consequently designated as  $\gamma_{jj+1}(\varphi|q)$  and is given by the following expression:

$$\gamma_{jj+1}(\varphi|q) = \int_0^\varphi \tau_{\varphi jj+1}(\varphi'|q) d\varphi' \quad (4.3)$$

The corresponding topological phase,  $\alpha_{jj+1}(q)$ , is defined similarly but for a *closed* circle:

$$\alpha_{jj+1}(q) = \int_0^{2\pi} \tau_{\varphi jj+1}(\varphi'|q) d\varphi' \quad (4.4)$$

[Thus the upper limit in the integral in Eq. (4.3) becomes  $\varphi = 2\pi$ .] Similar expressions are employed for the ADT **A**-matrix elements [see Eq. (2.29)]

$$\mathbf{A}(\varphi|q) = \wp \exp \left( - \int_0^\varphi \tau_\varphi(\varphi|q) d\varphi \right) \quad (4.5)$$

and the corresponding *topological* **D**-matrix elements [see Eq. (2.32)]

$$\mathbf{D}(q) = \wp \exp \left( - \int_0^{2\pi} \tau_\varphi(\varphi|q) d\varphi \right) \quad (4.6)$$

The symbol  $\wp$  in front of the integrals in Eqs. (4.5) and (4.6) implies that the integration has to be carried out in a given order.

## 4.3 QUANTIZATION OF NONADIABATIC COUPLING MATRIX: STUDY OF AB INITIO MOLECULAR SYSTEMS

### 4.3.1 Two-State Quasiquantization

#### 4.3.1.1 $\{\text{H}_2, \text{H}\}$ System

The  $\{\text{H}_2, \text{H}\}$  system is known for its equilateral  $D_{3h}$  conical intersection, which couples the two lowest states. In the present chapter we study the spatial distribution of the NACT – to be designated as (1,2) NACT – that results from this *ci*. However, in so doing we reveal that this spatial distribution is affected by two other *cis* that couple the second and the third states and are located not too far from the just-mentioned  $D_{3h}$  *ci*<sup>1</sup> (see Fig. 4.1). We note that these *cis* are located on the two sides of the symmetry line that connects the center of mass of the two *fixed* hydrogens and the (1,2) *ci* point. Consequently this type of *ci* is frequently referred to as “twin *cis*.”

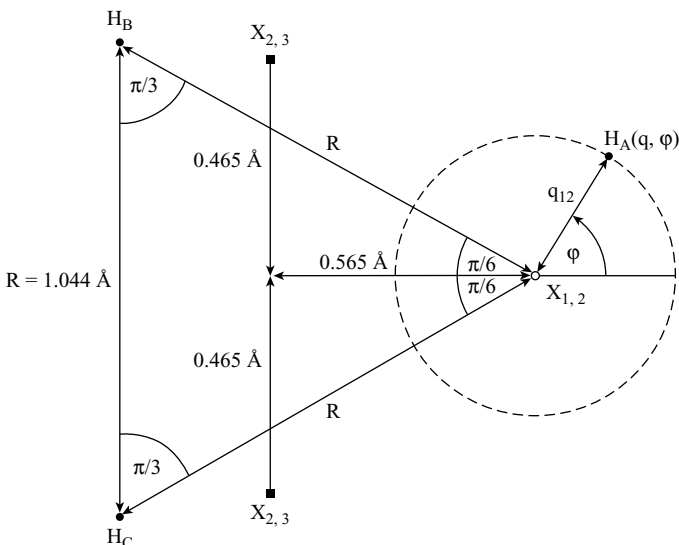


**Figure 4.1** Position of the three *cis* points of the  $\{\text{H}_2, \text{H}\}$  system. Shown is the  $(1,2)$   $D_{3h}$  *cis* (o) designated as  $X_{1,2}$  and the two (symmetric)  $(2,3)$  *cis* twins (■) designated as  $X_{2,3}$ . One of them is located at  $\{q_{12} = 0.73 \text{ \AA}, \varphi = 141.5^\circ\}$  and the other, at  $\{q_{12} = 0.73 \text{ \AA}, \varphi = 218.5^\circ\}$  both with respect to the  $(1,2)$  *cis*. The distance between these two *cis* is  $0.93 \text{ \AA}$ . The locations of the *cis* are calculated for the (fixed) HH distance,  $R_{\text{HH}} = 1.044 \text{ \AA}$ .

The  $\text{H}_2 + \text{H}$ ,  $D_{3h}$  *cis* has attracted numerous studies revealing various features that result from the existence of this *cis*. The earlier publications<sup>2–5</sup> concentrated mainly on the sign flip phenomenon (caused by the *cis*) more widely known as the *Jahn-Teller effect*,<sup>6,7</sup> and only the more recent publications emphasize the resulting NACT, formed by *cis*.<sup>1,8–18</sup>

Calculation of the NACTs was carried out at the state-average complete active-space self-consistent field (CASSCF) level using a 6-311G\*\* ( $3d, 3p$ ) basis set,<sup>19</sup> but extended with diffuse functions. Thus, in order to properly account, for the Rydberg states, two diffuse functions—one *s* function and one *p* function—were added to the basis set, in an even-tempered manner,<sup>20</sup> with the exponents of 0.0121424 and 0.046875, respectively. We used the active space including all three electrons distributed on nine orbitals. Three different electronic states, namely,  $1^2A'$ ,  $2^2A'$ , and  $3^2A'$ , were computed by the abovementioned state-average CASSCF method (with equal weights). Calculations of both the eigenfunctions and the NACTs were done by employing the MOLPRO program.<sup>21</sup>

We report here on results as calculated for the situation where two hydrogens are at a (fixed) distance  $R_{\text{HH}} = 1.044 \text{ \AA}$  and the third is used to probe the NACTs at the points of interest.<sup>1</sup> The calculations are carried out along circular contours. Four circles are considered; all of them are centered at the  $D_{3h}$  point and with radii  $q = 0.3, 0.5, 0.7, 0.75 \text{ \AA}$ . In the present section we concentrate on angular NACTs and the relevant ADT angles. The ab initio angular NACTs are presented in Figure 4.2. As

**TABLE 4.1** Topological Phases  $\alpha_{12}(q)$  and  $\cos \alpha_{12}(q)$  as Calculated for  $\{\text{H}_2, \text{H}\}$  System along Different Closed Circles

| Radius q ( $\text{\AA}$ ) | $\alpha_{12}$ | $\cos \alpha_{12}$ |
|---------------------------|---------------|--------------------|
| 0.010                     | 3.11          | -0.9995            |
| 0.015                     | 3.12          | -0.9998            |
| 0.020                     | 3.14          | -1.0000            |
| 0.030                     | 3.14          | -1.0000            |
| 0.050                     | 3.14          | -1.0000            |
| 0.100                     | 3.13          | -1.0000            |
| 0.200                     | 3.12          | -0.9998            |
| 0.300                     | 3.10          | -0.999             |
| 0.50                      | 3.08(5)       | -0.998             |
| 0.60                      | 3.10          | -0.999             |
| 0.7                       | 3.10          | -0.999             |
| 0.72                      | 3.09          | -0.999             |
| 0.75                      | 2.27          | -0.640             |
| 0.80                      | 2.27          | -0.640             |

is noted the figure is arranged in columns—each column for one situation related to a specified circle with an assigned radius  $q$ . Each column contains a set of upper and lower panels; the upper panel presents the (angular) NACT  $\tau_{\varphi 12}(\varphi|q)$ , and the lower one shows the corresponding  $\gamma_{12}(\varphi|q)$  angle, both presented as a function of  $\varphi$ . In addition, each lower panel gives the value of the corresponding  $\alpha_{12}(q)$ . Additional information is supplied in Table 4.1, which lists a set of phases,  $\alpha_{12}(q)$  [and  $\cos \alpha_{12}(q)$ ] as a function of  $q$ .

The main features to be noticed in Figure 4.2 are the wiggly  $\tau_{\varphi 12}(\varphi|q)$  functions, which, as long as  $q$  is small enough, are smooth with relatively small amplitudes and evenly distributed around the value  $\tau_{\varphi 12} = 0.5$ . However, as  $q$  increases, the  $\tau_{\varphi 12}$  functions become more erratic, with larger amplitudes and values rapidly approaching the  $\varphi$  axis. Finally, at  $q \sim 0.75 \text{ \AA}$ , the  $\tau_{\varphi 12}$  function crosses this axis to become negative. As for the topological phases [i.e.,  $\alpha_{12}(q)$ ], it is noted that as long as  $q$  is smaller than  $0.72 \text{ \AA}$ , all  $\alpha_{12}$  values are in close proximity to  $\pi$ . However, once  $q$  exceeds this value, the  $\alpha_{12}$  values drop abruptly, to become 2.27 [or  $\cos(\alpha_{12}) = -0.62$ ]. The fact that  $\alpha_{12}$  starts to deviate from  $\pi$  once  $q > 0.72 \text{ \AA}$  is, according to the theory, an indication that the two-state system is not isolated as it previously was for regions closer to the  $D_{3h}$  *cis*. In other words, we encounter strong disturbances, most probably, due to the next (third) state that acts via one or several (2,3) *cis*. These *cis* have to be located in the region defined by  $q > 0.72 \text{ \AA}$ . Indeed, more extensive studies revealed the existence of twin (2,3)  $C_{2v}$  *cis*, located on both sides of the symmetry line, at a distance of  $q = 0.73 \text{ \AA}$  from the (1,2)  $D_{3h}$  *cis*<sup>1</sup> (see Fig. 4.1).

The conclusion of this study is that the two-state quantization is fulfilled for a relatively large region surrounding the (1,2) *cis* (much beyond the “perturbation” region). However, it seems to be damaged by the third state once the region becomes large enough to include also the twin (2,3) *cis*. This situation is discussed further in Section 4.3.2.1.

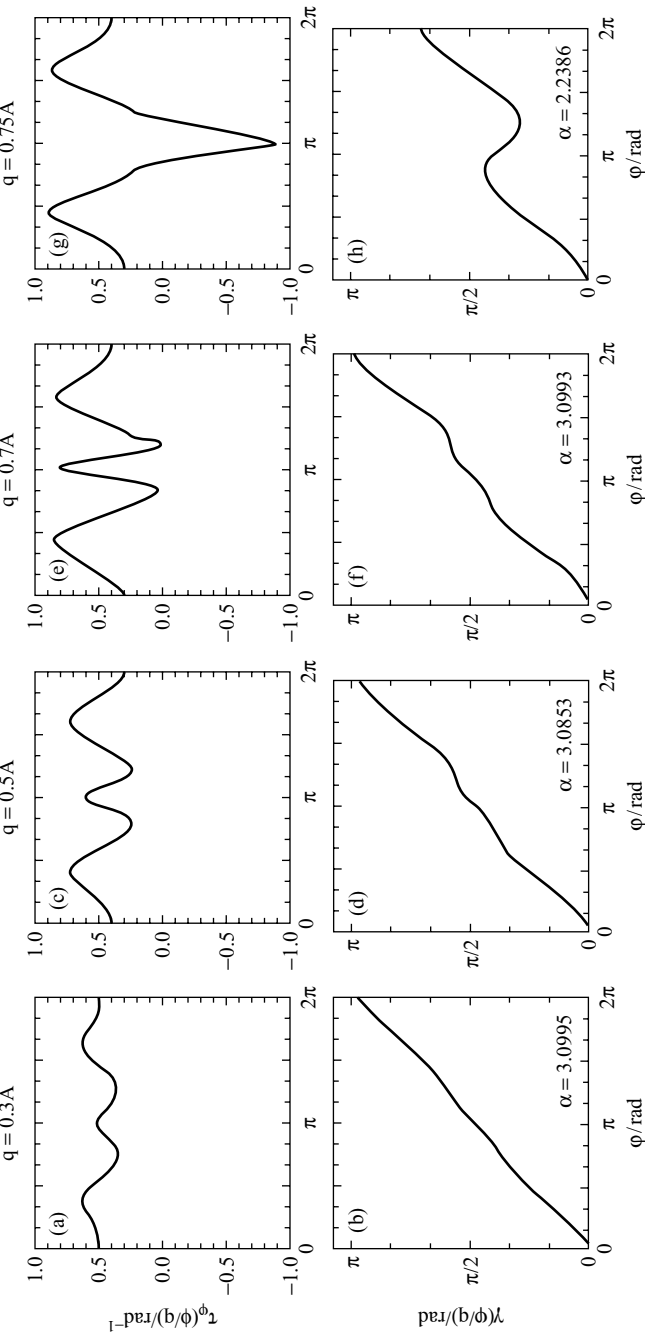


**Figure 4.2** Results for the fixed interatomic distance,  $R_{\text{HH}} = 1.044 \text{ \AA}$ , of the  $\{\text{H}_2, \text{H}\}$  system as obtained along circles located at the (1,2)  $cis$  and defined in terms of several radii  $q$ . Shown are the angular NACTs,  $\tau_{12\phi}(\varphi|q)$ , and the corresponding ADT angles,  $\gamma(\varphi|q)$  as calculated for four specified  $q$  values as listed in the figure. Note that the circular contours with  $q = 0.3, 0.5, 0.7 \text{ \AA}$  surround *only* the (1,2)  $cis$  but the circular contour with  $q = 0.75 \text{ \AA}$  surrounds three *cis*, namely, the (1,2)  $cis$  and the two (2,3)  $cis$ .

### 4.3.1.2 $\{H_2, O\}$ System

The ab initio calculation of the NACTs was carried out, as in the previous case, at the state-average CASSCF level employing the following basis functions.<sup>22</sup> For the oxygen we applied  $s$ ,  $p$ , and  $d$  functions from the aug-cc-pVQZ set and  $f$  functions from the cc-pVQZ set. For the hydrogens we employed  $s$  and  $p$  functions from the aug-cc-pVQZ set and  $d$  and  $f$  functions from the cc-pVQZ set. We used the active space including all eight valence electrons distributed on 10 orbitals. *Four* different electronic states, including the two studied states, were computed by the abovementioned state-average CASSCF method with equal weights. The required NACTs were obtained employing the MOLPRO program.<sup>21</sup>

As is known, the  $\{H_2, O\}$  system is characterized by two kinds of (1,2) *cis*: one located along collinear OHH arrangement channel and the other along the collinear HOH arrangement channel.<sup>23–27</sup> Here we consider only the *cis* belonging to the OHH configuration. To be more specific, we fixed the distance  $R_{OH}$  between the oxygen and the central hydrogen (i.e.,  $H_1$  in Fig. 4.3) and allowed the sideward hydrogen

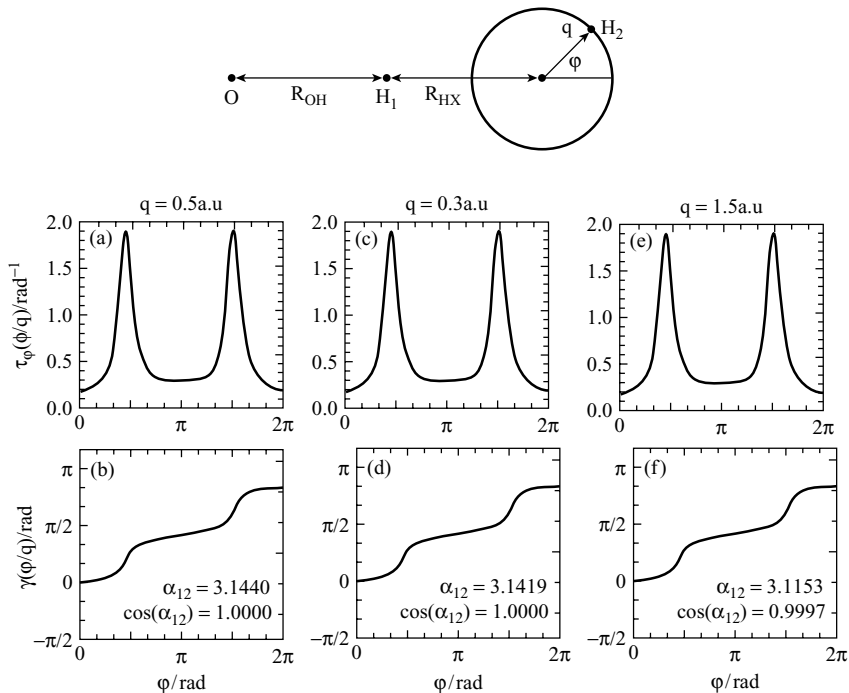


**Figure 4.3** Results related to the (1,2) *ci* for the collinear {OHH} arrangement as calculated along circles positioned at  $R_{HX}(=R_{HH})=1.6$  a.u. and different  $R_{OH}$  values. Panels (a) and (b) represent  $R_{OH}=2.5$  a.u. and  $q=0.5$  a.u.; panels (c) and (d),  $R_{OH}=3.0$  a.u. and  $q=0.3$  a.u.; panels (e) and (f),  $R_{OH}=3.0$  a.u. and  $q=1.5$  a.u. Panels (a), (c) and (e) present the angular NACTs,  $\tau_{\varphi 12}(\varphi|q)$  and panels (b), (d), and (f) present the ADT angle  $\gamma_{12}(\varphi|q)$ , both as a function of  $\varphi$ . A schematic representation of the configurations is given above each panel.

(i.e., H<sub>2</sub> in Fig. 4.3) to move along assumed circles surrounding the (1,2) *cis*. The results of this study are presented in Fig. 4.3. We note that the figure is arranged in columns—each column for one situation, specified by the abovementioned distance,  $R_{\text{OH}}$  and a radius  $q$  of the a specific circle [ $R_{\text{HX}}$ , the distance between H<sub>1</sub> and the position of the (1,2) *cis*, is fixed to be at 1.5 a.u. (atomic units)]. Each column contains two sets of panels; the upper panel presents the (angular) NACT  $\tau_{\varphi 12}(\varphi|q)$ , and the lower one shows the corresponding  $\gamma_{12}(\varphi|q)$  angle, both calculated along a circle and presented as a function of  $\varphi$ . In addition, each lower panel plots the corresponding values of  $\alpha_{12}(q)$  and  $\cos \alpha_{12}(q)$ . As for the shape of the curves, we note that they can be considered to be of the elliptic Jahn–Teller type (see Section 3.2.3 and Fig. 3.2). In this sense the present system differs from the {H<sub>2</sub>,H} system, which is a typical (circular) Jahn–Teller system.

Figure 4.3 shows results due to three circles and in all three of them the value of  $\alpha_{12}(q) \sim \pi$ . The most outstanding result is the one for  $q = 1.6$  a.u.; it is observed that although the circular contour is far away from the *cis*, the value of  $\alpha_{12}(q)$  is, for all practical purposes, still equal to  $\pi$ . This result contradicts all expectations because of the ability of the corresponding NACTs to form the value of  $\pi$  within such a large region—a result that cannot be justified, for instance, by perturbation theory. Our interpretation for this phenomenon is that inside the region surrounded by this large circle the system does not form any (2,3) *cis* so that the two lower states can form a quasiisolated two-state Hilbert subspace (see Section 2.1.3.1).

In this sense the two systems—{H<sub>2</sub>,H} and {H<sub>2</sub>,O}—behave differently. The two-state quantization for the {H<sub>2</sub>,O} system extends to large regions, whereas the quantization region for the {H<sub>2</sub>,H} system is relatively small [due to the existence of (2,3) *cis* as is discussed below].

#### 4.3.1.3 {C<sub>2</sub>,H<sub>2</sub>} System

The third system to be discussed is the four-atom molecule, C<sub>2</sub>H<sub>2</sub>. The electronic spectrum of the molecule has been a subject of numerous experimental<sup>28–31</sup> and numerical<sup>32–38</sup> studies (a detailed summary of studies related to this system can be found in Refs. 36 and 37). In this respect we mention that our preliminary results for acetylene are presented in Refs. 39 and 40. As in the two previous cases, here, too, the eigenfunctions and the eigenvalues are calculated at the state-average CASSCF level employing a 6-311G\*\* basis set.<sup>19</sup> We used the active space, including all 10 valence electrons distributed on 10 orbitals (a full-valence active space). Following convergence tests we included in the calculations, in addition to the four studied states (i.e., 1<sup>2</sup>A', 2<sup>2</sup>A', 3<sup>2</sup>A', and 4<sup>2</sup>A'), another four to six electronic states. The calculations were done employing the abovementioned state-average CASSCF method with equal weights.

In order to reveal the *cis* of this system, we restrict our study to a plane that contains all four atoms (in this way we have to consider five internal coordinates). Next, fixing the CC distance and the position of the l.h.s. hydrogen leaves the r.h.s. hydrogen free to move on this given plane (see Fig 4.4). The results to be presented are obtained for  $R_{\text{CC}} = 1.35$  Å,  $R_{\text{HC}} = 1.10$  Å, and  $\angle(\text{HCC}) = 109^\circ$ . In this section we discuss four *cis*, namely, one (1,2) *cis*, one (2,3) *cis*, and two (3,4) *cis* [designated as (3,4)<sub>x</sub> *cis*;

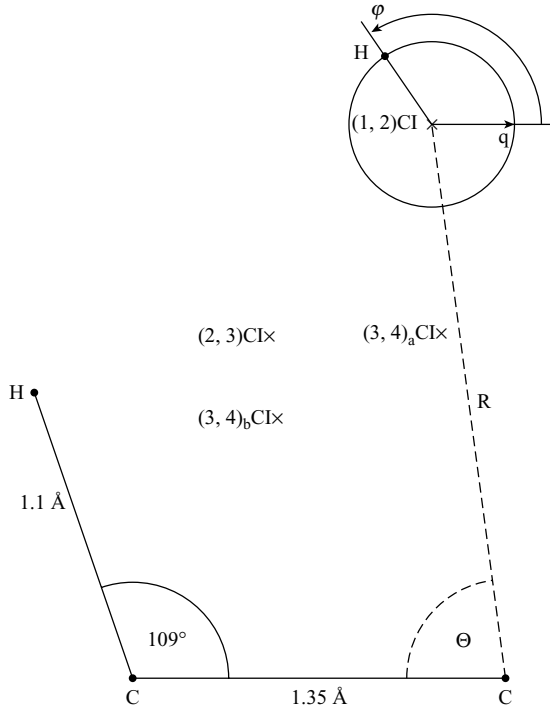


**Figure 4.4** The  $\{C_2H_2\}$  configuration and the four *cis* points for which the four angular NACTs,  $\tau_{\varphi jj+1}(\varphi|q)$ ;  $j = 1, 2, 3$ , were calculated. We present three fixed atoms, namely, one hydrogen (on the l.h.s.) and two carbons. The fourth hydrogen is moving on the plane that contains the four atoms. The calculations are done for  $R_{CC} = 1.35 \text{ \AA}$ ,  $R_{CH} = 1.10 \text{ \AA}$ , and  $\angle(HCC) = 109^\circ$ . The positions of the four  $(j, j + 1)$  *cis* with respect to the r.h.s. carbon are as follows:

$$(R_{XC}, \theta_{CCX}) = \{(2.04 \text{ \AA}, 82.7^\circ), (1.58 \text{ \AA}, 57.5^\circ), (1.37 \text{ \AA}, 80.0^\circ), (1.20 \text{ \AA}, 52.0^\circ)\}$$

$x = a, b]$  all located in the radial range between the two carbons (see Fig. 4.4). As is usually the case, this free-moving hydrogen is used as a test particle to locate *cis* and to examine their spatial intensities.

Figure 4.5 presents the corresponding, angular  $\varphi$ -dependent NACTs,  $\tau_{\varphi jj+1}(\varphi|q)$ ;  $j = 1, 2, 3$ , as calculated along equicentered circles that surround each of the four *cis* (12 cases altogether). In addition, the relevant topological phase  $\alpha_{jj+1}(q)$  is specified in each panel (a–l) (see Eq. (4.4)). The smallest radius,  $q$ , for each  $\tau_{\varphi jj+1}(\varphi|q)$  is chosen to show that in such a case the corresponding value of  $\alpha_{jj+1}(q)$  is, indeed, close to  $\pi$ , as expected. We encounter various shapes for the different NACTs, but the dominant shape is the double-hump shape. A double hump is, as mentioned earlier, typical for the elliptic Jahn–Teller model (see Section 3.2.3 and Fig. 3.2)—in particular, when the two humps are of identical size as, for instance, can be seen in panels (b) and (l). In most cases  $\alpha_{jj+1}(q)$  are close to  $\pi$  as expected, particularly for sufficiently small  $q$  values. In particular, we emphasize the encouraging results for the (1,2) NACT for which the double-hump structure survives even for relatively large  $q$  values.

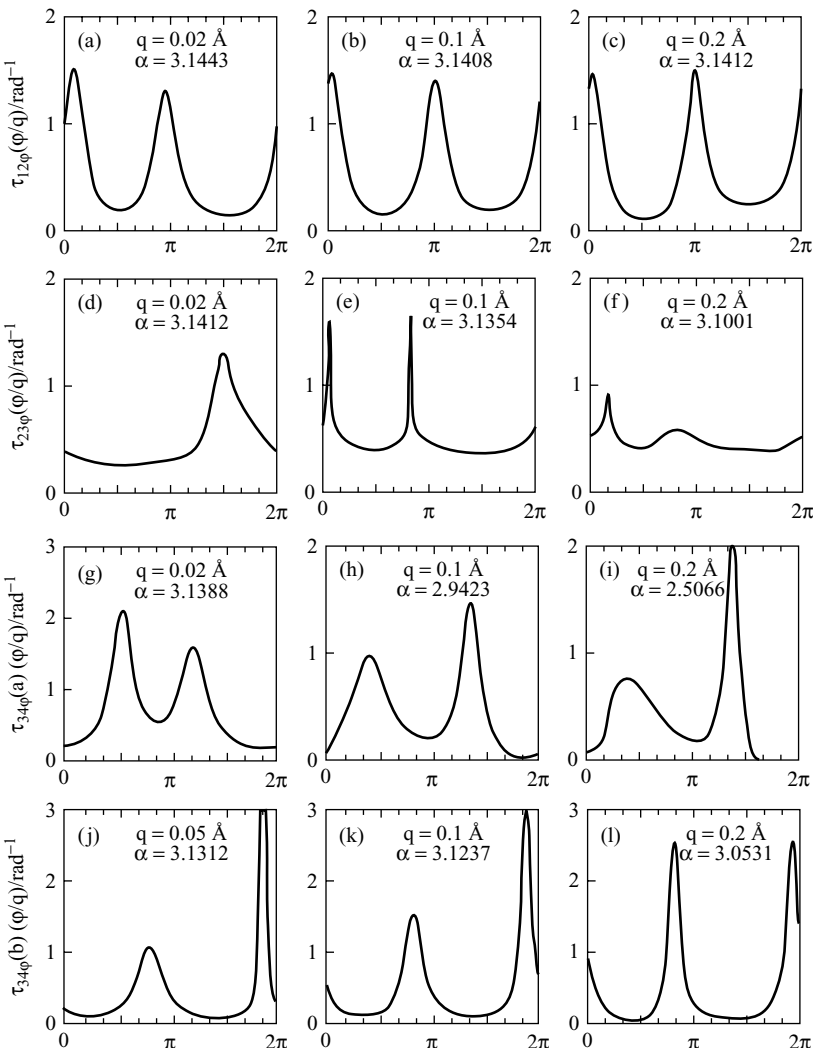


**Figure 4.5** The angular  $\varphi$ -dependent NACTs,  $\tau_{\varphi j j+1}(\varphi|q)$ ;  $j = 1, 2, 3$ , as calculated for acetylene along three different equicentered circles (characterized by different radii  $q$ ) that surround the four *cis* presented in Figure 4.4. The results for the (1,2) NACT, as calculated along circles centered at the (1,2) *ci*, are presented in panels (a)–(c); the results for the (2,3) NACT as calculated along circles centered at the (2,3) *ci*, are presented in panels (d)–(f); the results for the (3,4)<sub>a</sub> NACT as calculated along circles centered at the r.h.s. (3,4) *ci*, are presented in panels (g)–(i); and the results for the (3,4)<sub>b</sub> NACT as calculated along circles centered at the l.h.s. (3,4) *ci*, are presented in panels (j)–(l). Each panel also gives the corresponding value of the topological phase,  $\alpha_{jj+1}(q)$ .

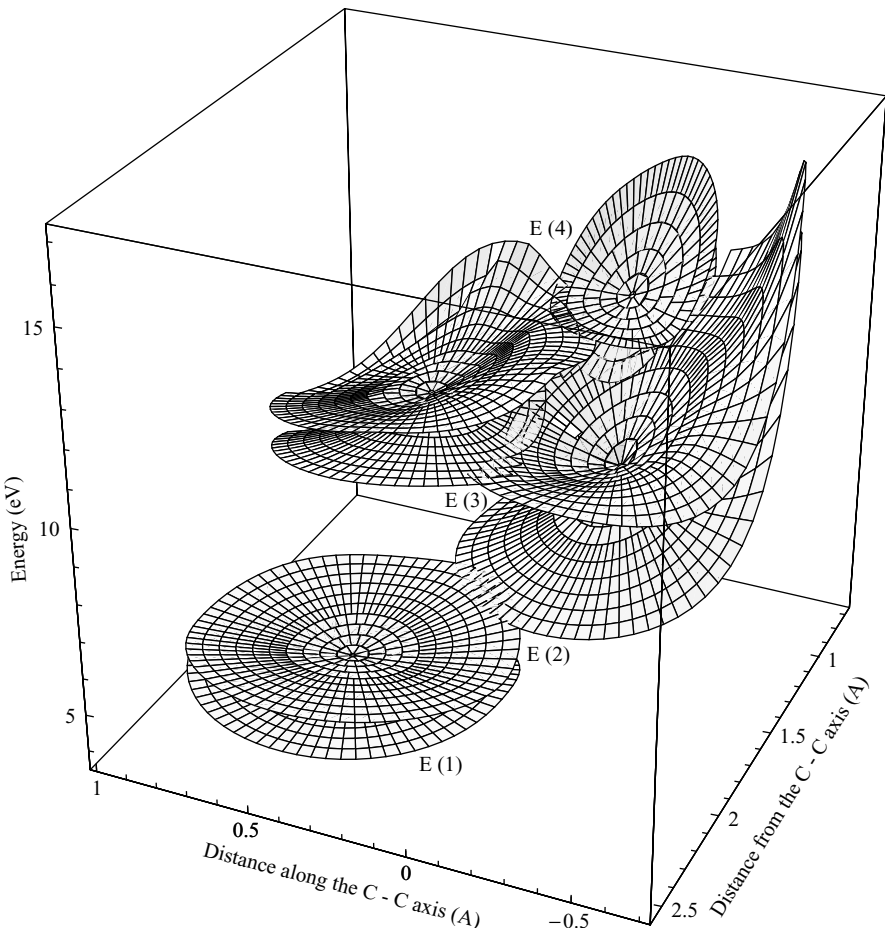


**Figure 4.6** A three-dimensional presentation of the four ab initio surfaces as calculated for acetylene for the configuration given in Figure 4.4. Also noted are the positions of the four *cis* points.

Figure 4.6 presents the four surfaces related to the first four lower  $A'$  states of acetylene. The figure emphasizes the existence of the four *cis* and shows how close they are located to each other. The values of the energies at the *cis* points (as compared to the collinear, ground-state, configuration:  $\{R_{HC}, R_{CC}, R_{CH}\} = \{1.076, 1.218, 1.076 \text{ \AA}\}$ ) are as follows:  $\{E_{12}, E_{23}, E_{34(a)}, E_{34(b)}\} = \{5.5, 9.1, 10.0, 11.2 \text{ eV}\}$ . The structure of the potential energy surfaces (PESs) and the corresponding *cis* points as presented in Figure 4.6 are interesting in the sense that they seem to form a system of *inlets* and *outlets* capable of driving a wavepacket, in a most efficient way, from the upper surface (in this case surface  $4^2 A'$ ) to the two lower surfaces, namely,  $1^2 A'$  and  $2^2 A'$ , which adiabatically are known to be related to the  $C_2H(X^2\Sigma)$  and  $C_2H(A^2\Pi)$  radicals,<sup>36</sup> respectively, by sheer potential gradients.

### 4.3.2 Multistate Quasiquantization

#### 4.3.2.1 $\{H_2, H\}$ System

We report here on NACTs, ADT angles, and, in particular, topological  $\mathbf{D}$ -matrix elements as calculated for three to five adiabatic states, where two hydrogens are at a fixed distance  $R_{HH} = 0.74 \text{ \AA}$ .<sup>40</sup> Four circular contours are considered, three of them centered, as in Section 4.2.2.1, at the (1,2)  $D_{3h}$  *cis* point with the radii  $q = 0.3, 0.4, 0.5 \text{ \AA}$  and the fourth, centered at a point shifted along the symmetry line by 0.25  $\text{\AA}$ , thus located at a distance of 0.89  $\text{\AA}$  from the HH axis (compared to 0.64  $\text{\AA}$  in the previous three cases), with radius  $q = 0.65 \text{ \AA}$ .

**Quasibreakup of  $\tau$  Matrix** Our first aim is to use this opportunity to show, employing ab initio results, that our assumption concerning the block structure of the  $\tau$  matrix as presented in Eq. (1.37) is encountered in real molecular systems. For this purpose, in Figure 4.7 we present 10 different  $\varphi$ -dependent NACTs, namely,  $\tau_{\varphi jk}(\varphi|q); j(< k) = 1,2,3,4$ , as calculated along the four circles mentioned above.

Here we emphasize the large values that are attached to the three tridiagonal elements  $\tau_{\varphi jj+1}; j = 1,2,4$ , formed by adjacent states [see Fig. 4.7 panels (a), (d), (g), (j), all in the first row], as compared to the values attached to the off-tridiagonal elements  $\tau_{\varphi jk}$  where  $k > j + 1$ , formed by nonadjacent states (see results presented in the two lower rows). Also, note the different scales used in the two types of figure panels (viz., those presented in the first row vs. those presented in the second and third rows); the ratio is 1 : 3.

Two additional observations are to be made:

1. The values of  $\tau_{\varphi 34}$  are exceptionally small, although they are formed by adjacent states (the third and fourth). These small values indicate that, most likely, no (3,4) *cis* exist in the regions given in Figure 4.7. This missing *cis*, in fact, the main reason for the formation of the  $3 \times 3$  upper block of the  $\tau$  matrix or, in other words, that the *three* lower states of the  $\{H_2, H\}$  system form a quasi-Hilbert subspace in these regions.
2. Out of all the *off-tridiagonal* elements,  $\tau_{\varphi 13}$  is the largest one. The reason is attributed to the overlap between  $\tau_{12}$  and  $\tau_{23}$ ,<sup>18,41</sup> which, according to the Curl equation, is responsible for forming this matrix element [see Eq. (6.35c) and, in particular, the following discussion on multistate quantization for the  $\{H_2, H\}$  system].

**Multistate Quantization for  $\{H_2, H\}$  System** The measure for the quantization of the  $\tau$  matrix is given in terms of the relevant topological  $\mathbf{D}$  matrix (discussed in Section 2.1.3.1 and in particular Eq. (2.32)]. According to the theory, an  $N$ -dimensional  $\tau$  matrix is quantized if the corresponding topological matrix,  $\mathbf{D}(N)$ , is diagonal (thus having  $\pm 1$  in its diagonal). Table 4.2 are presented the diagonal elements of the  $\mathbf{D}(N)$ , namely,  $\mathbf{D}_{jj}(q|N); j = 1, \dots, N$  as calculated for different  $N$  values, specifically,  $N = 2,3,4,5$  and different circles.<sup>40</sup>

Since in this analysis we also refer to the (4,5) *cis*, we briefly discuss this *cis* as it was not mentioned before. Within the numerical study as described earlier, the (4,5)

**TABLE 4.2** Diagonal Elements of Topological D Matrix as a Function of  $N$  Calculated for  $\{\mathbf{H}_2, \mathbf{H}\}$  System along Different Closed Contours

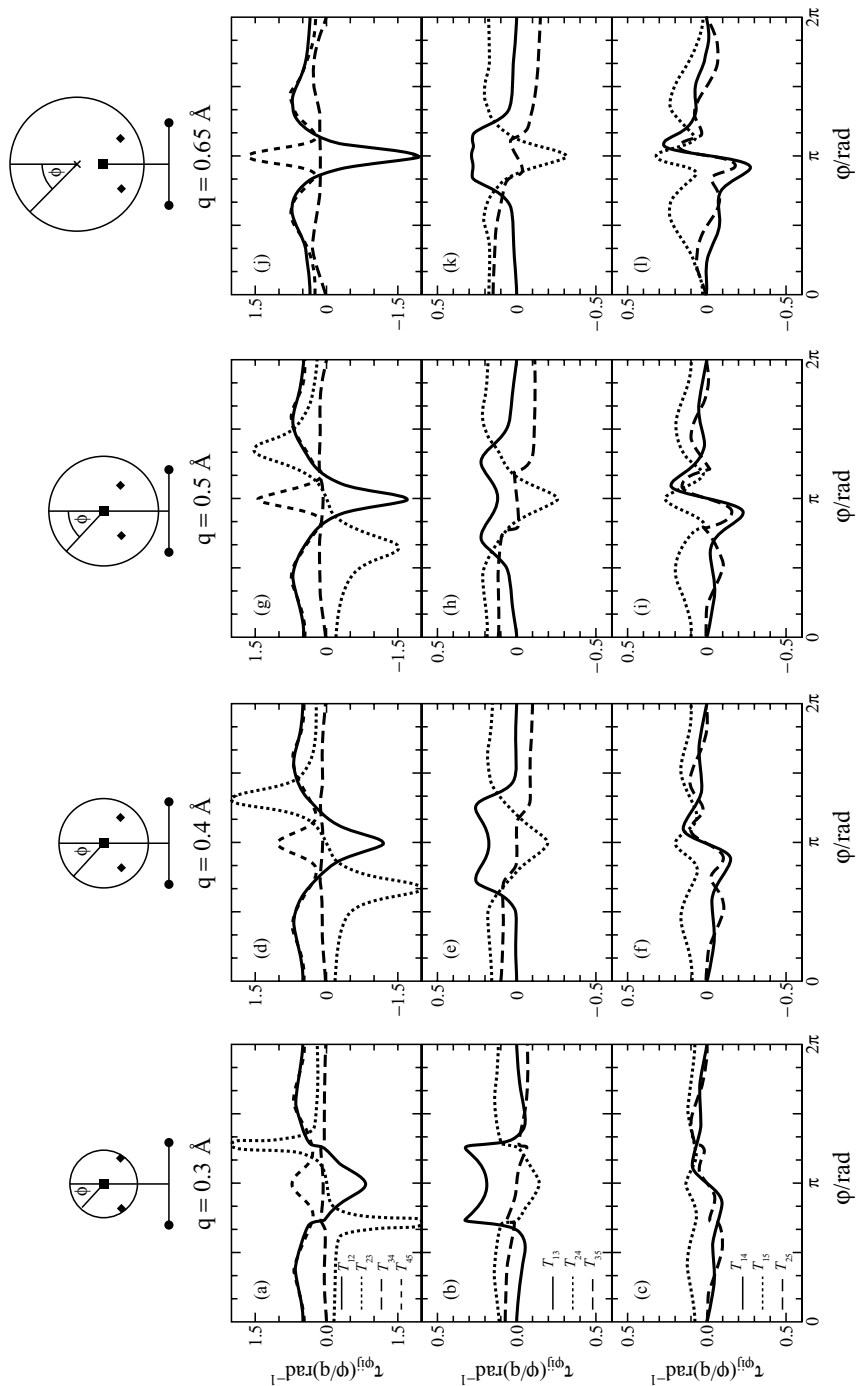
| $N$<br>$q$ (radius <sup>a</sup> ) | —        | 2                   | 3      | 4      | 5      |
|-----------------------------------|----------|---------------------|--------|--------|--------|
| 0.3 <sup>b</sup>                  | $D_{11}$ | -0.292 <sup>d</sup> | -0.986 | -0.810 | -0.995 |
|                                   | $D_{22}$ | -0.292 <sup>d</sup> | -0.986 | -0.996 | -0.996 |
|                                   | $D_{33}$ | —                   | +1.000 | +0.984 | +0.999 |
|                                   | $D_{44}$ | -0.998 <sup>e</sup> | —      | -0.798 | -0.991 |
|                                   | $D_{55}$ | -0.998 <sup>e</sup> | —      | —      | -0.990 |
| 0.4 <sup>b</sup>                  | $D_{11}$ | -0.361 <sup>d</sup> | -0.966 | -0.714 | -0.992 |
|                                   | $D_{22}$ | -0.361 <sup>d</sup> | -0.966 | -0.993 | -0.991 |
|                                   | $D_{33}$ | —                   | +0.999 | +0.963 | +0.997 |
|                                   | $D_{44}$ | -0.991 <sup>e</sup> | —      | -0.684 | -0.931 |
|                                   | $D_{55}$ | -0.991 <sup>e</sup> | —      | —      | -0.925 |
| 0.5 <sup>b</sup>                  | $D_{11}$ | -0.404 <sup>d</sup> | -0.940 | -0.629 | -0.986 |
|                                   | $D_{22}$ | -0.404 <sup>d</sup> | -0.938 | -0.990 | -0.985 |
|                                   | $D_{33}$ | —                   | +0.999 | +0.936 | +0.993 |
|                                   | $D_{44}$ | -0.975 <sup>e</sup> | —      | -0.576 | -0.931 |
|                                   | $D_{55}$ | -0.975 <sup>e</sup> | —      | —      | -0.925 |
| 0.65 <sup>c</sup>                 | $D_{11}$ | -0.406 <sup>d</sup> | -0.935 | -0.614 | -0.982 |
|                                   | $D_{22}$ | -0.406 <sup>d</sup> | -0.921 | -0.995 | -0.982 |
|                                   | $D_{33}$ | —                   | +0.986 | +0.674 | +0.987 |
|                                   | $D_{44}$ | -1.000 <sup>e</sup> | —      | -0.293 | -0.974 |
|                                   | $D_{55}$ | -1.000 <sup>e</sup> | —      | —      | -0.961 |

<sup>a</sup> Values in anstroms ( $\text{\AA}$ ).<sup>b</sup> Center at  $D_{3h}$  point.<sup>c</sup> Center, removed from  $D_{3h}$  point, by 0.25  $\text{\AA}$  “northway.”<sup>d</sup> Values for  $\cos \alpha_{12}$  where  $\alpha_{12}$  is calculated employing Eq. (4.4) for the (1,2) *ci*.<sup>e</sup> Values for  $\cos \alpha_{45}$  where  $\alpha_{45}$  is calculated employing Eq. (4.4) for the (4,5) *ci*.

$D_{3h}$  *ci* was revealed by employing Eq. (4.4) for  $\tau_{\varphi 45}$  to calculate  $\alpha_{45}$ . The results of this calculation are presented in Table 4.2 (third column, i.e.,  $N = 2$ ), where we show  $\mathbf{D}_{44}(q) = \mathbf{D}_{55}(q)$  ( $\equiv \cos \alpha_{45}$ ).

Returning now to the more general cases in Table 4.2, the following is to be noted:

1. Inspecting values of  $\mathbf{D}_{11}(q)$  ( $= \mathbf{D}_{22}(q)$ ) as calculated assuming  $N = 2$ , we see that these are far from being  $(-1)$ , the expected value. This result implies, as already mentioned in Section 4.3.1.2, that in the region surrounded by the circle with  $q = 0.3 \text{ \AA}$  [in this case the corresponding region contains also the (2,3) *cis*—see Fig. 4.7)], the corresponding  $2 \times 2 \tau$  matrix element, namely,  $\tau_{12}$ , is not quantized. The situation improves significantly once a third state is added. It is noted that the three  $\mathbf{D}$ -matrix elements are close to  $\pm 1$ , which implies that the three lower states form, approximately, a reasonably quantized  $\tau$  matrix; however, this quantization slowly deteriorates as the spatial region increases (compare results along the  $N = 3$  column for different  $q$  values).



2. Adding the two upper states (i.e., states 4 and 5), we note that for the smaller regions, the quantization holds for both the three lower states and the two upper states separately. This implies that the five-dimensional  $\tau$  matrix breaks up into two blocks: the lower part of dimension  $3 \times 3$  and the upper one of dimension  $2 \times 2$ . The main reason for this breakup is, as discussed earlier, the missing (3,4) *cis* in the region of interest.<sup>40</sup>

3. It is observed that increasing the dimension of the  $\tau$  matrix from 3 to 4 does not improve the quantization quality (cf. values along  $N = 3$  and the  $N = 4$  columns). In fact, the quality of the four diagonal  $\mathbf{D}$ -matrix elements deteriorated because the fourth state is strongly coupled with the fifth state [recall the existence of the (4,5) *cis*], and this coupling is ignored, thus affecting the conditions to achieve the quantization.

4. Increasing the dimension of the  $\tau$  matrix from  $N = 3$  to  $N = 5$  improves the quantization quality altogether. This is clearly evident while inspecting the five diagonal elements of the  $\mathbf{D}$  matrix (for each region) as presented in the last column. This addition improves not only the four-state quantization but even the three-state quantization—in particular the quantization for the larger regions (cf. results for  $q = 0.5$  and  $0.65 \text{ \AA}$ ).

5. Interesting and encouraging results are obtained for the region surrounded by the shifted circle (by  $0.25 \text{ \AA}$  from the  $D_{3h}$  point) with  $q = 0.65 \text{ \AA}$  (see results for the last five rows). Doing this shift enabled the increase of the relevant *circular* region without getting too close to the fixed hydrogens axis. We note that although the spatial region surrounded by this circle is almost doubled (compared to the one for  $q = 0.5 \text{ \AA}$ ), its diagonal  $\mathbf{D}$ -matrix elements are of the same quality. This implies that the slow deterioration of the nice quantization (along the first three regions) as  $q$  increases is not necessarily connected to the size of the region but can sometimes be attributed to the effect (damage) caused by the presence of the (fixed) atoms close to this region, in this case the two hydrogens.

### 4.3.2.2 $\{\mathbf{C}_2, \mathbf{H}\}$ System

As in Section 4.3.2.1, here, too, we concentrate on a three-state Hilbert subspace. For this purpose we consider the three *excited* states  $2^2A'$ ,  $3^2A'$  and  $4^2A'$  of the title

---

**Figure 4.7** Angular NACTs,  $\tau_{\varphi ij}(\varphi|q); i < j(i = 1, 2, 3, 4)$ , as calculated for the  $\{\text{H}_2, \text{H}\}$  system for  $R_{\text{HH}} = 0.74 \text{ \AA}$ . Panels (a)–(c) present results as calculated along a circle located at the (1,2)  $D_{3h}$  *cis* with radius  $q = 0.3 \text{ \AA}$ , panels (d)–(f) present results as calculated along a circle located at the (1,2)  $D_{3h}$  *cis* with radius  $q = 0.4 \text{ \AA}$ , panels (g)–(i) present results as calculated along a circle located at the (1,2)  $D_{3h}$  *cis* with radius  $q = 0.5 \text{ \AA}$  and panels (j)–(l) present results as calculated along a circle located at a point (designated as  $\times$ ) on the symmetry line shifted by  $0.25 \text{ \AA}$  from the (1,2)  $D_{3h}$  *cis* with radius  $q = 0.65 \text{ \AA}$ . It is important to emphasize that the  $D_{3h}$  (4,5) *cis* is located, in exactly the same way as is the  $D_{3h}$  (1,2) *cis*, at the equilateral position. Enlarged dots designate the two fixed hydrogens, solid squares denote the (1,2) *cis* points [and also the (4,5) *cis* points], solid diamonds designate the (2,3) *cis* points, and the circles describe the contours along which the  $\tau_{\varphi ij}(\varphi|q)$  were calculated. The straight line perpendicular to the HH axis connects the center-of-mass point of the two (fixed) hydrogens and the  $D_{3h}$  *cis* point. Note the *different scale* in panels (b), (c), (e), (f), (h), (i), (k), and (l) in contrast to the scale in panels (a), (d), (g) and (j).

system that were found to form, approximately, such a subspace.<sup>42</sup> The NACTs in this case are due to one (2,3) *cis*—a  $C_{2v}$  *cis*—located on the symmetry line that passes through the center-of-mass point of the two carbons and is perpendicular to the CC axis (sometimes referred to as the  $C_{2v}$  symmetry line) and two twin (3,4) *cis* located on both sides of this line in close vicinity to the (2,3) *cis*<sup>42</sup> (see Fig. 4.8). The (1,2)

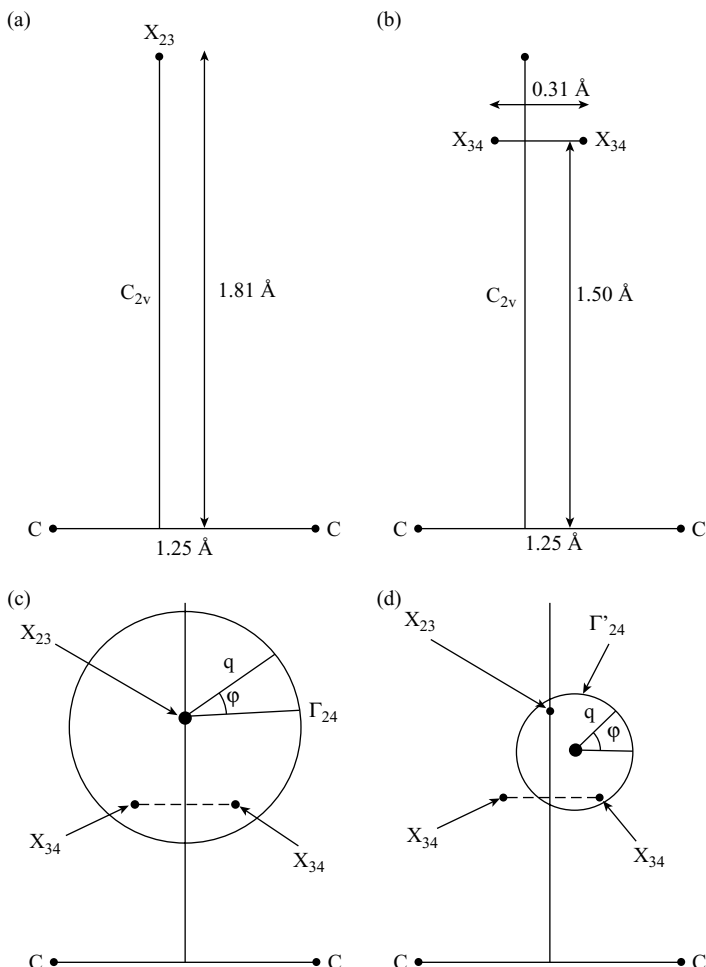


**Figure 4.8** This figure presents geometric magnitudes related to the  $\{\text{C}_2, \text{H}\}$  system as calculated for the interatomic distance  $R_{\text{CC}} = 1.25 \text{ \AA}$ . Panel (a) gives the geometric position of the (2,3) *cis* (designated as  $X_{23}$ ) that couples the  $2^2 \text{A}'$  and  $3^2 \text{A}'$  states; panel (b) gives the geometric positions of the two (3,4) *cis* twins (designated as  $X_{34}$ ) that couple the  $3^2 \text{A}'$  and the  $4^2 \text{A}'$  states. Panels (c) and (d) show the circular contours along which the ADT  $\mathbf{A}$ -matrix and the topological  $\mathbf{D}$ -matrix elements are calculated. In panel (c) circle  $\Gamma_{24}$ , for  $q = 0.4 \text{ \AA}$ , is centered on the  $C_{2v}$  line, at the (2,3) *cis*; in panel (d) circle  $\Gamma'_{24}$  for  $q = 0.2 \text{ \AA}$ , is centered at the midway between the (2,3) *cis* and the r.h.s. (3,4) *cis*. Circle  $\Gamma_{24}$  surrounds all three *cis*, namely, the (2,3) *cis* and the two (3,4) *cis*, while circle  $\Gamma'_{24}$  surrounds only two *cis*, namely, the (2,3) *cis* and one (3,4) *cis*.

NACT, revealed in earlier studies,<sup>43</sup> was found not to interact with the (2,3) NACT as not only are the two *cis* located too far from each other<sup>44,45</sup> but also their NACTs only slightly overlap.<sup>41,46</sup> In the same way the (4,5) *cis* are located far away from the symmetry line and therefore, in this case too, the overlap between the (4,5) and (3,4) NACTs is negligible.<sup>45</sup>

Ab initio calculations were carried out at the state-average CASSCF level with the 6-311G\*\* basis set. We used the active space, including all nine valence electrons distributed on nine orbitals (full-valence active space). Four different electronic states, namely,  $1^2 A'$ ,  $2^2 A'$ ,  $3^2 A'$ , and  $4^2 A'$  were computed by the state-average CASSCF with equal weights, employing MOLPRO<sup>21</sup>.

We report on the diagonal elements  $\mathbf{A}_{jj}(\varphi|q); j = 1, 2, 3$  of the ADT matrix [see Eq. (4.5)] and the corresponding diagonal elements of the **D** matrix [see Eq. (4.6)] as calculated for the situation where two carbon atoms are at a fixed distance  $R_{CC} = 1.25 \text{ \AA}$ . For this situation we find that the (2,3)  $C_{2v}$  *cis* is located at a distance of 1.81 Å from the CC axis and the two (3,4) *ci* twins are located at a distance of 1.50 Å from the CC axis and at a distance of 0.31 Å apart from each other (see Figs. 4.8a and 4.8b). The calculations are done along two contours,  $\Gamma_{24}$  and  $\Gamma'_{24}$  (see Figs. 4.8c and 4.8d, respectively). It is important to mention that in order to solve for **A** and **D**, we employ the procedure described in Section 1.3.3 and in particular, use series of ordered products as given in Eq. (1.91).

We start by reporting the results for the **A** matrix as calculated along  $\Gamma'_{24}$ . For this purpose we need the three NACM elements, namely,  $\tau_{23}(\varphi|q)$ ,  $\tau_{34}(\varphi|q)$ , and  $\tau_{24}(\varphi|q)$ , presented, as a function of  $\varphi$ , in Figures 4.9a, 4.9b, and 4.9c, respectively. The three *diagonal* terms of the  $\mathbf{A}(\varphi|q)$  matrix are shown in Figure 4.9d. The integration along the contour is started with an **A** matrix that is the unit matrix. We expect to find at the end of the circular contour, namely, at  $\varphi = \varphi_N (= 2\pi)$ , the matrix  $\mathbf{A}(\varphi_N|q)$  that is diagonal and whose elements are one (+1) and two (-1)s. The position of the (+1) along the diagonal depends on the chosen contour. As is noted from the figure, we obtain the following series  $(- + -)$ . More details are given in Ref. 42, but see also discussion in Section 5.3.2 related to Eq. (5.20).

The end values of the **A** matrix, just mentioned, are the **D**-matrix elements, and these values, as calculated along the two contours,  $\Gamma_{24}$  and  $\Gamma'_{24}$  in Figures 4.8c and 4.8d, are presented in Table 4.3. The following is to be noted:

1. The first three columns in the Table 4.3 give the three diagonal elements of the **D** matrix:  $\mathbf{D}_{kk}(q); k = 1, 2, 3$ . We pay attention to two features: (a) how close the values of  $\mathbf{D}_{kk}(q)$  are to the numbers to  $\pm 1$  and (b) the order of the minus signs along the diagonal. As for the first feature, the closer the numbers are to  $\pm 1$ , the more pronounced is the three-state *quantization*. As for the second feature, we encounter for the contour  $\Gamma_{24}$  the sign series  $(- - +)$  and for the  $\Gamma'_{24}$  contour the sign series  $(- + -)$ . In other words, the positions of the + sign along the diagonal of the **D** matrix are seen to depend on the chosen contour. At this stage we are not yet fully able to discuss the difference between the two situations. This is done in Section 5.3.2.

2. In the fifth and the sixth columns of Table 4.3 the cosine values, namely,  $\cos \alpha_{jj+1}$ ,  $j = 2, 3$ , respectively, are presented, where  $\alpha_{jj+1}$  is the corresponding

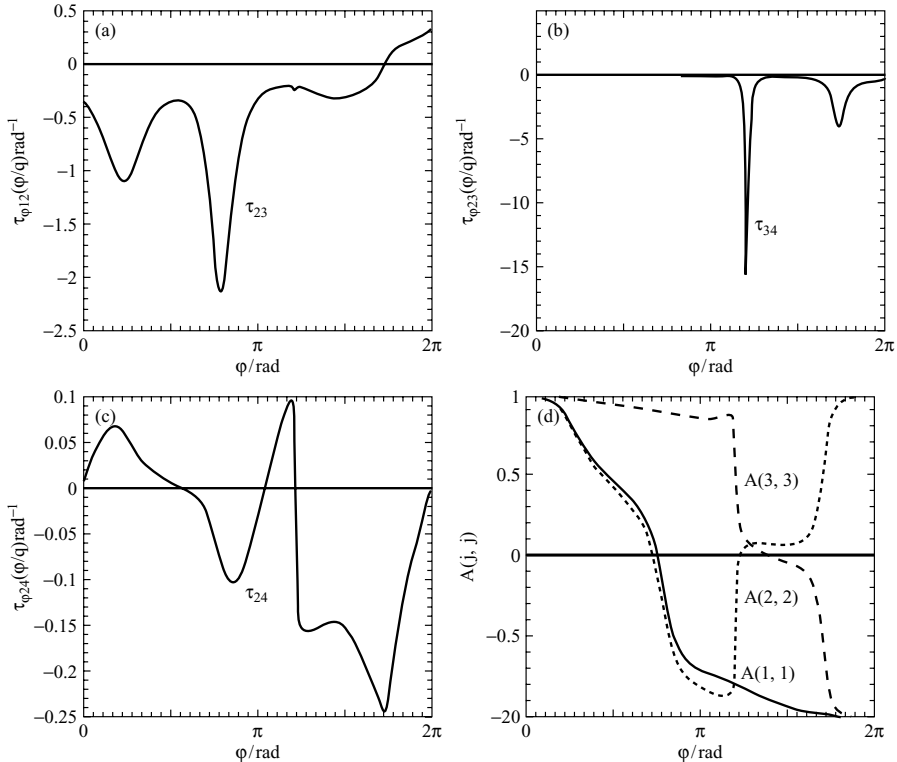


**Figure 4.9** The three elements of the angular NACM, namely,  $\tau_{12}$  ( $\equiv \tau_{23\varphi}(\varphi|q)$ ),  $\tau_{23}$  ( $\equiv \tau_{34\varphi}(\varphi|q)$ ), and  $\tau_{13}$  ( $\equiv \tau_{24\varphi}(\varphi|q)$ ) and the corresponding three diagonal elements of the ADT matrix,  $A_{jj}(\varphi|q)$ ;  $j = 1, 2, 3$  as calculated for the  $\{\text{C}_2, \text{H}\}$  system, along the contour  $\Gamma'_{24}$  that surrounds the (2,3) *cis* and *one* of the two (3,4) *cis* (see contour in Fig. 4.8d). The NACTs are presented in panels (a)–(c) and the ADT matrix elements, in (d).

topological phase [see Eq. (4.4)]. In case the (2,3) states and/or the (3,4) states form a two-state Hilbert subspace, the values of the relevant cosine functions are expected to be (a)  $\cos \alpha_{23} = (-1)$  for the (2,3) pair and (b) either  $\cos \alpha_{34} = (+1)$  (for the contour  $\Gamma_{24}$ ) or  $\cos \alpha_{34} = (-1)$  (for the contour  $\Gamma'_{24}$ ). As can be seen, in all four cases the ab initio values of the cosine functions are significantly different from the expected  $\pm 1$  values. These findings indicate that none of the two pairs of states form a two-state

**TABLE 4.3** Diagonal Elements of  $3 \times 3$  D Matrix and Corresponding Two-State Cosine Values as Calculated for  $\{\text{C}_2, \text{H}\}$  Molecule along Two Closed Contours

| Contour        | $D_{11}$ | $D_{22}$ | $D_{33}$ | $\cos \alpha_{23}$ | $\cos \alpha_{34}$ |
|----------------|----------|----------|----------|--------------------|--------------------|
| $\Gamma_{24}$  | -0.990   | -0.988   | +0.997   | -0.318             | +0.752             |
| $\Gamma'_{24}$ | -1.000   | +1.000   | -1.000   | -0.960             | -0.891             |

Hilbert subspace in the region of interest [cf., e.g., values for the {H<sub>2</sub>,O} system in Section 4.3.1.2 as presented in Fig. 4.3].

## REFERENCES

### Section 4.1

1. M. Baer and A. Alijah, *Chem. Phys. Lett.* **319**, 489 (2000).
2. M. Baer, *J. Phys. Chem.* **104**, 3181 (2000).
3. M. Baer, S. H. Lin, A. Alijah, S. Adhikari, and G. D. Billing, *Phys. Rev. A* **62**, 032506-1 (2000).
4. M. Baer, *Phys. Rep.* **358**, 75 (2002).

### Section 4.2

1. E. Renner, *Z. Phys.* **92**, 172 (1934).
2. H. C. Longuet-Higgins, *Adv. Spectrosc.* **2**, 429 (1961).
3. C. A. Mead, *J. Chem. Phys.* **78**, 807 (1983).
4. D. R. Yarkony, *J. Chem. Phys.* **105**, 10456 (1996).
5. M. Baer and A. Alijah, *Chem. Phys. Lett.* **319**, 489 (2000).
6. M. Baer, *J. Phys. Chem.* **104**, 3181 (2000).
7. M. Baer, S. H. Lin, A. Alijah, S. Adhikari, and G. D. Billing, *Phys. Rev. A* **62**, 032506-1 (2000).
8. A. M. Mebel, G. J. Halász, Á. Vibók, A. Alijah, and M. Baer, *J. Chem. Phys.* **117**, 991 (2002).
9. M. Baer, T. Vértesi, G. J. Halász, Á. Vibók, and S. Suhai, *Faraday Disc.* **127**, 337 (2004).
10. P. E. S. Wormer, *The Original Renner–Teller Effect* (preprint).

### Section 4.3

1. G. Halász, Á. Vibók, A. M. Mebel and M. Baer, *Chem. Phys. Lett.* **358**, 163 (2002).
2. H. C. Longuet-Higgins, *Proc. Roy. Soc., Lond. A* **344**, 147 (1975).
3. E. R. Davidson, *J. Am. Chem. Soc.* **99**, 397 (1977).
4. B. Lepetit and A. Kuppermann, *Chem. Phys. Lett.* **166**, 581 (1990).
5. M. S. Child, in *The Role of Degenerate States in Chemistry*, M. Baer and G. D. Billing, eds., *Adv. Chem. Phys.* **124**, 1 (2002).
6. H. A. Jahn and E. Teller, *Proc. Roy. Soc. Lond. A* **161**, 220 (1937).
7. G. Herzberg and H. C. Longuet-Higgins, *Disc. Faraday Soc.* **35**, 77 (1963).
8. M. Baer and R. Englman, *Molec. Phys.* **75**, 293 (1992).
9. D. R. Yarkony, *J. Chem. Phys.* **105**, 10456 (1996).
10. M. Baer, *J. Chem. Phys.* **107**, 2694 (1997).
11. R. Xu, M. Baer, and A. J. C. Varandas, *J. Chem. Phys.* **112**, 2746 (2000).
12. R. Abrol, A. Shaw, A. Kuppermann, and D. R. Yarkony, *J. Chem. Phys.* **115**, 4640 (2001).

13. R. Abrol and A. Kuppermann, *J. Chem. Phys.* **116**, 1035 (2002).
14. A. Kuppermann and R. Abrol, in *The Role of Degenerate States in Chemistry*, M. Baer and G. D. Billing, eds., *Adv. Chem. Phys.* **124**, 283 (2002).
15. G. Halász, Á. Vibók, A. M. Mebel, and M. Baer, *J. Chem. Phys.* **118**, 3052 (2003).
16. A. J. C. Varandas, in *Fundamental World of Quantum Chemistry*, E. J. Brandas and E. S. Kryachko, eds., Kluwer Academic Publishers, 2003, Vol. II, p. 32.
17. S. Han and D. R. Yarkony, *J. Chem. Phys.* **119**, 5058 (2003).
18. T. Vértesi, Á. Vibók, G. J. Halász, and M. Baer, *J. Chem. Phys.* **121**, 4000 (2004).
19. R. Krishnan, M. Frisch, and J. A. Pople, *J. Chem. Phys.* **72**, 4244 (1980).
20. D. F. Feller and K. Ruedenberg, *Theor. Chim. Acta* **52**, 231 (1978).
21. MOLPRO is a package of ab initio programs written by H.-J. Werner and P. J. Knowles, with contributions from J. Almlöf et al.
22. Á. Vibók, G. J. Halász, and M. Baer, *Chem. Phys. Lett.* **399**, 7 (2004).
23. J. Murrel, S. Carter, I. M. Mills, and M. F. Guest, *Molec. Phys.* **42**, 605 (1980).
24. G. Durand and X. Chapuisat, *Chem. Phys.* **96**, 381 (1985).
25. R. Polak, I. Paidarova, and P. J. Kuntz, *J. Chem. Phys.* **87**, 2863 (1987).
26. A. J. Dobbyn and P. J. Knowles, *Molec. Phys.* **91**, 1107 (1997).
27. D. R. Yarkony, *Molec. Phys.* **93**, 971 (1998).
28. C. W. King and C. K. Ingold, *Nature* (London) **169**, 1101 (1952).
29. P. D. Foo and K. K. Innes, *Chem. Phys. Lett.* **22**, 439 (1973).
30. P. Dupre, P. G. Green, and R. W. Field, *Chem. Phys.* **196**, 221 (1995).
31. J. Zhang, C. W. Riehn, M. Dulligan, and C. Wittig, *J. Chem. Phys.* **103**, 5860 (1995).
32. D. Dmoulin and M. Jungén, *Theor. Chim. Acta* **34**, 1 (1974).
33. H. Lischka and A. Karpfen, *Chem. Phys.* **102**, 77 (1986).
34. Y. Yamaguchi, G. Vacek, and H. F. Schaefer III, *Theor. Chim. Acta* **86**, 97 (1993).
35. J. F. Stanton, C. M. Huang, and P. G. Szalay, *J. Chem. Phys.* **101**, 356 (1994).
36. Q. Cui, K. Morokuma, and J. F. Stanton, *Chem. Phys. Lett.* **263**, 46 (1996).
37. E. Ventura, M. Dallos, and H. Lischka, *J. Chem. Phys.* **118**, 1702 (2003).
38. H. Koppel, *Faraday Disc.* **127**, 35 (2004).
39. Á. Vibók, G. J. Halász and M. Baer, *Chem. Phys. Lett.* **413**, 226 (2005).
40. M. Baer, T. Vértesi, G. J. Halász, Á. Vibók, and S. Suhai, *Faraday Disc.* **127**, 337 (2004).
41. M. Baer, A. M. Mebel, and G. D. Billing, *Int. J. Quant. Chem.* **90**, 1577 (2002).
42. A. M. Mebel, G. J. Halász, Á. Vibók, A. Alijha, and M. Baer, *J. Chem. Phys.* **117**, 991 (2002).
43. A. Mebel, M. Baer, and S. H. Lin, *J. Chem. Phys.* **112**, 10703 (2000).
44. A. M. Mebel, M. Baer, V. M. Rozenbaum, and S. H. Lin, *Chem. Phys. Lett.* **336**, 135 (2001).
45. A. M. Mebel, A. Yahalom, R. Englman, and M. Baer, *J. Chem. Phys.* **115**, 3673 (2001).
46. M. Baer, A. M. Mebel, and G. D. Billing, *J. Phys. Chem.* **106**, 6499 (2002).

# CHAPTER 5

---

## DEGENERACY POINTS AND BORN–OPPENHEIMER COUPLING TERMS AS POLES

---

### 5.1 RELATION BETWEEN BORN–OPPENHEIMER COUPLING TERMS AND DEGENERACY POINTS

In the late 1930s, Hellmann<sup>1</sup> and Feynman<sup>2</sup> independently derived a relation now known as the Hellmann–Feynman theorem, which enables the calculation of forces that directly act on molecules. It turns out that the Hellmann–Feynman theorem can be extended to a situation that yields a closed formula for the NACTs. This extension is attributed to Epstein,<sup>3</sup> as was recommended by Singh and Singh in 1989.<sup>4</sup>

Theorem 5.1 connects the NACTs and the topography of the Born–Oppenheimer surfaces and in particular refers to the possibility that NACTs may become singular at points where the Born–Oppenheimer surfaces become degenerate.

**Theorem 5.1** Considering two states  $j$  and  $k$  defined in terms of their two adiabatic eigenfunctions  $|\zeta_j(\mathbf{s}_e|\mathbf{s})\rangle$  and  $|\zeta_k(\mathbf{s}_e|\mathbf{s})\rangle$ , the corresponding NACT,  $\tau_{jk}(\mathbf{s})$ , fulfills the following relation

$$\tau_{jk} = \frac{\langle \zeta_j | \nabla \mathbf{H}_e | \zeta_k \rangle}{u_k - u_j} \quad (5.1)$$

where  $u_k$  and  $u_j$  are the two corresponding eigenvalues and  $\nabla$  is a grad operator with respect to the nuclear coordinates.

*Proof* To prove the theorem, we consider, following Eq. (1.1), the expression

$$\mathbf{H}_e(\mathbf{s}_e|\mathbf{s})|\zeta_k(\mathbf{s}_e|\mathbf{s})\rangle - u_k(s)|\zeta_k(\mathbf{s}_e|\mathbf{s})\rangle = 0; \quad k = 1, \dots, N \quad (5.2)$$

---

*Beyond Born–Oppenheimer: Conical Intersections and Electronic Nonadiabatic Coupling Terms*  
By Michael Baer. Copyright © 2006 John Wiley & Sons, Inc.

and differentiate it, employing the grad operator:

$$\nabla \mathbf{H}_e(\mathbf{s}_e|\mathbf{s})|\zeta_k(\mathbf{s}_e|\mathbf{s})\rangle + \mathbf{H}_e(\mathbf{s}_e|\mathbf{s})|\nabla \zeta_k(\mathbf{s}_e|\mathbf{s})\rangle - \nabla u_k(\mathbf{s})|\zeta_k(\mathbf{s}_e|\mathbf{s})\rangle - u_k(\mathbf{s})|\nabla \zeta_k(\mathbf{s}_e|\mathbf{s})\rangle = 0 \quad (5.3)$$

Next, multiplying Eq. (5.3) by  $\langle \zeta_j(\mathbf{s}_e|\mathbf{s})|$  for  $j \neq k$  (which implies also integration over the electronic coordinates), we get

$$\begin{aligned} \langle \zeta_j(\mathbf{s}_e|\mathbf{s})|\nabla \mathbf{H}_e(\mathbf{s}_e|\mathbf{s})|\zeta_k(\mathbf{s}_e|\mathbf{s})\rangle + \langle \zeta_j(\mathbf{s}_e|\mathbf{s})|\mathbf{H}_e(\mathbf{s}_e|\mathbf{s})|\nabla \zeta_k(\mathbf{s}_e|\mathbf{s})\rangle \\ - u_k(\mathbf{s})\langle \zeta_j(\mathbf{s}_e|\mathbf{s})|\nabla \zeta_k(\mathbf{s}_e|\mathbf{s})\rangle = 0 \end{aligned} \quad (5.4)$$

where the contribution of the third term in Eq. (5.3) is eliminated because of the orthogonality feature of the electronic basis set. To complete the derivation, we do the following:

1. We recall that  $\mathbf{H}_e$  is an operator that also acts on the l.h.s. eigenfunction so that

$$\langle \zeta_j(\mathbf{s}_e|\mathbf{s})|\mathbf{H}_e(\mathbf{s}_e|\mathbf{s}) - \langle \zeta_j(\mathbf{s}_e|\mathbf{s})|u_j(\mathbf{s}) = \mathbf{0}; \quad j = 1, \dots, N \quad (5.2')$$

2. Substituting Eq. (5.2') in Eq. (5.4), and recalling the definition of  $\tau_{jk}(\mathbf{s})$  yield:

$$\langle \zeta_j(\mathbf{s}_e|\mathbf{s})|\nabla \mathbf{H}_e(\mathbf{s}_e|\mathbf{s})|\zeta_k(\mathbf{s}_e|\mathbf{s})\rangle + (u_j(\mathbf{s}) - u_k(\mathbf{s}))\tau_{jk} = \mathbf{0} \quad (5.5)$$

It is noted that dividing Eq. (5.5) by  $(u_k(\mathbf{s}) - u_j(\mathbf{s}))$  asserts the theorem.

In what follows we briefly elaborate on the meaning of Eq. (5.1), in particular in the vicinity of a degeneracy point. In order to do that in a simple way, we consider a situation of a planar system, defined in terms of two polar coordinates  $(q, \varphi)$ , assume a point of degeneracy at  $q = 0$ , and concentrate on the angular component of Eq. (5.1). Since the angular component of  $\boldsymbol{\tau}$  is  $\tau_\varphi/q$  and the angular component of the grad operator is  $(1/q)(\partial/\partial\varphi)$ , we get

$$\frac{1}{q}\tau_{\varphi jk} = \frac{1}{q} \frac{\left\langle \zeta_j \left| \frac{\partial}{\partial\varphi} \mathbf{H}_e \right| \zeta_k \right\rangle}{u_k - u_j} \quad (5.6)$$

Next we assume that both  $u_k(q, \varphi)$  and  $u_j(q, \varphi)$ , behave in the vicinity of  $q \sim 0$ , in the following way:

$$\lim_{q \rightarrow 0} u_i \sim u_0(\varphi) + \lambda_i(\varphi)q^m + O(q^{m+1}); \quad i = j, k \quad (5.7a)$$

where  $m$  is an integer and  $u_0(\varphi)$  and  $\lambda_i(\varphi)$ ;  $i = j, k$  are analytic functions. It can be seen that in order to guarantee the quantization as presented in Eq. (3.62) [see also

Eq. (3.12)] the numerator near the degeneracy point has to behave in a similar way, namely

$$\lim_{q \rightarrow 0} \left\langle \zeta_j \left| \frac{\partial}{\partial \varphi} \mathbf{H}_e \right| \zeta_k \right\rangle \sim \eta(\varphi) q^m + O(q^{m+1}) \quad (5.7b)$$

where  $\eta(\varphi)$  is some function. The case of  $m = 1$  is the well-known Jahn–Teller conical intersection case<sup>5,6</sup> (see Sections 3.2.2, and 3.2.3) The case  $m = 2$  stands, among other things, for the Renner<sup>7</sup> model, also known as the *Renner–Teller model*.<sup>8</sup>

*Comment:* By mentioning the case  $m = 2$ , we referred to the Renner–Teller model; in fact, there is more to it because it is also characterized by a singularity that yields for the topological phase  $\alpha(q)$  the value of  $2n\pi$ , where  $n$  is an integer<sup>9</sup> (see also a brief discussion in Section 4.2).

So far we have discussed a general case where  $j$  and  $k$  refer to any two states. In fact, not any, arbitrary, pair of states forms a degeneracy point. For this purpose we have the following lemma.

**Lemma 5.1** *Degeneracy points can be formed only between two adjacent adiabatic states, namely, state  $j$  and state  $(j + 1)$ .*

*Proof* To prove this lemma, we consider the following two nonadjacent states: the  $j$  state and the  $(j + 2)$  state. From the way the adiabatic states are constructed, it is obvious that in order for these two states to be degenerate at a given point, each one of them has to form a degeneracy with the “in between”  $(j + 1)$  state at the *same* point. This situation leads to a formation of (a single) three-state degeneracy. Thus, we may have either the case where only two adjacent states form a degeneracy (and therefore  $k = j \pm 1$ ) or the case where the  $j$ th and the  $k$ th states, together with all the in-between states, form one single point of degeneracy (e.g., in case of the  $\{\text{H}_2, \text{H}\}$  system, we encounter a single point of degeneracy for its three lower states,  $\{1^2A', 2^2A', 3^2A'\}$ , formed at its  $D_{3h}$  *ci* point where  $R_{\text{HH}} \sim 0.52 \text{ \AA}^{(10)}$ ). This issue is discussed further in Section 5.3.4.

In Chapter 1 we discussed in some detail the extended Curl equation and referred to the possibility that the component  $\mathbf{H}$  of  $\mathbf{F}$  [see Eq. (1.15,16)] may not be defined at some points. Since the NACTs are singular at the degeneracy points, their derivatives cannot be formed and therefore  $\mathbf{H}$  (and also  $\mathbf{F}$ ) becomes undefined at these degeneracy points. In what follows we assume that the opposite is also valid; specifically, at the *pathological* points where  $\mathbf{H}$  cannot be formed, we attribute it to a singularity of one or several NACTs. Again, we emphasize that these singularities are all assumed to be simple poles. In what follows we refer to these points as *cis* points, or simply *cis* (although the potentials may not be conical as, e.g., in the case of the Renner model).

The subject of degeneracy points requires additional clarification because *cis* are not really points in configuration space but arrange themselves along “infinite”<sup>11–14</sup> (or semiinfinite<sup>15</sup>) long lines known as *seams*, namely, geometric objects of one or more dimensions. For instance, in case of three internal coordinates, the *seams* are lines that

usually extend from  $-\infty$  to  $+\infty$ . However, our studies, discussed in this book, are carried out on planes. For a system of  $N$  atoms we fix the position of  $(N - 1)$  atoms and allow the  $N$ th atom to move freely on an assigned plane. Under this assumption the motion of this atom can be described in terms of two polar coordinates  $(q, \varphi)$ , where  $q$  is a radial coordinate and  $\varphi$  is an angular coordinate. As is shown later, this single atom is used as a test particle to expose the *cis* on the particular plane.

As mentioned, the planes are formed by fixing the coordinates of the  $(N - 1)$  atoms. To move from one plane to another, we may vary the coordinates of one of the  $N - 1$  atoms. Doing that gradually for all the coordinates of the  $N - 1$  atoms, we finally trace the full configuration space.

Having defined the plane, which contains the *cis*, it is important to emphasize that the theory developed here does not apply for the whole plane but for a given region in this plane, usually defined by a closed contour.

## 5.2 CONSTRUCTION OF HILBERT SUBSPACE

In Chapters 1 and 2 we frequently discussed the possibility of breaking up, in a given region in configuration space, the Hilbert space into (quasi) Hilbert subspaces. We also discussed to some extent the conditions for that to happen; however, this discussion was limited, and it is our intention to extend it in the present section. As is presented next, the magnitudes to play a role in determining the extent a Hilbert space breaks up into Hilbert subspaces are the NACTs.

The basic assumption is as follows. We consider a *region* in configuration space and a given distribution of *cis*. Assuming that the Hilbert space contains  $N$  states and breaks up into  $L$  subspaces where the  $P$ th subspace contains  $N_P$  states so that  $N$  is given in the form:

$$N = \sum_{P=1}^L N_P \quad (5.8)$$

For the  $P$ th subspace we assume the following.<sup>1</sup>

1. Each two adjacent states form at least one *cis*. In other words, if  $\tau_{jj+1}^{(P)}$  defined as

$$\tau_{jj+1}^{(P)} = \langle \zeta_j^{(P)} | \nabla \zeta_{j+1}^{(P)} \rangle \quad (5.9a)$$

is the NACT between two such adjacent states, then this NACT has at least one singular point in the region of interest.

2. If  $P$  and  $Q$  are two adjacent subspaces (thus  $Q = P \pm 1$ ), then no  $P$  state forms a *cis* with a  $Q$  state. In other words, if  $\tau_{1N_p}^{(P+1,P)}$  defined as

$$\tau_{1N_p}^{(P+1,P)} = \left\langle \zeta_1^{(P+1)} \middle| \nabla \zeta_{N_p}^{(P)} \right\rangle \quad (5.9b)$$

is the NACT between the highest state in the  $P$  subspace and the lowest state of the  $(P + 1)$ th subspace, then this NACT does not possess a singularity in the region

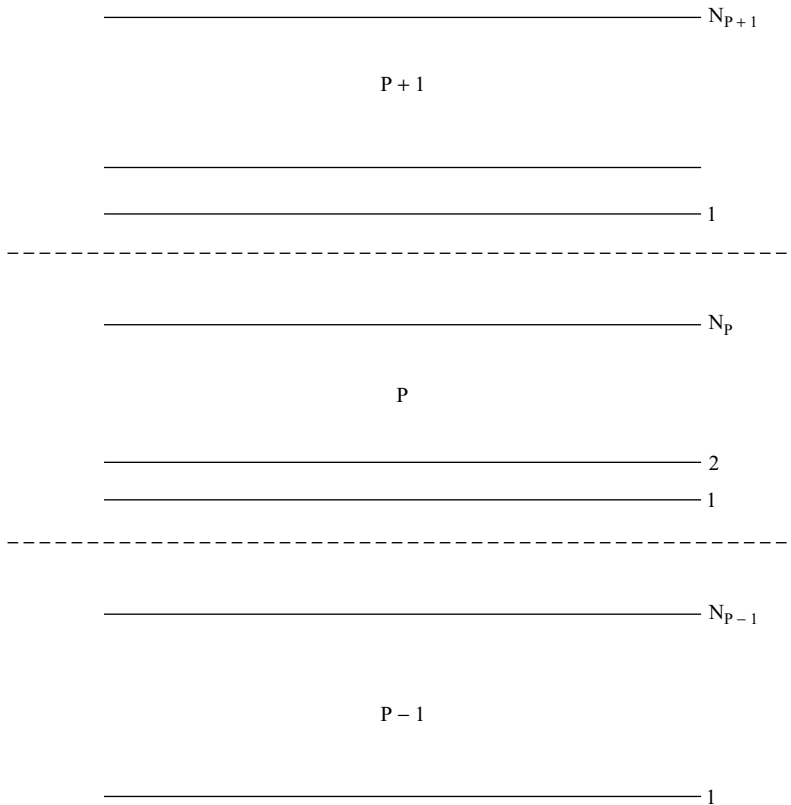


**Figure 5.1** A schematic representation of the three consecutive Hilbert subspaces, namely, the  $(P - 1)$ th, the  $P$ th, and the  $(P + 1)$ th. The dotted lines were drawn to differentiate the subspaces.

of interest. A similar assumption is made for the  $\tau_{1N_{P-1}}^{(P, P-1)}$  NACT, which is formed by the lowest  $P$  state and the highest  $(P - 1)$ -state (see Fig. 5.1).

The question to be asked is whether these two requirements are compatible with the conditions given in Eq. (1.36) or Eq. (1.37). In other words, is it enough to require that the upper and lower states of a group of states do not form any *cis* with their external neighbors to guarantee the breakup as presented in Eqs. (1.36) and (1.37). The answer to this question can be found only in Section 5.3, in which is discussed, in detail, the physical implication of the existence of *cis*.

## 5.3 SIGN FLIPS OF ELECTRONIC EIGENFUNCTIONS

### 5.3.1 Two-State Hilbert Subspace

In the late 1950s and the beginning of the 1960s Longuet-Higgins and colleagues<sup>1–4</sup> discovered one of the more interesting features in molecular physics related to the

Born–Oppenheimer electronic adiabatic eigenfunctions. They found that these functions, when surrounding a point of degeneracy, may acquire a phase that leads to a flip of sign of these functions. In particular, Herzberg and Longuet-Higgins<sup>2</sup> demonstrated this feature with respect to eigenfunctions of the Jahn–Teller model. This interesting observation implies that if a molecular system possesses a *cis* at a point in configuration space, the two relevant electronic eigenfunctions may become multivalued.

In Section 3.1.1 we considered the two-state system as an issue related to *analytical models*. In fact, this study is not limited to any model because the *two-state*  $\tau$  matrix, as written in Eq. (3.1), applies for the *general* (two-state) case. In the discussion that follows Eq. (3.12), we refer to the sign flips of the adiabatic eigenfunctions, which leads to the multivaluedness of these functions. In this sense the findings due to Longuet-Higgins et al.<sup>1–3</sup> and the general theory as expressed in terms of Eqs. (3.11), (3.12), and Eq. (2.31') lead to the same conclusions, namely, tracing a closed contour around a single *cis* causes the *two* functions to flip their signs *simultaneously*.

In case of several *cis*, this conclusion is generalized as will be done next. The line integral in Eq. (1.94) [see also Problem 1.1 (at the end of Chapter I)] can always be written as a sum of line integrals where each integral is performed along a closed contour that surrounds one single *cis*. In this situation each line integral contributes a value of  $\pm\pi$  to the total value of line integral formed for a contour  $\Gamma$  that surrounds *all* the *cis* in the region (assumed to be  $N$ ). The value of the line integral is not known at this stage (because of the two possible *signs*), but it is obvious that the value of  $n$ , in Eq. (3.12), is either even or odd when  $N$  is even or odd, respectively. In other words, the eigenfunctions flip their sign when this particular contour surrounds an *odd* number of *cis* but no sign-flips occur in case of an *even* number of *cis*.

Returning to Section 3.1.1 (or better, 3.1.1.2) and referring to the  $\mathbf{D}(\Gamma)$  matrix, we find that in case the closed contour  $\Gamma$  surrounds an even number of *cis*,  $\mathbf{D}(\Gamma)$  becomes a *unit* matrix but in case it surrounds an odd number of *cis*  $\mathbf{D}(\Gamma)$  becomes

$$\mathbf{D}(\Gamma) = \begin{pmatrix} -1 & 0 \\ 0 & -1 \end{pmatrix} \quad (5.10)$$

[see Eqs. (3.11) and (3.12)].

**Short Summary** We showed that sign flips of the eigenfunctions and the signs along the diagonal of the  $\mathbf{D}$  matrix are closely connected in view of Eq. (2.31'). Equation (2.31') explicitly states that each eigenfunction that traces a closed contour is identical to its original value multiplied by the corresponding (diagonal) element of the  $\mathbf{D}$  matrix. Therefore, if this element of the  $\mathbf{D}$  matrix is equal to  $(-1)$ , the corresponding eigenfunction flips its sign.

### 5.3.2 Three-State Hilbert Subspace

To study the possible sign flips for a three-state Hilbert subspace, we consider three states with two *cis*. One *cis* is formed between the two lower states and may be

considered as the source for the  $\tau_{12}$  NACT; the second  $ci$  is formed between the two upper states and may be considered as the source for the  $\tau_{23}$  NACT. It is known from numerous calculations that for a sufficiently small region surrounding a  $ci$  the two states that produce this  $ci$  form a two-state Hilbert subspace<sup>5,6</sup> (see Chapter 4). This also applies in the present case for the two lower states, namely, states 1 and 2 and their (1,2)  $ci$  and for the two upper states, namely, states 2 and 3 and their (2,3)  $ci$ . In other words, tracing a contour that surrounds, close enough, one of these  $cis$  will cause the two relevant eigenfunctions,  $j$  and  $(j+1)$ , to flip their signs.

Therefore, to construct the mathematical formulation to study possible sign flips for a three-state Hilbert subspace, we must first present the  $3 \times 3 \tau$  matrices for the two possible cases and the corresponding  $\mathbf{D}$  matrices.

As for the  $\tau$  matrices, we assume them to be

$$\mathbf{t}_{12}(\mathbf{s}) = \begin{pmatrix} \mathbf{0} & \tau_{12} & \mathbf{0} \\ -\tau_{12} & \mathbf{0} & \mathbf{0} \\ \mathbf{0} & \mathbf{0} & \mathbf{0} \end{pmatrix} \quad \text{and} \quad \mathbf{t}_{23}(\mathbf{s}) = \begin{pmatrix} \mathbf{0} & \mathbf{0} & \mathbf{0} \\ \mathbf{0} & \mathbf{0} & \tau_{23} \\ \mathbf{0} & -\tau_{23} & \mathbf{0} \end{pmatrix} \quad (5.11)$$

Having the  $\tau$  matrices, we are now in a position to derive the corresponding  $\mathbf{D}$  matrices. For this reason we employ Eq. (1.93) and the matrices  $\mathbf{t}_{12}$  and  $\mathbf{t}_{23}$  to calculate  $\mathbf{D}_{12}(\Gamma_{12})$  and  $\mathbf{D}_{23}(\Gamma_{23})$ , along the corresponding contours  $\Gamma_{12}$  and  $\Gamma_{23}$  that surround the (1,2)  $ci$  and the (2,3)  $ci$  respectively (see also detailed discussion on this subject in Sections 3.1.1.1 and 3.1.1.2)

$$\mathbf{D}_{12}(\Gamma_{12}) = \begin{pmatrix} -1 & 0 & 0 \\ 0 & -1 & 0 \\ 0 & 0 & 1 \end{pmatrix} \quad \text{and} \quad \mathbf{D}_{23}(\Gamma_{23}) = \begin{pmatrix} 1 & 0 & 0 \\ 0 & -1 & 0 \\ 0 & 0 & -1 \end{pmatrix} \quad (5.12)$$

The issue we intend to consider next is what happens when a contour,  $\Gamma_{13}$  surrounds both,  $cis$ , namely, the (1,2)  $ci$  and the (2,3)  $ci$  (see Fig. 5.2).<sup>7</sup>

**Lemma 5.2** If a contour in a given plane surrounds two  $cis$  belonging to two different (adjacent) pairs of states, only two eigenfunctions flip their sign—the one that belongs to the lower state and the one that belongs to the upper state—but the intermediate eigenfunction is left unchanged. Consequently the appropriate  $\mathbf{D}$  matrix takes the following form:

$$\mathbf{D}_{13}(\Gamma_{13}) = \begin{pmatrix} -1 & 0 & 0 \\ 0 & 1 & 0 \\ 0 & 0 & -1 \end{pmatrix} \quad (5.13)$$

*Proof* To prove the lemma, we consider the following three regions (see Fig. 5.2) In the first region, designated as  $\sigma_{12}$ , is located the main portion of the interaction,  $\tau_{12}$ , with the  $ci$  point at (1,2)  $ci$ . In the second region, designated as  $\sigma_{23}$ , is located the main portion of the interaction,  $\tau_{23}$ , and the  $ci$  point at (2,3)  $ci$ . In addition, we

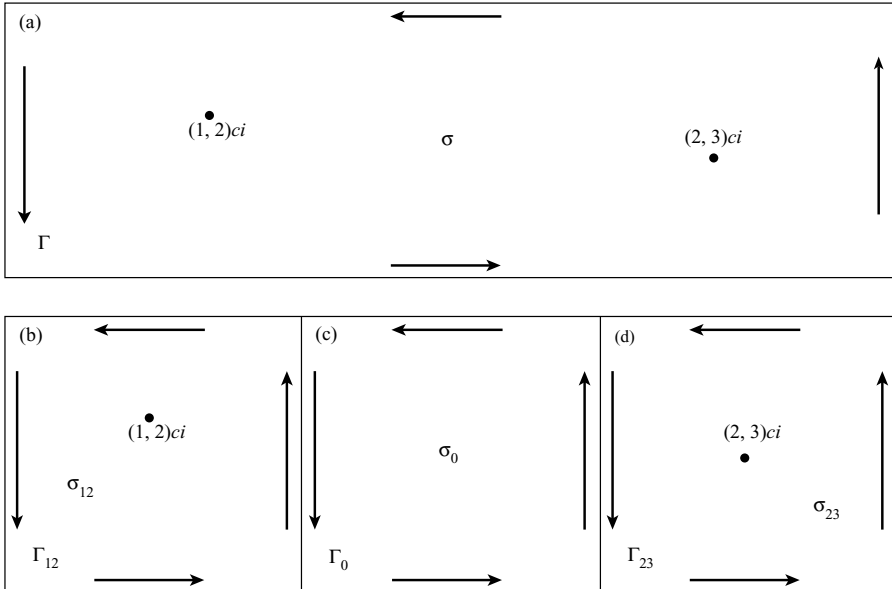


**Figure 5.2** This diagram shows a region  $\sigma$  that contains two  $cis$  designated as  $\bullet$ : (a) the full region,  $\sigma$ , defined in terms of the closed contour  $\Gamma$ ; (b) the region  $\sigma_{12}$ , which contains one  $(1,2)$   $ci$  and is defined by the closed contour  $\Gamma_{12}$ ; (c) the region  $\sigma_0$ , which does not contain any  $ci$  and is defined by the closed contour  $\Gamma_0$ ; (d) the region  $\sigma_{23}$ , which contains one  $(2,3)$   $ci$  and is defined by the closed contour  $\Gamma_{23}$ . It can be seen that  $\Gamma = \Gamma_{12} + \Gamma_0 + \Gamma_{23}$ .

assume a third region,  $\sigma_0$ , which is located in between the two and is used as a buffer zone. Next we assume that the intensity of  $\tau_{23}$  (i.e.,  $|\tau_{23}|$ ) in  $\sigma_{12}$  and the intensity of  $\tau_{12}$  (i.e.,  $|\tau_{12}|$ ) in  $\sigma_{23}$  is negligibly small (i.e.,  $|\tau_{jj+1}| \leq \varepsilon$ , where  $j = 1, 2$  and  $\varepsilon$  is a sufficiently small number). This situation can always be achieved by reducing area of  $\sigma_{12}$  ( $\sigma_{23}$ ) around the corresponding  $ci$  point. In  $\sigma_0$ , both  $\tau_{12}$  and  $\tau_{23}$  may be of arbitrary intensities.

To prove our statement, we consider the expression as derived in Section 1.3.2.2 [in particular, see Eq. (1.73)]

$$\mathbf{A}(\Gamma) = \mathbf{A}_0 - \oint_{\Gamma} \mathbf{ds} \cdot \boldsymbol{\tau}(\mathbf{s}) \mathbf{A}(s) \quad (5.14)$$

where the integration is carried out along a closed contour  $\Gamma$ ,  $\mathbf{A}_0$  is a (constant) given matrix,  $\mathbf{A}(\mathbf{s})$  is the  $3 \times 3$  ADT matrix to be calculated, the dot stands for a scalar product, and  $\boldsymbol{\tau}(\mathbf{s})$  is the  $3 \times 3$  matrix that contains the relevant NACTs,

$$\boldsymbol{\tau}(\mathbf{s}) = \begin{pmatrix} \mathbf{0} & \tau_{12} & \tau_{13} \\ -\tau_{12} & \mathbf{0} & \tau_{23} \\ -\tau_{13} & -\tau_{23} & \mathbf{0} \end{pmatrix} \quad (5.11')$$

The closed contour  $\Gamma$  can be presented as a sum of three closed contours:  $\Gamma_{12}$ ,  $\Gamma_{23}$  and  $\Gamma_0$  (see Fig. 5.2). Consequently, the integral in Eq. (5.14) becomes a sum of three integrals, namely

$$\mathbf{A}(\Gamma) = A_0 - \oint_{\Gamma_{12}} \mathbf{ds} \cdot \boldsymbol{\tau} \mathbf{A} - \oint_{\Gamma_0} \mathbf{ds} \cdot \boldsymbol{\tau} \mathbf{A} - \oint_{\Gamma_{23}} \mathbf{ds} \cdot \boldsymbol{\tau} \mathbf{A} \quad (5.14')$$

or to be more specific

$$\mathbf{A}(\Gamma) = A_0 - \oint_{\Gamma_{12}} \mathbf{ds} \cdot \mathbf{t}_{12} \mathbf{A} - \oint_{\Gamma_0} \mathbf{ds} \cdot \boldsymbol{\tau} \mathbf{A} - \oint_{\Gamma_{23}} \mathbf{ds} \cdot \mathbf{t}_{23} \mathbf{A} \quad (5.15)$$

where we assumed that the intensity of  $\boldsymbol{\tau}_{13}$  is negligibly small in the close vicinity of each of the *cis* (this assumption is consistent with what we know about the formation of  $\boldsymbol{\tau}_{13}$ —to be discussed in Chapter 6). Since there are no *cis* in the buffer zone,  $\sigma_0$ , the second integral is identically zero (see discussion in Section 1.3.2.2)) and therefore can be deleted so that we are left with the first and the third integrals:

$$\mathbf{A}(\Gamma) = A_0 - \oint_{\Gamma_{12}} \mathbf{ds} \cdot \mathbf{t}_{12} \mathbf{A} - \oint_{\Gamma_{23}} \mathbf{ds} \cdot \mathbf{t}_{23} \mathbf{A} \quad (5.15')$$

To carry out the integrations we need  $\mathbf{A}(\mathbf{s})$ , which is not given. Therefore we intend to obtain the  $\mathbf{D}$  matrix in a different way. For this purpose we introduce two (constant) matrices  $\mathbf{G}_{12}$  and  $\mathbf{G}_{23}$  that enable the presentation of Eq. (5.15') in two more different ways:

$$\mathbf{A}(\Gamma) = \mathbf{G}_{jj+1} - \oint_{\Gamma_{jj+1}} \mathbf{ds} \cdot \mathbf{t}_{jj+1} \mathbf{A}; \quad j = 1, 2 \quad (5.16)$$

Comparing Eqs. (5.15') and (5.16) yields the following expressions for  $\mathbf{G}_{jj+1}$ ;  $j = 1, 2$ :

$$\begin{aligned} \mathbf{G}_{12}(\Gamma_{23}) &= \mathbf{A}_0 - \oint_{\Gamma_{23}} \mathbf{ds} \cdot \mathbf{t}_{23} \mathbf{A} \\ \mathbf{G}_{23}(\Gamma_{12}) &= \mathbf{A}_0 - \oint_{\Gamma_{12}} \mathbf{ds} \cdot \mathbf{t}_{12} \mathbf{A} \end{aligned} \quad (5.17)$$

Using Eqs. (5.14) and (5.16), we have three different ways to present  $\mathbf{A}(\Gamma)$  in terms of three different  $\mathbf{D}$  matrices [see Eq. (2.47), recalling that  $\mathbf{D} \equiv \mathbf{B}$ ]: first, applying the definition of the  $\mathbf{D}$  matrix with respect to Eq. (5.14)

$$\mathbf{A}(\Gamma) = \mathbf{D}(\Gamma) \mathbf{A}_0 \quad (5.18a)$$

and then applying it for the two equations in Eq. (5.16):

$$\mathbf{A}(\Gamma) = \mathbf{D}_{12}(\Gamma_{12})\mathbf{G}_{12} \quad (5.18b)$$

$$\mathbf{A}(\Gamma) = \mathbf{D}_{23}(\Gamma_{23})\mathbf{G}_{23} \quad (5.18c)$$

In the same way the matrices  $\mathbf{D}_{jj+1}$  and  $\mathbf{G}_{jj+1}$ ;  $j = 1, 2$  are related as follows [see Eq. (5.17)]:

$$\begin{aligned}\mathbf{G}_{12} &= \mathbf{D}_{23}(\Gamma_{23})\mathbf{A}_0 \\ \mathbf{G}_{23} &= \mathbf{D}_{12}(\Gamma_{12})\mathbf{A}_0\end{aligned}\quad (5.19)$$

Substituting Eqs. (5.19) in Eqs. (5.18b) and (5.18c) (see Eq. (5.18a)) and recalling that the  $\mathbf{D}$  matrices, for the corresponding Hilbert subspaces, are diagonal, we obtain:

$$\mathbf{D}(\Gamma) = \mathbf{D}_{13} = \mathbf{D}_{12}(\Gamma_{12})\mathbf{D}_{23}(\Gamma_{23}) \quad (5.20)$$

Next, recalling the explicit form of  $\mathbf{D}_{12}$  and  $\mathbf{D}_{23}$  [see Eqs. (5.12)], we substitute Eqs. (5.12) in Eq. (5.20), and this leads directly to Eq. (5.13).

**Summary** We know from numerical calculations that tracing any contour that surrounds a single  $ci$  causes the sign flip of the two states that form the  $ci$ . In the present section we proved, analytically, that surrounding two  $cis$  as given in Lemma 5.2 again causes two sign flips, but this time these are the signs of eigenfunctions related to the lower and the upper states. Thus the sign related to the intermediate state is left unaffected. The conclusion of this study is that tracing any closed contour within the three-state Hilbert subspace yields at most two sign flips (however if the contour does not surround any  $ci$ , no sign flip takes place). This finding can be extended, in a straightforward way, to Hilbert subspaces of arbitrary dimensions, as will be done in the next section.

### 5.3.3 General Hilbert Subspace

In this section we present a geometric approach that yields possible sign flips for an electronic manifold,  $\zeta(s)$ , which traces a contour that surrounds one or several  $cis$  belonging to a given subspace. To be more specific, we assume that the subspace contains  $N$  states ( $N > 2$ ) where any adjacent pair of states forms at least *one*  $ci$ . The geometric approach is based on the analytical derivation in Section (5.3.2) carried out for  $N = 3$ .

[Comment: Two adjacent states may form more than one  $ci$ , but here, to simplify the discussion, we assume one  $ci$  for any two (adjacent) states. The extension is done at later stages.]

### Notations

1. Having two adjacent states,  $j$  and  $(j + 1)$ , the two form the  $ci$  to be assigned as  $C_j$  (see Fig. 5.3).
2. The contour that surrounds (only)  $C_j$  is assigned as  $\Gamma_{jj+1}$  (see Fig. 5.4a).
3. A contour that surrounds  $n$  consecutive  $cis$  (i.e.,  $C_j, C_{j+1} \dots C_{j+n}$ ) is assigned as  $\Gamma_{jj+n}$  (see Fig. 5.4b for  $n = 1$  and Fig. 5.4c for  $n = 2$ ).
4. A contour that surrounds only two  $cis$ , namely,  $C_j$  and  $C_k$  is assigned as  $\Gamma_{j,k+1}$ . For instance,  $\Gamma_{1,4}$  surrounds  $C_1$  and  $C_3$  but not  $C_2$  (see Fig. 5.4d).

These notations can be extended, in case of larger subspaces, to include other possibilities.

Having these notations, we return to describe the various possible sign flips. In case of  $N = 2$ , we have two possibilities:  $\Gamma (= \Gamma_{12})$  either (1) surrounds or (2) does not surround the  $ci$ . In case 1, the two functions,  $\zeta_1$  and  $\zeta_2$ , flip their sign so that  $K = 2$  ( $K$ , the topological number, is defined as the number of *minus* signs along the diagonal of the  $\mathbf{D}$  matrix). In case  $N = 3$ , we encounter two conical intersections:  $C_1$  and the  $C_2$  (see Fig. 5.4a). Moving the electronic manifold along the path  $\Gamma_{12}$  flips the signs of  $\zeta_1$  and  $\zeta_2$ , moving it along  $\Gamma_{23}$  flips the signs of  $\zeta_2$  and  $\zeta_3$ , but moving it along  $\Gamma_{13}$  (see Fig. 5.4b) causes the signs of  $\zeta_1$  and  $\zeta_3$  to be flipped once but the sign of  $\zeta_2$  to be flipped twice (once surrounding  $C_1$  and once surrounding  $C_2$ ) and therefore,

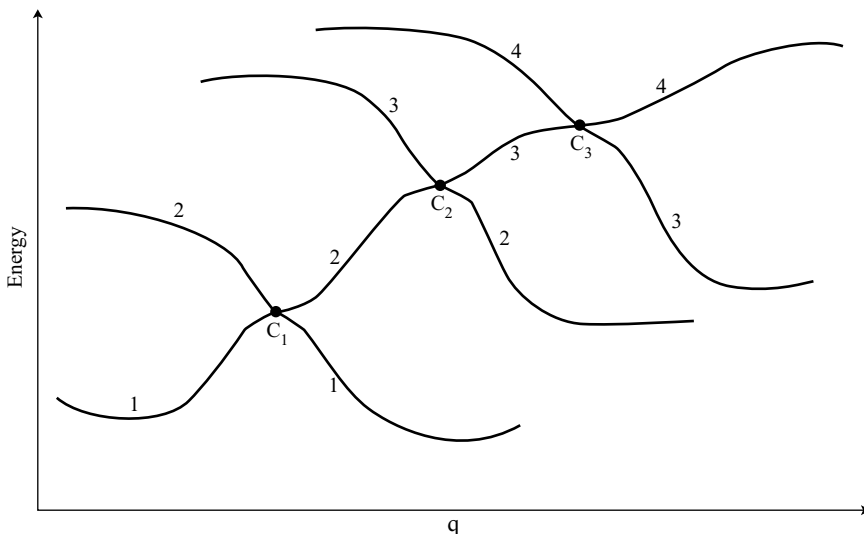


**Figure 5.3** A schematic representation of four interacting adiabatic surfaces presented in terms of four (adiabatic) curves;  $j = 1, 2, 3, 4$ . The three  $C_j$ 's where  $j = 1, 2, 3$ , stand for the three  $ci$  points formed by the intersections of the four surfaces. The curves are presented as a function of  $q$ .

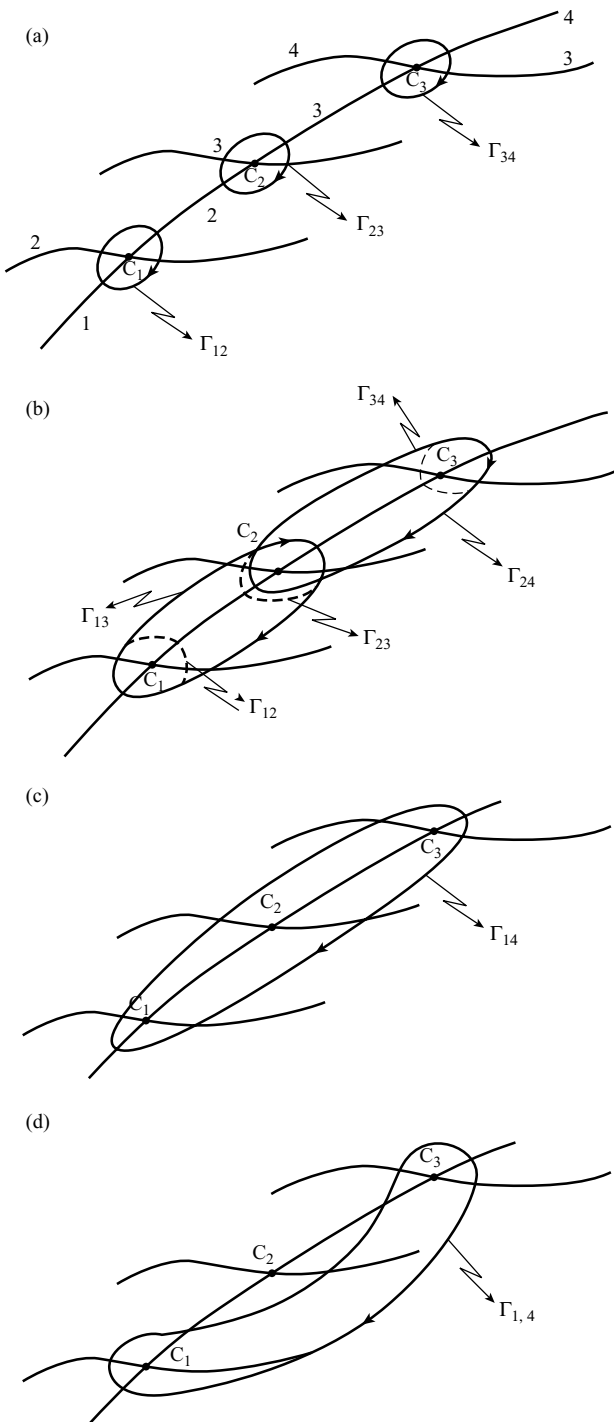


Figure 5.4

altogether, its sign remains unflipped. The conclusion for three-state systems is that we can have either no sign flip (when the  $\Gamma$  does not surround any  $ci$ ) or three cases where two different functions flip signs.

Next, we discuss the case  $N = 4$ . It is now obvious that tracing contours of the type  $\Gamma_{jj+1}; j = 1, 2, \dots$  that surround the relevant  $C_j$  (see Fig. 5.4a) flip the signs of the two corresponding functions,  $\zeta_j$  and  $\zeta_{j+1}$ . Next, tracing contours of the type  $\Gamma_{jj+2}; j = 1, 2$  (see Fig. 5.4b) flip the sign of the two external functions,  $\zeta_j$  and  $\zeta_{j+2}$ , but leave the sign of the intermediate function,  $\zeta_{j+1}$ , unchanged (see also Eq. (5.20)). We have two such situations: one related to the first and the second *cis* and one related to the second and the third *cis*. Then we have the contour  $\Gamma_{14}$  that surrounds all three *cis* (see Fig. 5.4c), and here, as in the previous three-state case, only the two external functions,  $\zeta_1$  and  $\zeta_4$ , flip signs whereas the signs of the two internal functions, namely,  $\zeta_2$  and  $\zeta_3$ , are left unchanged (they are flipped twice). Finally, we have the case where the contour  $\Gamma_{1,4}$  surrounds  $C_1$  and  $C_3$  but does not surround  $C_2$  (see Fig. 5.4d). In this case all four functions flip signs (none of the four functions get their sign flipped twice).

As an example, we present this particular situation in terms of a product of two matrices. Thus, defining  $\mathbf{D}_{12}$  and  $\mathbf{D}_{34}$  as

$$\mathbf{D}_{12}(\Gamma_{12}) = \begin{pmatrix} -1 & 0 & 0 & 0 \\ 0 & -1 & 0 & 0 \\ 0 & 0 & 1 & 0 \\ 0 & 0 & 0 & 1 \end{pmatrix} \quad (5.21a)$$

and

$$\mathbf{D}_{34}(\Gamma_{34}) = \begin{pmatrix} 1 & 0 & 0 & 0 \\ 0 & 1 & 0 & 0 \\ 0 & 0 & -1 & 0 \\ 0 & 0 & 0 & -1 \end{pmatrix} \quad (5.21b)$$

---

**Figure 5.4** Four interacting adiabatic surfaces, three  $ci$  points and the corresponding contours to study sign flips along the closed contours. (a) The contours  $\Gamma_{jj+1}$  each surrounding the respective  $C_j$  [i.e., the  $(j, j + 1) ci$ ] leads to sign flip of the  $j$ th and  $(j + 1)$ th eigenfunctions. (b) The contours  $\Gamma_{jj+2}$ , which surround two consecutive *cis* at  $C_j$  and  $C_{j+1}$ , lead to sign flip of the  $j$ th and  $(j + 2)$ th eigenfunctions but leave the sign of the intermediate  $(j + 1)$  eigenfunction unchanged. Also shown are the contours of type  $\Gamma_{jj+1}$  that surround the respective  $C_j$  points (designated by dotted lines). It can be seen that  $\Gamma_{jj+2} = \Gamma_{jj+1} + \Gamma_{j+1,j+2}$  (see Fig. 5.2). (c) The contour  $\Gamma_{14}$  that surrounds the three  $C_j$  points leads to sign flip of the first and the fourth eigenfunctions and leaves, unflipped, the signs of the second and the third eigenfunctions. Extending the situation in Eq. (5.4c), we obtain  $\Gamma_{14} = \Gamma_{12} + \Gamma_{23} + \Gamma_{34}$ . (d) The contour  $\Gamma_{1,4}$  surrounds the two external  $ci$  points but not the middle one. Based on Figure 5.4b, we have  $\Gamma_{1,4} = \Gamma_{12} + \Gamma_{34}$ .

we observe that the matrix that describes the sign flips along  $\Gamma_{1,4}$  is given in the form

$$\mathbf{D}(\Gamma_{1,4}) = \mathbf{D}_{1,4}(\Gamma_{1,4}) = \mathbf{D}_{12}(\Gamma_{12})\mathbf{D}_{34}(\Gamma_{34})$$

or

$$\mathbf{D}_{1,4}(\Gamma_{1,4}) = \begin{pmatrix} -1 & 0 & 0 & 0 \\ 0 & -1 & 0 & 0 \\ 0 & 0 & -1 & 0 \\ 0 & 0 & 0 & -1 \end{pmatrix} \quad (5.21c)$$

The four-state system can be summarized as follows. We revealed six different types of contours that lead to the sign flip of two functions and one kind that leads to the sign flip of all *four* functions.

The discussion above introduces the idea of attaching “algebra” of closed contours (based on the closed *line integral* approach as presented in Section 5.3.2). We present two examples:

1. The case of the contour  $\Gamma_{jj+n}$ , which surrounds *n consecutive cis*. It can be shown that

$$\Gamma_{jn} = \sum_{k=j}^{n-1} \Gamma_{kk+1} \quad (5.22)$$

2. The contour  $\Gamma_{j,k+1}$ , which surrounds two *nonconsecutive cis* (i.e., the *j*th and the *k*th):

$$\Gamma_{j,k+1} = \Gamma_{k,j+1} = \Gamma_{jj+1} + \Gamma_{kk+1}; \quad k \geq j + 1 \quad (5.23)$$

In case  $k = j + 1$  we have

$$\Gamma_{j,j+2} = \Gamma_{jj+1} + \Gamma_{j+1,j+2} = \Gamma_{jj+2} \quad (5.23')$$

As an example of an ab initio treatment for a real molecular system, we briefly discuss the three diagonal elements of the  $\mathbf{D}$  matrix as calculated for the {C<sub>2</sub>,H} system along the *two* contours presented in Figure 4.8.

For the contour that surrounds one (2,3) *ci* and one (3,4) *ci* (see Fig. 4.8d), we get the series {−+−}—a case treated analytically in Section 5.3.2 and discussed earlier [see also Eq. (5.20)]. For the contour that surrounds one (2,3) *ci* and two (3,4) *cis* (see Fig. 4.8c), we form the following series of products

$$\mathbf{D}(\Gamma_{24}) \equiv \mathbf{D}_{13} = \mathbf{D}_{12}\mathbf{D}_{23}\mathbf{D}_{23} \quad (5.20')$$

where  $\mathbf{D}_{12}$  and  $\mathbf{D}_{23}$  are as given in Eq. (5.12). This product yields for the  $\mathbf{D}(\Gamma_{24})$ -diagonal elements the series {−−+} as indeed is found in the calculation (see results along the first row of Table 4.3).

[*Caution:* There is some confusion regarding the indices because the analysis is done with respect to three *excited* state, ignoring the ground state (usually assigned as state 1).]

Returning, again, to the topological number,  $K$  we prove the following lemma:

**Lemma 5.3** The *topological* number  $K(\Gamma)$  is an even number.<sup>8</sup>

*Proof* We assume a system of  $N$  states and a closed contour  $\Gamma$  that surrounds  $n$  *cis* (to simplify this proof, we assume that each adjacent pair of states is coupled by one  $ci$ ) so that when the group of  $N$  states traces  $\Gamma$ ,  $K$  functions flip their signs. Next we assume a slightly different contour,  $\Gamma'$ , which surrounds one  $ci$  less, for instance, the  $(j, j + 1)$   $ci$ . As a result, the signs of two functions, the  $j$ th and the  $(j + 1)$ th, are affected. The change in  $K$  is either 2 [when the two functions flip their original signs, e.g., two  $(-1)$ s become two  $(+1)$ s] or zero [when, e.g., one  $(-1)$  becomes  $(+1)$  and one  $(+1)$  becomes  $(-1)$ ]. Thus any change in  $K$  caused by including or excluding *cis* is accompanied by a flip of an even number of signs only. Next, since the smallest value of  $K$  is zero (and never 1),  $K$  may attain even integers only.

As is noted  $K$  determines the number of possible sign flips along a given contour. Information regarding the *number* of different groups of functions with identical number of flipped signs is still missing.

**Corollary 5.1** If  $N$  is the number of states that form the subspace where each two adjacent states are coupled by a single  $ci$ , then  $N_K$ , the number of groups that contain *different* functions with  $K$  flipped signs, is as follows:

$$N_k = \binom{N}{K} \quad (5.24)$$

This expression is known to yield the number of different groups of  $K$  elements out of a group of  $N$  elements.

**Example 5.1** In the four-states case, the number of groups with two flipped signs is six (6), the number of groups with four flipped signs is one, and the number of groups with unflipped signs is also one.

**Short Summary** Extending Lemma 5.2 for any  $N$ -state Hilbert subspace with an arbitrary number of *cis*, the number of functions that flip their signs while the electronic manifold traces a given closed contour  $\Gamma$  is determined by the number  $K$  related to the  $\mathbf{D}$  matrix formed by the product

$$\mathbf{D}(\Gamma) = \prod_{j=1}^n {}' \mathbf{D}_{jj+1}(\Gamma) \quad (5.25)$$

where  $\mathbf{D}_{jj+1}(\Gamma)$  is an  $N \times N$  (diagonal) matrix that has  $(-1)$ s at positions  $(j, j)$  and  $(j + 1, j + 1)$  [and otherwise  $(+1)$ ], and the prime sign implies that the product is carried out only with respect to *cis* surrounded by  $\Gamma$ .

### 5.3.4 Multidegeneracy Point

#### 5.3.4.1 General Approach

The emphasis in our previous sections was on isolated two-state *cis*. Here we would like to refer to cases where at a given point three (or more) states form one degeneracy point.<sup>8</sup> This can happen, for instance, when two seams cross each other at a point so that at this point we have three surfaces intersecting each other or, in other words, a three-state degeneracy point. In fact we may even expect higher multistate degeneracy when several (more than two) seams cross each other all at the same point. The issue is how to incorporate this situation into the already existing theoretical framework.

In what follows we assume that each two adjacent states form only one *ci* (the extension to several *cis* is straightforward). We start by analyzing a three-state degeneracy point and consider the following situation:

1. The two lower states form a *ci*, presented in terms of  $\tau_{12}(\rho, \varphi)$ , located at the origin, namely, at  $\rho = 0$ .
2. The two upper states form a *ci*, presented in terms of  $\tau_{23}(\rho, \varphi | \rho_0, \varphi_0)$ , located at  $\rho = \rho_0, \varphi = \varphi_0$ .
3. The three-state degeneracy is formed by letting  $\rho_0 \rightarrow 0$ , namely

$$\lim_{\rho_0 \rightarrow 0} \tau_{23}(\rho, \varphi | \rho_0, \varphi_0) = \tau_{23}(\rho, \varphi | \varphi_0) \quad (5.26)$$

so that the two *cis* coincide (the angle  $\varphi_0$  becomes, in this case, redundant). Since the two *cis* are located at the same point, every closed contour that surrounds one of them surrounds the other so that this situation is the case of a contour  $\Gamma (= \Gamma_{13})$  surrounding two (adjacent) *cis* (see Fig. 5.4b) According to the analysis in Section (5.3.2), only two functions flip signs in such a case, that is, the ones belonging to the lower and the upper states.

Extending this situation to a degeneracy point formed by  $N$  states does not change the final result, namely, *only two functions flip signs: the one belonging to the lower state and the one belonging to the upper state*. This implies that along the diagonal of the  $\mathbf{D}$  matrix we encounter the series  $\{- + \cdots + -\}$  to be designated as  $\{- + (N - 2) + -\}$ .

This general result is at odds with some more recent models. First, it contradicts the conclusions given in Sections 3.1.2 and 3.1.3, which refer to specific models as presented there. Then it also contradicts a model discussed by Child and Manolopoulos.<sup>9</sup> On the other hand, they seem to be supported by an analysis given by Varandas and colleagues.<sup>10,11</sup> based on Lie algebra.

### 5.3.4.2 Model Studies

In Section 3.1.2 we treated a particular type of a three-state model and found that in this case *none* of the functions flip sign, which implies that along the diagonal of the  $\mathbf{D}$  matrix we have the  $\{+++$  series. In Section 3.1.3 a four-state model is treated and it is found that either all four functions flip sign or none of them flip sign. This implies that along the diagonal of the  $\mathbf{D}$  matrix we have the  $\{---$  series or the  $\{+++\}$  series, respectively. We explain these outcomes as follows.

**The Three-State System** To explain this case, we assume the existence of four *cis*: two of them formed by the two lower states and two formed by the two upper states. In Section 5.3.1 we briefly discussed the outcome of surrounding two or more *cis* formed by the *same* two states. We showed that in case the contour  $\Gamma$  surrounds an *even* number of *cis*, no sign flip takes place. Here we consider the extension of this situation for a three-state system where each two adjacent states form a *pair* of *cis* and the contour surrounds all four *cis*. To determine what the signs of the  $\mathbf{D}$  matrix diagonal elements are in such a situation, we apply a product similar to Eq. (5.20') [see also Eq. (5.25)] for the two matrices  $\mathbf{D}_{12}$  and  $\mathbf{D}_{23}$  in Eqs. (5.12):

$$\mathbf{D}(\Gamma_{1,3}) = \mathbf{D}_{1,3} = \mathbf{D}_{12}\mathbf{D}_{12}\mathbf{D}_{23}\mathbf{D}_{23} \quad (5.20'')$$

It is straightforward to verify that  $\mathbf{D}_{1,3} = \mathbf{I}$ , or in other words, we encounter the  $\{+++\}$  series. In case of a single three-state degeneracy point, since *any* contour surrounds all four *cis*, we always encounter the same series. As a final point on this issue, we mention an ab initio treatment carried out for the three lower states of the  $\{\text{H}_2, \text{H}\}$  system.<sup>12</sup> In this study Halász et al. revealed that for the equilateral configuration,  $R_{\text{HH}} \sim 0.52 \text{ \AA}$ , two *pairs* of *cis* (two *cis* formed by the lower states,  $1^2 A'$  and  $2^2 A'$ , and two *cis* formed by the upper states  $2^2 A'$ ,  $3^2 A'$ ) converge to form a single three-state degeneracy point (see also Refs. 13–15). It is shown, numerically, that the corresponding  $\mathbf{D}$  matrix is characterized by the  $\{+++\}$  series.

**The Four-State System** We mentioned earlier that while studying, the four-state system in Section 3.1.3, we found that either (1) none of or (2) all of the four functions flip sign. Case 1 (i.e., no sign flip) can be explained in the same way as the previous three-state case, namely, assuming that each two adjacent states form *two cis* (thus three pairs altogether). Therefore, enforcing the four-state degeneracy causes the shift of all *six cis* to the same point so that any contour surrounds the six *cis*. In this way we encounter the  $\{++++\}$  series. The second case where all four functions flip their signs is somewhat more complicated. Here states (1,2) and (3,4) each form one *ci*, but the two intermediate states, (2,3), form two *cis*. Therefore the four corresponding matrices to be employed are  $\mathbf{D}_{12}$  and  $\mathbf{D}_{34}$  given in Eqs. (5.21a) and (5.21b), respectively, and two  $\mathbf{D}_{23}$  matrices. Next, forming the relevant product

$$\mathbf{D}_{1,4}(\Gamma_{1,4}) = \mathbf{D}_{12}\mathbf{D}_{23}\mathbf{D}_{23}\mathbf{D}_{34} \quad (5.20'')$$

we note that the matrix  $\mathbf{D}_{1,4}$  is identical to the one given in Eq. (5.21c), thus characterized by the  $\{----\}$  series.

A different model was studied by Child and Manolopoulos.<sup>9</sup> Within their model they consider a diabatic potential matrix of the form

$$\mathbf{H}(q, \varphi) = \mathbf{F}(q) \cos \varphi + \mathbf{G}(q) \sin \varphi$$

where  $\mathbf{F}(q)$  and  $\mathbf{G}(q)$  are real symmetric matrices assumed to form an  $N$ -fold degeneracy at the vicinity of the origin and scale linearly with  $q$ . Once constructed, the two authors solved the corresponding eigenvalue problem for the eigenfunctions  $\chi_j(\varphi|q); j = \{1, N\}$ . These eigenfunctions were then followed along closed contours (formed by fixed  $q$  values) to determine their signs at the end of the contour. With this model a situation for  $N = 3$  was found, that yields the series  $\{-+-\}$ , a series identical to the one discussed in Section 5.3.4.1 and resulting from the existence of two *cis*: one (1,2) *cis* and one (2,3) *cis*. But they also report on the existence of the  $\{+++$  series, which has to be a result of at least four *cis*, namely, two (1,2) *cis* and two (2,3) *cis* formed by the corresponding product given in Eq. (5.20''). In other words, the model produces more than the minimal number of two *cis* (one *cis* for each adjacent pair of states). This conclusion is also supported by an analysis carried out by Pistolesi and Manini.<sup>16</sup>

We also briefly discuss the  $N = 4$  case. For this case, the Child–Manolopoulos model produces either the series  $\{++++\}$  or the series  $\{----\}$ . As discussed earlier, we need to have at least six *cis* to form a  $\{++++\}$  series and four *cis* to form a  $\{----\}$  series. Thus in both cases more than just the minimal number of three *cis* are involved (again, one *cis* for each adjacent pair of states). However, strangely enough, this model does not produce the  $\{-++-\}$  series, which requires only three *cis* as discussed in Section 5.3.4.1. In the same way their model requires, in case of higher  $N$  values, many more *cis* than the necessary minimal number of  $N - 1$  *cis* as discussed in the previous section.

In this respect we also mention a model applied by Varandas et al.,<sup>10,11</sup> based on Lie algebra, who derive essentially the same results as discussed in Section 5.3.4.1. They obtain, in case of an  $N$ -state degeneracy point, the following series  $\{-+(N-2)+-\}$ —a result formed by  $N - 1$  *cis*. In other words, regardless of the value of  $N$ , only two functions flip their signs, namely, those relate to the lowest and the highest states.

## 5.4 TOPOLOGICAL SPIN

The concept of spin in quantum mechanics was introduced because experiments indicated that elementary particles such as electrons and nucleons are not completely identified in terms of their three spatial coordinates.<sup>1</sup> To be more specific, to ensure a complete description of the state of a particle, one has to consider the possibility that these particles may have intrinsic angular momentum, which is known by the name *spin*. This magnitude, like any other classical angular momentum, is a vector.

Hence the wavefunction of a particle must be a function of four variables: the three spatial coordinates and the spin variable, which determines the values of all possible projections of the spin along a given direction. Next, precisely as in the case of the ordinary angular momentum, these variables—for a given spin—are allowed to have a limited number of discrete values. Usually these values are added as a subscript to the wavefunction that describes the state of the particle. This implies that in fact a wavefunction of a particle (with a nonzero spin) is not a single function but a set of functions that are characterized by their spin subscripts.

Returning now to NACTs and their matrix  $\tau$ , we intend to construct a concept that is somewhat similar to what is understood as a spin. For this purpose we mention the two-state NACT,  $\tau_{12}$ , which was found to fulfill the quantization condition as presented in Eq. (3.12). As was discussed, the number  $n$  in this equation has to be an integer but not necessarily an even integer (as required by the spatial Bohr-Sommerfeld quantization law<sup>2</sup>) and therefore can also be an odd integer. In this sense the quantization as required for  $\tau_{12}$  is reminiscent of the spin of an elementary particle rather than the quantization of spatial angular momentum.

In case the two states are coupled by several *cis*, the value for the total spin for a region surrounded by a given closed contour is simply the algebraic sum of the individual spin values in the same way as is done in case of the ordinary electronic spins. Thus in this case the meaning of the ordinary spin is conserved. See also a more detailed discussion in Section 5.3.1.

As we have shown, the magnitude that most characterizes a Hilbert subspace is its *cis*. In the present section we are interested mainly in the *topological* features produced by the *cis*. For instance, a two-state system may have several *cis* but it is immaterial how many *cis* it possesses, the *topological* number  $K$  is either 2 or 0 (see discussion in Section 5.3.1).

To extend these ideas to an  $N$ -state system ( $N > 2$ ), we encounter a major obstacle, specifically, the fact that the system becomes non-Abelian; namely, the usual Abelian (functional) variables now become matrices. This difficulty, as we discussed in previous sections of this Chapter, is resolved by the topological  $\mathbf{D}(\Gamma)$  matrix. In order to introduce the *topological spin* for an  $N$ -state system, we need to introduce some order regarding the various numbers that define the  $N$ -state system (in a given region).

We start by defining  $N_c$ , as the smallest *possible* number of *cis*, which an  $N$ -state Hilbert subspace is capable of forming. It is, in fact, straightforward to show that  $N_c = N - 1$  (we recall that any pair of adjacent states has to form at least one *ci*). It is important to emphasize that in general, one may encounter more than one *ci* between a pair of states<sup>3–9</sup> so that the number of *cis* is usually larger than  $N_c$ .

The second number of interest is the abovementioned  $K$  value, which, like the  $\mathbf{D}$  matrix, depends on the chosen (closed) contour  $\Gamma$ ; thus  $K = K(\Gamma)$ . On the other hand,  $K$  does not depend on how many *cis* exist in the  $N$ -state system, but it is constrained in two ways: (1)  $K$  has to be an even integer and (2) the  $K$  values are limited by  $N (= N_c + 1)$  because  $K$  yields the possible numbers of  $(-1)$ s along the diagonal of the  $\mathbf{D}$  matrix and this number cannot exceed the dimension  $N$  of the  $\mathbf{D}$  matrix.

Thus,  $K$  attains the following values:

$$K = \{0, 2, \dots, K_c\} \begin{cases} K_c = N_c; & N_c = \text{even} \\ K_c = (N_c + 1); & N_c = \text{odd} \end{cases} \quad (5.27)$$

In order to construct a relation between  $N_c$  and  $K$  that is similar to the relation between  $\mathbf{S}$ —the total spin of a given system—and its *magnetic* components  $\mathbf{M}_S = \{-S, \dots, +S\}$ , we define the quantum numbers  $S$  as

$$S = \frac{1}{2} \frac{K_c}{2} \quad (5.28a)$$

and, accordingly, its *magnetic* component numbers  $M_S$ :

$$M_S = S - K/2 \quad (5.28b)$$

As examples for  $\mathbf{S}$  and  $M_S$ , we present their values for  $N_c = \{0, 7\}$ :

$$\begin{aligned} \text{For } N_c = 0 : \quad & \{S = 0 \quad M_s = 0\} \\ \text{For } N_c = 1 : \quad & \left\{S = \frac{1}{2} \quad M_s = \frac{1}{2}, -\frac{1}{2}\right\} \\ \text{For } N_c = 2 : \quad & \left\{S = \frac{1}{2} \quad M_s = \frac{1}{2}, -\frac{1}{2}\right\} \\ \text{For } N_c = 3 : \quad & \{S = 1 \quad M_s = 1, 0, -1\} \\ \text{For } N_c = 4 : \quad & \{S = 1 \quad M_s = 1, 0, -1\} \\ \text{For } N_c = 5 : \quad & \left\{S = \frac{3}{2} \quad M_s = \frac{3}{2}, \frac{1}{2}, -\frac{1}{2}, -\frac{3}{2}\right\} \\ \text{For } N_c = 6 : \quad & \left\{S = \frac{3}{2} \quad M_s = \frac{3}{2}, \frac{1}{2}, -\frac{1}{2}, -\frac{3}{2}\right\} \\ \text{For } N_c = 7 : \quad & \{S = 2 \quad M_s = 2, 1, 0, -1, -2\} \end{aligned} \quad (5.29)$$

The general formula and the individual cases listed above indicate that the *smallest* number of *cis* to form a particular Hilbert subspace and the number of possible sign flips within this subspace are indeed interrelated, and this relation is similar to the relation between a given spin value  $S$  and its magnetic components  $\mathbf{M}_S$ . Thus, each Hilbert subspace is now characterized by a *spin quantum number*  $S$ , which is related to the number of states that form the Hilbert subspace and the topological effects that take place within the assigned region in configuration space, namely, how many *possible* (or different) sign flips may occur while following all possible contours in this assigned region.

Since there is a one-to-one relation between the values of  $(S, M_S)$  and  $(K_c, K)$ , Eqs. (5.28) yield the following results

$$\begin{aligned} K_c &= 4S \\ K &= 2(S - M_S) \end{aligned} \quad (5.30)$$

However, the value of  $N_c$  is not uniquely determined here because  $K_c$  has to be even whereas  $N_c$  can be either even or odd, independent of  $K_c$  (or  $K$ ). The reason for not having a unique relation with  $N_c$  is the fact that in every sign flip *two* functions are involved regardless of whether the number of *cis*,  $N_c$ , is even or odd.

Although the whole idea of the topological spin and its components may seem somewhat artificial, it seems to contain physical information in case the molecule is exposed to an external (adiabatic) magnetic field. In this situation a magnetic dipole interaction should theoretically be formed because of the existence of the topological spin as, for instance, in case of an ordinary electronic spin.

According to the procedure above described a system with a given spin  $\mathbf{S}$  has a  $(2S + 1)$  degeneracy. It is obvious that the molecular system, in a field-free situation, is not affected by the sign flip of one function or another as the diabatic potential is a well-defined magnitude of the subspace as a whole. However, exposing the molecular system to a cyclic, electromagnetic field causes parts of the molecule to move, one with respect to the other, along various (closed) contours. This motion may cause some of the eigenfunctions to flip their sign. For a given molecule, the number of flipped signs is determined by the contours enforced by the electromagnetic field. This situation causes the creation of the topological spin, which in turn interacts with the magnetic field.<sup>10</sup> The intensity of this novel type of interaction is not dependent on what happens along a given contour but is related to the structure of the Hilbert subspace. In other word the issue is not how many different sign flips *may* be formed along a particular contour but rather the *probability* of producing a certain number of sign flips in a given molecule (or subspace), and this probability is related to the number of possible *bundles* of contours to form this number of sign flips.

So let us summarize as follows. The multiplicity of the  $\mathbf{D}$  matrix due to an electromagnetic field depends on what happens along a given contour (viz., how many sign flips are encountered), but the probability for that to occur depends on the number of possible *bundles* of contours that lead to this multiplicity.

As examples, we consider the cases of four and five states where each two adjacent states are coupled by a single  $ci$ . In case of  $N = 4$  (or  $N_c = 3$ ), there are six bundles of contours that lead to two (different) sign flips and one bundle of contours that lead to four sign flips [see Eq. (5.24)]. Thus, the multiplicity is equal to 3 because  $M_S = (1, 0, -1)$  as given in the list above, but the probability of having the value  $M_S = 0$  (i.e.,  $K = 2$ ) is 6 times greater than having the value  $M_S = -1$  (i.e.,  $K = 4$ ). In case of  $N = 5$  (or  $N_c = 4$ ), the multiplicity is the same as before, namely, equal to 3 (because  $M_S = (1, 0, -1)$ ) but the probability of having two sign flips is only 2 times greater than having four sign flips because Eq. (5.24) yields the ratio for the two types of contours as 10:5.

## 5.5 EXTENDED EULER MATRIX AS A MODEL FOR ADIABATIC-TO-DIABATIC TRANSFORMATION MATRIX

### 5.5.1 Introductory Comments

In deriving a model for the ADT matrix  $\mathbf{A}$ , we have to make sure that it is capable of forming a matrix with the following features:

1. The matrix has to be orthogonal at any point in configuration space (see Section 1.3.1.3).

2. Its elements are cyclic functions with respect to a single given parameter  $\lambda$ , so that, starting with a diagonal (unit) matrix, the model matrix has to become diagonal again after one cycle (it does not have to return to a unit matrix)
3. While becoming diagonal, it has to contain an *even* number  $K$  of  $(-1)$ s along the diagonal.

It is important to realize that the first condition is due to the fact that  $\mathbf{A}$  is a solution of Eq. (1.50) and the two other conditions are a result the quantization condition (see Section 2.1.3.1 and 2.1.3.3).

In this section we intend to present the general  $N \times N$  ADT matrix  $\mathbf{A}$  as a product of single angle  $N \times N$  rotation matrices. This resulting matrix, which becomes similar to the Euler matrix<sup>1</sup> in case of  $N = 3$ , will be termed, for  $N > 3$ , the *extended Euler matrix*. In what follows this matrix is labeled  $\mathbf{A}^N$ .

Before describing the general situation, we discuss two cases:  $N = 2$  and  $N = 3$ . Once we find that  $\mathbf{A}^{(2)}$  and  $\mathbf{A}^{(3)}$  fulfill the abovementioned, conditions we continue to the general case.

### 5.5.2 Two-Dimensional Case

The matrix  $\mathbf{A}^{(2)}$  is discussed in Section 3.1.1, but for completeness, we describe all its features here.

The matrix  $\mathbf{A}^{(2)}(\gamma_{12})$  takes the form

$$\mathbf{A}^{(2)}(\gamma_{12}(\mathbf{s})) = \begin{pmatrix} \cos \gamma_{12}(\mathbf{s}) & \sin \gamma_{12}(\mathbf{s}) \\ -\sin \gamma_{12}(\mathbf{s}) & \cos \gamma_{12}(\mathbf{s}) \end{pmatrix} \quad (5.31)$$

where  $\gamma_{12}(\mathbf{s})$  fulfills the first-order vector differential equation [see Eq. (3.5)]:

$$\nabla \gamma_{12}(\mathbf{s}) + \boldsymbol{\tau}_{12}(\mathbf{s}) = \mathbf{0} \quad (5.32)$$

This equation is solved along a contour  $\Gamma$  [and consequently the solution of Eq. (5.32) becomes  $\Gamma$ -dependent] given by Eq. (3.6), which in the present notation becomes

$$\gamma_{12}(\mathbf{s}|\Gamma) = - \int_{\mathbf{s}_0}^{\mathbf{s}} d\mathbf{s} \cdot \boldsymbol{\tau}_{12}(\mathbf{s}|\Gamma) \quad (5.33)$$

In deriving Eq. (5.33), we assumed that the initial value of  $\gamma_{12}$ , namely,  $\gamma_{12}(\mathbf{s} = \mathbf{s}_0)$ , is zero.

Next we consider the  $\mathbf{D}$  matrix, which is presented in Eq. (3.11):

$$\mathbf{D}^{(2)}(\Gamma) = \begin{pmatrix} \cos \alpha_{12}(\Gamma) & \sin \alpha_{12}(\Gamma) \\ -\sin \alpha_{12}(\Gamma) & \cos \alpha_{12}(\Gamma) \end{pmatrix} \quad (5.34)$$

As a result of the quantization condition, the matrix  $\mathbf{D}^{(2)}$  has to be diagonal for any closed contour in the region of interest, which implies that  $\alpha_{12}(\Gamma)$  ( $\equiv \gamma_{12}(s = s_0|\Gamma)$ ) fulfills the condition

$$\alpha_{12}(\Gamma) = \gamma_{12}(s = s_0|\Gamma) = n\pi \quad (5.35)$$

where  $n$  is an integer (or zero). From these findings we note that the *two* (diagonal) elements of the  $\mathbf{D}$  matrix are either  $+1$  or  $-1$ , which implies that  $K$  is an even number ( $=2$ ) or zero. Thus the only two possibilities for  $\mathbf{D}^{(2)}$  are as follows

$$\mathbf{D}^{(2)}(\Gamma) = (-1)^k \mathbf{I} \quad (5.36)$$

where  $\mathbf{I}$  is the unit matrix and  $k$  is either even or odd.

### 5.5.3 Three-Dimensional Case

In case of  $N = 3$ , we encounter a matrix, namely,  $\mathbf{A}^{(3)}$ , with nine elements. However, since  $\mathbf{A}^{(3)}$  has to be an orthogonal matrix, the orthonormality criterion requires the fulfillment of six conditions, which leaves three free unknowns that, according to Euler, are three angles of rotation, namely,  $\gamma_{12}$ ,  $\gamma_{13}$ , and  $\gamma_{23}$ .<sup>1</sup> Consequently construction of the  $\mathbf{A}$  matrix as a product of three rotation matrices was suggested. For this purpose we define the three matrices  $\mathbf{Q}_{12}^{(3)}(\gamma_{12})$ ,  $\mathbf{Q}_{23}^{(3)}(\gamma_{23})$ , and  $\mathbf{Q}_{13}^{(3)}(\gamma_{13})$ , where, for instance,  $\mathbf{Q}_{13}^{(3)}(\gamma_{13})$  is given in the form

$$\mathbf{Q}_{13}^{(3)}(\gamma_{13}) = \begin{pmatrix} \cos \gamma_{13} & 0 & \sin \gamma_{13} \\ 0 & 1 & 0 \\ -\sin \gamma_{13} & 0 & \cos \gamma_{13} \end{pmatrix} \quad (5.37)$$

(the other two are similar in structure with the respective cosine and sine functions in the appropriate positions). Thus,  $\mathbf{A}^{(3)}$  becomes

$$\mathbf{A}^{(3)} = \mathbf{Q}_{12}^{(3)} \mathbf{Q}_{23}^{(3)} \mathbf{Q}_{13}^{(3)} \quad (5.38)$$

which, following multiplication, takes the form

$$\mathbf{A}^{(3)} = \begin{pmatrix} c_{12}c_{13} - s_{12}s_{13}s_{23} & -s_{12}c_{23} & c_{12}s_{13} + s_{13}s_{12}s_{23} \\ -s_{12}c_{13} - c_{12}s_{13}s_{23} & c_{12}c_{23} & -s_{12}s_{13} + c_{12}c_{13}s_{23} \\ -c_{23}s_{13} & -s_{23} & c_{13}c_{23} \end{pmatrix} \quad (5.39)$$

Here  $c_{kj} = \cos(\gamma_{kj})$  and  $s_{kj} = \sin(\gamma_{kj})$ . It is important to note that deriving the matrix  $\mathbf{A}^{(3)}$  in this way guarantees that the matrix is orthogonal (i.e., is a product of three orthogonal matrices).

The relevant  $\mathbf{D}^{(3)}$  matrix is obtained from  $\mathbf{A}^{(3)}$  by replacing the  $\gamma_{kj}$  angles by  $\gamma_{kj}(\mathbf{s} = \mathbf{s}_0|\Gamma)$ , which are the values,  $\gamma_{kj}$ , at the end of the (closed) contour. These end-of-contour angles are designated as  $\alpha_{kj}(\Gamma)$

$$\alpha_{kj}(\Gamma) = \gamma_{kj}(\mathbf{s} = \mathbf{s}_0|\Gamma) \quad (5.40)$$

Next it is known that the  $\mathbf{D}^{(3)}$  matrix formed in this way has to be a diagonal matrix; this condition can be achieved if and only if  $\alpha_{kj}(\Gamma) = n_{kj}\pi$ , where  $n_{kj}$  are integers. Since the diagonality of the  $\mathbf{D}^{(3)}$  matrix is guaranteed by the quantization condition (see Sections 2.1.3.1 and/or 2.1.3.3), it is expected that if the suggested model is correct, then the quantization also guarantees that  $\alpha_{kj}(\Gamma) = n_{kj}\pi$ .

To obtain the three angles, Eq. (5.39) is substituted in Eq. (1.50) (instead of  $\Omega$ ) and it can be shown that the three angles have to satisfy the following three coupled first-order differential equations:<sup>2,3</sup>

$$\begin{aligned} \nabla\gamma_{12} &= -\tau_{12} - \tan\gamma_{23}(-\tau_{13}\cos\gamma_{12} + \tau_{23}\sin\gamma_{12}) \\ \nabla\gamma_{23} &= -(\tau_{23}\cos\gamma_{12} + \tau_{13}\sin\gamma_{12}) \\ \nabla\gamma_{13} &= (\cos\gamma_{13})^{-1}(-\tau_{13}\cos\gamma_{12} + \tau_{23}\sin\gamma_{12}) \end{aligned} \quad (5.41)$$

Next we examine the possible signs of the diagonal elements of  $\mathbf{D}^{(3)}$ . Because of the product in Eq. (5.38) (see also Eq. (5.39)), these diagonal elements can be written as

$$D_{ij}^{(3)} = \delta_{ij} \cos\alpha_{jn} \cos\alpha_{jm}; \quad j \neq n \neq m; \quad j = 1, 2, 3 \quad (5.42)$$

where all the terms that contain sine functions are obviously zero [ $\sin(\pm n\pi) = 0$ ]

The expressions in Eq. (5.42) show that the  $\mathbf{D}^{(3)}$  matrix may have either (1) three (+1)s in the diagonal (this happens when all cosine functions are either positive or negative) or (2) two (-1)s and one (+1) (which happens when one or two of the three cosine functions are negative). Case 1 can occur if the contour surrounds an even number of conical intersections for each pair of *adjacent* states (or does not surround any conical intersection), whereas case 2 applies for all other situations. It is straightforward to see that according to this model,  $K$  is either 2 or 0 as, indeed, is required.

Equations (5.41) were solved on various occasions either for model systems<sup>3,4</sup> or for real molecular systems such as the {C<sub>2</sub>H} molecule<sup>5</sup> and the {H,H<sub>2</sub>} system.<sup>6</sup>

In the present section we show a few results obtained for the {C<sub>2</sub>,H} system.<sup>5</sup> These calculations are performed along circular contours for the various *angular* components, namely,  $(1/q)\tau_{\varphi kj}$  [see Eq. (4.2)] only. Consequently the grad operator  $\nabla$  in Eq. (5.41) is replaced by the corresponding angular component  $(1/q)(\partial/\partial\varphi)$ . These calculations yield the  $\varphi$ -dependent  $\gamma$  angles [i.e.,  $\gamma_{kj}(\varphi|q)$ , calculated for given values of  $q$ ].

As discussed in section 4.3.2.2, the three lower *excited* states of the  $\{\text{C}_2\text{H}\}$  system, namely, the  $2^2A'$ ,  $3^2A'$ , and  $4^2A'$  states, form a *three-state* Hilbert subspace. These states are coupled by three *cis*, the *lower* two states, namely, the  $2^2A'$  and  $3^2A'$  states are coupled by one  $C_{2v}$  *ci* and the two upper ones, the  $2^2A'$  and  $3^2A'$  states, are coupled by two twin *cis* (see Figs. 4.8c and 4.8c). Employing MOLPRO, we derived the three angular NACTs  $\tau_{ijk}(\varphi|q)$ ;  $j(>k) = 1, 2$ , which were then substituted in Eqs. (5.41) to be solved for the three Euler angles:  $\gamma_{23}(\varphi|q)$ ,  $\gamma_{34}(\varphi|q)$  and  $\gamma_{24}(\varphi|q)$ <sup>5</sup>. The subindices are shifted by one because we consider three excited states and ignore the ground state.

In Figure 5.5 these three angles are presented as a function of  $\varphi$ , calculated along two different circles shown in Figure 4.8 (one is the  $\Gamma_{24}$  contour given in Fig. 5.5c and one is the  $\Gamma'_{24}$  contour in Fig. 5.5d). In general, the results speak for themselves, but we refer to one particular issue—the values of the topological phases  $\alpha_{jk}$  ( $\equiv \gamma_{jk}(\varphi = 2\pi|q)$ ), as calculated for different circles, are all either zero or  $\pm\pi$ . This, in turn, guarantees that the relevant  $\mathbf{D}$  matrix is a diagonal matrix with numbers of  $(\pm 1)$  in the diagonal [see Eq. (5.42)]. Moreover, we note that for the results in Figure 5.5a we get  $\{\alpha_{23}, \alpha_{24}, \alpha_{34}\} = \{\pi, 0, 0\}$ , which correspond to  $\{D_{11}, D_{22}, D_{33}\} = \{--+\}$  [see Eq. (5.42)] and for the results in Figure 5.5b we get  $\{\alpha_{23}, \alpha_{24}, \alpha_{34}\} = \{0, -\pi, 0\}$ , which

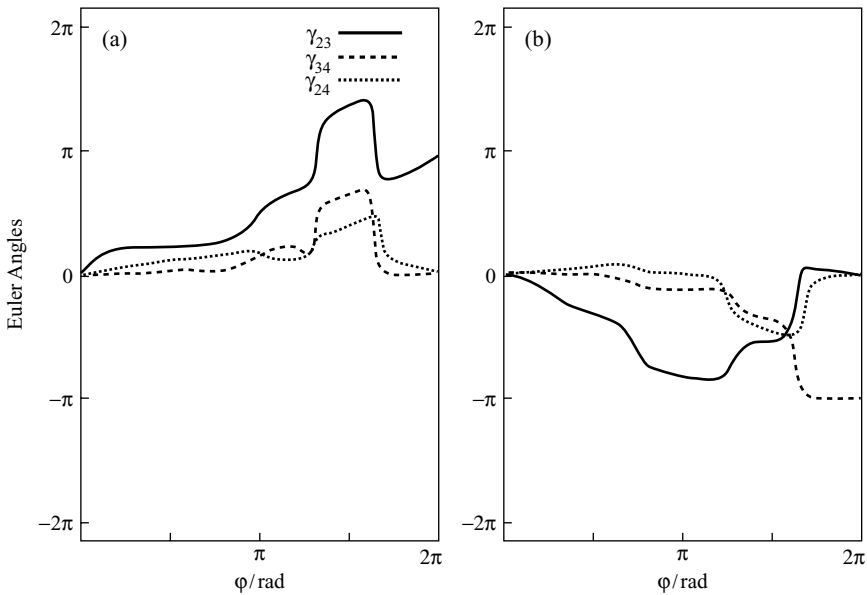


**Figure 5.5** The three Euler angles ( $\gamma_{23}, \gamma_{34}, \gamma_{24}$ ) as a function  $\varphi$ , calculated along contours that surround *cis* of the  $\{\text{C}_2\text{H}\}$  system, namely, the (2,3) *ci* and the two (3,4) *cis*: (a) calculations along the contour  $\Gamma_{24}$  (see Fig. 4.8c); (b) calculations along the contour  $\Gamma'_{24}$  (see Fig. 4.8d): —  $\gamma_{23}$ ; ---  $\gamma_{24}$ ; ....  $\gamma_{34}$ .

correspond to  $\{D_{11}, D_{22}, D_{33}\} = \{-+-\}$  [see Eq. (5.42)]. The diagonal elements of the  $\mathbf{D}$  matrix calculated solving the Euler angles are identical to the one listed in Table 4.3.

### 5.5.4 Multidimensional Case

The  $N$ -dimensional ADT matrix  $\mathbf{A}^N$  can be written as a product of elementary rotation matrices similar to that given in Eq. (5.38):<sup>7-9</sup>

$$\mathbf{A}^{(N)} = \prod_{i=1}^{N-1} \prod_{j>i}^N \mathbf{Q}_{ij}^{(N)}(\gamma_{ij}) \quad (5.43)$$

where  $\mathbf{Q}_{ij}^{(N)}(\gamma_{ij})$  [as in Eq. (5.37)] is an  $N \times N$  matrix with the following elements. The two relevant cosine functions are located at its  $(ii)$  and  $(jj)$  positions and  $(+1)$ s are located at the remaining  $(N - 2)$  positions along the diagonal the two relevant  $\pm$  sine functions are located at the  $(ij)$  and  $(ji)$  off-diagonal positions, and all other remaining positions are zeros. From Eq. (5.43) it can be seen that the number of matrices contained in this product is  $N(N - 1)/2$  and that this is also the number of independent  $\gamma_{ij}$  angles needed to describe an  $N \times N$  unitary matrix [we recall that the missing  $N(N + 1)/2$  conditions follow from the orthonormality conditions]. The matrix  $\mathbf{A}^{(N)}$  as presented in Eq. (5.43) is characterized by two important features: (1) every *diagonal* element contains at least one term that is a product of cosine functions only and (2) all *off-diagonal* elements are formed by a summation of products where each one contains at least one sine function.

To obtain the  $\gamma_{ij}$  angles, one usually has to solve the first-order differential equations of the type given in Eq. (5.41). Next, as before, the  $\alpha_{ij}$  angles are defined as the  $\gamma_{ij}$  angles at the end of a closed contour. In order to obtain the matrix  $\mathbf{D}^{(N)}$ , one replaces, in Eq. (5.43), the angles  $\gamma_{ij}$  by the corresponding  $\alpha_{ij}$  angles. In order for  $\mathbf{D}^{(N)}$  to be a diagonal matrix, all  $\alpha_{ij}$  angles have to be multiples of  $\pi$  (or zero) to guarantee that all sine functions become zero and all cosine functions become  $\pm 1$ . The only nonzero elements, if these requirements are fulfilled, are the diagonal ones, which are made up of products of cosine functions [see also Eq. (5.42)], that is

$$D_{ij}^{(N)} = \delta_{ij} \prod_{k \neq i}^N \cos \alpha_{ik} = \delta_{ij} (-1)^{\sum_{i \neq k}^N n_{ik}}; \quad i = \{1, N\} \quad (5.44)$$

where  $n_{ik}$  are integers that fulfill  $n_{ik} = n_{ki}$ . From Eq. (5.44) we note that one encounters  $(\pm 1)$ s along the diagonal of  $\mathbf{D}^{(N)}$ . Our next assignment is to prove the following lemma.

**Lemma 5.4** The number of  $(-1)$ s,  $K$ , along the diagonal is an even number for any  $\mathbf{D}^{(N)}$  matrix.

*Proof* We start with a given matrix  $\mathbf{D}^{(N)}$  and consider the various  $\alpha_{ik}$  phases in Eq. (5.44). Next we consider a slightly different matrix  $\mathbf{D}^{(N)}$  [to be assigned as  $\mathbf{D}'^{(N)}$ ] for which one of the phases, say,  $\alpha_{nm}$ , is changed from zero to  $\pi$ . It is obvious that all matrix elements that do not contain  $\alpha_{nm}$  are unaffected by this change and those that contain it flip their sign. Since  $\alpha_{nm} \equiv \alpha_{mn}$ , it can be shown that only two products (or two matrix elements) contain this particular angle, namely,  $D_{mm}^{(N)}$  and  $D_{nn}^{(N)}$ . Thus, the sign flip of the single  $\cos(\alpha_{nm})$  function causes two sign flips along the diagonal of  $\mathbf{D}^{(N)}$ , namely, one at  $D_{mm}^{(N)}$  and one at  $D_{nn}^{(N)}$ . This implies that, in general, sign flips can occur only to an even number of terms of the  $\mathbf{D}^{(N)}$  matrix. Since the group of all possible matrices  $\mathbf{D}^{(N)}$  contains also the unit matrix, this implies that  $K$  has to be even, and its values are given as

$$K = \{0, 2, \dots, K_f\} \quad (5.45)$$

where  $K_f$  is equal to either  $N$  or  $N - 1$  (depending on whether  $N$  is even or odd).

**Short Summary** At the beginning of this section we listed three requirements for the extended Euler matrix to be a model matrix for the ADT matrix. In this section we proved that these Euler matrices fulfill these requirements and therefore can be considered as suitable for presentation of a general ADT matrix.

## 5.6 QUANTIZATION OF $\tau$ MATRIX AND ITS RELATION TO SIZE OF CONFIGURATION SPACE: MATHIEU EQUATION AS A CASE OF STUDY

The way to estimate the degree that a given  $\tau$  matrix of dimension  $N \times N$  is quantized in a region  $\Lambda$ , formed by a closed contour  $\Gamma$ , is to form the relevant  $\mathbf{D}(\Gamma|N)$  matrix [see, eg., Eq. (4.6)] and to determine the extent to which it is diagonal [we recall that since the  $\mathbf{D}$  matrix is an orthogonal (real) matrix, its diagonal elements are expected to be close to  $\pm 1$ ]. In Section 5.3 we discussed various ab initio molecular systems and found strong evidence that for a given region in configuration space the matrix  $\mathbf{D}(N)$  becomes more and more diagonal as  $N$  gets larger. However, a consistent convergence study of this kind could not be done for ab initio systems because numerical instabilities are enhanced as  $N$  increases. In this section we present such a study, but employing eigenfunctions derived from the (appropriate) Mathieu equation. Because of its simplicity, we face no instabilities, and the wall time it takes to produce a sizable electronic manifold is relatively short.

### 5.6.1 Mathieu Equation and Its Eigenfunctions

The Mathieu equation considered in this section is of the form<sup>1-8</sup>

$$\left(-\frac{1}{2}E_{\text{el}}\frac{\partial^2}{\partial\theta^2} - U(\theta|\varphi, q) - u_j(\varphi, q)\right)\zeta_j(\theta|\varphi, q) = 0 \quad (5.46)$$

where  $U(\theta|\varphi, q)$  is the electronic potential:

$$U(\theta|\varphi, q) = G(\varphi, q) \cos(2\theta - \varphi) \quad (5.47)$$

Here,  $\theta$  serves as an electronic (cyclic) coordinate,  $(\varphi, q)$  are two nuclear polar coordinates,  $G(\varphi, q)$  is the nuclear-electronic interaction coefficient,  $u_j(\varphi, q)$  and  $\zeta_j(\theta|\varphi, q)$  are the  $j$ th eigenvalue and eigenfunction, respectively, which parametrically depend on the nuclear coordinates, and  $E_{\text{el}}$  is a characteristic electronic quantity. Equation (5.46) is recognized as the well-known Mathieu equation. For the present study we assume that  $G(\varphi, q)$  is independent of  $\varphi$  and linearly dependent on  $q$ , namely, equal to  $kq$ , where  $k$  is a constant. This choice of the interaction term has several numerical advantages, discussed below.

To simplify the forthcoming treatment somewhat, we introduce a new parameter,  $x$ , defined as follows:

$$x = q(k/E_{\text{el}}) \quad (5.48)$$

Thus,  $x$  replaces  $q$  as the *radial* coordinate. As was mentioned earlier, the size of the  $\Lambda$  region plays an important role in our study. In the present notation  $q$  is a (nuclear) coordinate directly associated with the size of  $\Lambda$  so that the larger is  $q$ , the larger is the  $\Lambda$  region. The same rule now applies for  $x$ ; the larger is  $x$ , the larger is the  $\Lambda$  region. Therefore, the numerical study reported here concentrates on the relation between  $x$  and  $N$ , the dimension of the  $\tau$  matrix. With all these changes, Eq. (5.46) takes the following form:

$$\left( -\frac{1}{2} \frac{\partial^2}{\partial \theta^2} - x \cos(\theta - \varphi/2) - u_j(\varphi, x) \right) \zeta_j(\theta|\varphi, x) = 0 \quad (5.49)$$

To solve the Mathieu equation, we expand the  $\zeta_j(\theta|x,\varphi)$  eigenfunctions in Fourier series. For our purposes and in the notation of Ref. 7, we select the following two families of solutions

$$\begin{aligned} ce_{2n+1}(z, -x) &= \sum_{m=0}^{\infty} A_{2m+1}^{2n+1}(-x) \cos(2m + 1)z \\ se_{2n+1}(z, -x) &= \sum_{m=0}^{\infty} B_{2m+1}^{2n+1}(-x) \sin(2m + 1)z \end{aligned} \quad (5.50)$$

where  $z$  is given as

$$z = \theta - \frac{\varphi}{2} \quad (5.51)$$

Here the cosine series stands for the  $\zeta_j(\theta|x,\varphi)$  functions with odd  $j$  values and the sine function, for those with the even  $j$  values.

It is well known that the geometric series as presented in Eqs. (5.50) does not converge at points close to the real  $z$  axis. This feature may affect the rate of convergence for points on the real axis. For this reason, the convergence in each case has to be treated with care. In this respect it is important to mention that we had to include 200 terms in the series in Eq. (5.50) to guarantee the required convergence.

### 5.6.2 Nonadiabatic Coupling Matrix ( $\tau$ ) and Topological Matrix ( $\mathbf{D}$ )

Solving Eq. (5.49) yields a set of  $N$  eigenvalues with the following features: (1) all the eigenvalues are  $\varphi$ -independent and depend on  $x$  only—thus  $u_j(x, \varphi) \equiv u_j(x)$ ;  $j = \{1, N\}$ ; (2) the eigenvalues become degenerate at  $x = 0$  only; (3) the degenerate states are arranged in pairs, namely, the first and the second states are degenerate (at  $x = 0$ ), and so are the third and the fourth states, the fifth and the sixth states, and so on. Consequently, close enough to  $x = 0$ , each pair of this kind forms a two-state Hilbert subspace.

We continue by considering the NACTs themselves and their NACMs; they, just like the eigenvalues, are found to be  $\varphi$ -independent.<sup>4</sup> The fact that the degenerate states are arranged in the pattern described above implies that in the close vicinity of  $x = 0$ , the NACM,  $\boldsymbol{\tau}_\varphi$ , becomes

$$\boldsymbol{\tau}_\varphi(x \sim 0|N) = \begin{pmatrix} 0 & \boldsymbol{\tau}_{\varphi 12} & 0 & 0 & 0 \\ -\boldsymbol{\tau}_{\varphi 12} & 0 & 0 & 0 & 0 \\ 0 & 0 & 0 & \boldsymbol{\tau}_{\varphi 34} & 0 \\ 0 & 0 & -\boldsymbol{\tau}_{\varphi 34} & 0 & 0 \\ 0 & 0 & 0 & 0 & 0 \end{pmatrix} \quad (5.52)$$

The two-state case was studied in Ref. 2, and it was found that  $\boldsymbol{\tau}_{\varphi 12}(x \sim 0) = \frac{1}{2}$ . Therefore, here, too,  $\boldsymbol{\tau}_{\varphi j+1} = \boldsymbol{\tau}_{\varphi j+1}(x \sim 0) = \frac{1}{2}$  for  $j = 2n + 1$ , where  $n$  is an integer (or zero).

Next we consider the  $\mathbf{D}$  matrix, which, for our case, takes the form<sup>4</sup>

$$\mathbf{D}(x|N) = \wp \exp(-2\pi \boldsymbol{\tau}_\varphi(x|N)) \quad (5.53)$$

because, as mentioned earlier, the various NACTs are  $\varphi$ -independent. This  $\mathbf{D}$  matrix, for the NACM in Eq. (5.52), can be shown to be equal to  $-\mathbf{I}$ , where  $\mathbf{I}$  is the unit matrix.

In order to obtain the  $\mathbf{D}$  matrix for arbitrary  $x$  values, we solve Eq. (5.49), form the required NACM, and substitute it in Eq. (5.53).

From the results it was verified that the last *diagonal* element of the matrix  $\mathbf{D}(x|N)$ , namely,  $D_{NN}(x|N)$ , shows the largest deviation from  $(-1)$ .<sup>4</sup> In Figure 5.6 these  $D_{NN}(x|N)$  elements are presented as a *function* of  $N$  for different  $x$  values. It is noticed that the each  $D_{NN}(x|N)$  curve decays asymptotically toward the value of  $(-1)$  as  $N$  increases but the rate of decay becomes slower when  $x$  is greater (i.e., when the region in configuration space is larger). Thus it is noted that, for example, at

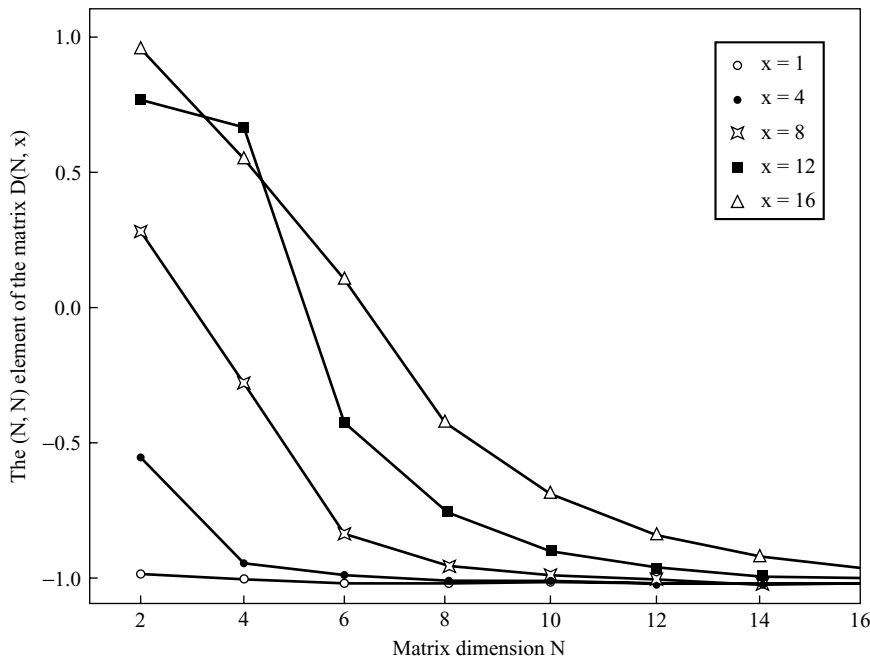


**Figure 5.6** The last diagonal matrix element of the topological  $\mathbf{D}$  matrix,  $D_{NN}(N, x)$  (derived by solving the Mathieu equation) as a function of  $N$ , presented for various  $x$  values (empty circles— $x = 1.0$ ; enlarged dots— $x = 4.0$ ; diamonds— $x = 8.0$ ; squares— $x = 12.0$ ; triangles— $x = 16.0$ ).

$x = 4$  the rate of decay is relatively fast (all diagonal elements for  $N \geq 4$  are already  $-1$ ) but for  $x = 16$  the rate of convergence is so slow that we may reach the value of  $(-1)$  only when  $N > 16$ .

**Short Summary** We showed here that the more extended is the region in configuration space (expressed in terms of  $x$ ), the larger is the required size  $N$  of a group of states in order to become a Hilbert subspace. Our study is not typical for Born–Oppenheimer states because the various  $ci$  points for this system are located at the same point, but nevertheless this study illuminates some aspects of the relation between  $x$  and  $N$ .

## PROBLEMS

- 5.1** In Section 5.1 we expressed the NACT matrix elements  $\tau_{jk}(\mathbf{s})$  in terms of  $\nabla\mathbf{H}_e(\mathbf{s}_e|\mathbf{s})$  [see Eq. (5.1)]. Here, we express  $\tau_{jk}(\mathbf{s})$  in terms of the diabatic potential matrix  $\mathbf{W}(\mathbf{s})$  [see Eq. (2.39)]:

$$\mathbf{W} = \mathbf{A}^\dagger \mathbf{u} \mathbf{A} \quad (5.54)$$

and the corresponding ADT matrix  $\mathbf{A}$ .

*Solution* We start by differentiating Eq. (5.54) and rearranging somewhat the result:

$$\mathbf{A} \nabla \mathbf{W} \mathbf{A}^\dagger = \mathbf{A} (\nabla \mathbf{A}^\dagger) \mathbf{u} + \nabla \mathbf{u} + \mathbf{u} (\nabla \mathbf{A}) \mathbf{A}^\dagger \quad (5.55)$$

Next, employing Eq. (2.37), we express the derivates  $\nabla \mathbf{A}$  and  $\nabla \mathbf{A}^\dagger$  in terms of the matrix  $\tau(\mathbf{s})$ :

$$\mathbf{A} \nabla \mathbf{W} \mathbf{A}^\dagger = \boldsymbol{\tau} \mathbf{u} + \nabla \mathbf{u} - \mathbf{u} \boldsymbol{\tau} \quad (5.56)$$

If  $\Omega$  is defined as the sum of the three terms on the r.h.s. of Eq. (5.56), we find its elements to be of the form

$$\Omega_{jk} = \begin{cases} \nabla u_j; & j = k \\ (u_j - u_k) \boldsymbol{\tau}_{jk}; & j \neq k \end{cases} \quad (5.57)$$

Since  $\Omega$  is also equal to the l.h.s. of Eq. (5.56), we get the following result for  $\boldsymbol{\tau}_{jk}(\mathbf{s})$ :

$$\boldsymbol{\tau}_{jk} = \frac{\mathbf{A}_j \nabla \mathbf{W} \mathbf{A}_k^\dagger}{u_j - u_k}; \quad j \neq k \quad (5.58)$$

which is the requested expression. Equation (5.58) implies that having the diabatic matrix  $\mathbf{W}$ , one can produce the corresponding NACM by employing only the  $\mathbf{W}$  matrix and its eigenvalues and eigenvectors.

## 5.2 Given the $2 \times 2$ diabatic potential matrix $\mathbf{W}$

$$\mathbf{W} = \begin{pmatrix} W_{11} & W_{12} \\ W_{12} & W_{22} \end{pmatrix} \quad (5.59)$$

prove the following:

(a) If  $\mathbf{A}$ , written in the form

$$\mathbf{A}(\beta) = \begin{pmatrix} \cos \beta & \sin \beta \\ -\sin \beta & \cos \beta \end{pmatrix} \quad (5.60)$$

is the matrix that diagonalizes  $\mathbf{W}$ , then the angle  $\beta$  fulfills the following relation:

$$\beta = \frac{1}{2} \tan^{-1} \frac{2W_{12}}{W_{11} - W_{22}} \quad (5.61)$$

- (b) Employ Eq. (5.59) to show that the corresponding (1,2) NACT,  $\tau_{12}$ , is given in the following form:

$$\tau_{12}(\mathbf{s}) = \nabla \beta \quad (5.62)$$

*Solution:*

- (a) To derive Eq. (5.61), we consider Eqs. (3.13), subtract the second equation from the first, and divide the third equation by respective differences

$$\frac{W_{12}(\mathbf{s})}{W_{11}(\mathbf{s}) - W_{22}(\mathbf{s})} = \frac{\cos \beta(\mathbf{s}) \sin \beta(\mathbf{s})}{\cos^2 \beta(\mathbf{s}) - \sin^2 \beta(\mathbf{s})}$$

or

$$\frac{1}{2} \tan 2\beta(\mathbf{s}) = \frac{W_{12}(\mathbf{s})}{W_{11}(\mathbf{s}) - W_{22}(\mathbf{s})} \quad (5.63)$$

which, following simple rearrangements, leads to Eq. (5.61).

- (b) To prove Eq. (5.62), we consider Eq. (5.58) for the case that  $j = 1$  and  $k = 2$  and again employ Eq. (3.13):

$$\tau_{12}(\mathbf{s}) = \frac{\mathbf{A}_2 \nabla \mathbf{W} \mathbf{A}_1^\dagger}{u_2 - u_1} = \frac{\sin 2\beta}{2W_{12}} \mathbf{A}_2 \nabla \mathbf{W} \mathbf{A}_1^\dagger \quad (5.64)$$

where  $\mathbf{A}_j$ ;  $j = 1, 2$  are the two rows of the  $\mathbf{A}$  matrix in Eq. (5.60). Substituting the explicit expressions for  $\mathbf{A}_j$ ;  $j = 1, 2$  in Eq. (5.64) yields

$$\tau_{12}(\mathbf{s}) = \frac{\sin 2\beta}{2W_{12}} \left( -\frac{\sin 2\beta}{2} \nabla (W_{11} - W_{22}) + \cos 2\beta \nabla W_{12} \right) \quad (5.65)$$

Next, differentiating Eq. (5.61), we obtain

$$\frac{1}{2} \nabla (W_{11} - W_{22}) = W_{12} \nabla (\cot 2\beta) + \cot 2\beta \nabla W_{12} \quad (5.66)$$

and substituting Eq. (5.66) in Eq. (5.65) finally yields Eq. (5.62)

## REFERENCES

### Section 5.1

1. H. Hellmann, *Einführung in die Quantenchemie*, Deuticke, Leipzig, 1937.
2. R. P. Feynman, *Phys. Rev.* **56**, 340 (1940).
3. S. T. Epstein, *Am. J. Phys.* **22**, 613 (1954).

4. S. B. Singh and C. A. Singh, *Am. J. Phys.* **57**, 894 (1989).
5. H. A. Jahn and E. Teller, *Proc. Roy. Soc. Lond. A* **161**, 220 (1937).
6. M. Baer, A. M. Mebel, and R. Englman, *Chem. Phys. Lett.* **354**, 243 (2002).
7. E. Renner, *Z. Phys.* **92**, 172 (1934).
8. G. Herzberg, *Molecular Spectra and Molecular Structure*, Vol. III, Krieger, Malabar, 1991.
9. H. C. Longuet-Higgins, *Adv. Spectrosc.* **2**, 429 (1961).
10. G. Halász, Á. Vibók, A. M. Mebel, and M. Baer, *J. Chem. Phys.* **118**, 3052 (2003).
11. M. Baer, *Chem. Phys. Lett.* **349**, 84 (2001).
12. R. Englman and A. Yahalom, *Acta Univ. Debreceniensis (Series Physica et Chimica)* **34–35**, 283 (2002).
13. T. Vértesi, Á. Vibók, G. J. Halász, and M. Baer, *J. Chem. Phys.* **121**, 4000 (2004).
14. T. Vértesi, Á. Vibók, G. J. Halász, and M. Baer, *J. Phys. B* **37**, 4603 (2004).
15. T. Vértesi and E. Bene, *Chem. Phys. Lett.* **392**, 17 (2004).

## Section 5.2

1. M. Baer, *Chem. Phys. Lett.* **329**, 450 (2000).

## Section 5.3

1. H. C. Longuet-Higgins, U. Opik, M. H. L. Pryce, and R. A. Sack, *Proc. Roy. Soc. Lond. A* **244**, 1 (1958).
2. G. Herzberg and H. C. Longuet-Higgins, *Disc. Faraday Soc.* **35**, 77 (1963).
3. H. C. Longuet-Higgins, *Proc. Roy. Soc. Lond. A* **344**, 147 (1975).
4. M. S. Child, in *The Role of Degenerate States in Chemistry*, M. Baer and G. D. Billing, eds., *Adv. Chem. Phys.* **124**, 1 (2002).
5. A. M. Mebel, G. J. Halász, Á. Vibók, A. Alijah, and M. Baer, *J. Chem. Phys.* **117**, 991 (2002).
6. G. Halász, Á. Vibók, A. M. Mebel, and M. Baer, *Chem. Phys. Lett.* **358**, 163 (2002).
7. M. Baer, *J. Phys. Chem. A* **105**, 2198 (2001).
8. M. Baer, *Chem. Phys. Lett.* **329**, 450 (2000).
9. M. S. Child and D. E. Manolopoulos, *Phys. Rev. Lett.* **82**, 2223 (1999).
10. A. J. C. Varandas and Z. R. Xu, *Int. J. Quant. Chem.* **99**, 385 (2004).
11. A. J. C. Varandas, *Fundamental World of Quantum Chemistry*, E. J. Brandas and E. S. Kryachko, eds., Vol. II, 2003, p.33.
12. G. Halász, Á. Vibók, A. M. Mebel, and M. Baer, *J. Chem. Phys.* **118**, 3052 (2003).
13. E. R. Davidson, *J. Am. Chem. Soc.* **99**, 397 (1977).
14. S. L. Mielke, B. C. Garret, and K. A. Peterson, *J. Chem. Phys.* **116**, 4142 (2002).
15. S. Han and D. R. Yarkony, *J. Chem. Phys.* **119**, 5058 (2003).
16. P. Pistoletti and N. Manini, *Phys. Rev. Lett.* **85**, 1585 (2000).

## Section 5.4

1. L. Landau and E. Lifshitz, *Quantum Mechanics*, Pergamon Press, London, 1959, p. 186.
2. D. Bohm, *Quantum Theory*, Dover Publications, New York, 1959, p. 41.
3. A. Mebel, A. Yahalom, R. Englman, and M. Baer, *J. Chem. Phys.* **115**, 3673 (2001).
4. N. Matsunaga and D. R. Yarkony, *J. Chem. Phys.* **107**, 7825 (1997).
5. A. Mebel, M. Baer, V. M. Rozenbaum, and S. H. Lin, *Chem. Phys. Lett.* **336**, 135 (2001).
6. G. Halász, Á Vibók, A. M. Mebel, and M. Baer, *J. Chem. Phys.* **118**, 3052 (2003).
7. S. Han and D. R. Yarkony, *J. Chem. Phys.* **119**, 5058 (2003).
8. S. S Xantheas, G. J. Atchty, S. T. Ebert, and K Ruedenberg, *J. Chem. Phys.* **95**, 1862 (1991).
9. M. S. Gordon, V.-A. Glezakou, and D. R. Yarkony, *J. Chem. Phys.* **108**, 5657 (1998).
10. M. V. Berry, *Proc. Roy. Soc. London A*, **392**, 45 (1984).

## Section 5.5

1. H. Goldstein, *Classical Mechanics*, Addison-Wesley, Reading, MA, 1966, p. 107.
2. Z. H. Top and M. Baer, *J. Chem. Phys.* **66**, 1363 (1977).
3. A. Alijah and M. Baer, *J. Phys. Chem. A* **104**, 389 (2000).
4. S. Adhikari, G. D. Billing, A. Alijah, S. H. Lin, and M. Baer, *Phys. Rev. A* **62**, 032507-1 (2000).
5. A. M. Mebel, G. J. Halász, Á Vibók, A. Alijah, and M. Baer, *J. Chem. Phys.* **117**, 991 (2002).
6. T. Vértesi, E. Bene, Á Vibók, G. J. Halász, and M. Baer, *J. Phys. Chem.* **109**, 3476 (2005).
7. M. Baer, *Chem. Phys. Lett.* **329**, 450 (2000).
8. M. Baer, in *The Role of Degenerate States in Chemistry*, M. Baer and G. D. Billing, eds., *Adv. Chem. Phys.* **124**, 39, (2002).
9. A. Kuppermann and R. Abrol, in *The Role of Degenerate States in Chemistry*, M. Baer and G. D. Billing, eds., *Adv. Chem. Phys.* **124**, 283 (2002).
10. D. E. Manolopoulos and M. S. Child, *Phys. Rev. Lett.* **82**, 2223 (1999).

## Section 5.6

1. M. Baer and R. Englman, *J. Molec. Phys.* **75**, 283 (1992).
2. M. Baer, A. Yahalom, and R. Englman, *J. Chem. Phys.* **109**, 6550 (1998).
3. R. Englman, Yahalom, A. and M. Baer, *Int. J. Quant. Chem.* **90**, 266 (2002).
4. T. Vértesi, Á Vibók, G. J. Halász, A. Yahalom, R. Englman, and M. Baer, *J. Phys. Chem. A* **107**, 7189 (2003).
5. H. C. Longuet-Higgins, U. Opik, M. H. L. Pryce, and R. A. Sack, *Proc. Roy. Soc. Lond. A* **244**, 1 (1958).
6. V. Aquilanti, S. Cavalli, and G. Grossi, *Theor. Chim. Acta*, **75**, 33 (1989).
7. N. W. MacLachlan, *Theory and Application of Mathieu Functions*, (Clarendon, Oxford, 1947).
8. E. T. Whittaker and G. N. Watson, *A Course of Modern Analysis*, Cambridge Univ. Press, 1996.

# CHAPTER 6

---

## MOLECULAR FIELD

---

### 6.1 SOLENOID AS A MODEL FOR THE SEAM

In Sections 1.1.2 and 1.1.3 we showed that the adiabatic Born–Oppenheimer eigenfunctions that form a Hilbert space produce Curl–divergence equations [see Eqs. (1.24) and (1.34), respectively] that are similar to the Curl–divergence equations encountered in electrodynamics<sup>1</sup> (in what follows we refer to these equations as *C-D equations*).

On the basis of this feature, we present a new approach to treat the NACTs, namely, to consider their spatial distribution as *fields* where at least some of them are produced by source points reminiscent of electromagnetic fields formed by charged particles (electrons, protons, etc.). It will be shown that the source points in our case are the *cis* points—the points at which certain NACTs become singular (see Section 5.1). Since *cis* arrange themselves along (semi)*infinite* long contour lines—*seams*<sup>2–4</sup>—and since electric charges do not exist within the Born–Oppenheimer framework, formation of an analogy with the magnetic component of the electromagnetic field is suggested.<sup>5–13</sup> This analogy almost speaks for itself because a *seam* is reminiscent of the infinite (or semiinfinite) long and infinitesimal narrow *solenoid* that forms a magnetic field,  $\mathbf{H}$  (see Fig. 6.1). However, from experiments it is known that solenoids produce magnetic fields only inside the solenoid whereas outside the solenoid the field is zero. Thus  $\tau$ , which is different from zero in configuration space, cannot be identified with  $\mathbf{H}$ , but if it can at all, then with the *vector potential*  $\mathbf{A}$ , which, like  $\tau$ , differs from zero in the space surrounding the solenoid. Indeed, as will be shown in this chapter, the similarity between  $\tau$  and  $\mathbf{A}$  is rather striking. Having formed this similarity, we are

---

*Beyond Born–Oppenheimer: Conical Intersections and Electronic Nonadiabatic Coupling Terms*  
By Michael Baer. Copyright © 2006 John Wiley & Sons, Inc.

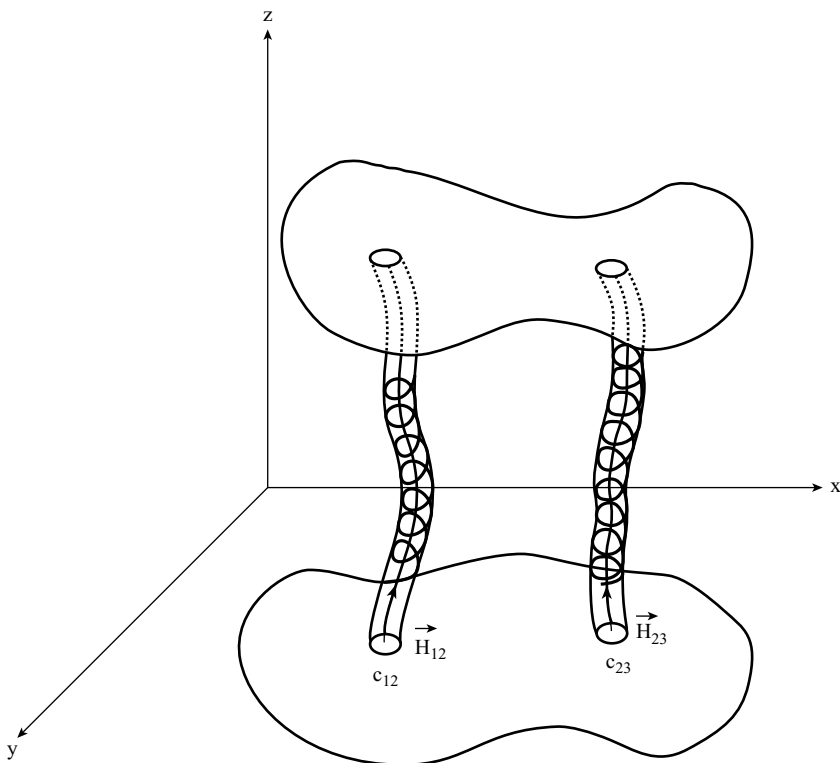


**Figure 6.1** Simulation of a seam as a helical (electric) wire characteristic for a solenoid. Two seams are shown: one formed by a (1,2) *ci* and one by a (2,3) *ci*.

in a position to add a few more features to the NACTs based on this similarity. These assumptions were justified by detailed numerical treatments as discussed throughout the present chapter.

For this purpose we first summarize our knowledge regarding the solenoid and its field.<sup>14</sup> Recalling the theory of electrodynamics, the magnetic field  $\mathbf{H}$  is formed by a vector potential  $\mathbf{A}$  according to the following relation:

$$\mathbf{H} = \text{Curl } \mathbf{A} \quad (6.1)$$

Since the direction of  $\mathbf{H}$  in the solenoid is along the solenoid's axis, Eq. (6.1) implies that  $\mathbf{A}$  is orthogonal to  $\mathbf{H}$  and therefore also to the solenoid's axis. Thus, if for a given value of  $z$  the  $x$ - $y$  plane is chosen in such a way that the axis of the solenoid is perpendicular to it (and therefore is along the  $z$  axis), then  $\mathbf{H}$  possesses only a  $z$  component and  $\mathbf{A}$ , only the (nonzero) components  $A_x$  and  $A_y$ . Assuming that the  $\mathbf{A}$ -solenoid system correctly simulates the  $\tau$ -seam system, this implies that if the seam is in the  $z$  direction, then  $\tau_z \sim 0$  and  $\tau_x$  and  $\tau_y$  differ from zero.

There are, however, two major differences between the solenoid ( $\mathbf{A}$ ) and the seam ( $\tau$ ) systems that cannot be ignored:

1. The vector potential  $\mathbf{A}$  is Abelian, namely, made up of vector functions whereas  $\tau$  is usually a non-Abelian magnitude made up of (vector) *matrices*. Because of this difference, the simulation may fail. However, in Corollary 1.1 it was shown that the  $2 \times 2 \tau$  matrices exhibit Abelian behavior and therefore a simulation can be formed for a two-state Hilbert subspace. Moreover, the two-state case is exceptionally important because any non-Abelian  $\tau$  matrix usually reduces, at the vicinity of any  $c_i$ , to a  $2 \times 2$  matrix and therefore becomes Abelian so that the simulation is always valid close enough to a given  $c_i$ . (We remind the reader that as the distance from the given  $c_i$  increases, the  $\tau$  matrix, as a result of interactions with other *cis*, expands to become  $N$ -dimensional, where  $N > 2$ , and therefore is non-Abelian.)
2. The  $\mathbf{A}$  vector produced by a solenoid possesses a cylindrical symmetry whereas the spatial distribution of a NACT (formed even by a *single*  $c_i$ ) is rarely circular. For instance, in case of a three-atom system it is frequently elliptic<sup>15</sup> (see Section 3.2.3). This difference is a source for difficulties because for a solenoid,  $\mathbf{A}$  can be chosen so that it fulfills the equation  $\text{Div } \mathbf{A} = 0$ <sup>14</sup> (by this we do not mean that  $\text{Div } \mathbf{A}$  *has* to be zero), whereas in our case we usually have  $\text{Div } \tau \neq 0$ . It is important to emphasize that for molecular systems  $\text{Div } \tau$  *has* to differ from zero.

In the present chapter the molecular C-D equations are reconsidered for a different reason, namely, to prove that indeed the various elements of the  $\tau$  matrix behave like (molecular) fields.<sup>16–18</sup> It will be shown that part of them have sources just as in electrodynamics and others, which lack sources, are induced by the fields with sources—a situation not encountered in electrodynamics. Both types will be studied employing the ordinary mathematical tools as applied within field theory.

In Section 6.2 we show, step by step, to what extent the two-state NACT behaves like an Abelian system, whereas in Section 6.3 we discuss in some detail the multistate non-Abelian system.

## 6.2 TWO-STATE (ABELIAN) SYSTEM

### 6.2.1 Nonadiabatic Coupling Term as a Vector Potential

We start by stating the following lemma.

**Lemma 6.1** Given a two-state Hilbert subspace, the corresponding two coupled adiabatic Schrödinger equations in Eq. (2.12) can be decoupled, for sufficiently low energy, so that one equation is for a function  $\phi(\mathbf{s})$  and the second for its complex conjugate, namely,  $\phi(\mathbf{s})^*$ .<sup>1</sup>

*Proof* For the sake of completeness, Eq. (2.12) is repeated here:

$$-\frac{\hbar^2}{2m} (\nabla + \boldsymbol{\tau})^2 \Psi + (\mathbf{u} - E) \Psi = \mathbf{0} \quad (2.12)$$

and the same applies to  $\tau$  given in Eq. (1.26):

$$\tau = \begin{pmatrix} 0 & \tau_{12} \\ -\tau_{12} & 0 \end{pmatrix}$$

Next,  $\Psi$  is replaced by  $\Phi$  following the (constant) unitary transformation, thus

$$\Psi = \mathbf{G}\Phi \quad (6.2)$$

where  $\mathbf{G}$  is chosen in such a way that it diagonalizes the  $\tau$  matrix.<sup>1,2</sup>

$$\mathbf{G} = \frac{1}{\sqrt{2}} \begin{pmatrix} 1 & 1 \\ i & -i \end{pmatrix} \quad (6.3)$$

Substituting Eqs. (6.2), (6.3), and (1.26) in Eq. (2.12) (see above) yields the two coupled equations:

$$\begin{aligned} -\frac{\hbar^2}{2m}(\nabla + i\tau)^2\phi_1 + \left(\frac{1}{2}(u_1 + u_2) - E\right)\phi_1 + \frac{1}{2}(u_1 - u_2)\phi_2 &= 0 \\ -\frac{\hbar^2}{2m}(\nabla - i\tau)^2\phi_2 + \left(\frac{1}{2}(u_1 + u_2) - E\right)\phi_2 + \frac{1}{2}(u_1 - u_2)\phi_1 &= 0 \end{aligned} \quad (6.4)$$

where  $\tau_{12}$  is replaced by  $\tau$  to simplify the notation. These two equations can be rearranged to become

$$\begin{aligned} -\frac{\hbar^2}{2m}(\nabla + i\tau)^2\phi_1 + (u_1 - E)\phi_1 + i\frac{1}{\sqrt{2}}(u_2 - u_1)\psi_2 &= 0 \\ -\frac{\hbar^2}{2m}(\nabla - i\tau)^2\phi_2 + (u_1 - E)\phi_2 - i\frac{1}{\sqrt{2}}(u_2 - u_1)\psi_2 &= 0 \end{aligned} \quad (6.5)$$

where  $\psi_2$ , the (nuclear) adiabatic function associated with the upper state  $u_2$ , is put back again to replace the difference  $(\phi_1 - \phi_2) = -i\sqrt{2}\psi_2$  [employing Eqs. (6.2) and (6.3)]. Next we assume the energy to be low enough so that  $u_2$  is classically forbidden and therefore  $|\psi_2| \sim 0$  at every point. Consequently the term that contains  $\psi_2$  can be neglected so that the two coupled equations become decoupled<sup>1,2</sup>

$$-\frac{\hbar^2}{2m}(\nabla \pm i\tau)^2\phi + (u_1 - E)\phi = 0 \quad (6.6)$$

where the subscripts 1 and 2 become redundant and are deleted. Thus we managed to derive a single (decoupled) Schrödinger equation that keeps its NACT contrary to the ordinary Born–Oppenheimer approximation.<sup>3–5</sup> It is important to mention that

the derivation of a decoupled single Schrödinger equation from a (general)  $N$ -state system is discussed in Chapter 8.

The outcome of this proof is that the NACT appears in the single-state Schrödinger equation in the same way as the magnetic vector potential appears in a Hamiltonian that describes the interaction of a charged particle with an external magnetic field.<sup>6,7</sup>

It is important to remind the reader that writing the Hamiltonian as in Eq. (6.6) guarantees, classically, that the magnetic force that acts on a charged particle is the Lorentz force:<sup>7</sup>

$$\mathbf{F} = \frac{e}{mc} [\mathbf{p} \times \mathbf{H}]$$

However, due to Eq. (1.28) [see also Eq. (6.8)],  $\mathbf{H} = \mathbf{0}$ , and consequently the Lorentz force for the charged particles within the molecule (at least in close vicinity of the  $c_i$ ) is identically zero.

### 6.2.2 Two-State Curl Equation

The two-state Curl equation is introduced in Section 1.1.2, in particular through Eqs. (1.27) and (1.28), where it is presented, in terms of cartesian coordinates. Here and in what follows we are interested in a planar system described by two polar coordinates  $(\varphi, q)$ , where the two are related to the Cartesian coordinates as follows:

$$\varphi = \tan^{-1}(y/x); \quad q = \sqrt{x^2 + y^2} \quad (6.7)$$

Transforming from the Cartesian to the polar coordinates yields the following expression for the Curl equation in polar coordinates [see Eq. (1.25)–(1.28)]

$$\mathbf{F}_{q\varphi} = \frac{1}{q} \left( \frac{\partial \tau_\varphi}{\partial q} - \frac{\partial \tau_q}{\partial \varphi} \right) = 0 \Rightarrow \frac{\partial \tau_\varphi}{\partial q} - \frac{\partial \tau_q}{\partial \varphi} = 0 \quad (6.8)$$

where

$$\boldsymbol{\tau}_\lambda = \left\langle \zeta_1 \left| \frac{\partial}{\partial \lambda} \zeta_2 \right. \right\rangle; \quad \lambda = \varphi, q \quad (6.9)$$

Next we prove the following lemma.

**Lemma 6.2** For a two-state Hilbert subspace, the line integral of which is quantized in Eq. (3.12), the radial component of  $\boldsymbol{\tau}$ , namely,  $\tau_q$ , has to be singlevalued.<sup>8</sup>

*Proof* Integrating Eq. (6.8) with respect to both  $q$  and  $\varphi$  yields the following result:

$$\int_0^{2\pi} \tau_\varphi(\varphi, q_2) d\varphi - \int_0^{2\pi} \tau_\varphi(\varphi, q_1) d\varphi - \int_{q_1}^{q_2} dq (\tau_q(\varphi = 2\pi, q) - \tau_q(\varphi = 0, q)) = 0 \quad (6.10)$$

The quantization implies that Eq. (3.12) holds for every radius  $q$  so that we have

$$\int_0^{2\pi} \tau_\varphi(\varphi, q_2) d\varphi = \int_0^{2\pi} \tau_\varphi(\varphi, q_1) d\varphi (= n\pi) \quad (3.12')$$

Returning to Eq. (6.10), we obtain the following for  $\tau_q(\varphi, q)$ :

$$\int_{q_1}^{q_2} dq (\tau_q(\varphi = 2\pi, q) - \tau_q(\varphi = 0, q)) = 0 \quad (6.11)$$

Thus,  $\tau_q(\varphi, q)$  is a singlevalued function with respect to  $\varphi$  for any  $q$ .

### 6.2.3 (Extended) Stokes Theorem

The Stokes theorem implies that

$$\oint_{\Gamma} d\mathbf{s} \cdot \boldsymbol{\tau}(\mathbf{s}) = \iint_{\sigma} \mathbf{F} d\boldsymbol{\sigma} \quad (6.12)$$

where  $\mathbf{F}$  is introduced in Eq. (6.8),  $\boldsymbol{\tau}$  is the (1,2) NACT vector (not a matrix) mentioned earlier, and the closed contour  $\Gamma$  is the borderline of the assigned planar region  $\sigma$ . On the l.h.s. of Eq. (6.12) we encounter a *line* integral and on the r.h.s., a *surface* integral.

It seems as if Eq. (6.12) is not fulfilled within the present formalism because the expression on the r.h.s. is always zero [see Eq. (6.8)] whereas the expression on the l.h.s., due to the quantization condition [see Eq. (3.12)], usually differs from zero. This discrepancy is due to the integration over  $\sigma$ , which cannot be carried out correctly because  $\mathbf{F}$  is not defined at the singular  $ci$  points (these points were termed in Section 1.3.2.2 as *pathological* points). To correct for this defect, we recall that the  $ci$  points form a *finite* group of (isolated) points and therefore at each such point the  $(q, \varphi)$  tensorial component of  $\mathbf{F}$ , namely,  $F_{q\varphi}$ , has to be infinitely large to ensure that the surface integral in Eq. (6.12) yields a *nonzero* contribution. To continue, we consider the case of one single  $ci$ . In order to guarantee the quantization in Eq. (3.12), we assume for  $F_{q\varphi}$ , at the  $ci$  point, the following expression:<sup>9</sup>

$$F_{q\varphi} = 2\pi f(\varphi, q) \frac{\delta(q)}{q} \quad (6.13)$$

Here  $\delta(q)$  is the Dirac delta function and  $f(\varphi, q)$  is an analytic, as yet undetermined, function.

To continue, we concentrate on a circular region that contains one  $ci$  at  $q = 0$  and unite Eqs. (6.13) and (6.8) to form an extended version of the Curl equation:

$$F_{\varphi q} = \frac{1}{q} \left( \frac{\partial \tau_\varphi}{\partial q} - \frac{\partial \tau_q}{\partial \varphi} \right) - 2\pi f(\varphi, q) \frac{\delta(q)}{q} \quad (6.14)$$

Next, considering again Eq. (6.12) and employing Eq. (6.14) for  $F_{q\varphi}$ , we observe that the Stokes theorem leads to the following expression:<sup>10,11</sup>

$$\oint_{\Gamma} \frac{1}{q} \tau_\varphi(\varphi, q) q d\varphi = 2\pi \iint_{\sigma} \frac{1}{q} f(\varphi, q) \delta(q) q d\varphi dq \quad (6.15)$$

In writing Eq. (6.15) it is assumed that Eq. (6.8) is fulfilled at every point in  $\sigma$  (including  $q = 0$ ).

To continue, we perform the integrations on both sides of Eq. (6.15) and find that in order to guarantee equality, the function  $f(\varphi, q = 0)$  has to fulfill the following condition:

$$\int_0^{2\pi} \tau_\varphi(\varphi, q) d\varphi = \pi \int_0^{2\pi} f(\varphi, q = 0) d\varphi \quad (6.15')$$

However, recalling Eq. (3.12') (see previous page) we see that  $f(\varphi)\{ \equiv f(\varphi, q = 0)\}$ , just like  $\tau_\varphi(\varphi, q)$ , has to be quantized, namely

$$\int_0^{2\pi} f(\varphi) d\varphi = n \quad (6.16)$$

where  $n$  is an integer.

We continue to elaborate on Eq. (6.14). This equation is defined for both  $q = 0$  and  $q > 0$  and therefore can be considered as the extension of Eq. (6.8).<sup>9</sup>

$$\frac{\partial \tau_\varphi}{\partial q} - \frac{\partial \tau_q}{\partial \varphi} = 2\pi f(\varphi) \delta(q) \quad (6.17)$$

We note that adding the r.h.s in Eq. (6.17) is, in fact, a way to incorporate, in Eq. (6.8), the boundary condition at  $q = 0$ .

The solution of Eq. (6.17) (for  $q > 0$ ) is given in the form

$$\tau_\varphi(q, \varphi) - \int_{\varepsilon}^q dq \frac{\partial \tau_q}{\partial \varphi} = \pi h(q) f(\varphi) \quad (6.18)$$

where  $\varepsilon \rightarrow 0$  and  $h(q)$  is the Heaviside function:

$$h(q) = \begin{cases} 1 & q > 0 \\ 0 & q < 0 \end{cases} \quad (6.19)$$

The fact that Eq. (6.18) is a solution of Eq. (6.17) can be verified by substitution.

Since  $q$  is a radius, it is always positive and therefore Eq. (6.18) can be written, without loss of generality, as follows:

$$\tau_\varphi(q, \varphi) - \int_{\varepsilon}^q dq \frac{\partial \tau_q}{\partial \varphi} = \pi f(\varphi) \quad (6.20)$$

Next, assuming  $\tau_q(\varphi, q)$  to be *finite* at the vicinity of  $q \sim 0$ , we note that the second term on the l.h.s. of Eq. (6.20) for  $q \rightarrow \varepsilon$  ( $\sim 0$ ) can be ignored, so that we find<sup>9</sup>

$$f(\varphi) = \frac{1}{\pi} \tau_\varphi(q \sim 0, \varphi) \quad (6.21)$$

This result implies that the angular dependence of the *Curl* term in Eq. (6.13) is identical (up to a division by  $\pi$ ) to the *angular* component of  $\boldsymbol{\tau}$  as calculated (at any  $q$  but in particular in the close vicinity of the *ci*, i.e.,  $q \sim 0$ ). In what follows the angular component at  $q \sim 0$  is termed the *virgin* function—virgin in the sense that its values are not damaged by NACTs of other *cis*. The virgin functions are used as boundary conditions to solve the C-D equations.

An unavoidable difficulty of the present theory is that the radial component of  $\boldsymbol{\tau}$ , namely,  $\tau_q(\varphi, q)$ , remains, in fact, unknown. Moreover, except for its singlevaluedness in configuration space (see Section 6.2.2), we are not aware of any special features. We *assumed* it to be finite for  $q \sim 0$ , but no clue is given with regard to its values for  $q > 0$ . In fact, distinguishing, for  $\tau_q(\varphi, q \sim 0)$ , between being finite or identically zero is not essential because the angular component of  $\boldsymbol{\tau}$ , namely,  $\tau_\varphi(\varphi, q)/q$ , becomes infinitely large and therefore completely dominates  $\boldsymbol{\tau}$  in this region. Since the values of  $\tau_q(\varphi, q)$  are of minor importance at the *ci* point, we continue to ignore it at the whole region of interest. In other words, we *assume* that for an isolated *ci*,  $\tau_q(\varphi, q) \sim 0$  for any  $q$  value. We are aware that this is a far-reaching *assumption* and therefore, this assumption has been under detailed scrutiny in more recent numerical treatments.<sup>12–14</sup>

#### 6.2.4 Application of Stokes Theorem for Several Two-State Conical Intersections

We start by extending Eq. (6.14) to the case of several *cis*

$$\mathbf{F} = \text{Curl } \boldsymbol{\tau} - \sum_{j=1}^n \vec{\mathbf{S}}_j \quad (6.14')$$

where  $\vec{\mathbf{S}}_j$  is the intensity due to the  $j$ th  $ci$  [see Eq. (6.13')]:

$$\vec{\mathbf{S}}_j(\vec{q}) = 2\pi f_j(\varphi_j) \frac{\delta(\vec{q} - \vec{q}_{j0})}{|\vec{q} - \vec{q}_{j0}|} \vec{\mathbf{n}}_j \quad (6.13')$$

Here  $\vec{\mathbf{n}}_j$  is a unit vector normal to the plane under consideration, thus pointing either up or down.

Consequently the line integral in Eq. (6.15), which now is assumed to surround  $N$  *cis*, is given in the form

$$\oint_{\Gamma} d\mathbf{s} \cdot \boldsymbol{\tau}(\mathbf{s}) = \oint_{\sigma} \sum_{j=1}^n \mathbf{S}_j \cdot d\boldsymbol{\sigma} = \sum_{j=1}^n \oint_{\sigma} \mathbf{S}_j d\boldsymbol{\sigma}$$

or

$$\oint_{\Gamma} d\mathbf{s} \cdot \boldsymbol{\tau}(\mathbf{s}) = \sum_{j=1}^n \oint_{\sigma_j} \mathbf{S}_j d\boldsymbol{\sigma}_j \quad (6.22)$$

where  $\sigma_j$ ,  $j = 1, \dots, N$  is an infinitely small area element that surrounds the  $j$ th  $ci$ .

As an example of what happens in case of two *cis*, we consider the two (3,4) *ci twins* that couple the third and the fourth states of the {C<sub>2</sub>H} system (see Fig. 4.8c). Assuming the contour  $\Gamma = \Gamma_{24}$  to surround both *cis*, it was found that the line integral in Eq. (6.22) yields the value *zero*, indicating that the two *cis annihilate* each other.<sup>15,16</sup> This result implies, following the substitution of Eq. (6.13') in Eq. (6.22), that the two unit vectors  $\vec{\mathbf{n}}_j$ ;  $j = 1, 2$  have opposite signs. At first it was not clear why the two vectors posses opposite signs. For instance, they could both have the same sign, thus yielding, for the line integral in Eq. (6.22), the value of  $2\pi$ . An explanation that supports these findings was given by Vértesi and Bene<sup>17</sup> and is schematically, presented in Figure 6.2. Mebel et al.<sup>15</sup> found that by increasing the distance between the two fixed carbons in Figure 4.8b, the two *cis*, originally located on a plane *A*, approach each other, as schematically described in Figure 6.2, so that at  $R_{CC} = 1.35 \text{ \AA}$  they coalesce at point *P* on plane *B*. It is clearly noted that since the two seams coalesce and because the direction of the NACT along the common seam (up and down) has to be continuous, these two conditions cause the two (3,4) NACTs related to the two *cis*, located on plane *A*, to have different signs.

### 6.2.5 Application of Vector Algebra to Calculate the Field of a Two-State Hilbert Space

In the previous section we analyzed a system with a *single ci* and ended up with the conclusion that the NACT,  $\boldsymbol{\tau}$ , associated with a single *ci* does not possess a radial component; in other words,  $\tau_q(\varphi, q) \equiv 0$  for any  $q$ . Recalling the Curl equation [Eq. (6.8)], this assumption implies that  $\boldsymbol{\tau}_\varphi(\varphi, q)$  does not depend on  $q$ . Therefore the NACT,  $\boldsymbol{\tau}$ , due to one single *ci* located at  $q = 0$  (viz., at the origin) can be presented

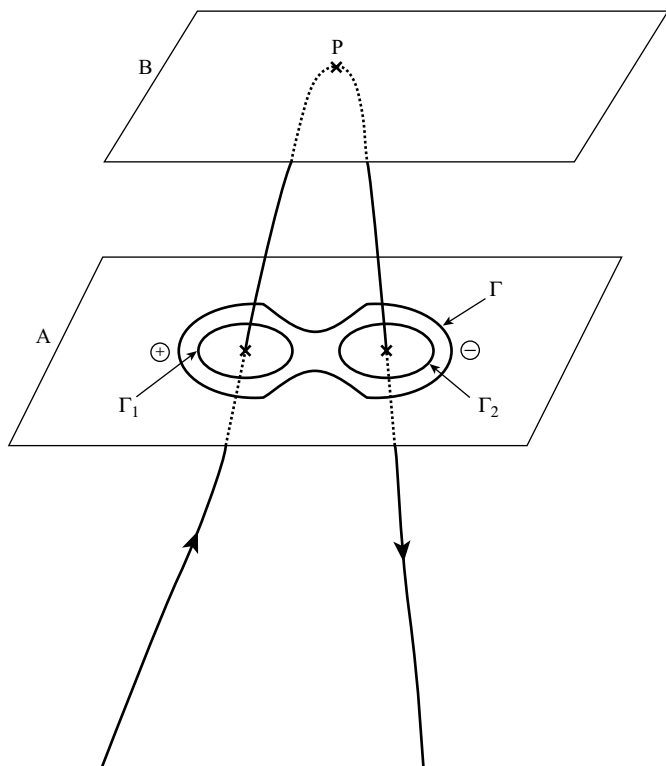


**Figure 6.2** A schematic representation of two semiinfinite long (directed) seams, each formed by a series of *cis* as encountered for the  $C_2H$  system (see Fig. 4.8c). Also shown are two planes, A and B as obtained by assigning the carbon-carbon distance,  $R_{CC}$ , two different values. On plane A, where the two *cis* twins are well separated from each other, are drawn a contour  $\Gamma$  that surrounds the two (3,4) *cis* and the two infinitesimal small contours  $\Gamma_1$  and  $\Gamma_2$  that (each) surround only one *cis*. Plane B contains the point  $P$ , where the two *cis* coalesce or the two seams intersect each other.

as  $\tau(\varphi, q) = (f(\varphi)/q, 0)$  at any point  $(q, \varphi)$  in configuration space. Next we consider the situation where the two states form several *cis*. In this case, just as in the case of a vector potential that is formed by several solenoids, vector algebra is employed on the basis of the contribution of each *cis*, namely adding up the contributions of the various *cis* to obtain the resultant intensity of the field at a given point.

For this purpose we first derive the mathematical expression for field due to a single *cis* located at an arbitrary point  $(q_{j0}, \varphi_{j0})$ . The procedure is as follows. Having  $\tau = (f(\varphi)/q, 0)$ , we present it in terms *Cartesian* components  $(\tau_x, \tau_y)$  and then *shift* (but not rotate) the vector  $\tau$  to the point of interest, namely,  $(0, 0) \rightarrow (x_{j0}, y_{j0})$  ( $\equiv (q_{j0}, \varphi_{j0})$ ). Since no rotation is involved in the transformation, the shift of the origin to a new point is parallel. Once completed, the solution is transformed back into polar coordinates. The details of the derivation are given as a solution of Problem 6.1

at the end of this chapter. This derivation yields the following results<sup>9,12</sup> for a given point  $P(q,\varphi)$  (as measured from the new origin)

$$\begin{aligned}\tau_q(q,\varphi) &= -f_j(\varphi_j)\frac{1}{q_j} \sin(\varphi - \varphi_j) \\ \tau_\varphi(q,\varphi) &= f_j(\varphi_j)\frac{q}{q_j} \cos(\varphi - \varphi_j)\end{aligned}\quad (6.23)$$

where the connection between the various coordinates is as follows:

$$\begin{aligned}q_j &= \sqrt{(q \cos \varphi - q_{j0} \cos \varphi_{j0})^2 + (q \sin \varphi - q_{j0} \sin \varphi_{j0})^2} \\ \cos \varphi_j &= \frac{q \cos \varphi - q_{j0} \cos \varphi_{j0}}{q_j}\end{aligned}\quad (6.24)$$

It is noted that for  $q_{j0} \rightarrow 0$  (and therefore  $\varphi_j \rightarrow \varphi$ ), the solution in Eq. (6.23) yields  $(\tau_\varphi(q,\varphi)/q, \tau_q(q,\varphi)) \equiv (f_j(\varphi_j)/q, \tau_q \rightarrow 0)$ , which is the solution for the case where the *cis* is at the origin. A similar situation is encountered as  $q \gg q_{j0}$ . Here, too,  $\varphi_j \rightarrow \varphi$ , and therefore  $\tau_q \rightarrow 0$ .

We attached to each *cis* a different  $f(\varphi)$  function, specifically  $f_j(\varphi_j)$ , to indicate that each such *cis* (in this case the  $j$ th one) may form a *different* virgin distribution.

With this modified expression we can now extend the solution of Eq. (6.23) to any number of *cis*. Since  $\tau_\varphi(q,\varphi)$  and  $\tau_q(q,\varphi)$  are scalars, the solution in case of  $N$  *cis* is obtained by summing up the contributions of all *cis*:<sup>12,18</sup>

$$\begin{aligned}\tau_q(q,\varphi) &= -\sum_{j=1}^N f_j(\varphi_j)\frac{1}{q_j} \sin(\varphi - \varphi_j) \\ \tau_\varphi(q,\varphi) &= q \sum_{j=1}^N f_j(\varphi_j)\frac{1}{q_j} \cos(\varphi - \varphi_j)\end{aligned}\quad (6.25)$$

Equation (6.25) yields the two components of  $\boldsymbol{\tau}(q,\varphi)$ , for a distribution of two-state *cis* expressed in terms of the *virgin* distributions of the NACTs at their *cis*. These functions have to be obtained from ab initio treatments, however, the entire field is formed by Eq. (6.25).

### 6.2.6 A Numerical Example: Study of {H<sub>2</sub>,Na} System

In 2003 we completed an extensive study of the {H<sub>2</sub>,Na} system<sup>19</sup> and found two features that allow us to test our two-state vector algebra approach for a situation where 4 two-state *cis* form the NACT field.

Within this study the four lowest states of this system, namely, 1<sup>2</sup>A', 2<sup>2</sup>A', 3<sup>2</sup>A', 4<sup>2</sup>A' were considered and the relevant NACTs were calculated employing MOLPRO<sup>20</sup>

(see Chapter 4). For this purpose we concentrate on configurations for which the distance  $R_{\text{HH}}$  between the two hydrogen atoms is fixed, namely,  $R_{\text{HH}} = 2.18$  a.u., and allow the sodium to be *free* and serve as the *test particle* to determine the values of the NACTs at various points. The main finding for the present study is that the *third* and the *fourth* states form a quasi-*two-state* Hilbert subspace coupled by *four* (3,4) *cis*. Consequently this system furnishes a unique opportunity to apply the vector algebra for a relatively complicated system with four sources and test the ideas presented in the previous sections (particularly in Section 6.2.4).

The aim of the numerical treatment is to compare the ab initio values of  $\tau_{34\varphi}(q, \varphi)$  and  $\tau_{34q}(q, \varphi)$  with those derived by applying Eq. (6.25).

In order to apply Eq. (6.25), we need the *virgin* distributions,  $f_j(\varphi_j)$ , for the four (3,4) *cis*. These are calculated, employing MOLPRO, along circles of small radii ( $\sim 0.01$  a.u.) that surround each of the four *cis* and are presented in Figure 6.3.

The comparison is carried out along four circles that surround various numbers of *cis* (see Fig. 6.4). The comparison itself is presented in Figure 6.5, and the results speak for themselves. It is observed that although the ab initio distributions are frequently rather complicated and show a lot of structure, the vector algebra approach produces functions that are capable of accurately following the ab initio points.

Before closing this section, we refer to one issue related to the assumption that radial component  $\tau_{qj}(q_j, \varphi_j)$  that originate from the  $j$ th *ci* are small enough for any  $q$  value and hence can be ignored in numerical treatments. The ability of the vector algebra approach to correctly simulate the NACTs of the  $\{\text{H}_2, \text{Na}\}$  (and also those of the  $\{\text{H}_2, \text{H}\}^{12,13}$ ) may not be the ultimate proof for the relevance of this assumption but does yield strong support for it.

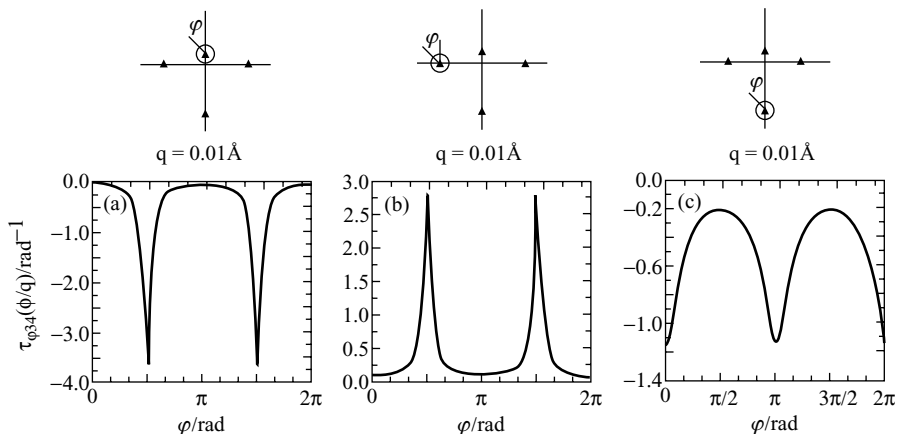


**Figure 6.3** The three ab initio virgin distributions of the (3,4) *cis* as calculated for the  $\{\text{H}_2, \text{Na}\}$  system for the configuration formed by  $R_{\text{HH}} = 2.18$  a.u.: (a)  $f_1(\varphi_1) (= \tau_{\varphi 34}(\varphi_1 | q_1))$  calculated for the upper (3,4) *ci* located on the symmetry line; (b)  $f_2(\varphi_2) (= \tau_{\varphi 34}(\varphi_2 | q_2))$  [and its mirror image  $f_3(\varphi_3)$ ] calculated for the sideward (3,4) *ci*; (c)  $f_4(\varphi_4) (= \tau_{\varphi 34}(\varphi_4 | q_4))$  calculated for the lower (3,4) *ci* located on the symmetry line.

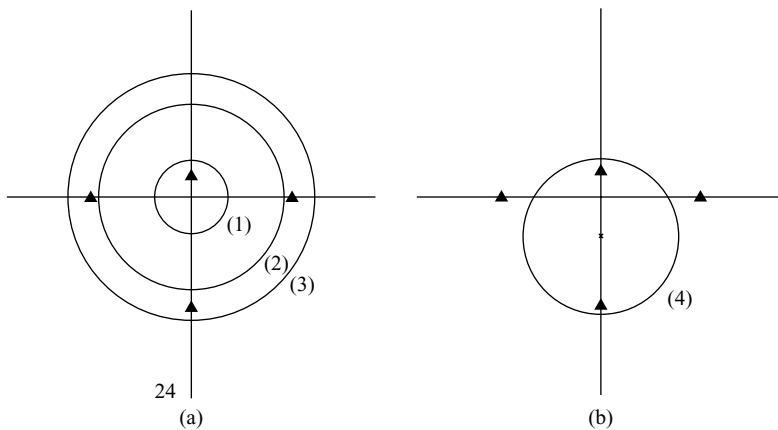


**Figure 6.4** Four circular contours along that are calculated the various NACTs for the  $\{\text{H}_2, \text{Na}\}$  system: (a) three concentric circles with their centers at  $O(0,0)$  surrounding different numbers of *cis*; (b) a circle with its center shifted downward at  $O(0, -0.135 \text{ a.u.})$  surrounding two *cis* located on the symmetry line. The positions of the *cis* are designated as (full) triangles.

### 6.2.7 A Short Summary

In this section we presented an approach implying that the field produced by the two-state NACTs—termed the *molecular field*—is formed at *cis* points. Moreover, numerical examples<sup>12,13</sup> (one of which is presented in Section 6.2.6) indicate that *cis* not only form the molecular fields but also seem to be the *only* sources to form these fields.

## 6.3 MULTISTATE HILBERT SUBSPACE

### 6.3.1 Non-Abelian Stokes Theorem

The multistate extended Curl equation is discussed in Section 1.1.2, and it is shown that for a Hilbert space it takes the form

$$\mathbf{F} = \mathbf{H} - \mathbf{T} = 0 \quad (6.26)$$

where  $\mathbf{H}$  and  $\mathbf{T}$  are as given in Eqs. (1.16) and (1.17), respectively.

Next we extend this equation in order to include the various source terms similar to the extension of Eq. (6.14). Thus Eq. (6.26) is assumed to be of the form

$$\mathbf{F} = \mathbf{H} - \mathbf{T} - \mathbf{S} \quad (6.27)$$

where  $\mathbf{S}$  is an antisymmetric *tridiagonal* vector matrix that contains at its two tridiagonals [viz., at the  $(k, k \pm 1)$  locations] the various source terms. Thus

$$\mathbf{S}_{kk\pm 1}(\vec{q}) = \sum_{j=1} \vec{\mathbf{S}}_{kk\pm 1j}(\vec{q}) \quad (6.28)$$

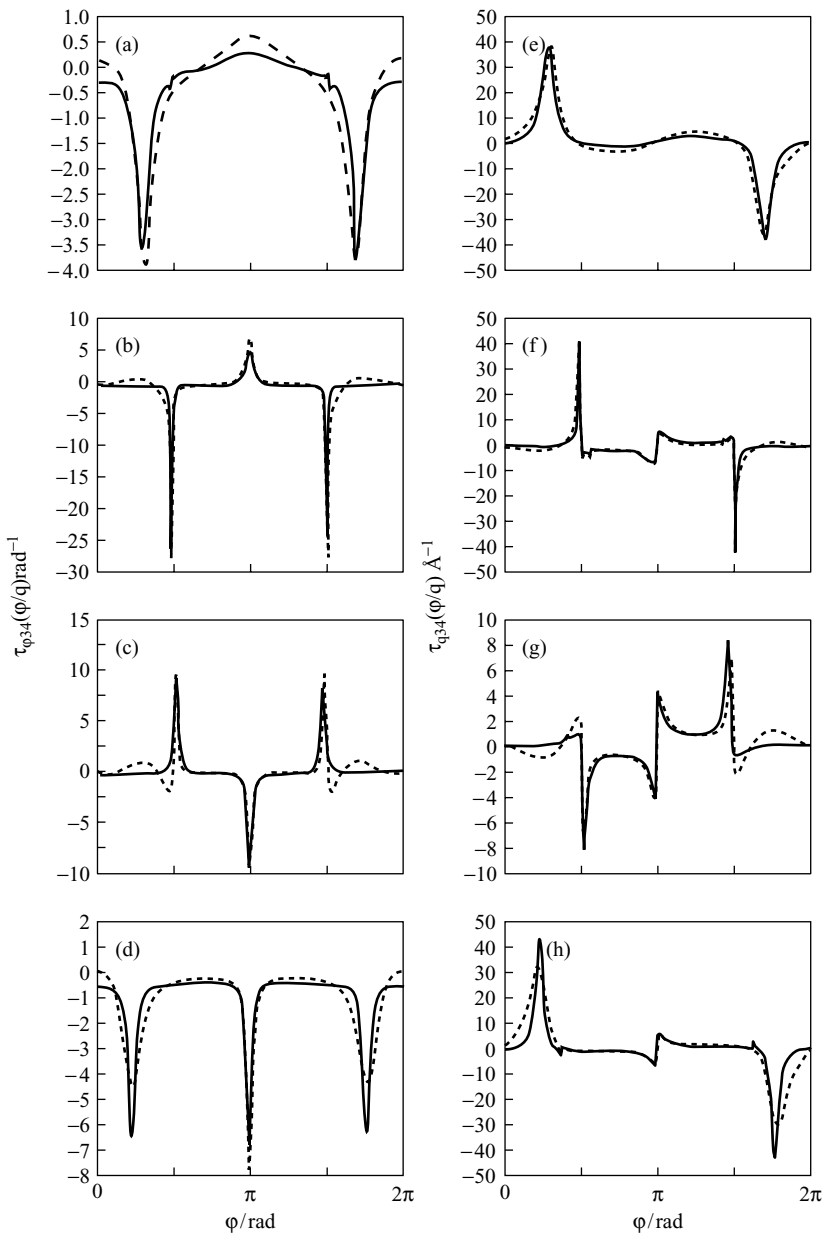


**Figure 6.5** A comparison between ab initio and vector algebra results, for the two components of  $\tau_{34}(\varphi|q)$ , calculated along four circles presented in Figure 6.4. Panels (a)–(d) present the angular components,  $\tau_{\varphi 34}(\varphi|q)$ , and panels (e)–(h), the radial components,  $\tau_{q34}(\varphi|q)$ . Full lines are results due to ab initio calculations; dashed lines are results due to the vector algebra model.

where  $\vec{\mathbf{S}}_{kk\pm 1j}(\vec{q})$  is the contribution of a  $j$ th  $ci$  located at  $\vec{q}_{j0}$  to the  $(k,k \pm 1)$  source terms [see also Eq. (6.13') on p. 147]:

$$\vec{\mathbf{S}}_{kk\pm 1j}(\vec{q}) = \pm 2\pi f_{kk\pm 1}^{(j)}(\varphi_j) \frac{\delta(\vec{q} - \vec{q}_{j0})}{|\vec{q} - \vec{q}_{j0}|} \quad (6.29)$$

Here  $\vec{q}$  is the (polar) coordinate of a point in a given system of coordinates,  $\varphi_j$  is angular coordinate relating the point of interest to the  $j$ th  $ci$ ,  $f_{kk\pm 1}^{(j)}(\varphi_j)$  is the angular component of the field as formed by the corresponding  $(k,k \pm 1)$   $ci$  at the point  $\vec{q}_{j0}$ , and  $\delta(\vec{q} - \vec{q}_{j0})$  is the relevant Dirac  $\delta$  function. It is important to emphasize that, due to the Dirac  $\delta$  function, the expression in Eq. (6.29) is an Abelian system source term.

Having prepared these numerical tools, we intend to show that the topological  $\mathbf{D}$  matrix—the magnitude that most characterizes a given Hilbert subspace (in a given region)—is formed by the (Abelian)  $cis$  located in this region.

In order to show that we consider the line integral given in Eq. (1.94) for a circle on a plane

$$\mathbf{D}(\Gamma) = \mathbf{I} - \oint_{\Gamma} d\mathbf{s} \cdot \boldsymbol{\tau}(\mathbf{s}|\Gamma) \mathbf{A}(\mathbf{s}|\Gamma) \quad (1.94')$$

We employ the Stokes theorem to present it as a surface integral:

$$\mathbf{D}(\Gamma) = \mathbf{I} - \iint_{\sigma} d\sigma \cdot \text{Curl } (\boldsymbol{\tau}(\mathbf{s}) \mathbf{A}(\mathbf{s})) \quad (6.30)$$

Next, performing a few algebraic rearrangements, we find

$$\mathbf{D}(\Gamma) = \mathbf{I} - \iint_{\sigma} d\sigma \cdot (\mathbf{H} - \mathbf{T}) \mathbf{A}(\mathbf{s}) \quad (6.31)$$

As in the Abelian, two-state, case, here, too, the surface integral yields the zero matrix, which causes the  $\mathbf{D}$  matrix to be the unity matrix. The reason for this mishap is that the integration is carried out over pathological points where  $\mathbf{H}$  is not well defined (viz., at the  $ci$  points). To correct for this malfunction, we have to replace, in the integrand, the matrix  $(\mathbf{H} - \mathbf{T})$  by the expression in Eq. (6.27), and then we obtain for the  $\mathbf{D}$  matrix the expression:

$$\mathbf{D}(q) = \mathbf{I} - \int_0^{2\pi} \int_0^q dq' q' d\varphi \mathbf{S}(\varphi, q') \mathbf{A}(\varphi, q') \quad (6.32)$$

where we also introduced explicitly the polar coordinates and assumed  $\Gamma$  to be a circle (so that  $\sigma$  becomes a circular region).

As is noted, the integrand in Eq. (6.32) yields nonzero contributions only at  $ci$  points. In other words, the multistate  $\mathbf{D}$  matrix is formed solely by the two-state  $cis$  where the corresponding  $\delta$  functions guarantee that the contribution for the  $\mathbf{D}$  matrix

comes only from regions infinitesimally close to the various *cis* [we recall that the corresponding **A**-matrix elements appearing in the integrand are, in fact, two-state matrix elements of the type discussed in Section 3.11.1—see Eq. (3.4)].

While calculating the **D** matrix, we recall that it is expected to be (approximately) a diagonal matrix (for a Hilbert subspace). In case one is interested in calculating it employing Eq. (6.32), we suggest first studying Problem 1.1 (in Chapter 1).

### 6.3.2 The Curl–Divergence Equations

In Section 6.2 we concentrated on NACTs belonging to a two-state Hilbert space, which implies that all the *cis* are formed by the *same* two states. However, once we encounter a multistate Hilbert subspace with three or more states, we face a different type of system, the non-Abelian system, characterized by a new type of interaction, namely, an interaction between *cis* formed by *different* pairs of states, for instance, a (1,2) *ci* interacting with a (2,3) *ci*. Thus, we argue that the non-Abelian system behaves differently than just a *collection* of Abelian systems.

Although the non-Abelian system behaves differently, we still carry out the study of such a system by applying the numerical tools presented in the previous sections. This becomes possible because any non-Abelian system *reduces* to an Abelian system in the vicinity of any *ci*. Since *cis*, as mentioned in Section 6.2.6, are the sources of Abelian fields, they are in fact also the sources of those fields encountered in the *non-Abelian* system. Indeed, in Section 6.3.1 we showed, *explicitly*, that the topological **D** matrix related to a multistate system is produced solely by the two-state *cis*.

In case of the *Abelian* system, one is able to derive the intensity of the molecular field (viz., the NACT) at every point by simply applying a vector algebra approach as described in Section 6.2.4 because, in so doing, we observe that the *j*th extended Curl equation that is fulfilled in the vicinity of the *j*th *ci* is also fulfilled for a given group of *n cis* because of the *sum rule* expressed in Eqs. (6.14') and (6.25).

Since the interactions in non-Abelian systems are not always additive, vector algebra cannot be applied and therefore other means have to be developed to derive the molecular fields. More recent publications have suggested solving, for this purpose, C-D equations subject to boundary conditions formed at *cis*. This approach is discussed to some extent in the following sections<sup>1–4</sup>.

In applying the C-D equations, we encounter two difficulties:

1. To solve the differential equations, we need the source terms as were just discussed. However, not all molecular fields are formed by sources of this type. For instance, the field related to the  $\tau_{13}(q,\varphi)$ -matrix element is not formed in this way because  $\tau_{13}(q,\varphi)$  is a NACT between two *nonadjacent* states and two such states do not produce a *ci*. Thus in what follows we need to distinguish between NACTs of the type  $\tau_{jj\pm 1}(q,\varphi)$  that have source terms and NACTs of the kind  $\tau_{jj\pm k}(q,\varphi)$ ;  $k > 1$  that do not have source terms.

2. The divergence equation is given in the form

$$\text{Div } \boldsymbol{\tau} = \boldsymbol{\tau}^{(2)} - \boldsymbol{\tau} \cdot \boldsymbol{\tau} \quad (6.33)$$

[see Eq. (1.34), where it is presented in a slightly different form]. The main difficulty with applying this equation is that it contains the  $\tau^{(2)}$ -matrix elements [see Eq. (1.29)] that are not explicitly given and have to be obtained independently. In what follows this matrix is termed the *Strange matrix* and its elements are referred to as the *Strange elements*.

### 6.3.2.1 Three-State Hilbert Subspace

*Derivation of C-D Equations for Three-State System* The three-state  $\tau$  matrix is given in the form

$$\boldsymbol{\tau} = \begin{pmatrix} \mathbf{0} & \boldsymbol{\tau}_{12} & \boldsymbol{\tau}_{13} \\ -\boldsymbol{\tau}_{12} & \mathbf{0} & \boldsymbol{\tau}_{23} \\ -\boldsymbol{\tau}_{13} & -\boldsymbol{\tau}_{23} & \mathbf{0} \end{pmatrix} \quad (6.34)$$

and the corresponding three-state Curl equations that follow from the Eq. (1.13) are expressed as follows:<sup>1,4</sup>

$$\text{Curl } \boldsymbol{\tau}_{12} = [\boldsymbol{\tau}_{23} \times \boldsymbol{\tau}_{13}] \quad (6.35a)$$

$$\text{Curl } \boldsymbol{\tau}_{23} = [\boldsymbol{\tau}_{13} \times \boldsymbol{\tau}_{12}] \quad (6.35b)$$

$$\text{Curl } \boldsymbol{\tau}_{13} = [\boldsymbol{\tau}_{12} \times \boldsymbol{\tau}_{23}] \quad (6.35c)$$

As is noted, the extension from a two-state system to a three-state one is much more complicated than just adding another equation. A comparison between Eqs. (6.35) and (6.8) already reveals part of the difficulty with this extension. Moreover, in the two-state case we do not solve for differential equations; all we have to do is to employ vector algebra to obtain the components of  $\boldsymbol{\tau}$  (see Section 6.2.4). In the three-state system, not only do we have to solve differential equations to obtain the NACTs but also these equations are nonlinear [see r.h.s. of Eq. (6.35)], a fact that may introduce additional complications.

Equation (6.35) contain six unknown functions, namely,  $(\tau_{\varphi jk}, \tau_{qjk})$ ;  $j > k$ ,  $j = 1, 2$ . Thus, in order to solve them, we need three more equations that, as discussed earlier, follow from the divergence equations:

$$\text{Div } \boldsymbol{\tau}_{12} = \boldsymbol{\tau}_{12}^{(2)} - \boldsymbol{\tau}_{23} \cdot \boldsymbol{\tau}_{13} \quad (6.36a)$$

$$\text{Div } \boldsymbol{\tau}_{23} = \boldsymbol{\tau}_{23}^{(2)} - \boldsymbol{\tau}_{13} \cdot \boldsymbol{\tau}_{12} \quad (6.36b)$$

$$\text{Div } \boldsymbol{\tau}_{13} = \boldsymbol{\tau}_{13}^{(2)} + \boldsymbol{\tau}_{12} \cdot \boldsymbol{\tau}_{23} \quad (6.36c)$$

It is noted that each of these Equations (6.36) contains one *Strange* term, namely,  $\boldsymbol{\tau}_{12}^{(2)}$ ,  $\boldsymbol{\tau}_{23}^{(2)}$  and  $\boldsymbol{\tau}_{13}^{(2)}$ , respectively—the corresponding elements of the  $\boldsymbol{\tau}^{(2)}$  matrix [see Eq. (1.29)].

*Ab-Initio Verification for the Curl Equation* In this section we briefly examine to what extent an ab initio three-state Hilbert subspace fulfills the Curl equation as

presented in Eq. (6.35c). To be more specific, we consider the expression (written in polar coordinates)

$$\frac{\partial \tau_{q13}}{\partial \varphi} - \frac{\partial \tau_{\varphi13}}{\partial q} = (\tau_{\varphi12}\tau_{q23} - \tau_{q12}\tau_{\varphi23}) \quad (6.35c')$$

and apply it for the three lower states of the {H<sub>2</sub>, H} system (for details regarding this system, see Section 4.3.1.1 and in particular Section 4.3.2.1).

According to this equation, the ( $q, \varphi$ ) component of  $\text{Curl } \tau_{13}$  can be presented as a difference between two products, each related to the components of the two NACTs,  $\tau_{12}$  and  $\tau_{23}$ . As is noted, the required  $\text{Curl } \tau_{13}$  expression can be calculated in two different ways: (1) applying MOLPRO<sup>5</sup> to derive the two (1,3) components  $\tau_{\lambda13}(\varphi|q)$ ;  $\lambda = \varphi, q$  and then producing, *numerically*, the relevant derivatives to form the respective  $\text{Curl}$  expression [i.e., the l.h.s. term in Eq. (6.35c')] or (2) applying MOLPRO to derive the two components of the (1,2) and (2,3) NACTs, namely,  $\tau_{\lambda12}(\varphi|q)$  and  $\tau_{\lambda23}(\varphi|q)$ ;  $\lambda = \varphi, q$ , respectively, and form the required commutator [i.e., the r.h.s. of Eq. (6.35c')]. The calculations were done along two circles with radii  $q = 0.2, 0.35$  Å centered at the (1,2)  $D_{3h}$ , *ci* point. The geometry and the corresponding results are presented in Figure 6.6. As is noted, the fit is practically complete. For more details, see Refs. 6 and 7.

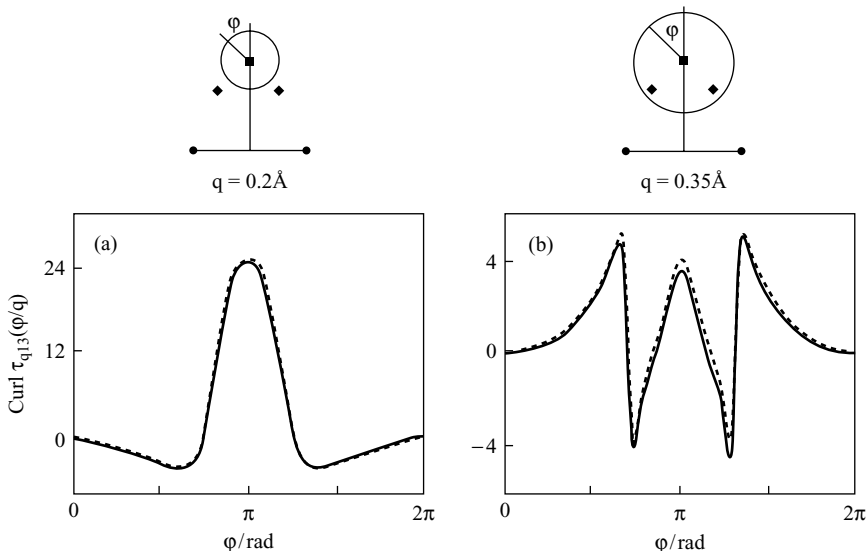


**Figure 6.6** Results for the H+H<sub>2</sub> system as calculated along the two circles centered at the  $D_{3h}$ , *ci*: (a) results for  $\text{Curl } \tau_{13}(\varphi|q = 0.2 \text{ \AA})$ ; (b) results for  $\text{Curl } \tau_{13}(\varphi|q = 0.35 \text{ \AA})$ . Full lines present results due to the l.h.s. of Eq. (6.35c') (derived from numerical differentiations of the relevant magnitudes as obtained from MOLPRO), and dotted lines present results due to the r.h.s. of Eq. (6.35c') [derived from the vectorial product and therefore based on  $\tau_{12}(\varphi|q)$  and  $\tau_{23}(\varphi|q)$ ].

In 2004 a similar calculation was carried out by Barragan et al. while studying the two lower states of the ( $H_2, H^+$ ) system.<sup>8</sup>

### 6.3.2.2 Derivation of Poisson Equations

As mentioned earlier, the divergence equations have their own source terms, namely, *Strange* terms,  $\tau_{12}^{(2)}$ ,  $\tau_{23}^{(2)}$ , and  $\tau_{13}^{(2)}$ . However, as in the Curl equations, here, too, we distinguish between two types of *Strange* terms: those formed at *cis*, like  $\tau_{12}^{(2)}$  and  $\tau_{23}^{(2)}$ , and those that are not formed at any particular point, such as  $\tau_{13}^{(2)}$ . As will be shown in see Section 6.2.4, two of the three *Strange* elements, namely,  $\tau_{12}^{(2)}$  and  $\tau_{23}^{(2)}$ , are essential to obtain correct results or in other words are *nonremovable*, for instance, by a gauge transformation, but  $\tau_{13}^{(2)}$  is less essential and therefore can be removed by a gauge transformation.

Equations (6.35) and (6.36) can be arranged as three pairs of C-D equations

$$\text{Curl } \boldsymbol{\tau}_{jk} = [\boldsymbol{\tau}_{j\ell} \times \boldsymbol{\tau}_{\ell k}]; \quad j \neq \ell \neq k > j \quad (6.37a)$$

$$\text{Div } \boldsymbol{\tau}_{jk} = \boldsymbol{\tau}_{jk}^{(2)} + \boldsymbol{\tau}_{j\ell} \cdot \boldsymbol{\tau}_{\ell k}; \quad j \neq \ell \neq k > j \quad (6.37b)$$

(where  $\boldsymbol{\tau}_{jk} = -\boldsymbol{\tau}_{kj}$ , etc.). Each of the two equations contains on the l.h.s. the same unknown function, namely,  $\boldsymbol{\tau}_{jk}$ , whereas the other two (unknown) functions,  $\boldsymbol{\tau}_{j\ell}$  and  $\boldsymbol{\tau}_{\ell k}$ , show up on the r.h.s. of these two equations and appear to be part of the inhomogeneity terms. In fact, it is these *inhomogeneities* that not only cause the three pairs of equations to be coupled but also form the nonlinear part of the equations, which may cause additional difficulties while solving them.

The structure of Eqs. (6.37) hints at the possibility that these equations can eventually be solved iteratively where values of a previous step are employed on the r.h.s. Thus, if the  $\boldsymbol{\tau}_{j\ell}$  and  $\boldsymbol{\tau}_{\ell k}$  are replaced by  $\boldsymbol{\tau}_{j\ell}^{(0)}$  and  $\boldsymbol{\tau}_{\ell k}^{(0)}$ , then Eqs. (6.37) become, essentially, two equations decoupled from the other four equations:

$$\text{Curl } \boldsymbol{\tau}_{jk} = [\boldsymbol{\tau}_{j\ell}^{(0)} \times \boldsymbol{\tau}_{\ell k}^{(0)}]; \quad j \neq \ell \neq k > j \quad (6.38a)$$

$$\text{Div } \boldsymbol{\tau}_{jk} = \boldsymbol{\tau}_{jk}^{(2)} + \boldsymbol{\tau}_{j\ell}^{(0)} \cdot \boldsymbol{\tau}_{\ell k}^{(0)}; \quad j \neq \ell \neq k > j \quad (6.38b)$$

These two coupled equations are further processed to prepare for the numerical treatment. To achieve this purpose, we present Eqs. (6.38) in a more explicit form

$$\frac{1}{q} \left( \frac{\partial \tau_\varphi}{\partial q} - \frac{\partial \tau_q}{\partial \varphi} \right) = F_C(\varphi, q) \quad (6.39a)$$

$$\frac{1}{q^2} \frac{\partial \tau_\varphi}{\partial \varphi} + \frac{\partial \tau_q}{\partial q} + \frac{\tau_q}{q} = F_D(\varphi, q) \quad (6.39b)$$

where  $F_C(\varphi, q)$  and  $F_D(\varphi, q)$  are the corresponding inhomogeneities as shown in Eqs. (6.38).

Next, defining  $q\tau_q$  as  $\tilde{\tau}_q$ , these equations take the more familiar form:

$$\frac{\partial \tau_\varphi}{\partial q} - \frac{1}{q} \frac{\partial \tilde{\tau}_q}{\partial \varphi} = q F_C(\varphi, q) \quad (6.40a)$$

$$\frac{1}{q} \frac{\partial \tau_\varphi}{\partial \varphi} + \frac{\partial \tilde{\tau}_q}{\partial q} = q F_D(\varphi, q) \quad (6.40b)$$

To derive the two decoupled equations, we do the following:

*1. Derivation of Angular Component*

- a. Multiply the first equation by  $q$  and differentiate it with respect to  $q$ .
- b. Differentiate the second equation with respect to  $\varphi$ .
- c. Add up the two resultant expressions and divide the result by  $q$ . Thus

$$\frac{1}{q^2} \frac{\partial^2 \tau_\varphi}{\partial \varphi^2} + \frac{\partial^2 \tau_\varphi}{\partial q^2} + \frac{1}{q} \frac{\partial \tau_\varphi}{\partial q} = F_\varphi(\varphi, q) \quad (6.41a)$$

where

$$F_\varphi(\varphi, q) = \frac{\partial F_D}{\partial \varphi} + \frac{1}{q} \frac{\partial (q^2 F_C)}{\partial q} \quad (6.42a)$$

*2. Derivation of Radial Component*

- a. Multiply the second equation by  $q$  and differentiate it with respect to  $q$ .
- b. Differentiate the first equation with respect to  $\varphi$ .
- c. Subtract the first resultant expression from the second and divide the result by  $q$ . Thus

$$\frac{1}{q^2} \frac{\partial^2 \tilde{\tau}_q}{\partial \varphi^2} + \frac{\partial^2 \tilde{\tau}_q}{\partial q^2} + \frac{1}{q} \frac{\partial \tilde{\tau}_q}{\partial q} = F_q(\varphi, q) \quad (6.41b)$$

where

$$F_q(\varphi, q) = -\frac{\partial F_C}{\partial \varphi} + \frac{1}{q} \frac{\partial (q^2 F_D)}{\partial q} \quad (6.42b)$$

The two inhomogeneous terms given in Eqs. (6.42) can be written in a somewhat more compact way:

$$(F_\varphi, F_q) = \left( \frac{\partial}{\partial \varphi}, \frac{1}{q} \frac{\partial q^2}{\partial q} \right) \begin{pmatrix} F_D & -F_C \\ F_C & F_D \end{pmatrix} \quad (6.42c)$$

Equations (6.41) are the expected (two-dimensional) decoupled Poisson equations: one for the angular component of  $\tau$ , namely,  $\tau_\varphi(\varphi, q)$ , and one for its radial component, namely,  $\tau_q(\varphi, q)$ .

### 6.3.2.3 Strange Matrix Element and Gauge Transformation

Since the *Strange* elements appear as inhomogeneous terms in the divergence equations [see, e.g., Eqs. (6.38)], one may hope that they can be eliminated by a gauge transformation. In order to carry out the gauge transformation, we consider Eqs. (6.38) and replace  $\tau_{jk}$  by  $\tilde{\tau}_{jk}$  so that

$$\tau_{jk} = \tilde{\tau}_{jk} + \nabla\Phi \quad (6.43)$$

where  $\Phi$  is an unknown function that fulfills the following equation:

$$\nabla^2\Phi = \tau_{jk}^{(2)} \quad (6.44)$$

Next, we replace, in Eq. (6.38a),  $\tau_{jk}$  by Eq. (6.43):

$$\text{Curl } \tau_{jk} = \text{Curl} (\tilde{\tau}_{jk} + \nabla\Phi) \quad (6.45)$$

Now, if the function  $\Phi$ , which is a solution for Eq. (6.44), is an *analytic* function, then

$$\text{Curl } \nabla\Phi = \nabla \times \nabla\Phi = 0 \quad (6.46)$$

and Eq. (6.44) yields

$$\text{Curl } \tau_{jk} \equiv \text{Curl } \tilde{\tau}_{jk} \quad (6.47)$$

With this result and recalling Eq. (6.44), we finally obtain for Eqs. (6.38) the results

$$\text{Curl } \tau_{jk} = [\tau_{j\ell}^{(0)} \times \tau_{\ell k}^{(0)}]; \quad j \neq \ell \neq k > j \quad (6.48a)$$

$$\text{Div } \tau_{jk} = \tau_{jl}^{(0)} \cdot \tau_{lk}^{(0)}; \quad j \neq \ell \neq k > j \quad (6.48b)$$

where the tilde sign is dropped from  $\tau_{jk}$ .

From numerical studies [see Section 6.4], we found that the preceding gauge transformation is fully justified for  $\tau_{13}^{(2)}$  and like terms (which are not formed at any particular *ci* point and therefore are analytic functions) but cannot be applied for *Strange* terms formed at *ci* points [e.g.,  $\tau_{12}^{(2)}$  and  $\tau_{23}^{(2)}$ ]. It is important to mention that in case Eqs. (6.48) are valid, there is really no need to calculate the function  $\Phi$  because Eqs. (6.48) are solved for a set of boundary conditions and they uniquely determine  $\tau_{13}$ .

In fact, gauge transformation may also be applied when  $\tau_{jk}^{(2)}$  are formed at *cis*. However, in this case the gauge transformation eliminates the removable component of  $\tau_{jk}^{(2)}$  but leaves the nonremovable one, which can eventually be estimated by other means (this possibility is discussed to some extent in Section 6.4).

## 6.4 A NUMERICAL STUDY OF {H<sub>2</sub>,H} SYSTEM

### 6.4.1 Introductory Comments

In this chapter we briefly discuss the numerical solution of the decoupled Poisson equations [see Eqs. (6.41)] and then present a few results to show that, indeed, the C-D equations are capable of correctly simulating the two components of  $\tau_{12}$ ,  $\tau_{23}$ , and  $\tau_{13}$  as obtained by the ab initio treatment.

To solve the coupled equations in Eq. (6.41), one has to develop a series of iterations in order to establish the inhomogeneity terms at each stage. This process can, in principle, be carried out because we may produce the terms for the *initial* step without necessarily solving differential equations. A way to do that is to calculate these terms employing the *vector algebra* approach as described in Section 6.2.5 (see also Refs. 1 and 2). This procedure may resolve most of the difficulties related to the iteration process but not all of them. In particular, we may encounter difficulties related to the *Strange* elements  $\tau_{jk}^{(2)}$  formed by adjacent states. In Ref. 3 these strange elements are analyzed and, accordingly, a recipe is given as to how they can, eventually be derived. The studies on this issue are not yet completed.

So far none of these ideas were tested in actual calculations. It is true that Eqs. (6.41) were solved as described in Ref. 3, but without iterations. At this early stage, we were interested to find out to what extent the newly derived Poisson equations are capable of reproducing the ab initio NACTs (thus, at most, forming an *existence* theorem for these equations) and not so much in testing the relevance of the iteration process. This aim was achieved by solving the Poisson equations for inhomogeneities supplied by the ab initio treatment. In other words, we assume the inhomogeneities to be given at every point, and the differential equations, for  $\tau_{12}$ ,  $\tau_{23}$ , and  $\tau_{13}$ , are solved, as will be briefly discussed in the next section.

### 6.4.2 Introducing Fourier Expansion

Within the numerical study the two decoupled Poisson equations (for each component of the three NACTs,  $\tau_{12}$ ,  $\tau_{23}$ , and  $\tau_{13}$ ) are solved separately.<sup>3</sup> In the present section we elaborate, to some extent, on how these equations are solved.

Considering the two equations in Eq. (6.41), both are observed to be essentially similar (their l.h.s expressions are identical) and differ only in their inhomogeneity terms. In addition, they are solved for different sets of boundary conditions.

To solve these equations, we expand the unknown functions in terms of Fourier series. In what follows we treat Eq. (6.41a) and for this purpose present  $\tau_\varphi(\varphi, q)$  as follows:

$$\tau_\varphi(\varphi, q) = \sum_{k=0}^{\infty} \{T_{\varphi Ck}(q) \cos(\lambda(k)\varphi) + T_{\varphi Sk}(q) \sin(\lambda(k)\varphi)\} \quad (6.49)$$

The Fourier series is usually characterized assuming  $\lambda(k)$  to be integers, namely,  $\lambda(k) = k$ . In the present case we found the expansion to be more efficient by assuming that  $\lambda(k)$  is equal to half-integers, namely,  $\lambda(k) = (1 + 2k)/2$ . A similar expansion is assumed for  $\tilde{\tau}_q(\varphi, q)$ .

Substituting Eq. (6.49) in Eq. (6.41a) and recalling that  $\{\cos(\lambda(k)\varphi), \sin(\lambda(k)\varphi)\}$  form an orthonormal set, we note that each of the coefficients fulfills the equation

$$T_{\varphi Rk}'' + \frac{1}{q} T_{\varphi Rk}' - \frac{1}{q^2} \lambda(k)^2 T_{\varphi Rk} = F_{\varphi Rk}; \quad R = C, S, \quad k \geq 1 \quad (6.50)$$

where the two prime signs label first and second derivatives with respect to  $q$  and  $F_{\varphi Rk}$ , on the r.h.s., are the corresponding inhomogeneities as obtained from Eq. (6.42a).

The equations for the Fourier coefficients of  $\tilde{\tau}_q(\varphi, q) (= q \tau_q(\varphi, q))$  are identical to those in Eq. (6.50) except that the inhomogeneity is now taken from Eq. (6.42b) and becomes  $F_{q Rk}$ .

### 6.4.3 Introducing Boundary Conditions

The Poisson equations are solved for a (circular) region centered at the equilateral  $D_{3h}$  *ci* and surrounded by a circle with a radius  $q = q_0$ , where  $q_0 = 0.5 \text{ \AA}$ . However, since this region contains the two troublesome (2,3) *cis* located at a distance of  $q \sim 0.29 \text{ \AA}$ , we divided this region into two subregions: (1) the *internal region*, defined within the (radial) range  $0 \leq q \leq q_i$ , where  $q_i = 0.285 \text{ \AA}$ ; and (2) the *external region*, defined within the circular strip in the interval  $q_e \leq q \leq q_0$ , where  $q_e = 0.295 \text{ \AA}$ . With these two regions, the two (2,3) *cis* are located outside both of them (see Fig. 6.7). In this

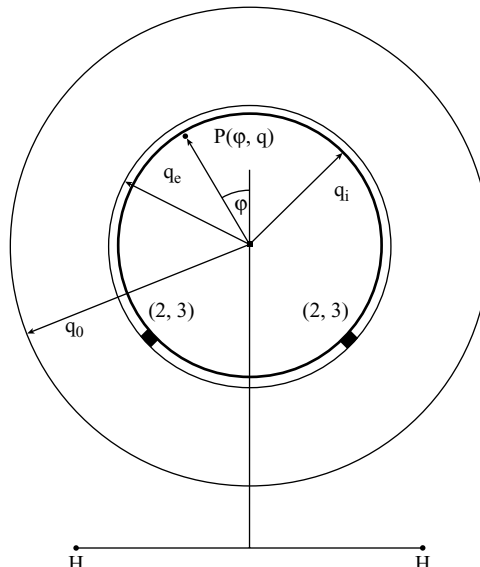


**Figure 6.7** Division of configuration space into two circular regions: (a) internal region defined along the interval  $(0 \leq q \leq q_i)$ ; (b) external region defined (as a circular strip) along the interval  $(q_e \leq q \leq q_0)$ . The full square presents the (1,2)  $D_{3h}$  *ci* and the two full diamonds, the two (2,3)  $C_{2v}$  *cis*.

section we report on a few results related to the internal region only (more results for both regions can be found in Ref. 3).

To solve the equations, we assume Dirichlet-type boundary conditions, derived by ab initio calculations, along the internal circle with the radius  $q = q_i$ . In addition, at the origin, all five NACTs [i.e.,  $\tau_{\varphi 23}(\varphi, q = 0)$ ,  $\tau_{\varphi 13}(\varphi, q = 0)$ ,  $\tau_{q 12}(\varphi, q = 0)$ ,  $\tau_{q 23}(\varphi, q = 0)$ ,  $\tau_{q 13}(\varphi, q = 0)$ ] are assumed to be identically zero. The only exception is  $\tau_{\varphi 12}(\varphi, q = 0)$  for which it is assumed to be  $0.5 \text{ rad}^{-1}$ , as was verified on numerous occasions.<sup>4,5</sup>

#### 6.4.4 Numerical Results

A detailed numerical study is presented in Ref. 3. Here we report on only a few results emphasizing the fact that the calculation seems to justify the promised *existence* theorem mentioned in Section 6.4.1. Before presenting the results, we mention only that all the details required to carry out the numerical study for the  $\{\text{H}_2, \text{H}\}$  are given in Sections 4.3.1.1 and 4.3.2.1. In particular, the fixed interatomic distance is  $R_{\text{HH}} = 0.74 \text{ \AA}$ .

Figures 6.8–6.10 present the angular and the radial components of  $\tau_{12}$ ,  $\tau_{23}$ , and  $\tau_{13}$ , respectively, as calculated along various circles surrounding the  $D_{3h}$  *ci* (see Fig. 6.7). We remind the reader that boundary conditions are attached only along the circle with the radius  $q = q_i = 0.285 \text{ \AA}$  (see Fig. 6.7). At the origin, namely, at  $q = 0$ , all functions are assumed to be equal to zero (as was also mentioned earlier) except for  $\tau_{\varphi 12}$ , which is assumed to be equal to  $0.5 \text{ rad}^{-1}$ . As is noted, the fit for the two components of all three  $\tau$ -matrix elements is very promising.

The ability of the Poisson equations to produce such encouraging fits has to be appreciated because (1) the initial integration point is the  $D_{3h}$  *ci* point, namely, a singular point; and (2) ab initio boundary conditions were attached to only one boundary (at  $q = q_i$ ).

The nice fit between two types of results for all six functions has important implications for the physical contents of the assumed model. However, the more important message due to this numerical study is that in the vicinity of a given *ci* [in this case the (1,2) *ci*] the other NACTs (in this case  $\tau_{23}$  and  $\tau_{13}$ ) become negligibly small. Another important outcome is that for the relevant NACT, namely,  $\tau_{12}$ , only the angular component remains nonzero (actually becomes singular) whereas the radial one is practically zero.

### 6.5 MULTISTATE HILBERT SUBSPACE: BREAKUP OF NONADIABATIC COUPLING MATRIX

In this section we discuss the possibility of forming finite Hilbert subspaces in a given region. For this purpose we consider a group of  $N$  states and for simplicity assume them to be the  $N$  lowest states. Next, it is assumed that within this group each two adjacent states form at least one *ci* but the  $N$ th state does not form a *ci* with its upper neighbor—the ( $N + 1$ )th state. As discussed in the previous sections, we distinguish

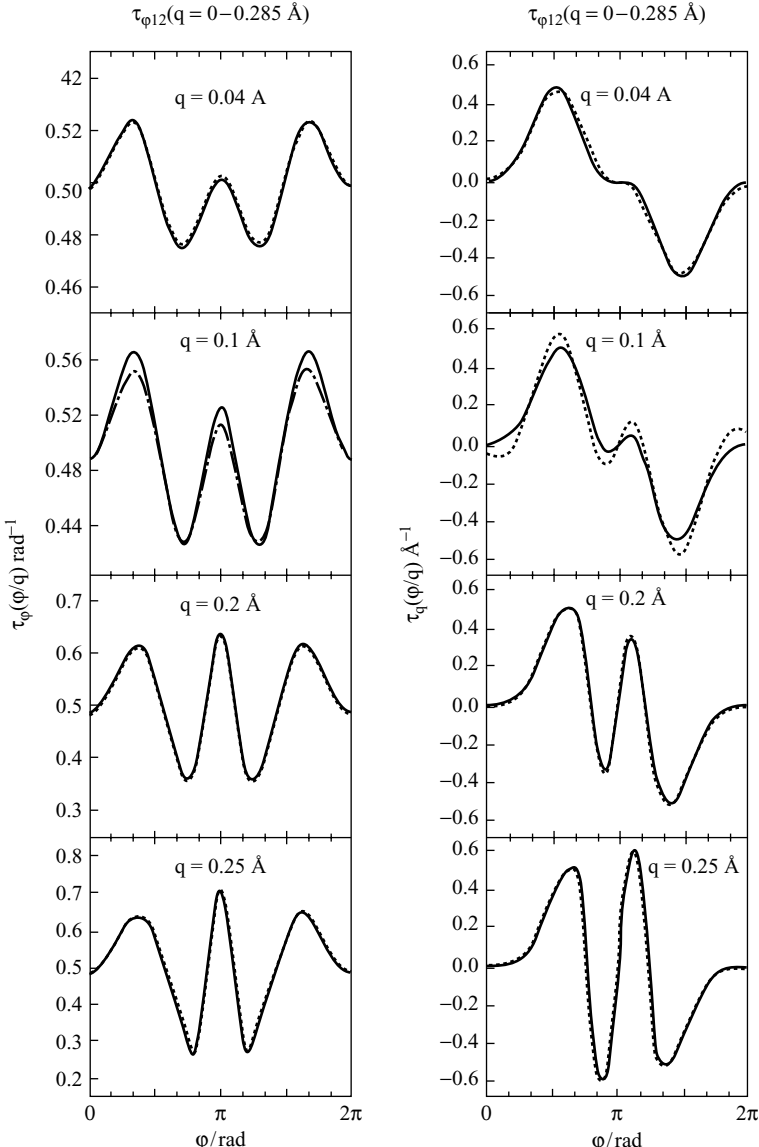


**Figure 6.8** Results for the (1,2) NACT  $\tau_{12}(\varphi|q)$ , namely,  $\tau_{\varphi 12}(\varphi|q)$  and  $\tau_{q12}(\varphi|q)$  presented as a function  $\varphi$  along specified concentric circles centered at the equilateral (1,2)  $D_{3h}$  ci (see Fig. 6.7). Solid lines describe results due to ab initio calculations; dotted lines describe results obtained from the Poisson equations. Along the first column results are shown for the angular component  $\tau_{\varphi 12}$  and along the second, results for the radial component  $\tau_{q12}$ . The Dirichlet (ab initio) boundary conditions are given along the circle with the radius  $q (= q_i) = 0.285 \text{ \AA}$ .

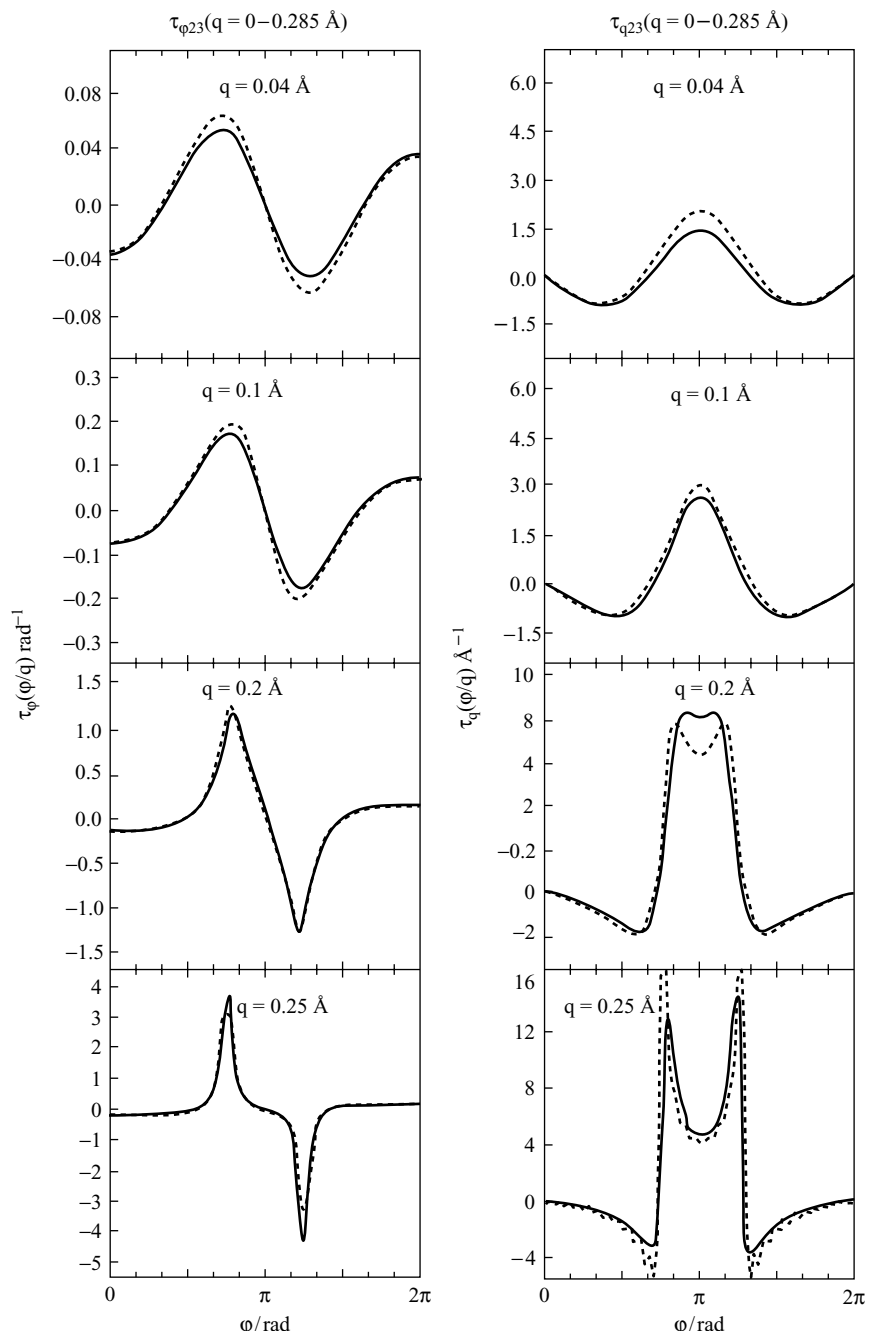


**Figure 6.9** Similar to the scenario depicted in Figure 6.8 but for the (2,3) NACTs, namely,  $\tau_{\phi 23}(\phi)$  and  $\tau_{q 23}(\phi)$ . [Note how well the Poisson equations produce the nonsymmetric  $\tau_{\phi 23}(\phi)$  function.]

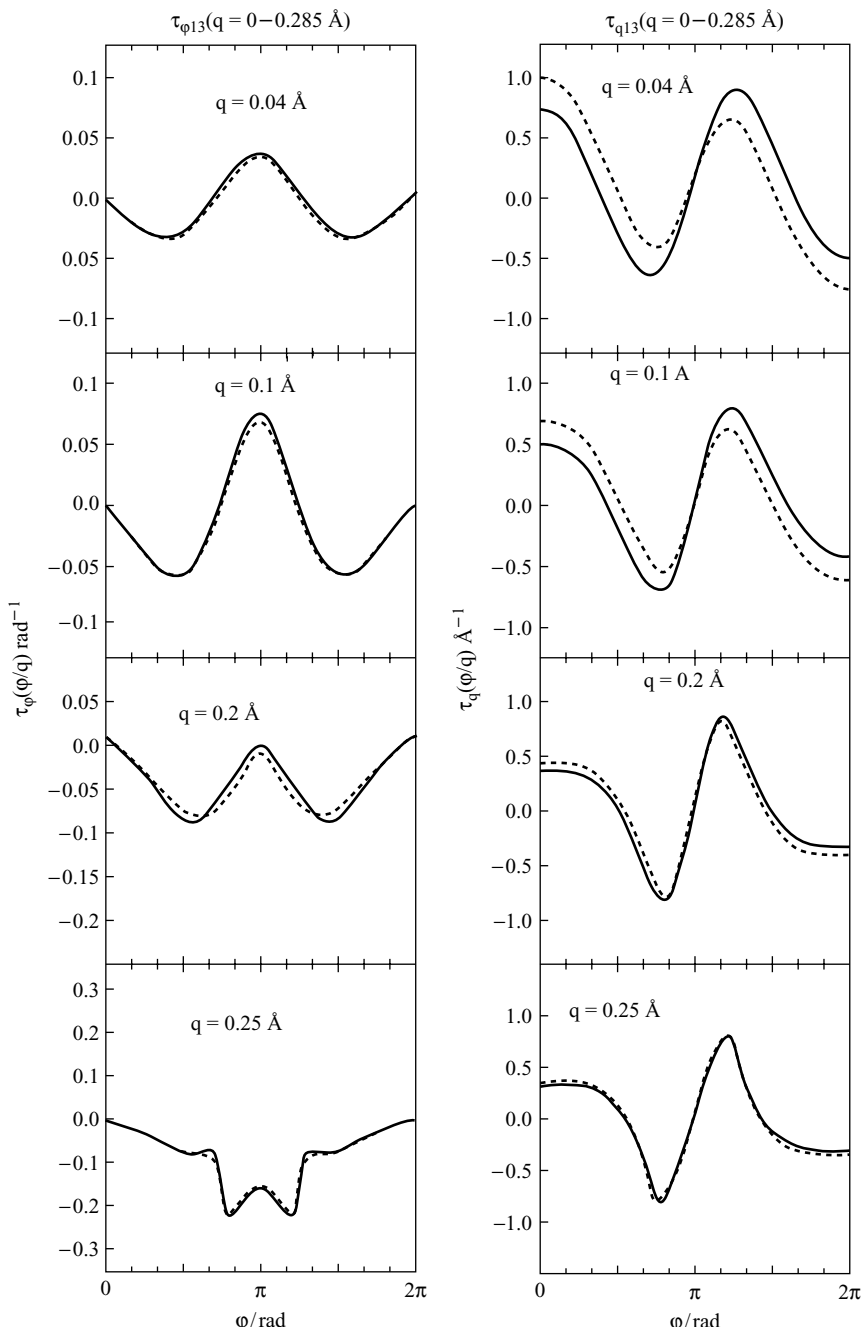


**Figure 6.10** Similar to the results shown in Figure 6.8 but for the (1,3) NACTs, namely,  $\tau_{\phi 13}(\phi)$  and  $\tau_{q 13}(\phi)$ .

between NACTs that are created by sources located at  $ci$  points and NACTs that do not have a source and are maintained by other NACTs. In what follows we concentrate on the second type, namely, on  $\tau_{jk}$  NACTs, where  $|j - k| > 1$ , determined by the C-D equations (see Eqs. (6.37)):

$$\text{Curl } \boldsymbol{\tau}_{jk} = \sum_{\ell=1}^{\infty} [\boldsymbol{\tau}_{j\ell} \times \boldsymbol{\tau}_{\ell k}]; \quad k > j + 1 \quad (6.51\text{a})$$

$$\text{Div } \boldsymbol{\tau}_{jk} = \sum_{\ell=1}^{\infty} [\boldsymbol{\tau}_{j\ell} \cdot \boldsymbol{\tau}_{\ell k}]; \quad k > j + 1 \quad (6.51\text{b})$$

Since we consider only NACTs without a source, the corresponding *Strange* terms are eliminated by gauge transformations.

Having these general expressions, we prove the following lemma.

**Lemma 6.3** For a system of  $(N + 1)$  states that lacks the  $(N, N + 1) ci$ , all elements of the type  $\boldsymbol{\tau}_{jN+1}$ , where  $j \leq N$ , are expected to be (negligibly) small.

*Proof* To prove the lemma, we assume that all the elements  $\boldsymbol{\tau}_{jk}$  (and  $\boldsymbol{\tau}_{kj}$ ) where  $j \leq N$  and  $k \leq N$  are given (eventually formed step by step employing iteration procedures—see Section 6.4) and we concentrate on the elements located along the  $N + 1$  column, namely,  $\boldsymbol{\tau}_{jN+1}; j = \{1, \infty\}$ . The relevant set of equations to determine the  $N$  first elements in this column are as follows:

$$\text{Curl } \boldsymbol{\tau}_{jN+1} = \sum_{\ell=1}^{\infty} [\boldsymbol{\tau}_{j\ell} \times \boldsymbol{\tau}_{\ell N+1}]; \quad j = \{1, N\} \quad (6.52\text{a})$$

$$\text{Div } \boldsymbol{\tau}_{jN+1} = \sum_{\ell=1}^{\infty} [\boldsymbol{\tau}_{j\ell} \cdot \boldsymbol{\tau}_{\ell N+1}]; \quad j = \{1, N\} \quad (6.52\text{b})$$

Equation (6.52a) can be rewritten in a more explicit form:

$$\sum_{\ell=1}^N [(\delta_{j\ell} \nabla - \boldsymbol{\tau}_{j\ell}) \times \boldsymbol{\tau}_{\ell N+1}] = \sum_{\ell=N+2}^{\infty} [\boldsymbol{\tau}_{j\ell} \times \boldsymbol{\tau}_{\ell N+1}]; \quad \{j = 1, N\} \quad (6.53)$$

A similar equation can be written for Eq. (6.52b) (where the dot replaces the  $\times$  sign).

In what follows we concentrate first on the l.h.s. of Eq. (6.53), for which the *unknown terms* are the  $\boldsymbol{\tau}_{\ell N+1}$  (where  $\ell \leq N$ ) and the  $\boldsymbol{\tau}_{j\ell}$ ;  $j, \ell \leq N$  serve as the *coefficients* for the equations (and, as mentioned earlier, are assumed to be given). It is important to realize that in this set of equations each of the unknown elements,  $\boldsymbol{\tau}_{\ell N+1}$ , is multiplied at least once (and sometimes twice) by  $\boldsymbol{\tau}_{\ell \pm 1, \ell}$ , namely, NACTs of a well-defined intensity, formed at  $cis$ , located in the region of interest. This fact guarantees that each unknown is properly presented within this set of equations.

Next we discuss the r.h.s., where we note that the summation starts at  $\ell = N + 2$  (and not at  $\ell = N + 1$ ) because  $\boldsymbol{\tau}_{N+1N+1} \equiv 0$ . The expressions on the r.h.s. serve, in

this case, as the  $N$  *inhomogeneous* terms for the equations on the l.h.s. These terms are usually formed by products of two NACTs where at least one, and usually both, are of weak intensity (because they are not of the type  $\tau_{\ell\pm 1,\ell}$  produced directly by sources). The only exception is the NACT  $\tau_{N+2,N+1}$ , which appears in the inhomogeneity of the  $N$ th equation but still is multiplied by  $\tau_{N,N+2}$ , and is again of weak intensity.

Equation (6.53), together with its divergence counterpart, form a set of differential equations for the  $N$  NACTs,  $\tau_{\ell,N+1}; \ell \leq N$ . This set of equations does not have a source term [as we assumed that this system lacks the only possible  $(N,N+1)$  *cis*] and all its inhomogeneous terms are expected to be relatively weak except, eventually, the inhomogeneous terms associated with the  $N$ th Curl equation and the  $N$ th divergence (Div) equation. These two inhomogeneous terms are of the form  $\tau_{N,N+2} \times \tau_{N+2,N+1}$  and  $\tau_{N,N+2} \cdot \tau_{N+2,N+1}$ , respectively, and in principle can be substantial [due to the  $(N+1,N+2)$  *cis*]. However, for that to happen, two conditions have to be satisfied: their multiplier,  $\tau_{NN+2}$ , must (1) have nonnegligible intensity and (2) overlap significantly with  $\tau_{N+2,N+1}$ . The conclusion is that if the  $N$ th inhomogeneous terms  $\tau_{NN+2} \times \tau_{N+2,N+1}$  and  $\tau_{N,N+2} \cdot \tau_{N+2,N+1}$  are small enough, the NACTs  $\tau_{\ell,N+1}; \ell \leq N$  along the  $(N+1)$ th column, are expected to be weak, specifically, of order  $O(\varepsilon)$ .

**Corollary 6.1** The same procedure can be applied for any column  $k$  outside the  $N \times N$  sub-NACM (viz., where  $k > N+1$ ) so that in general all elements of the type  $\tau_{jk}$  (and  $\tau_{kj}$ ) where  $j \leq N$  and  $k > N$  are expected to be of the order  $O(\varepsilon)$  or less.

This lemma contains one of the most fundamental features of the Born–Oppenheimer coupling terms, namely, that the absence of *cis* between two adjacent states, in a given region in configuration space, is likely to yield a breakup of the NACM to the level of  $O(\varepsilon)$ , as assumed in Eqs. (1.36) and (1.37). The size of  $O(\varepsilon)$  is expected to depend mainly on how far are the relevant  $(N, N+1)$  *cis* located from the region of interest.

In Section 4.3.2.1, the paragraphs under the heading “Quasibreakup of  $\tau$  Matrix” present a detailed study on this subject as carried out for the  $\{\text{H}_2, \text{H}\}$  system (see also Ref. 1). It is shown that in the region of interest the three lower states of this system form one (1,2) *cis*, two (2,3) *cis*, but no (3,4) *cis*. The implication of this finding is that the three lower states of the  $\{\text{H}_2, \text{H}\}$  system form approximately a Hilbert subspace as shown numerically in Section 4.3.2.1, text under heading “Multistate Quantization for  $\{\text{H}_2, \text{H}\}$  System.”

## 6.6 PSEUDOMAGNETIC FIELD

The present chapter is devoted to the possibility that the NACTs form fields that were previously termed *molecular fields*. It is important to realize that these are neither electric nor magnetic fields. These are vector-potential-type fields, which, as is known from the seminal Aharonov–Bohm publication,<sup>1</sup> are capable of affecting the phases of moving (charged) particles but are not capable of affecting the route

of these particles.<sup>1,2</sup> In this section we discuss the pseudomagnetic field as generated by the NACTs.

### 6.6.1 Quantization of Pseudomagnetic Field along the Seam

In Section 6.2.3 we discussed the Stokes theorem and found that for this theorem to apply, the tensorial (Abelian) component  $F_{q\varphi}$  has to be of the form as given in Eq. (6.13). Next, it was found that the function  $f(\varphi)$ , which yields the angular distribution of  $\mathbf{F}_{q\varphi}$  (with regard to the *seam*), has to be quantized.

In order to understand these two outcomes, we remind the reader of two facts: (1) for the Abelian case we have  $\mathbf{F} = \text{Curl } \boldsymbol{\tau}$ ; and (2) we assume the existence of pseudomagnetic field  $\tilde{\mathbf{H}}$ , which is formed by  $\boldsymbol{\tau}$  in the same way that a real magnetic field  $\mathbf{H}$  is formed by  $\mathbf{A}$  [see Eq. (6.1)]. Combining these two results, we have  $\mathbf{F} = \tilde{\mathbf{H}}$ . Next, since  $F_{q\varphi}$  fulfills Eq. (6.13), the same applies for  $\tilde{\mathbf{H}}$ :

$$\tilde{\mathbf{H}} = 2\pi f(\varphi) \frac{\delta(q)}{q} \mathbf{n} \quad (6.54)$$

This equation, in conjunction with the fact that  $f(\varphi)$  is quantized [see Eq. 6.17)], implies that the pseudomagnetic field  $\tilde{\mathbf{H}}$ , formed along the seam, is quantized.<sup>3,4</sup> This result is reminiscent of Dirac's quantization of the magnetic monopole.<sup>5</sup> Although we have the interesting analogy between  $\mathbf{H}$  and  $\tilde{\mathbf{H}}$ , we note that  $\tilde{\mathbf{H}}$  is quantized but that  $\mathbf{H}$ , as formed along the solenoid, is not.

### 6.6.2 Non-Abelian Magnetic Fields

Whereas an Abelian system is not capable of generating a pseudomagnetic field, unless it is located along the seam itself, we found that non-Abelian systems form pseudomagnetic fields distributed in configuration space. To see that, we call the reader's attention to a three-state system and Eqs. (6.35). Defining  $\tilde{\mathbf{H}}_{jk}$  as the field formed by  $\text{Curl } \boldsymbol{\tau}_{jk}$ , we, obtain

$$\tilde{\mathbf{H}}_{jk} = [\boldsymbol{\tau}_{j\ell} \times \boldsymbol{\tau}_{\ell k}]; \quad j \neq \ell \neq k > j \quad (6.55)$$

In other words, within the non-Abelian framework pseudomagnetic fields are formed as a result of interactions between NACTs belonging to different Abelian systems.

## PROBLEMS

### 6.1 Derive Eqs. (6.25).

*Solution* Equations (6.25) can be derived in two different approaches. In the first approach the  $ci$  is shifted to an arbitrary point employing Cartesian coordinates and the field is calculated for this shifted  $ci$ . In the other approach we employ straightforward vector algebra.

- (a) Shift transformation employing change of variables.** We start by writing the Curl equation in Eq. (6.8) for a vector  $\tau(x,y)$  in Cartesian coordinates

$$\frac{\partial \tau_x}{\partial y} - \frac{\partial \tau_y}{\partial x} = 0 \quad (6.56)$$

and assume  $\tau(x,y)$  to be of the form

$$\tau(x,y) = f\left(\frac{y}{x}\right) \frac{-y\mathbf{i}_x + x\mathbf{i}_y}{x^2 + y^2} \quad (6.57)$$

where  $\mathbf{i}_x$  and  $\mathbf{i}_y$  are unit vectors along the  $x$  and the  $y$  axes, respectively [it can be shown, by substitution, that the expression in Eq. (6.57) fulfills Eq. (6.56)]. To shift this solution (without rotation) from the origin to some given point  $(x_{j0},y_{j0})$ , the variables  $x$  and  $y$  are replaced by  $(x - x_{j0})$  and  $(y - y_{j0})$  so that the solution of Eq. (6.57) takes the following form:

$$\tau(x,y) = f\left(\frac{y - y_{j0}}{x - x_{j0}}\right) \frac{-(y - y_{j0})\mathbf{i}_x + (x - x_{j0})\mathbf{i}_y}{(x - x_{j0})^2 + (y - y_{j0})^2} \quad (6.58)$$

Our next step is to express this result in terms of polar coordinates  $(q,\varphi)$ . For this purpose we recall the relations:

$$x = q \cos \varphi; \quad y = q \sin \varphi \quad (6.59)$$

and introduce the following definitions (see Fig. 6.11):

$$x - x_{j0} = q_j \cos \varphi_j; \quad y - y_{j0} = q_j \sin \varphi_j \quad (6.60)$$

Since we are interested in the polar components of  $\tau(q,\varphi)$ , namely,  $\tau_q$  and  $\tau_\varphi$ , we also need to know their relation with  $\tau_x$  and  $\tau_y$ , which can be derived by chain rules (for the derivatives)

$$\begin{aligned} \tau_q &= \left\langle \zeta_1 \left| \frac{\partial}{\partial q} \zeta_2 \right. \right\rangle = \cos \varphi \tau_x + \sin \varphi \tau_y \\ \tau_\varphi &= \left\langle \zeta_1 \left| \frac{\partial}{\partial \varphi} \zeta_2 \right. \right\rangle = q(-\sin \varphi \tau_x + \cos \varphi \tau_y) \end{aligned} \quad (6.61)$$

where  $\zeta_1$  and  $\zeta_2$  are the two electronic adiabatic wavefunctions. Employing Eqs. (6.58), (6.60), and (6.61), we finally get

$$\begin{aligned} \tau_q(q,\varphi) &= -f(\varphi_j) \frac{1}{q_j} \sin(\varphi - \varphi_j) \\ \tau_\varphi(q,\varphi) &= \frac{q}{q_j} f(\varphi_j) \cos(\varphi - \varphi_j) \end{aligned} \quad (6.62)$$

Equations (6.62) are employed in the main text [see Eqs. (6.23)].

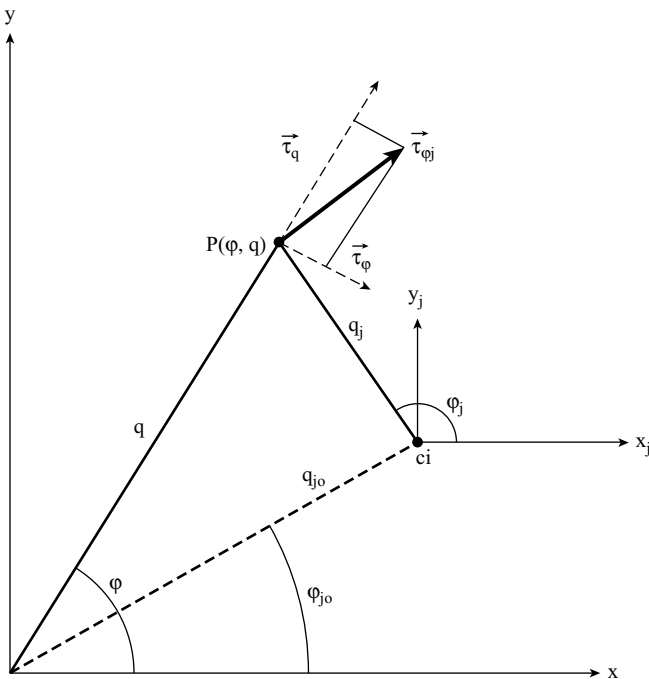


**Figure 6.11** Two systems of coordinates, one shifted parallel with respect to the other. The first system, with the axes  $(x_j, y_j)$ , is located at the  $ci$  point and the second system, with axes  $(x, y)$ , is located at some arbitrary point (on the same plane). Also shown is the angular component  $\vec{\tau}_{\varphi_j} (\equiv \vec{\tau}_{\varphi_j}/q_j)$  related to the  $ci$  (body) system and the two polar components  $(\vec{\tau}_\varphi, \vec{\tau}_q) (\equiv (\vec{\tau}_\varphi/q, \vec{\tau}_q))$  related to the  $(x, y)$  (space-fixed) system, both evaluated at point  $P(\varphi, q)$ .

- (b) *Shift transformation employing vector algebra.* We consider two parallel systems of coordinates (see Fig. 6.11): one at the  $ci$  point described by  $(q_j, \varphi_j)$  and the other at the assumed new system of coordinates described in terms of  $(q, \varphi)$ . The component of interest is the angular component  $-f_j(\varphi_j)/q_j$  along  $\hat{\varphi}_j$ , which at the point  $P(q, \varphi)$  is projected into the corresponding  $(\hat{q}, \hat{\varphi})$  axes:

$$\begin{aligned}\tau_q(q, \varphi) &= -\frac{1}{q_j} f(\varphi_j) \cos \left( \varphi_j - \frac{\pi}{2} - \varphi \right) \\ \frac{1}{q} \tau_\varphi(q, \varphi) &= \frac{1}{q_j} f(\varphi_j) \sin \left( \varphi_j - \frac{\pi}{2} - \varphi \right)\end{aligned}\quad (6.63)$$

Next, making the required changes yields the expression in Eqs. (6.62)

- 6.2** Prove the following statement: “The farther a  $\tau$ -matrix element is located from the diagonal, the weaker is its intensity.”

*Solution* In this problem we consider matrix elements that do not couple two adjacent states and therefore are located along the *off*-tridiagonals and even farther out. To prove the statement, we consider Eqs. (6.51). In fact, we consider only the Curl equations as any statement that applies to the Curl equations applies to the divergence equation as well. We consider the following Curl equations:

$$\text{Curl } \boldsymbol{\tau}_{jj+k} = \sum_{\ell=1}^N [\boldsymbol{\tau}_{j\ell} \times \boldsymbol{\tau}_{\ell j+k}] \quad (6.64)$$

where  $k \geq 2$ , and therefore this equation does not contain any terms,  $\boldsymbol{\tau}_{jj\pm 1}$ , unless they are multiplied by other elements of the NACM (see Eqs. (6.65) and (6.66)). The statement above is proved as follows.

- (a) We start by considering the case  $k = 2$  (viz., the elements along the first off-tridiagonal). Rewriting Eq. (6.64) for these elements, we get

$$\text{Curl } \boldsymbol{\tau}_{jj+2} = [\boldsymbol{\tau}_{jj+1} \times \boldsymbol{\tau}_{j+1j+2}] + \sum_{\ell=1}^N [\boldsymbol{\tau}_{j\ell} \times \boldsymbol{\tau}_{\ell j+2}] \quad (6.65)$$

where the summation does not include the index  $\ell = j + 1$ . We note that the separated product  $[\boldsymbol{\tau}_{jj+1} \times \boldsymbol{\tau}_{j+1j+2}]$  contains two NACTs, where each is of a well-defined intensity as both are formed by *sources* and therefore have to fulfill the quantization as presented in Eq. (3.12') [which follows Eq. (6.10)]. All other terms contained in the summation are formed by products where at least one of the multipliers is not a *source* term and therefore are expected to be of reduced intensity. Thus the differential equations for terms of the kind  $\boldsymbol{\tau}_{jj+2}$  are dominated by the abovementioned products.

- (b) To treat the other terms, we rewrite Eq. (6.64) in the following form:

$$\begin{aligned} \text{Curl } \boldsymbol{\tau}_{jj+k} &= [\boldsymbol{\tau}_{jj+1} \times \boldsymbol{\tau}_{j+1j+k}] + [\boldsymbol{\tau}_{jj+k-1} \times \boldsymbol{\tau}_{j+k-1j+k}] \\ &\quad + \sum_{\ell=1}^N' [\boldsymbol{\tau}_{j\ell} \times \boldsymbol{\tau}_{\ell j+k}] \end{aligned} \quad (6.66)$$

where  $k > 2$  and the summation does not include terms with the indices  $\ell = j + 1, j + k - 1$ . We note that the two separated products are expected to form the largest contributions to the inhomogeneity of the equation for  $\boldsymbol{\tau}_{jj+k}$  because each one of them contains one source term and another term of reduced intensity. For instance, in case of  $k = 3$ , these two terms are  $\boldsymbol{\tau}_{jj+1} \times \boldsymbol{\tau}_{j+1j+3}$  and  $\boldsymbol{\tau}_{jj+2} \times \boldsymbol{\tau}_{j+2j+3}$  and in case of  $k = 4$ ,  $\boldsymbol{\tau}_{jj+1} \times \boldsymbol{\tau}_{j+1j+4}$  and  $\boldsymbol{\tau}_{jj+3} \times \boldsymbol{\tau}_{j+3j+4}$ . Therefore, the  $\boldsymbol{\tau}_{jj+3}$  elements located along the fourth diagonals are expected to be of a lower intensity than the previously discussed  $\boldsymbol{\tau}_{jj+2}$  elements located along the third diagonals but of an intensity higher than that of the  $\boldsymbol{\tau}_{jj+4}$  elements located along the fifth diagonals.

These kinds of arguments can be further pursued for larger  $k$  values.

## REFERENCES

### Section 6.1

1. J. D. Jackson, *Classical Electrodynamics*, 2nd ed., Wiley, New York, 1998, Chapter 6 (in particular, see Eqs. 6.37 and 6.38).
2. E. E. Nikitin, in *Chemische Elementarprozesse*, H. Hartman ed., Springer Verlag, Berlin, 1968.
3. Z. H. Top and M. Baer, *Chem. Phys.* **25**, 1 (1977).
4. T. Vértesi and E. Bene, *Chem. Phys. Lett.* **392**, 17 (2004).
5. Y. Aharonov, E. Ben-Reuven, S. Popescu, and D. Rohrlich, *Nucl. Phys. B.* **350**, 818 (1991).
6. T. Pacher, L.S. Cederbaum, and H. Köppel, *Adv. Chem. Phys.* **84**, 293 (1993).
7. M. Baer, *Chem. Phys. Lett.* **349**, 84 (2001).
8. A. Kuppermann and R. Abrol, in *The Role of Degenerate States in Chemistry*, M. Baer and G. D. Billing, eds., *Adv. Chem. Phys.* **124**, 283 (2002).
9. R. Englman and A. Yahalom, *Acta Univ. Debreceniensis (Series Physica et Chimica)* **34–35**, 283 (2002).
10. M. Baer, A. M. Mebel, and G. D. Billing, *Int. J. Quant. Chem.* **90**, 1577 (2002).
11. M. S. Child, in *The Role of Degenerate States in Chemistry*, M. Baer and G. D. Billing, eds., *Adv. Chem. Phys.* **124**, 1 (2002).
12. R. Englman and A. Yahalom, in *The Role of Degenerate States in Chemistry*, M. Baer and G. D. Billing, eds., *Adv. Chem. Phys.* **124**, 197 (2003).
13. M. Baer, in *The Role of Degenerate States in Chemistry*, M. Baer and G.D. Billing, eds., *Adv. Chem. Phys.* **124**, 39 (2003).
14. R. P. Feynman, R. B Leighton, and M. Sands, *The Feynman Lectures on Physics*, Addison-Wesley, Reading, MA, 1964, Vol. II: (a) Section 14.1; (b) Section 14.4.
15. M. Baer, A. M. Mebel, and R. Englman, *Chem. Phys. Lett.* **354**, 243 (2002).
16. M. Baer, *Chem. Phys. Lett.* **360**, 243 (2002).
17. T. Vértesi, Á Vibók, G. J. Halász, and M. Baer, *J. Chem. Phys.* **121**, 4000 (2004).
18. Á Vibók, G. J. Halász, A. M. Mebel, S. Hu, and M. Baer, *Int. J. Quant. Chem.* **99**, 594 (2004).

### Section 6.2

1. M. Baer and R. Englman, *Chem. Phys. Lett.* **265**, 105 (1997).
2. M. Baer, S. H. Lin, A. Alijah, S. Adhikari, and G. D. Billing, *Phys. Rev. A.* **62**, 032506-1 (2000).
3. M. Born and J. R. Oppenheimer, *Ann. Phys. (Leipzig)* **84**, 457 (1927).
4. M. Born, *Festschrift Goett. Nach. Math. Phys.* **K1**, 1 (1951).
5. M. Born and K. Huang, *Dynamical Theory of Crystal Lattices*, Oxford Univ. Press, New York, 1954, Chapter 4.
6. P. A. M. Dirac, *Proc. Roy. Soc. Lond. A.* **133**, 60 (1931).
7. H. Goldstein, *Classical Mechanics*, Addison-Wesley, Reading, MA, Cambridge, MA, 1956, Section 1–5.

8. M. Baer, A. M. Mebel, and G. D. Billing, *Int. J. Quant. Chem.* **90**, 1577 (2002).
9. M. Baer, *Chem. Phys. Lett.* **349**, 84 (2001).
10. R. Englman and A. Yahalom, *Acta Univ. Debreceniensis (Series Physica et Chimica)* **34–35**, 283 (2002).
11. T. Vértesi, Á Vibók, G. J. Halász, A. Yahalom, R. Englman, and M. Baer, *J. Phys. Chem. A.* **107**, 7189 (2003).
12. T. Vértesi, Á Vibók, G. J. Halász, and M. Baer, *J. Chem. Phys.* **120**, 8420 (2004).
13. Á Vibók, T. Vértesi, E. Bene, G. J. Halász, and M. Baer, *J. Phys. Chem. A.* **108**, 8590 (2004).
14. T. Vértesi, Á Vibók, G. J. Halász, and M. Baer, *J. Chem. Phys.* **121**, 4000 (2004).
15. A. M. Mebel, M. Baer, and S. H. Lin, *J. Chem. Phys.* **114**, 5109 (2001).
16. A. M. Mebel, A. Yahalom, R. Englman, and M. Baer, *J. Chem. Phys.* **115**, 3673 (2001).
17. T. Vértesi and E. Bene, *Chem. Phys. Lett.* **392**, 17 (2004).
18. J. Avery, M. Baer, and D. G. Billing, *Molec. Phys.* **100**, 1011 (2002).
19. Á Vibók, G. J. Halász, T. Vértesi, S. Suhai, M. Baer, and J. P. Toennies, *J. Chem. Phys.* **119**, 6588 (2003).
20. MOLPRO is a package of ab initio programs written by H.-J. Werner and P. J. Knowles, with contributions from J. Almlöf et al.

### Section 6.3

1. T. Vértesi, Á Vibók, G. J. Halász, and M. Baer, *J. Chem. Phys.* **121**, 4000 (2004).
2. M. Baer, *Chem. Phys. Lett.* **360**, 243 (2002).
3. Á Vibók, G. J. Halász, A. M. Mebel, S. Hu, and M. Baer, *Int. J. Quant. Chem.* **99**, 594 (2004).
4. M. Baer, A. M. Mebel, and G. D. Billing, *Int. J. Quant. Chem.* **90**, 1577 (2002).
5. MOLPRO is a package of ab initio programs written by H.-J. Werner and P. J. Knowles, with contributions from J. Almlöf et al.
6. T. Vértesi, Á Vibók, G. J. Halász, and M. Baer, *J. Chem. Phys.* **120**, 8420 (2004).
7. Á Vibók, T. Vértesi, E. Bene, G. J. Halász, and M. Baer, *J. Phys. Chem. A.* **108**, 8590 (2004).
8. P. Barragan, L. F. Errea, A. Macias, L. Mendez, I. Rabadan, A. Riera, J. M. Lucas, and A. Aguilar, *J. Chem. Phys.* **121**, 11629 (2004).
9. G. Halász, Á Vibók, A. M. Mebel, and M. Baer, *Chem. Phys. Lett.* **358**, 163 (2002).

### Section 6.4

1. T. Vértesi, Á Vibók, G. J. Halász, and M. Baer, *J. Chem. Phys.* **120**, 8420 (2004).
2. Á Vibók, T. Vértesi, E. Bene, G. J. Halász, and M. Baer, *J. Phys. Chem. A.* **108**, 8590 (2004).
3. T. Vértesi, Á Vibók, G. J. Halász, and M. Baer, *J. Chem. Phys.* **121**, 4000 (2004).
4. G. Halász, Á Vibók, A. M. Mebel, and M. Baer, *J. Chem. Phys.* **118**, 3052 (2003).
5. M. Baer, T. Vértesi, G. J. Halász, Á Vibók, and S. Suhai, *Faraday Disc.* **127**, 337 (2004).

### Section 6.5

1. M. Baer, T. Vértesi, G. J. Halász, Á Vibók, and S. Suhai, *Faraday Disc.* **127**, 337 (2004).

**Section 6.6**

1. Y. Aharonov and D. Bohm, *Phys. Rev.* **115**, 485 (1959).
2. R. P. Feynman, R. B. Leighton, and M. Sands, *The Feynman Lectures on Physics*, Addison-Wesley, Reading, MA, 1964, Vol. II, pp. 15–12.
3. M. Baer, *Chem. Phys. Lett.* **349**, 84 (2001).
4. R. Englman and A. Yahalom, *Acta Univ. Debreceniensis (Series Physica et Chimica)* **34–35**, 283 (2002).
5. J. D. Jackson, *Classical Electrodynamics*, 2nd ed., Wiley, New York, 1998, Chapter 6.12.

# CHAPTER 7

---

## OPEN PHASE AND BERRY PHASE FOR MOLECULAR SYSTEMS

---

### 7.1 STUDIES OF AB INITIO SYSTEMS

#### 7.1.1 Introductory Comments

Since the early 1980s, one of the discoveries in quantum mechanics has been the *geometric phase* by Berry.<sup>1</sup> He showed that transporting a system in a *given* eigenstate  $|\zeta_n(\mathbf{s}(t))\rangle$  along a contour  $\Gamma$  will acquire a time-dependent phase factor  $\exp(i\tilde{\gamma}(t))$ . In case  $\Gamma$  becomes a *closed* contour and the time  $T$  it takes for the excursion along that closed contour is long enough, the acquired phase  $\tilde{\gamma}(t = T|\Gamma)$  becomes independent of  $T$ . In general this phase depends on  $\Gamma$  but not on any particular point along,  $\Gamma$ .

We can summarize Berry's findings by saying that if  $\Gamma$  lies in a plane that contains a *ci*, then the phase factor at  $t = T$  becomes<sup>1</sup>

$$\exp(i\tilde{\gamma}(\Gamma)) = \begin{cases} -1; & \text{if } \Gamma \text{ encircles the degeneracy} \\ +1; & \text{otherwise} \end{cases} \quad (7.1)$$

This result is reminiscent of a study by Herzberg and Longuet-Higgins,<sup>2</sup> who, a few years before Berry's study, revealed the somewhat unexpected result that in the Jahn–Teller model<sup>2–6</sup> the eigenfunctions flip their sign on completing a closed circle around a degeneracy point. Although their finding is not related to the time-dependent framework as presented by Berry, these two phenomena nevertheless seem to be closely connected.

---

*Beyond Born–Oppenheimer: Conical Intersections and Electronic Nonadiabatic Coupling Terms*  
By Michael Baer. Copyright © 2006 John Wiley & Sons, Inc.

One of the clearest observable manifestations of the geometric phase is in the ordering of the vibronic energy levels in molecular systems.<sup>7,8</sup> Moreover, it was proved that the geometric phase is gauge-invariant<sup>9–11</sup> and therefore is also a measurable quantity. Indeed, the existence of the Berry phase was also established experimentally.<sup>12,13</sup>

Although the geometric phase exists within Born–Oppenheimer systems, the final part in Berry’s derivation is, as will be shown, inapplicable for these systems.<sup>14</sup> Thus, for completeness, Berry’s derivation is presented with the aim of showing why it becomes inappropriate for Born–Oppenheimer systems (see Section 7.1.2). Next, in Section 7.1.3, we discuss the derivation which is suitable for these systems, and an examples based on an ab initio treatment of the {H<sub>2</sub>, H} system is worked out in Section 7.1.3.4.

### 7.1.2 Open Phase and Berry Phase for Singlevalued Eigenfunctions: Berry’s Approach

We consider the function  $|\psi(\mathbf{s}_e|\mathbf{s})\rangle$ , which is assumed to be a solution of the time-dependent Schrödinger equation, namely

$$i\hbar \frac{\partial |\psi(\mathbf{s}_e|\mathbf{s})\rangle}{\partial t} = \mathbf{H}_e |\psi(\mathbf{s}_e|\mathbf{s})\rangle \quad (7.2)$$

where  $\mathbf{s}_e$  is an electronic coordinate and  $\mathbf{s}$  is a nuclear coordinate, which may depend on time. Next we consider the electronic function  $|\chi_k(\mathbf{s}_e|\mathbf{s})\rangle$ , which is assumed to be an eigenstate of the electronic Hamiltonian  $\mathbf{H}_e = \mathbf{H}_e(\mathbf{s}_e|\mathbf{s})$  and therefore solves the following eigenvalue equation

$$\mathbf{H}_e |\chi_k(\mathbf{s}_e|\mathbf{s})\rangle = w_k(\mathbf{s}) |\chi_k(\mathbf{s}_e|\mathbf{s})\rangle \quad (7.3)$$

where  $w_k(\mathbf{s})$  is the corresponding eigenvalue. Since Eq. (7.3) is valid for any attached (nuclear) phase factor, we may choose it in such a way that  $|\chi_k(\mathbf{s}_e|\mathbf{s})\rangle$  is singlevalued in the region of interest.

In what follows we trace the motion of  $|\psi(\mathbf{s}_e|\mathbf{s}(t))\rangle$  [the function that solves Eq. (7.2)] along a *closed* contour  $\Gamma$ . Assuming the system to be at a given eigenstate  $|\chi_k(\mathbf{s}_e|\mathbf{s}(t=0))\rangle$  at  $t=0$  and  $T$  to be the time period of the cycle, we consider situations for which  $T$  is large enough so that at any time  $t$  the system is in the state  $|\chi_k(\mathbf{s}_e|\mathbf{s}(t))\rangle$  (eventually multiplied by some phase factors). Making this assumption, the function  $|\psi(\mathbf{s}_e|\mathbf{s}(t))\rangle$  can be written as follows:

$$|\psi(\mathbf{s}_e|\mathbf{s}(t))\rangle = \exp\left(\frac{-i}{\hbar} \int_0^t dt' w_k(\mathbf{s}(t'))\right) \times \exp\left(i\gamma_k(t)\right) |\chi_k(\mathbf{s}_e|\mathbf{s}(t))\rangle \quad (7.4)$$

In this expression the first exponential is the dynamical phase factor, a typical term that accompanies any eigenstate involved in the solution of Eq. (7.2), and the second term is the phase factor assumed to develop while the system moves along the contour.

Our interest is in the phase  $\gamma(t)$ , termed the *open phase*, and to obtain it, we substitute Eq. (7.4) in Eq. (7.2) and, recalling Eq. (7.3), we get

$$\frac{d\gamma_k}{dt} = i \left\langle \chi_k(\mathbf{s}_e|\mathbf{s}(t)) \left| \nabla_{\mathbf{s}} \chi_k(\mathbf{s}_e|\mathbf{s}(t)) \right. \right\rangle \cdot \frac{d\mathbf{s}(t)}{dt} \quad (7.5)$$

where the dot stands for scalar product. The value of  $\gamma_k$ , once the system reached the end of the closed contour [viz., when  $t = T$ ] is  $\gamma_k(t = T)$ . In what follows this value is denoted as  $\alpha_k(\Gamma)$  and is recognized as the *geometric phase* (or the *Berry phase*), which, according to this approach, is given in the following form:

$$\alpha_k(\Gamma) = i \oint_{\Gamma} \left\langle \chi_k(\mathbf{s}_e|\mathbf{s}) \left| \nabla_{\mathbf{s}} \chi_k(\mathbf{s}_e|\mathbf{s}) \right. \right\rangle \cdot d\mathbf{s} \quad (7.6)$$

It is noted that  $\alpha_k(\Gamma)$  depends on the chosen contour  $\Gamma$  but not on any particular point along  $\Gamma$ .

As mentioned earlier, this is Berry's original derivation. Nevertheless, we stop here because the rest of the derivation applies to an isolated degeneracy point in a three-dimensional system whereas in molecular systems this type of degeneracy does not exist. The degeneracy points in molecular systems arrange themselves along infinitely long seams. Therefore the procedure suggested by Berry in order to evaluate Eq. (7.6), namely, to convert the line integral into a surface integral by applying Stokes' theorem (thus circumventing the need to treat the poles produced at the degeneracy points—see Section 5.1), cannot be materialized because each such surface is crossed by the infinitely long seams that contain degeneracy points. Any other procedure requires the evaluation of  $|\nabla_{\mathbf{s}} \chi_k\rangle$  (which in this derivation is a singlevalued function) in terms of locally singlevalued basis functions  $|\chi_k\rangle$ , which can be an insurmountable difficulty.

In the next section we show how the existence of Berry's phase becomes apparent in molecular systems and how it is derived.

### 7.1.3 Open Phase and Berry Phase for Multivalued Eigenfunctions: Present Approach

#### 7.1.3.1 Derivation of Time-Dependent Equation

The approach presented next is similar to the one applied in the previous section, but instead of employing adiabatic, singlevalued eigenfunctions, we employ *real* eigenfunctions, which are not necessarily singlevalued.

We consider the following time-dependent Schrödinger equation

$$i\hbar \frac{\partial |\xi(\mathbf{s}_e|\mathbf{s})\rangle}{\partial t} = \mathbf{H}_e |\xi(\mathbf{s}_e|\mathbf{s})\rangle \quad (7.7)$$

where all notations are similar to the ones in Section 7.1.2. Next, we assume a Hilbert subspace of dimension  $N$  in a given region  $\Lambda$  of configuration space. This implies that any (normalized) function  $|\xi(\mathbf{s}_e|\mathbf{s})\rangle$  defined in this region can be presented in terms

of  $N$  eigenfunctions of  $\mathbf{H}_e$ , calculated at a given (fixed) point  $\mathbf{s}_0$  and are denoted as  $\{|\zeta_k(\mathbf{s}_e|\mathbf{s}_0)\rangle; k = 1, N\}$ . Thus

$$|\xi(\mathbf{s}_e|\mathbf{s})\rangle = \sum_{k=1}^N \tilde{\zeta}_k(\mathbf{s}) |\zeta_k(\mathbf{s}_e|\mathbf{s}_0)\rangle \quad (7.8)$$

where  $\{\tilde{\zeta}_k(\mathbf{s}); k = 1, N\}$  are coefficients that depend solely on nuclear coordinates and are normalized in such a way that  $|\xi(\mathbf{s}_e|\mathbf{s})\rangle$  is guaranteed to be normalized as mentioned earlier. It is important to emphasize that  $|\xi(\mathbf{s}_e|\mathbf{s})\rangle$  does not have to be singlevalued and therefore also the coefficients  $\{\tilde{\zeta}_k(\mathbf{s}); k = 1, N\}$  are not necessarily singlevalued.

To be more efficient in the derivation, we employ matrix notation so that Eq. (7.8) is written as

$$|\xi(\mathbf{s}_e|\mathbf{s})\rangle = \left| \zeta^*(\mathbf{s}_e|\mathbf{s}_0) \right\rangle \tilde{\zeta}(\mathbf{s}) \quad (7.8')$$

where  $|\zeta^*(\mathbf{s}_e|\mathbf{s}_0)\rangle$  is a row vector and  $\tilde{\zeta}(\mathbf{s}(t))$  is the corresponding column vector that contains the coefficients  $\{\tilde{\zeta}_k(\mathbf{s}); k = 1, N\}$ .

Substituting Eq. (7.8') in Eq. (7.7) and integrating over  $\mathbf{s}_e$  yields the matrix-equation to be solved, namely

$$i\hbar \frac{\partial \tilde{\zeta}(\mathbf{s}(t))}{\partial t} = \mathbf{V}(\mathbf{s}(t)) \tilde{\zeta}(\mathbf{s}(t)) \quad (7.9)$$

where  $\mathbf{V}(\mathbf{s}(t))$  is the (diabatic) potential matrix formed by the basis set  $\{|\zeta_k(\mathbf{s}_e|\mathbf{s}_0)\rangle; k = 1, N\}$  introduced above [see Section 2.1.2, and in particular Eq. (2.17), for details].

Next are introduced the matrix  $\mathbf{A}$  that diagonalizes  $\mathbf{V}(\mathbf{s})$  and  $\mathbf{u}$ , a diagonal matrix that contains the eigenvalues of  $\mathbf{V}$ :

$$\mathbf{V}(\mathbf{s}) = \mathbf{A}^\dagger(\mathbf{s}) \mathbf{u}(\mathbf{s}) \mathbf{A}(\mathbf{s}) \quad (7.10)$$

Matrix  $\mathbf{A}$  is recognized as the adiabatic-to-diabatic transformation (ADT) matrix introduced earlier [see section 2.1.3.2, and specifically Eq. (2.39)]. Substituting Eq. (7.10) in Eq. (7.9) and replacing  $\tilde{\zeta}(\mathbf{s}(t))$  by  $\boldsymbol{\eta}(t)$  where

$$\boldsymbol{\eta}(t) = \mathbf{A}(\mathbf{s}(t)) \tilde{\zeta}(\mathbf{s}(t)) \quad (7.11)$$

yields, for Eq. (7.9), the result<sup>14–16</sup>

$$i\hbar \frac{\partial \boldsymbol{\eta}(t)}{\partial t} = \mathbf{u}(\mathbf{s}(t)) \boldsymbol{\eta}(t) - i\hbar \mathbf{A}(\mathbf{s}(t)) \dot{\mathbf{A}}^\dagger(\mathbf{s}(t)) \boldsymbol{\eta}(t) \quad (7.12)$$

or

$$i\hbar \frac{\partial \boldsymbol{\eta}(t)}{\partial t} = \mathbf{u}(\mathbf{s}(t)) \boldsymbol{\eta}(t) - i\hbar \mathbf{A}(\mathbf{s}(t)) (\dot{\mathbf{s}} \cdot \nabla_{\mathbf{s}} \mathbf{A}^\dagger(\mathbf{s}(t))) \boldsymbol{\eta}(t) \quad (7.13)$$

In what follows Eq. (7.13) is solved for a closed contour  $\Gamma$ . If  $\mathbf{s}$  is chosen to be proportional to  $t$  and if  $T$ , as before, is the corresponding time period, then  $\mathbf{s}$  can be written as  $\mathbf{s} = s\mathbf{i}_\Gamma$ , where  $\mathbf{i}_\Gamma$  is a unit vector along the contour  $\Gamma$  and  $s = 2\sigma_0\pi(t/T)$  so that Eq. (7.13) becomes

$$i\hbar \frac{\partial \boldsymbol{\eta}(t)}{\partial t} = \mathbf{u}(\mathbf{s}(t))\boldsymbol{\eta}(t) - i\hbar\sigma_0 \frac{2\pi}{T} \mathbf{A}(s(t)) \frac{\partial \mathbf{A}^\dagger(s(t))}{\partial s} \boldsymbol{\eta}(t) \quad (7.14)$$

Here  $\sigma_0$  is either a constant or, at most, a weakly time-dependent function.

### 7.1.3.2 Treatment of Adiabatic Case

*Connection between Berry Phases and D-Matrix Elements* In this section we discuss the solution of Eq. (7.14) in the adiabatic limit, namely, when  $T \rightarrow \infty$ .

From the structure of Eq. (7.14) we note that in the adiabatic case its second term may be deleted. Consequently the solution of Eq. (7.14) becomes

$$\lim_{T \rightarrow \infty} \boldsymbol{\eta}(t) = \exp\left(-\frac{i}{\hbar} \int_0^t \mathbf{u}(t) dt\right) \boldsymbol{\eta}(t=0) \quad (7.15)$$

where  $\mathbf{u}(t) \equiv \mathbf{u}(s(t))$  and the exponential function is a *diagonal* matrix that contains in its  $k$ th position the  $k$ th dynamic phase factor:  $\exp(-i/\hbar) \int_0^t u_k(t) dt$ .

Next, recalling Eq. (7.11), we get the following solution for  $\tilde{\zeta}(t)$ :

$$\lim_{T \rightarrow \infty} \tilde{\zeta}(t) = \mathbf{A}^\dagger(t) \exp\left(-\frac{i}{\hbar} \int_0^t \mathbf{u}(t) dt\right) \mathbf{A}(t=0) \tilde{\zeta}(t=0) \quad (7.16)$$

and following that, the expression for  $|\xi(\mathbf{s}_e|t)\rangle$  [see Eq. (7.8')]:

$$\begin{aligned} \lim_{T \rightarrow \infty} |\xi(\mathbf{s}_e|t)\rangle &= |\zeta^*(\mathbf{s}_e|\mathbf{s}_0)\rangle \mathbf{A}^\dagger(t) \exp\left(-\frac{i}{\hbar} \int_0^t \mathbf{u}(t) dt\right) \\ &\quad \times \mathbf{A}(t=0) \tilde{\zeta}(t=0) \end{aligned} \quad (7.17)$$

To continue, we distinguish between two situations:

1. For  $t = 0$  we have the result

$$|\xi(\mathbf{s}_e|t=0)\rangle = |\zeta^*(\mathbf{s}_e|\mathbf{s}_0)\rangle \tilde{\zeta}(t=0) \quad (7.18)$$

which is identical to the one given in Eq. (7.8') by assuming  $\mathbf{s}_0 \equiv \mathbf{s}(t=0)$ .

2. For  $t = T$  we have the result

$$\begin{aligned} \lim_{T \rightarrow \infty} |\xi(s_e|t = T)\rangle &= |\zeta^*(s_e|s_0)\rangle A^\dagger(t = T) \\ &\times \exp\left(-\frac{i}{\hbar} \int_0^T \mathbf{u}(t)dt\right) A(t = 0) \tilde{\zeta}(t = 0) \end{aligned} \quad (7.19)$$

where  $A(t = T)$  is identified with  $A(\beta|\Gamma)$  as presented in Eq. (2.48). Recalling the definition of the  $\mathbf{D}$  matrix in Eq. (2.47) [where the matrix  $\mathbf{B}(\Gamma)$ , in Eq. (2.47), is later identified as the  $\mathbf{D}(\Gamma)$ —see discussion following Eq. (2.49)] we replace  $A^\dagger(t = T)$  by  $A^\dagger(t = 0)\mathbf{D}^\dagger$ :

$$\begin{aligned} \lim_{T \rightarrow \infty} |\xi(s_e|t = T)\rangle &= |\zeta^*(s_e|s_0)\rangle A^\dagger(t = 0)\mathbf{D}^\dagger(\Gamma) \\ &\times \exp\left(-\frac{i}{\hbar} \int_0^T \mathbf{u}(t)dt\right) A(t = 0) \tilde{\zeta}(t = 0) \end{aligned} \quad (7.20)$$

In what follows we recall that the  $\mathbf{D}$  matrix is real (because the electronic basis set is assumed to be real) and therefore  $\mathbf{D}^\dagger = \mathbf{D}$ .

To complete the derivation, we check the case where  $A(t = 0)$  is a unit matrix, namely, the case where  $s_0 = s(t = 0)$ :

$$\begin{aligned} \lim_{T \rightarrow \infty} |\xi(s_e|t = T)\rangle &= |\zeta^*(s_e|s_0)\rangle \mathbf{D}(\Gamma) \\ &\times \exp\left(-\frac{i}{\hbar} \int_0^T \mathbf{u}(t)dt\right) \tilde{\zeta}(t = 0) \end{aligned} \quad (7.21)$$

Comparing Eq. (7.21) with Eq. (7.18), we note that the main difference is the appearance of the  $\mathbf{D}$  matrix, which contains, in fact, Berry's phase factors [see also Eq. (7.4) and compare for a single state].

**Short Summary** We showed that in the adiabatic limit the solution of the *time-dependent* Schrödinger equation produces, at the end of a *closed* contour, the diagonal elements of the *topological*  $\mathbf{D}$  matrix as introduced within the *time-independent* formulation [see Eq. (2.32)]. These diagonal matrix elements are identified with Berry's phase factors as produced by an  $N$ -state Hilbert space (or produced, approximately, by an  $N$ -state Hilbert subspace). In Problem 7.1 it is proved that, in the adiabatic limit, the present derivation yields a system that moves along a contour while being in an eigenstate of the time-dependent Hamiltonian.

**Open-Path Phase and Principal Open-Path Phase** Having prepared the analytical background, the question to be asked is whether we are in a position to derive the open-path phase (OPP), namely, the time-dependent phase associated with the eigenstate of the system at time  $t$  while the system is moving adiabatically. It seems that using the (adiabatic) solution given in Eq. (7.17), substituting it in Eq. (7.7), and employing the fact that this solution also produces the relevant eigenvalue of the Hamiltonian (as is shown in the next section) will yield the required equation for calculating the OPP. It turns out that this procedure fails because  $\mathbf{A}(t)$  is, in general, not a diagonal matrix (it is diagonal only at  $t = 0$  and  $t = T$ ), and therefore this goal cannot be achieved within such a framework.

In what follows we derive the OPP, not of the whole eigenfunction but for the components associated with the individual vector elements,  $\{\tilde{\zeta}_j^{(k)}(t); j = 1, \dots, N\}$ . Thus, once Eq. (7.14) is solved, we again employ Eq. (7.11) to derive the vector elements,  $\{\tilde{\zeta}_j^{(k)}(t); j = 1, \dots, N\}$  for any time  $t$ . However, we concentrate on one particular component, the  $\tilde{\zeta}_k^{(k)}(t)$  element, namely, the only element that at  $t = 0$  is equal to 1 (the rest are all assumed to be zero) and at  $t = T$  is expected to be, again, the *only* nonzero element. Employing Eq. (7.21), it can be shown to be of the form:

$$\lim_{T \rightarrow \infty} \tilde{\zeta}_k^{(k)}(t = T) = \mathbf{D}_{kk}(\Gamma) \exp \left( -\frac{i}{\hbar} \int_0^T \mathbf{u}_k(t) dt \right) \quad (7.22)$$

where

$$\mathbf{D}_{kk}(\Gamma) = \exp \left( i\alpha^{(k)}(\Gamma) \right) \quad (7.23)$$

[see Eq. (2.33)], and we also recall that in case of real eigenfunctions  $\alpha^{(k)}(\Gamma)$  has to be an integer multiple of  $\pi$ .

This  $\tilde{\zeta}_k^{(k)}(t)$  term becomes, for any intermediate time  $t$  [see Eq. (7.16)]

$$\lim_{T \rightarrow \infty} \tilde{\zeta}_k^{(k)}(t) = \mathbf{A}_{kk}^\dagger(t) \exp \left( -\frac{i}{\hbar} \int_0^t \mathbf{u}_k(t) dt \right) \quad (7.24)$$

In the numerical study to be presented later we concentrate on this particular ( $k$ th) OPP, which in the adiabatic limit, when  $t = T$ , becomes the Berry phase. In what follows this phase is termed the *principal open-path phase* (POPP). For real molecular eigenfunctions, we show not only that the Berry phase is a multiple of  $\pi$  but also that the POPP is, at any given instant, a multiple of  $\pi$ .

### 7.1.3.3 Treatment of Nonadiabatic (General) Case

To treat the general case, we return to Eq. (7.9) and solve it numerically for different  $T$  values and show that once  $T$  becomes large enough, the computations converge to results obtained analytically, namely, for  $\tilde{\zeta}(t)$  in Eq. (7.16), where that the whole dependence of  $\tilde{\zeta}(t)$  is expressed in terms of the  $\mathbf{A}$ -matrix elements.

The calculations are carried out for circular contours—circles—with given centers and fixed radii. As a result, we apply polar coordinates  $(q, \varphi)$ , where  $q$  is the radial coordinate (usually fixed) and  $\varphi$  is the angular coordinate that is applied as the independent variable. However, the independent variable in the present study is the time  $t$  and, therefore, we assume that  $\varphi$  and  $t$  are related as  $\varphi = (2\pi/T)t$ . Equation (7.9) is solved for the following boundary conditions; namely,  $\tilde{\zeta}(t = 0)$  as given in the form  $\{\tilde{\zeta}_j^{(k)}(t = 0) = \delta_{kj}; j = 1, N\}$ .

For our purposes we present the  $k$ th element as<sup>14,17–20</sup>

$$\tilde{\zeta}_k^{(k)}(t) = \rho_k^{(k)}(t) \exp\left(i\gamma_k^{(k)}(t)\right) \exp\left(-\frac{i}{\hbar} \int_0^t \mathbf{u}_k(t) dt\right) \quad (7.25)$$

where  $\rho_k^{(k)}(t)$  is a positive number in the range  $\{0,1\}$  and describes the  $k$ th amplitude in the expansion of  $\xi^{(k)}(t)$  in terms of the original electronic basis set, namely,  $\{|\zeta_k(\mathbf{s}_e|t = 0)\rangle; k = 1, N\}$  and  $\gamma_k^{(k)}(t)$  is the ( $k$ th) associated POPP. It is important to emphasize that Eq. (7.25) is relevant for both the nonadiabatic case and the adiabatic one.

Next, comparing Eq. (7.25) with Eq. (7.24) (in case of the adiabatic limit), it is seen that

$$\lim_{T \rightarrow \infty} \rho_k^{(k)}(t) \exp\left(i\gamma_k^{(k)}(t)\right) = \mathbf{A}^\dagger_{kk}(t) \quad (7.26)$$

which implies

$$\lim_{T \rightarrow \infty} \rho_k^{(k)}(t) = |\mathbf{A}^\dagger_{kk}(t)| \quad (7.27a)$$

$$\lim_{T \rightarrow \infty} \gamma_k^{(k)}(t) = \arg(\mathbf{A}^\dagger_{kk}(t)) \quad (7.27b)$$

Since in case of real electronic eigenfunctions the  $\mathbf{A}$ -matrix elements are always real, we obtain from Eq. (7.27b) the fact that the POPP has to be an integer multiple of  $\pi$ . This implies that the phase function  $\gamma_k^{(k)}(t)$  is a step function (or Heaviside function), which may vary discontinuously along the time axis. In other words

$$\lim_{T \rightarrow \infty} \gamma_k^{(k)}(t) = n(t)\pi \quad (7.27c)$$

where  $n(t)$  is an integer. The discontinuous jumps in  $n(t)$  take place at times  $t$  when the corresponding diagonal matrix element,  $\mathbf{A}_{kk}(t)$  flips its sign.

This process also guarantees that at  $t = T$  the value of  $\gamma_k^{(k)}(t = T)$ , which becomes Berry's topological phase,  $\alpha^{(k)}(\Gamma)$ , is an integer multiple of  $\pi$ ; that is,  $n(t = T)$  is also an integer.

From previous studies we found that the most reliable way to extract the  $\gamma_k^{(k)}(t)$  is by employing the following expression:<sup>14,17,18</sup>

$$\gamma_k^{(k)}(t) = \text{Re} \left( i \int_0^t dt' \frac{\langle \frac{d}{dt} \zeta_k^{(k)}(\mathbf{s}_e|t') | \zeta_k^{(k)}(\mathbf{s}_e|t') \rangle}{\langle \zeta_k^{(k)}(\mathbf{s}_e|t') | \zeta_k^{(k)}(\mathbf{s}_e|t') \rangle} \right) \quad (7.28a)$$

In the adiabatic limit  $\gamma_k^{(k)}(t)$  is expected to be a step function [see Eq. (7.27c)] and the absolute value of  $\zeta_k^{(k)}(t)$  becomes

$$\rho_k^{(k)}(t) = |\zeta_k^{(k)}(t)| \quad (7.28b)$$

In the next section this approach is applied for the {H<sub>2</sub>,H} system.<sup>14</sup>

#### 7.1.4 {H<sub>2</sub>,H} System as a Case Study

In order to understand the meaning of the numerical results to be presented next, we first discuss a general molecular system for which this approach is applicable and then analyze numerical results for the title system.

We assume a system of electrons and nuclei that is composed of two “floppy” parts, but otherwise the two parts are rigid. Next, at time  $t = 0$  an external electromagnetic field is turned on that causes one part of the molecule (or both) to revolve around some (common) point. Assuming the molecular system to be in a given Born–Oppenheimer eigenstate, this induced rotational motion may cause transitions to other (electronic) states with (oscillating) time-dependent probabilities. To calculate these transition probabilities, we employ the time-dependent semiclassical treatment as presented in Section 7.1.3.3. These equations will be applied for the {H<sub>2</sub>,H} system for which we have available the necessary *ab initio* information (Section 4.3.1.1 and 4.3.2.1).

The main emphasis in these numerical treatments is to study the dependence of the amplitude  $\rho_k^{(k)}(t)$  and the POPP  $\gamma_k^{(k)}(t)$  on time as obtained for different values of  $T$ . We recall that both  $\rho_k^{(k)}(t)$  and  $\gamma_k^{(k)}(t)$  relate to the principal term in the expansion of the electronic wavefunction  $|\xi(\mathbf{s}_e|\mathbf{s}(t))\rangle$  in terms of the adiabatic set  $\{|\zeta_k(\mathbf{s}_e|\mathbf{s}_0 = \mathbf{s}(t=0))\rangle; k = 1, N\}$  (for more details, see Section 7.1.3.2, text under heading “Open-Path Phase and Principal Open-Path Phase”). The aim in this study is to repeat the calculation of these two magnitudes for increasing values of  $T$  with the aim of justifying the theoretical asymptotic adiabatic limits as obtained for  $T \rightarrow \infty$ .

The study to be presented next is related to a three-state system, namely, the three lower states of the H + H<sub>2</sub> system: the 1<sup>2</sup>A', the 2<sup>2</sup>A', and the 3<sup>2</sup>A' states known to be coupled to each other.<sup>21–24</sup> We recall that the two lower states of the H<sub>3</sub> system are coupled by an *equilateral ci*, labeled as a D<sub>3h</sub> ci and that the second and the third states are coupled by two C<sub>2v</sub> *cis* formed for the corresponding isosceles triangles

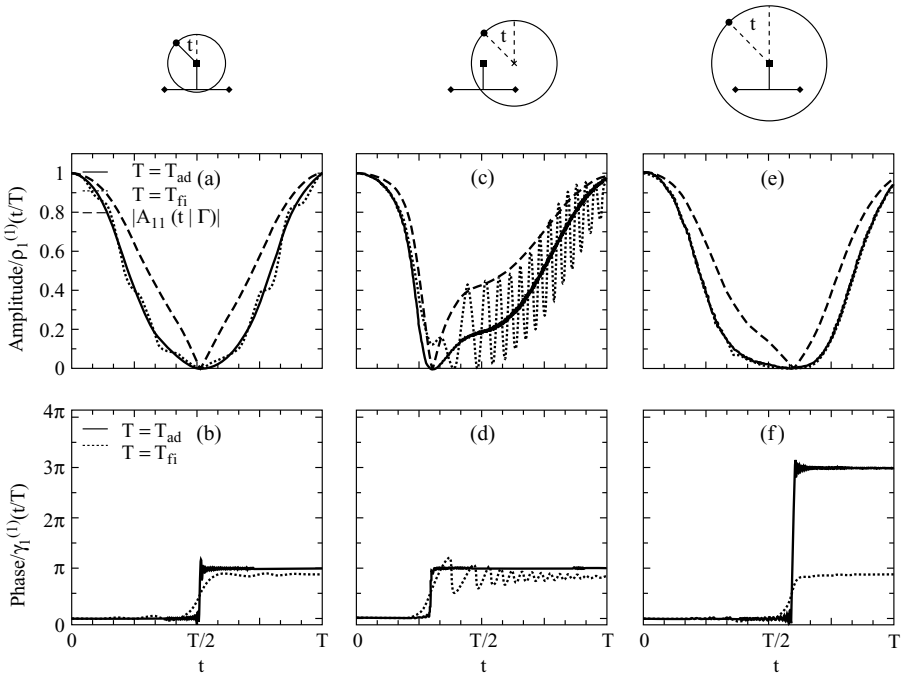


**Figure 7.1** Results for the ab initio  $\text{H}+\text{H}_2$  system as calculated along three circles surrounding the  $(1,2)$  *cis* and the  $(2,3)$  *cis* (labeled  $\blacksquare$  and  $\blacklozenge$ , respectively). All calculations are done once for  $T = T_{\text{fi}} = 10^3$  a.u. and once for  $T = T_{\text{ad}} = 2 \times 10^4$  a.u. The values of  $|A_{11}(\varphi(t)|\Gamma)|$  [presented in panels (a), (c), and (e)] are obtained from the (time-independent) ab initio treatment [see Eq. (7.27a)]. The  $\rho_1^{(1)}(t|T)$  functions, presented in the same panels, are the amplitudes of the components related to the *first* state (as obtained from solving the semiclassical time-dependent Schrödinger equation). Panels (b), (d), and (f) present the corresponding POPPs,  $\gamma_1^{(1)}(t|T)$ .

(see also Section 4.3.2.1. Our numerical study is related to a situation where two of the hydrogen atoms are at a (fixed) distance  $R_{\text{HH}} = 0.74$  Å and the third is free to move on a plane.

We discuss results (shown in Figs. 7.1–7.3) as calculated along three circular contours (formed by the free hydrogen): two of them, centered at the  $D_{3h}$  point, with the radii  $q = 0.2$  and  $0.4$  Å and a third centered at a sideward point between the  $D_{3h}$  point and one of the  $C_{2v}$  points. It is observed that the first circle for  $q = 0.2$  Å [in panels (a) and (b)] surrounds only the  $D_{3h}$  *cis*, the second circle for  $q = 0.4$  Å [in panels (e) and (f)] surrounds the  $D_{3h}$  *cis*, and two  $C_{2v}$  *cis* and the third circle for  $q = 0.3$  Å [in panels (c) and (d)] surrounds the  $D_{3h}$  *cis* and one of the two  $C_{2v}$  *cis*. Figure 7.1 (as well as in Figs. 7.2 and 7.3) schematically present the positions of the various *cis* and the corresponding circular contours.

For each such circle (in Figs. 7.1–7.3) the only variable is  $t$ , defined in the range  $0 \leq t \leq T$ . To calculate the relevant amplitude  $\rho_k^{(k)}(t|T)$  and the POPP  $\gamma_k^{(k)}(t|T)$ ;  $k = 1, 2, 3$ , we first solve Eq. (7.9) to obtain  $\zeta_j^{(k)}(t|T)$ ;  $j = 1, 2, 3$ , for an initial state

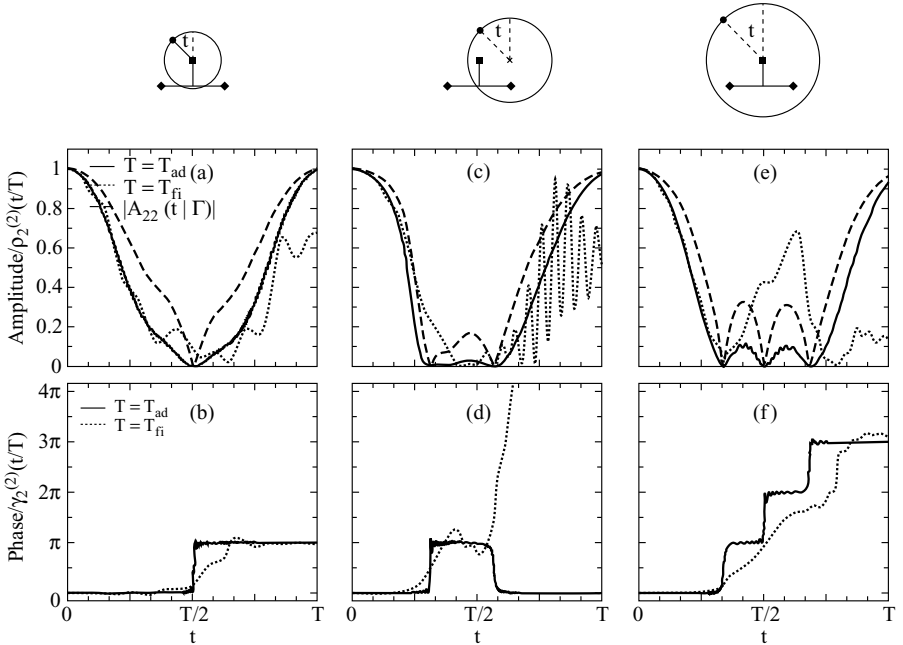


**Figure 7.2** The same as in Figure 7.1, but for the *second* state of the H + H<sub>2</sub> system, namely, the principal amplitudes related to the *second* state,  $\rho_2^{(2)}(t|T)$ , and the corresponding POPPs,  $\gamma_2^{(2)}(t|T)$ .

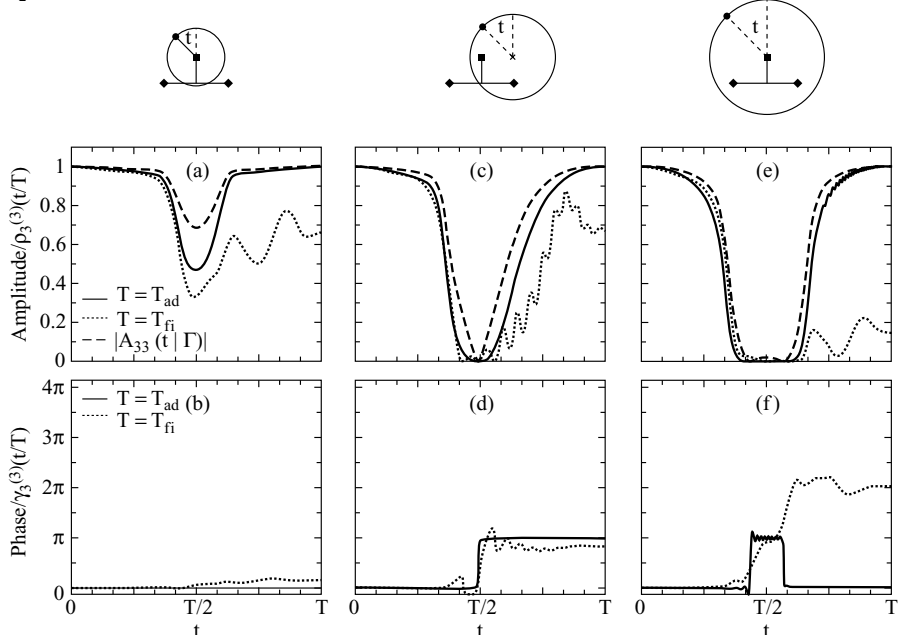


**Figure 7.3** The same as in Figure 7.1 but for the *third* state of the H + H<sub>2</sub> system, namely, the principal amplitudes related to the *third* state,  $\rho_3^{(3)}(t|T)$ , and the corresponding POPPs,  $\gamma_3^{(3)}(t|T)$ .

$k$  and then employ Eqs. (7.28) to extract the results presented in Figures 7.1–7.3. In panels (a), (c), and (e) of these figures, we find the amplitudes,  $\rho_k^{(k)}(t|T)$ , as calculated, once by solving Eq. (7.9) for a finite  $T = T_{\text{fi}}$  (i.e., a period too short to yield the adiabatic limit) and once for  $T = T_{\text{ad}}$  (a period closer to the adiabatic limit). Also shown are the diagonal matrix elements  $\mathbf{A}_{kk}(\varphi|\Gamma)$  [for  $\varphi = (t/T)2\pi$ ] [see Eq. (7.27a)], which yield the theoretical adiabatic limit (in this particular case the  $\mathbf{A}$  matrix is of dimension  $3 \times 3$ ). The same applies to panels (b), (d), and (f), which contain the POPP  $\gamma_k^{(k)}(t|T)$  [in particular, see Eq. (7.27b)].

Figures 7.1–7.3 present results for the three (different) relevant initial states. This means that Figure 7.1 presents the amplitudes,  $\rho_1^{(1)}(t|T)$ , and the POPPs,  $\gamma_1^{(1)}(t|T)$ , where the *initial* state is the lowest state (state 1); Figure 7.2 gives the amplitudes and the OPPPs,  $\rho_2^{(2)}(t|T)$ , and  $\gamma_2^{(2)}(t|T)$  for the case where the *initial* state is the intermediate state (state 2), and in Figure 7.3 shows the amplitudes and the POPPs  $\rho_3^{(3)}(t|T)$ , and  $\gamma_3^{(3)}(t|T)$  for the case where the initial state is the higher state (state 3).

The two main issues to be discussed are as follows:

1. The curves for the principal amplitudes  $\rho_k^{(k)}(t|\Gamma)$ ;  $k = 1, 2, 3$  as calculated for the adiabatic case (viz.,  $T = T_{\text{ad}} = 2 \times 10^4$  a.u.) overlap to some extent with the curves presenting the corresponding values of  $|\mathbf{A}_{kk}(t|\Gamma)|$ . This is far from be the case when  $T = T_{\text{fi}} = 10^3$  a.u.
2. The POPPs as calculated for the case with larger  $T$  values become Heaviside functions along the whole  $t$  axis.

Whereas the figures for the amplitudes speak for themselves, we encounter some interesting features for the POPPs that should be discussed to some extent. The shapes of the Heaviside functions vary, not only from one contour to the, other, but also from one initial state to the other. We find the dependence on the initial state more interesting because this dependence was, to a certain extent, not expected. So let us briefly discuss each column separately:

1. Comparing the three adiabatic POPPs related to panels (a) and (b) in Figures 7.1–7.3, we note that the first two POPPs for  $k = 1, 2$  (in Figs. 7.1 and 7.2) are similar and are characteristic for a case of a single  $ci$  but the third POPP (in Fig. 7.3) is entirely different and is typical for a situation where the contour does not surround any  $ci$ . Indeed, the contours for  $k = 1, 2$  surround the (1,2)  $ci$  related to *their* initial state (whether it is state 1 or state 2). However, this contour does not surround any  $ci$  related to state 3, and therefore this POPP does not show any effect due to a  $ci$ .

2. The POPPs in panels (e) and (f) of Figures 7.1–7.3 are somewhat similar to those in panels (a) and (b). Again, the contour surrounds one single (1,2)  $ci$ , and therefore the Berry phase should be  $(2n + 1)\pi$  except that  $n \neq 0$  and is equal to 1 probably because of the strong interaction between the (1,2) and the (2,3) NACTs, which is known to exist.<sup>21,22</sup> As for the third POPP (in Fig. 7.3), here this POPP, in contrast to the corresponding POPP in panels (a) and (b), is produced along a contour that surrounds two (2,3)  $cis$ , known to be of different signs, and therefore the resultant Berry phase is zero.

3. A new situation is encountered for the POPP presented in panels (c) and (d). Here the contour surrounds one (1,2) and one (2,3) *cis*. Therefore the Berry phases related to states 1 and 3 are equal to  $\pi$  but the phase of the intermediate function is turned twice (once up and once down) so that the resultant Berry phase is zero.

Details about similar findings as revealed within the time-independent framework can be found Sections 4.3.1.1 and 4.3.2.1.

## 7.2 PHASE-MODULUS RELATIONS FOR AN EXTERNAL CYCLIC TIME-DEPENDENT FIELD

In this section we discuss an interesting observation made by Englman et al.<sup>1–5</sup> that instead of deriving the OPP employing Eq. (7.28a), one may apply, for this purpose, reciprocal relations between phase and amplitude moduli, characteristic for a molecular system exposed to an external, periodic, time-dependent field. In the next section we derive these equations, known also as *dispersion relations* or *Kramers-Kronig dispersion equations*,<sup>6</sup> and then apply them, in Section 7.2.2, for a two-state model derived from the Mathieu equation (see Section 5.6.1)

### 7.2.1 Derivation of Reciprocal Relations

The starting point for deriving the reciprocal relation is the Cauchy integral formula<sup>7</sup>

$$w(z) = \frac{1}{2\pi i} \oint_{\Gamma} \frac{w(z')}{z' - z} dz' \quad (7.29)$$

where  $w(z)$  is an *analytic* function in a region formed by a closed contour  $\Gamma$  in the complex plane. In what follows  $\Gamma$  is assumed to be the real axis  $t$  (i.e.,  $-\infty \leq t \leq +\infty$ ), traversed in the reverse direction and an infinite semicircle in the lower half of the complex plane. Consequently,  $w(z)$  is assumed to be an *analytic* function in the lower half-plane. In general the variables  $z$  and  $z'$ , in Eq. (7.29), are identified as complex variables. However, in what follows we limit our discussion to  $z$  points located along the real axis only and consequently  $z$  becomes  $t$ . With these two additional requirements Eq. (7.29) takes the form<sup>2</sup>

$$w(t) = -\frac{1}{\pi i} P \int_{-\infty}^{\infty} \frac{w(t')}{t' - t} dt' + \frac{1}{\pi i} \oint_{SC} \frac{w(z')}{z' - t} dz' \quad (7.30)$$

where  $P$  stands for the *principal* value of the integral and the subscript “SC”, in the second term, stands for *semicircle*. Next we replace the variable  $z'$ , which is defined along the semicircle by an angular variable,  $\theta$ , namely

$$z' = \lambda \exp(i\theta); \Rightarrow \quad dz' = i\lambda \exp(i\theta) d\theta \quad (7.31)$$

where  $\lambda$  is the radius of the semicircle, and we recall that  $\lambda \rightarrow \infty$ . In what follows we consider cases for which  $w(z)$  is essentially zero along the semicircle except, eventually, on the real axis itself, namely

$$\lim_{|z| \rightarrow \infty} w(z) = 0 \quad (7.32)$$

so that  $w(t)$  in Eq. (7.30) becomes

$$w(t) = -\frac{1}{\pi i} P \int_{-\infty}^{\infty} \frac{w(t')}{t' - t} dt' \quad (7.33)$$

To continue, we recall that  $w(z)$  is a complex function, and therefore, although  $t$  is a real variable, the function  $w(t)$  remains complex:

$$w(t) = u(t) + i v(t) \quad (7.34)$$

Substituting Eq. (7.34) in Eq. (7.33) and equating the real and the imaginary components leads to the following two equations:

$$u(t) = -\frac{1}{\pi} P \int_{-\infty}^{\infty} \frac{v(t')}{t' - t} dt' \quad \text{and} \quad v(t) = \frac{1}{\pi} P \int_{-\infty}^{\infty} \frac{u(t')}{t' - t} dt' \quad (7.34)$$

These are the (previously mentioned) Kramers–Kronig relations, and they are applied to form a relation between the topological phase of a wavefunction and its amplitude-modulus. To be more specific, we refer to Eq. (7.25) and, for convenience, rewrite it, deleting all indices and ignoring the fast oscillating (dynamic) phase, namely

$$\zeta(t) = \rho(t) \exp(i\gamma(t)) \quad (7.35)$$

where both  $\rho(t)$  and  $\gamma(t)$  are real functions. Defining  $w(z)$  as

$$w(z) = \ell n(\zeta(z)) = \ell n(\rho(z)) + i\gamma(z) \quad (7.36)$$

we assume that  $\ell n(\rho(z))$  and  $\gamma(z)$  fulfill the necessary conditions to obey the Kramers–Kronig equations. This implies (1) that  $\rho(z)$  is not only an analytic function throughout the lower complex half-plane but is also free of zeros in that region (however, it can have simple zeros along the real axis<sup>5,8,9</sup>) and (2) that  $\rho(z)$  becomes, along the corresponding infinite semicircle, a constant [in fact, the constant has to be equal to 1 – so that  $\ell n(\rho(z)) = 0$ —but if it is  $\neq 1$ , the analysis is applied to  $w(z)$  divided by this constant].

Identifying  $\ell n(\rho(t))$  with  $u(t)$  and  $\gamma(t)$ , with  $v(t)$ , we obtain the following relations for Eqs. (7.34):

$$\ell n(\rho(t)) = -\frac{1}{\pi} P \int_{-\infty}^{\infty} \frac{\gamma(t')}{t' - t} dt' \quad (7.37)$$

$$\gamma(t) = \frac{1}{\pi} P \int_{-\infty}^{\infty} \frac{\ell n(\rho(t'))}{t' - t} dt' \quad (7.38)$$

In case  $\rho(t)$  is an even function, the equation for  $\gamma(t)$  can be written as

$$\gamma(t) = \frac{2t}{\pi} P \int_0^{\infty} \frac{\ell n(\rho(t'))}{t'^2 - t^2} dt' \quad (7.39)$$

and if  $\rho(t)$  is a periodic function, then Eq. (7.39) can be written as<sup>2</sup>

$$\gamma(t) = \frac{2t}{\pi} P \int_0^T \ell n(\rho(t')) \sum_{n=0}^{\infty} \frac{1}{(t' + nT)^2 - t^2} dt' \quad (7.40)$$

where  $T$  is the relevant period.

It is important to mention that the application of the reciprocal relation demands the fulfillment of a few more conditions. These were discussed extensively elsewhere<sup>2–5</sup> and will not be considered here.

## 7.2.2 Mathieu Equation

### 7.2.2.1 Time-Dependent Schrödinger Equations

In order to gain more insight, we consider the Hamiltonian<sup>1,10–12</sup>

$$\mathbf{H} = -\frac{1}{2} E_{\text{el}} \frac{\partial^2}{\partial \theta^2} - G_1(q, \varphi) \cos(2\theta) + G_2(q, \varphi) \sin(2\theta) \quad (7.41)$$

which is recognized as being related to the Mathieu equation (see Section 5.6.1). Here  $\theta$  is an electronic coordinate and  $(q, \varphi)$  are nuclear polar coordinates. As in the previous case,  $\varphi$  is assumed to change linearly with time; thus  $\varphi = \omega t$ , where  $\omega = 2\pi/T$  and  $T$  is the periodicity.

The time-dependent equation to be considered is

$$i\hbar \frac{\partial \Psi}{\partial t} = \mathbf{H}\Psi \quad (7.42)$$

and we solve it within the first-order approximation in  $G/E_{\text{el}}$ , thus yielding the ground-state doublet. For this situation  $\Psi$  is expanded as<sup>1,13</sup>

$$\Psi = \chi_1(t) \cos \theta + \chi_2(t) \sin \theta \quad (7.43)$$

and we seek an *analytic* solution for the initial conditions:  $\chi_1(t = 0) = 1$  and  $\chi_2(t = 0) = 0$ . To derive this solution, the coefficients  $\chi_1(t)$  and  $\chi_2(t)$  are replaced by  $\psi_+(t)$  and  $\psi_-(t)$ , defined as

$$\psi_{\pm}(t) = \frac{1}{2} \exp \left( i\hbar \frac{E_{\text{el}}}{2} t \right) (\chi_1(t) \pm \chi_2(t)) \quad (7.44)$$

and we get the corresponding equations for  $\psi_{\pm}(t)$

$$i\hbar \dot{\psi}_+ = -\frac{1}{2} \tilde{G} \psi_- \quad \text{and} \quad i\hbar \dot{\psi}_- = -\frac{1}{2} \tilde{G}^* \psi_+ \quad (7.45)$$

where  $\tilde{G}$  is defined as  $\tilde{G} = G_1 + iG_2$  ( $\tilde{G}^*$  is its complex conjugate) and the dot represents the time derivative.

Differentiating the two equations in Eq. (7.45) leads to decoupling of the two equations for  $\psi_{\pm}(t)$ . The equation for  $\psi_+(t)$  is<sup>2</sup>

$$\hbar^2 \frac{d^2 \psi_+}{dt^2} - \hbar^2 \frac{d}{dt} (\ln(\tilde{G})) \frac{d \psi_+}{dt} + \frac{1}{4} |\tilde{G}|^2 \psi_+ = 0 \quad (7.46)$$

and a similar equation can be formed for  $\psi_-(t)$  where  $\tilde{G}^*$  replaces  $\tilde{G}$ . Next, assuming that  $|\tilde{G}|$  is a constant,  $G$ , and presenting  $\tilde{G} = G \exp(i\Phi)$ , the two equations for  $\psi_{\pm}(t)$  become

$$\psi_{\pm} \mp i\dot{\Phi} \dot{\psi}_{\pm} + \frac{1}{4} G^2 \psi_{\pm} = 0 \quad (7.47)$$

The aim of this treatment is to obtain the phase,  $\gamma(t)$ , which along the terminology introduced in Section 7.1.3.2, text under heading “Open-Path Phase and *Principal Open-Path Phase*,” is recognized as POPP for the lower state. Consequently  $\gamma(t)$  is expected to be related to the phase  $\chi_1(t)$ ; however, this phase factor contains also the dynamical phase  $(G/2)t$ , and therefore, to eliminate this rapidly oscillating phase, we consider the smooth function  $\hat{\chi}_1(t)$  defined as

$$\hat{\chi}_1(t) = \chi_1(t) \exp \left( i \frac{1}{2} G t \right) = \rho(t) \exp(i\gamma(t)) \quad (7.48)$$

The function  $\hat{\chi}_1(t)$  is governed only by the POPP,  $\gamma(t)$ .

As it turns out, Eq. (7.47) can be solved analytically employing trigonometric functions. Thus

$$\begin{aligned} \hat{\chi}_1(t) &= \exp \left( i \frac{1}{2} G t \right) \\ &\times \left[ \cos(kt) \cos \left( \frac{1}{2} \omega t \right) + \frac{\omega}{2k} \sin(kt) \sin \left( \frac{1}{2} \omega t \right) - i \frac{G}{2k} \sin(kt) \cos \left( \frac{1}{2} \omega t \right) \right] \end{aligned} \quad (7.49)$$

where

$$k = \frac{1}{2}\sqrt{G^2 + \omega^2} \quad (7.50)$$

Considering the expression in Eq. (7.49), it is clear that it is governed by two periodicities: one,  $\omega$ , is a periodicity due to the external field and the other,  $k$ , is a periodicity due to the electronic coupling term,  $G$ .

### 7.2.2.2 Numerical Study of Topological Phase

As an example, we calculate  $\ell n(\rho(t))$  and  $\gamma(t)$  for the *nonadiabatic*, cyclic case ( $k = \omega$ ,  $G = \omega\sqrt{3}$ ). The calculations are done in one of two ways: (1) deriving the values for  $\ell n(\rho(t))$  and  $\gamma(t)$  from Eqs. (7.48) and (7.49) or (2) using the reciprocal relations, as given in Eqs. (7.37) and (7.38) where  $\gamma(t)$  serves as the input to calculate  $\ell n(\rho(t))$  and, in the same way  $\ell n(\rho(t))$  serves as an input to calculate  $\gamma(t)$ . The results are presented in Figure 7.4, where we note that the fit between the two types of calculation is very encouraging.

Whereas this example applies for a nonadiabatic case, in what follows we briefly refer to the (near-) adiabatic case but concentrate on the POPP only. The calculations were done for different values of  $\omega (= 2\pi/T)$  and the coupling intensity  $G$ . The results for three different cases are presented in Figure 7.5. Again, as in the nonadiabatic case, the fit between the two types of calculation is satisfactory. However, in contrast to the previous case, this time we encounter the discontinuous jump, typical for the adiabatic case.<sup>1–4,14</sup> Such discontinuous jumps were discussed in Section 7.1.4, but here we analyze them again in a somewhat different way.

As a final subject in this section, we analyze (again) the adiabatic case, namely, when  $T \rightarrow \infty$ . The most characteristic feature for the adiabatic case is the fact that  $\gamma(t)$  is constant along the whole cycle except for sporadic discontinuous jumps of size of  $n\pi$ , where  $n$  is an integer. For instance, employing Eq. (7.49), we derive  $\dot{\gamma}(t)$

$$\frac{d\gamma}{dt} = -\frac{G}{8} \frac{\left(\frac{\omega}{k}\right)^2 \sin^2(kt)(1 - \cos(\omega t)) + \frac{\omega}{k} \sin(2kt) \sin(\omega t)}{\cos^2(\frac{1}{2}\omega t) + \frac{\omega}{4k} \sin(2kt) \sin(\omega t) - \left(\frac{\omega}{2k}\right)^2 \sin^2(kt) \cos(\omega t)} \quad (7.51)$$

and it can be shown that  $\dot{\gamma}(t) \rightarrow 0$  along (almost the entire) interval  $0 \leq t \leq T$  when  $T \rightarrow \infty$ . The only exception takes place at the close vicinity of  $t \sim T/2$ . In other words, we have for  $\dot{\gamma}(t)$  the presentation:

$$\frac{d\gamma}{dt} = \begin{cases} 0; & \text{when } t < T/2 \\ G/2; & \text{when } t \sim T/2 \\ 0; & \text{when } t > T/2 \end{cases} \quad (7.52)$$

which implies that  $\gamma(t)$  is a constant ( $= 0$ ) along the interval  $0 \leq t < T/2$  and then becomes a constant again (but not necessarily zero) for  $t > T/2$ .

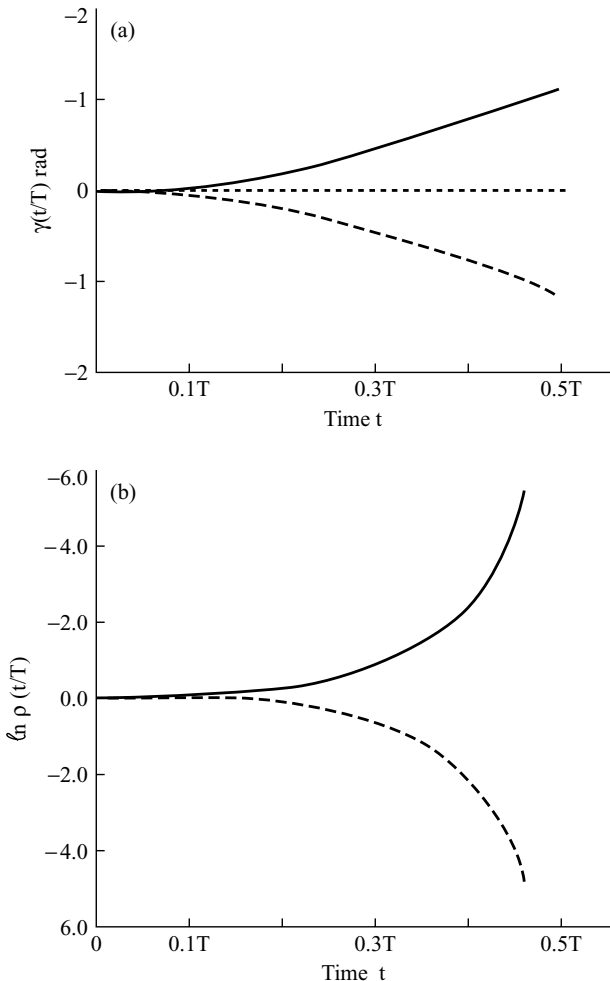


**Figure 7.4** Test of the reciprocal relations: Comparing inputs and outputs of Eqs. (7.37a) and (7.37b) for  $\hat{\chi}_1(t)$  in (7.49). The calculations were done for the *nonadiabatic*, cyclic case ( $k = \omega$ ,  $G = \omega\sqrt{3}$ ). (a) The POPP,  $\gamma(t)$ , as calculated along the time interval  $0 \leq t \leq T/2$ . The solid curve describes  $\gamma(t)$  as obtained from the  $\arg\{\hat{\chi}_1(t)\}$ , namely, extracting it from Eq. (7.49), and the, broken curve yields  $\gamma(t)$  as obtained from the numerical integration of Eq. (7.38), with  $\rho(t)$  values obtained from Eq. (7.49). (b) The  $\ln(\rho(t))$ —the  $\ln$  of the amplitude modulus—as calculated employing Eq. (7.49) (solid lines) and Eq. (7.37), where  $\gamma(t)$  was obtained from Eq. (7.49) (broken lines). The phase axis and the axis for the  $\ln$  of the amplitude modulus both have the same sign but are presented upward and downward in order to distinguish between the two types of results (which are, in fact, identical).

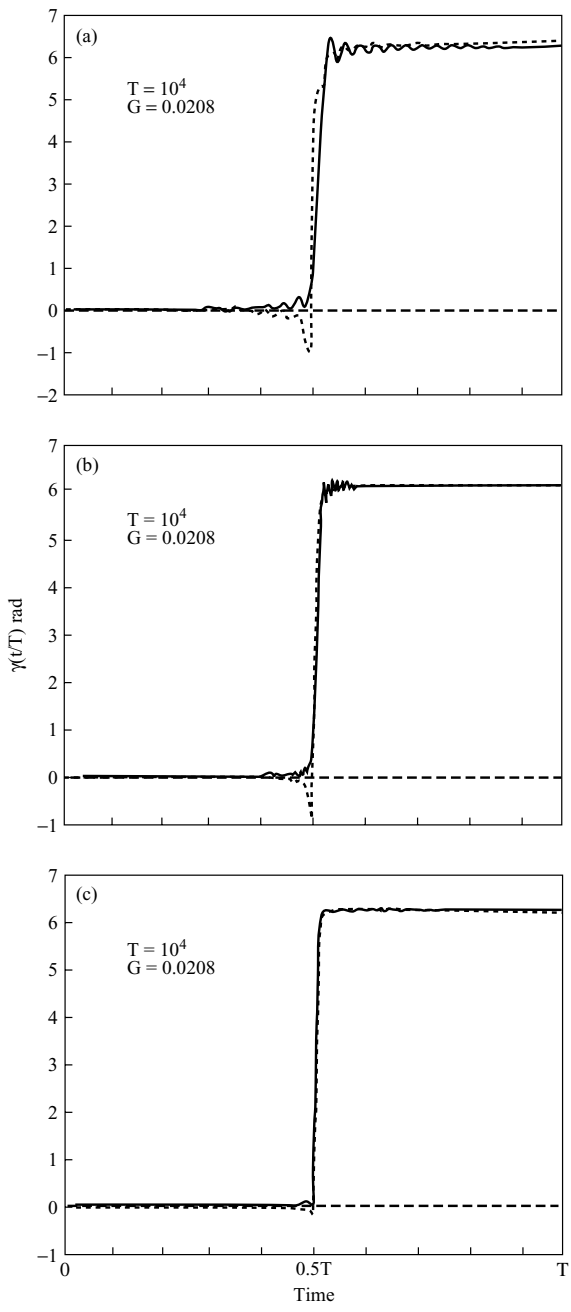


**Figure 7.5** The time-dependent POPP,  $\gamma(t)$ , as a function of time, calculated for the near-adiabatic case. The calculations were done for different values of the external field frequency  $\omega (= 2\pi/T)$  and the coupling intensity  $G$ . Two curves are shown in each panel; one, drawn as a solid line, is the curve calculated employing Eq. (7.49) and the other, drawn as a dashed line, obtained as in Figure 7.4, from numerical integration of Eq. (7.38). (a)  $T = 10^4$ ,  $G = 0.208$ ; (b)  $T = 10^4$ ,  $G = 0.0659$ ; (c)  $T = 10^5$ ,  $G = 0.0208$ .

This discontinuous step can be further understood by employing the Eq. (7.48) and writing the POPP in the form

$$\gamma(t) = \Im\{\ell\ln(\hat{\chi}_1(t))\} \quad (7.53)$$

where  $\Im$  stands for the imaginary part. Considering Eq. (7.49) for the case where  $T \rightarrow \infty$ , it can be seen that

$$\gamma(t) = \Im\left\{\ell\ln\left[\cos\left(\frac{1}{2}\omega t\right) + O(\omega)\right]\right\} \quad (7.54)$$

With this expression, the following is noted: (1) Since for  $t \leq (T/2)$  we have  $\cos\frac{1}{2}\omega t > 0$ , this implies that along the interval  $0 \leq t \leq (T/2)$ , the phase  $\gamma(t) \cong 0$ ; and (2) since for  $t \geq (T/2)$  we have  $\cos\frac{1}{2}\omega t < 0$ , this implies that along the interval  $(T/2) \leq t \leq T$ , the phase  $\gamma(t) \cong \pi$ .

Similar arguments were applied to explain the discontinuous steps encountered in the three-state study for the  $\{\text{H}_2, \text{H}\}$  system (see Section 7.1.4)

As a byproduct, we also reveal that the geometric (Berry) phase is, for the present model,  $\pi$  (see Fig. 7.5).

### 7.2.3 Short Summary

The existence of the reciprocity relations for the phase–amplitude moduli functions is interesting as it is, but it seems to carry with it an important physical message; specifically, the part of the phase that is given by the second reciprocal relation [Eq. (7.38)], is a measurable quantity (and therefore is also gauge-invariant). Thus one may measure the instant population of a given state as produced by a cyclic external field and deduce for it, employing Eq. (7.38), not only the Berry phase but also the complete POPP.

## PROBLEM

- 7.1** Starting an excursion at  $t = 0$  while the system is in its  $k$ th eigenstate, prove that in the adiabatic case the system remains in the same  $k$ th eigenstate throughout its motion along a given contour.

*Solution* To prove this statement, we consider Eq. (7.17) and assume that  $\mathbf{A}(t = 0)$  is the unit matrix and that  $\tilde{\zeta}(t = 0)$  is a column vector with the elements  $\{\tilde{\zeta}_{j1}(t = 0) = \delta_{kj}; j = 1, N\}$ . Next, we define the column vector  $\mathbf{E}^{(k)}(t)$ , which contains one single nonzero element at the  $k$ th position:

$$\mathbf{E}_{j1}^{(k)}(t) = \delta_{kj} \exp\left(-\frac{i}{\hbar} \int_0^t \mathbf{u}_k(t) dt\right); \quad j = \{1, N\} \quad (7.55)$$

With these definitions, Eq. (7.17) takes the form

$$\lim_{T \rightarrow \infty} |\xi^{(k)}(\mathbf{s}_e|t)\rangle = |\zeta^*(\mathbf{s}_e|t=0)\rangle \mathbf{A}^\dagger(t) \mathbf{E}^{(k)}(t) \quad (7.56)$$

and our aim is to show that  $|\xi^{(k)}(\mathbf{s}_e|t)\rangle$  is an eigenfunction of  $\mathbf{H}_e(\mathbf{s}(t))$  and the corresponding eigenvalue is  $\mathbf{u}_k(\mathbf{s}(t))$ , and thus to prove the following:

$$\langle \xi^{(k)}(\mathbf{s}_e|s(t)) | \mathbf{H}_e | \xi^{(k)}(\mathbf{s}_e|s(t)) \rangle = u_k(s(t)) \quad (7.57)$$

To show this, we consider the following matrix element:

$$\begin{aligned} & \lim_{T \rightarrow \infty} \langle \xi^{(k)}(\mathbf{s}_e|\mathbf{s}) | \mathbf{H}_e | \xi^{(k)}(\mathbf{s}_e|\mathbf{s}) \rangle \\ &= \mathbf{E}^{(k)\dagger}(t) [\mathbf{A}(t) \langle \zeta(\mathbf{s}_e|t=0) | \mathbf{H}_e | \zeta^*(\mathbf{s}_e|t=0) \rangle \mathbf{A}^\dagger(t)] \mathbf{E}^{(k)}(t) \end{aligned} \quad (7.58)$$

The expression within the angular bracket notation on the r.h.s. produces the diabatic matrix  $\mathbf{V}(\mathbf{s})$  [mentioned in Eq. (7.9) and given in Eq. (7.10)], and the product inside the square brackets on the r.h.s. produces the diagonal adiabatic potential matrix  $\mathbf{u}(\mathbf{s})$  [see Eq. (7.10)]. The remaining two products, from left and right [where  $\mathbf{E}^{(k)}(t)$  is a column vector—see Eq. (7.55)] finally yield the requested  $k$ th eigenvalue,  $\mathbf{u}_k(\mathbf{s}(t))$ . Thus, the validity of Eq. (7.57) is proved.

[In this problem we have shown that in the adiabatic limit, the solution of the time-*dependent* Schrödinger equation produces, at the end of a *closed* contour, the diagonal elements of the topological  $\mathbf{D}$  matrix as introduced within the time-*independent* formulation (see Section 2.1.3.1.). These diagonal matrix elements are identified as Berry's phase factors produced by a Hilbert subspace of  $N$  states. We also showed that in the adiabatic limit the system moves along the contour (not necessarily a closed contour) while being in its eigenstate.]

## REFERENCES

### Section 7.1

1. M. V. Berry, *Proc. Roy. Soc. Lond. A* **392**, 45 (1984).
2. G. Herzberg and H. C. Longuet-Higgins, *Disc. Faraday Soc.* **35**, 77 (1963).
3. H. A. Jahn and E. Teller, *Proc. Roy. Soc. Lond. A* **161**, 220 (1937).
4. H. C. Longuet-Higgins, *Proc. Roy. Soc. Lond. A* **344**, 147 (1975).
5. M. S. Child and H. C. Longuet-Higgins, *Phil. Trans. Roy. Soc. Lond. A* **254**, 259 (1961).
6. M. S. Child, *Adv. Chem. Phys.* **124**, 1 (2002).
7. H. Koizumi and I. B. Bersuker, *Phys. Rev. Lett.* **83**, 3009 (1999).
8. F. S. Ham, *Phys. Rev. Lett.* **78**, 725 (1987).
9. J. Samuel and R. Bhandari, *Phys. Rev. Lett.* **60**, 2339 (1988).
10. R. Bhandari, *Phys. Lett. A* **157**, 221 (1991).

11. J. Samuel and A. Dhar, *Phys. Rev. Lett.* **87**, 260401-1 (2001).
12. D. Suter, K. T. Mueller, and A. Pines, *Phys. Rev. Lett.* **60**, 1218 (1988).
13. S. Fuentes-Guridi, S. Bose, and V. Vedral, *Phys. Rev. Lett.* **85**, 5018 (2000).
14. T. Vértesi, Á. Vibók, G. J. Halász, and M. Baer, *J. Phys. B* **120**, 2565 (2004).
15. J. Anandan and L. Stodolsky, *Phys. Rev. D* **35**, 2597 (1987).
16. Y. Aharonov and J. Anandan, *Phys. Rev. Lett.* **58**, 1593 (1987).
17. Y. C. Ge and M. S. Child, *Phys. Rev. Lett.* **78**, 2507 (1997).
18. M. Baer, A. Yahalom, and R. Englman, *J. Chem. Phys.* **109**, 6550 (1998).
19. R. Englman, A. Yahalom, and M. Baer, *Phys. Lett. A* **251**, 223 (1999).
20. R. Englman, A. Yahalom, and M. Baer, *Eur. Phys. J. D* **8**, 1 (2000).
21. M. Baer, T. Vértesi, G. H. Halász, Á. Vibók and S. Suhai, *Faraday Disc.* **127**, 337 (2004).
22. G. J. Halász, Á. Vibók, A. M. Mebel, and M. Baer, *J. Chem. Phys.* **118**, 3052 (2003).
23. G. J. Halász, Á. Vibók, A. M. Mebel, and M. Baer, *Chem. Phys. Lett.* **358**, 163 (2002).
24. S. Han and D. R. Yarkony, *J. Chem. Phys.* **119**, 5058 (2003).

## Section 7.2

1. M. Baer, A. Yahalom, and R. Englman, *J. Chem. Phys.* **109**, 6550 (1998).
2. R. Englman, A. Yahalom and M. Baer, *The European Phys. J. D.* **8**, 1 (2000).
3. R. Englman, A. Yahalom, and M. Baer, *Phys. Lett. A* **251**, 223 (1999).
4. R. Englman and A. Yahalom, *Phys. Rev. A* **60**, 1890 (1999).
5. R. Englman and A. Yahalom, *Adv. Chem. Phys.* **124**, 197 (2002).
6. M. L. Goldberger and K. M. Watson, *Collision Theory*, Wiley, New York, 1967, p. 560.
7. R. V. Churchill, *Complex Variables and Applications*, McGraw-Hill, New York, 1960, Chapter 11.
8. J. H. Shapiro and R. S. Shepard, *Phys. Rev. A* **43**, 3795 (1991).
9. E. C. Titchmarsh, *The Theory of Functions* Clarendon Press, Oxford, 1932, Sections 7.8 and 8.1.
10. H. C. Longuet-Higgins, U. Opik, M. H. L. Pryce, and R. A. Sack, *Proc. Roy. Soc. Lond. A* **244**, 1 (1958).
11. M. Baer and R. Englman, *Molec. Phys.* **75**, 293 (1992).
12. T. Vértesi, Á. Vibók, G. J. Halász, A. Yahalom, R. Englman, and M. Baer, *J. Phys. Chem. A* **107**, 7189 (2003).
13. D. J. Moore and G. E. Stedman, *J. Phys. A Math. Gen.* **23**, 2049 (1990).
14. T. Vértesi, Á. Vibók, G. J. Halász, and M. Baer, *J. Phys. B* **120**, 2565 (2004).

# CHAPTER 8

---

## EXTENDED BORN–OPPENHEIMER APPROXIMATIONS

---

### 8.1 INTRODUCTORY COMMENTS

The Born–Oppenheimer approximation is a direct outcome of the Born–Oppenheimer treatment of molecular systems<sup>1–3</sup> (see Chapter 2) and follows from the fact that the NACTs (responsible for the coupling between the various states) contain a mass factor that in usual situations keeps them small enough to be of minor importance.<sup>2–3</sup>

In general, a derivative of an electronic eigenfunction with respect to a *nuclear* coordinate is expected to result in a much smaller value than is the corresponding derivative with respect to an *electronic* coordinate. The reason is that the electronic eigenfunctions that describe the electron density in (relatively) large regions in configuration space with typical distances of a several angstroms do not vary much along distances of a few tenths of angstroms, which are typical dimensions for a nuclear region. This is also how Eq. (1.10) is to be understood. Equation (1.10) is written here, again, in a slightly different form:

$$\langle \zeta_k(\mathbf{s}_e|\mathbf{s}) | (\zeta_k(\mathbf{s}_e|\mathbf{s} + \Delta\mathbf{s}) - \zeta_k(\mathbf{s}_e|\mathbf{s})) \rangle = O(\Delta\mathbf{s}^2) \langle \zeta_k(\mathbf{s}_e|\mathbf{s}) | \zeta_k(\mathbf{s}_e|\mathbf{s}) \rangle \quad (8.1)$$

Next, dividing Eq. (8.1) by  $\Delta\mathbf{s}$  and removing the integration over  $\mathbf{s}_e$  yields the following expression:

$$\frac{|\Delta\zeta_k(\mathbf{s}_e|\mathbf{s})\rangle}{\Delta\mathbf{s}} \sim O(\Delta\mathbf{s}) |\zeta_k(\mathbf{s}_e|\mathbf{s})\rangle \quad (8.2)$$

---

*Beyond Born–Oppenheimer: Conical Intersections and Electronic Nonadiabatic Coupling Terms*  
By Michael Baer. Copyright © 2006 John Wiley & Sons, Inc.

This implies that differentiating an *electronic* wavefunction with respect to a *nuclear* coordinate is expected to be much smaller than the corresponding differentiation with respect to an *electronic* coordinate (which is of the same order of magnitude as the function itself). Because of Eq. (8.2), the corresponding NACTs are also expected to be small. It is known that in order for a NACT to be effective in causing nonadiabatic transitions, its product with the nuclear momentum  $\mathbf{P}$  has to be of the order of the energy gap  $\Delta E$  between two states.<sup>4</sup> In this context we mention the Massey parameter known to be related to the ratio  $\Delta E/(\mathbf{P} \cdot \boldsymbol{\tau})$ , which is expected to be  $\leq 1$ .<sup>4</sup> Due to Eq. (8.2) the Massey condition is not likely to be fulfilled unless the expansion in Eq. (1.10) fails in the vicinity of the pathological (or *ci*-) points mentioned in Section 1.1.1. For all these reasons, the relevance of the Born–Oppenheimer approximation is not considered to be dependent on the energy of the system as long the kinetic energy is not too large (at most a few electronvolts). However, the Born–Oppenheimer approximation is also employed for cases where the NACTs become *very large* (and eventually *infinite* usually close to *ci* points) but assuming that the kinetic energy can be made as low as required (to avoid transition to excited states). The justification for this approximation is that for a sufficiently low energy, the upper *adiabatic* surface is classically forbidden, implying that the component of the total wavefunction related to this (closed) state is negligibly small. As a result, terms that contain the product of this component with the relevant NACT are also small and therefore are expected to have a minor effect on the dynamical process. This assumption, which underlies many of the single-state dynamical calculations, becomes questionable under these conditions.<sup>5–16</sup> The reason is that although the components of the total wavefunction are negligibly small, their products with (infinitely) large NACTs may result in non-negligible values. In that case the Born–Oppenheimer approximation breaks down for any (kinetic) energy, irrespective of how low it is (see Section 1.1).

In fact, the case of infinitely large NACTs is even more complicated. As we have shown in Chapter 5, the singularities associated with NACTs are not *accidental* (viz., of the type  $q^{-n}$  where  $n > 1$ ) but, most likely, are poles (viz.,  $n = 1$ ), and it is well known that poles form nonlocal effects (also known as *topological effects*) that extend to infinity and mathematically cannot be ignored. However, the ordinary Born–Oppenheimer approximation ignores this situation. In Section 8.2 we discuss how to rigorously incorporate the topological effect within the Born–Oppenheimer approximation. Unfortunately the theoretical treatment is limited to a certain type of NACTs and does not apply for a general case (except for two-state systems, for which it is general).

In Section 8.3 we discuss a different type of an approximation, which can be regarded more as a Born–Oppenheimer-type approximation.<sup>17,18</sup> For this purpose we consider a system of  $N$  *diabatic* coupled Schrödinger equations (see Section 2.1.2) and study the possibility of rigorously reducing this number to  $M$  equations ( $N > M$ ). The main idea here is to form a smaller number of diabatic Schrödinger equations with the aim of affecting as little as possible the topological features contained within the original system of equations.

## 8.2 BORN–OPPENHEIMER APPROXIMATION AS APPLIED TO A MULTISTATE MODEL SYSTEM

### 8.2.1 Extended Approximate Born–Oppenheimer Equation

As is well known, the NACM is an antisymmetric matrix and consequently contains nonzero elements at the off-diagonal positions only [see, e.g., Eq. (1.37)]. In order to form an *extended* approximate Born–Oppenheimer equation (that contains as much as possible the relevant topological effects), these terms have first to be shifted to the diagonal positions following an orthogonal transformation before any further steps are taken.

The starting equation is the adiabatic Born–Oppenheimer equation as presented in Eq. (2.12), where  $\tau$  is a model matrix<sup>1–3</sup> of the type presented in Eq. (3.1) and is, for reason of completeness, presented again here:

$$\tau(\mathbf{s}) = \mathbf{g}\lambda(\mathbf{s}) \quad (3.1)$$

Here  $\lambda(\mathbf{s})$  is a *vector* whose components are functions of the coordinates and  $\mathbf{g}$  is a *constant antisymmetric* matrix of dimensions  $M \times M$ . Because of its particular format, it presents the multidegeneracy case as discussed, to some extent, in Section 3.1. The reason for this limited choice is that the unitary matrix that diagonalizes it, is a *constant* matrix  $\mathbf{G}$ . Thus, returning to Eq. (2.12), replacing  $\Psi$  by  $\chi$ , where both are

$$\Psi = \mathbf{G}\chi \quad (8.3)$$

and continuing in the usual way leads to the following equation for  $\chi$ :

$$-\frac{\hbar^2}{2m}(\nabla + \mathbf{t}\lambda(\mathbf{s}))^2\chi + (\mathbf{W} - E)\chi = \mathbf{0} \quad (8.4)$$

Here,  $\mathbf{t}$  is a *diagonal imaginary* matrix that contains the eigenvalues of the  $\mathbf{g}$  matrix and  $\mathbf{W}$  is the corresponding diabatic potential matrix; thus

$$\mathbf{W} = \mathbf{G}^\dagger \mathbf{u} \mathbf{G} \quad (8.5)$$

where  $\mathbf{G}^\dagger$  is the complex conjugate of  $\mathbf{G}$ .

Considering Eq. (8.4), it is seen that the first term in front of the (column) vector  $\chi$  is a diagonal matrix because the expression in parentheses is diagonal according to the preceding definition of  $\mathbf{t}$ . However, the constant transformation matrix  $\mathbf{G}$  produced a nondiagonal potential matrix  $\mathbf{W}$ , and it is the off-diagonal elements of this matrix that couple the  $M$  differential equations. It is important to emphasize that so far the derivation has been rigorous and no approximations have been imposed. Thus, the solution of Eq. (8.4) is the same as the solution of Eqs. (2.12).

Having arrived at Eq. (8.4), we are now in a position to impose the Born–Oppenheimer approximation in case the energy is low enough. As was stated earlier, in such a situation all upper *adiabatic* states are energetically closed so that each of the corresponding *adiabatic* functions  $\psi_j$ ,  $j = \{2, M\}$  is negligibly small. Therefore, in all those regions of configuration space where the lower surface is energetically allowed we expect the fulfillment of the following condition:

$$|\psi_1(\mathbf{s})| \gg |\psi_k(\mathbf{s})|; \quad k = \{2, M\} \quad (8.6)$$

Our next step is to analyze the product  $\mathbf{W}\chi$ , for the  $j$ th equation of Eq. (8.4). Recalling Eqs. (8.3) and (8.5), we have<sup>4</sup>

$$(\mathbf{W}\chi)_j = \{(\mathbf{G}^\dagger \mathbf{u} \mathbf{G})(\mathbf{G}^\dagger \Psi)\}_j = \sum_{k=1}^M \mathbf{G}^\dagger_{jk} u_k \psi_k \quad (8.7)$$

which by adding and subtracting  $u_1(\mathbf{s})\chi_j$  can also be written as

$$(\mathbf{W}\chi)_j = u_1 \chi_j - u_1 \sum_{k=1}^M \mathbf{G}^\dagger_{jk} \psi_k + \sum_{k=1}^M \mathbf{G}^\dagger_{jk} u_k \psi_k$$

or

$$(\mathbf{W}\chi)_j = u_1 \chi_j + \sum_{k=2}^M \mathbf{G}^\dagger_{jk} (u_k - u_1) \psi_k; \quad j = \{1, M\} \quad (8.8)$$

It is noticed from Eq. (8.8) that for each  $j = \{1, M\}$ , the column  $(\mathbf{W}\chi)_j$  contains the product of the function  $\chi_j$  and the lowest *adiabatic* potential surface,  $u_1(\mathbf{s})$ , in addition to a summation of products of (finite) potential terms with the negligibly small  $\psi_k$  values (viz., only those for  $k \geq 2$ ). Substituting Eq. (8.8) in Eq. (8.4) and deleting the summation term in each of the equations yields the following system of equations

$$-\frac{\hbar^2}{2m} (\nabla + i\omega_j \boldsymbol{\lambda}(\mathbf{s}))^2 \chi_j + (u_1 - E) \chi_j = \mathbf{0}; \quad j = \{1, M\} \quad (8.9)$$

where the *imaginary* eigenvalue,  $t_j$ , is replaced by  $i\omega_j$  [and therefore  $\omega_j$  is a real constant (or zero)]. This system of  $M$  equations for the  $M$  functions,  $\chi_j$ ;  $j = \{1, M\}$  is obviously decoupled, or in other words we encounter here  $M$  equations where each one has to be solved separately (independently of the rest). However, it is also seen that all these equations contain the same (adiabatic) potential energy surface  $u_1(\mathbf{s})$  and differ only in the values of  $\omega_j$ .

### 8.2.2 Gauge Invariance Condition for Approximate Born–Oppenheimer Equations

The various (independent) equations presented in Eq. (8.9) do not necessarily yield solutions that are related to each other even if solved for identical boundary conditions. However, the whole approach is meaningless if each equation or even some of them will yield different solutions. In other words, we have to form conditions that guarantee that all these equations yield the *same* solution.

Since the equations may differ only because their imaginary components [i.e.,  $\omega_j \lambda(\mathbf{s})$ ;  $j = \{1, M\}$ ] are not necessarily identical, the question to be posed is: “What are the necessary conditions for having identical solutions even if not all  $\omega_j$  values are the same?” It is well known from gauge theory that these equations are gauge-invariant (i.e., yielding the same solution) if and only if the products  $\omega_j \lambda(\mathbf{s})$  appearing in Eq. (8.9) satisfy the following condition

$$\omega_j \oint_{\Gamma} \mathbf{d}\mathbf{s} \cdot \lambda(\mathbf{s}) = 2\pi n_j; \quad j = \{1, M\} \quad (8.10)$$

where the  $n_j$  numbers form either a series of integers or a series of half-integers. These conditions are similar to those discussed in Sections 3.1.1–3.1.3 [see Eqs. (3.12), (3.22), and (3.34)] and, in particular, in Section 3.1.4 (in which the general case is considered) for the type of  $\tau$  matrices defined in Eq. (3.1). We remind the reader that Eqs. (8.10), for  $\lambda(\mathbf{s})$  and the  $\mathbf{g}$ -matrix elements, have to be fulfilled, and also in order for the topological matrix  $\mathbf{D}$  to be diagonal—which implies having  $\pm 1$  in its diagonal (see Section 2.1.3.1).

We mentioned earlier that the  $n_j$  series have to consist of *either* integers or half-integers. This implies that in case of integers, we may have any number of coupled states; namely,  $M$  can be (any number);  $M = 2, 3, 4, \dots$ , but in case of half-integers,  $M$  is restricted to even numbers only, namely,  $M = 2, 4, \dots$ . Since a NACM that produces even  $n_j$  numbers does not form topological effects, their importance is limited. The only systems of interest are those that produce odd  $n_j$  numbers.

At the beginning we emphasized the fact that the derivation of the extended Born–Oppenheimer approximation applies only to a model system of the type given in Eq. (3.1). This statement is correct as long as  $M > 2$ . However, the case where  $M = 2$  is, in fact, the general case, and therefore Eq. (8.10) is valid for any two-state system. We remind the reader that the two-state case is already discussed in Section 6.2.1.

## 8.3 MULTISTATE BORN–OPPENHEIMER APPROXIMATION: ENERGY CONSIDERATIONS TO REDUCE DIMENSIONS OF DIABATIC POTENTIAL MATRIX

### 8.3.1 Introductory Comments

In Section 2.1.3.2 we showed that diabatization overcomes one major difficulty related to the adiabatic Born–Oppenheimer equations; namely, it eliminates the singular

NACTs but then may create a new difficulty, namely, forming a large system of (coupled) diabatic equations to be solved [see Eq. (2.38)]. As we recall, the size of the system of equations is dictated by the ability of the NACTs to form decoupled blocks within the  $\tau$  matrix [see Eq. (1.37)]. Thus the number of *diabatic* equations (just like the number of *adiabatic* equations) is an inherent feature of the molecular system under consideration and is not related to the method used to carry out the diabatization process.<sup>1</sup> In the present section we discuss an approach that reduces the size of this set of equations, for sufficiently low kinetic energies and, on the basis of a convergence process, is expected to yield the relevant dynamical results.

### 8.3.2 Derivation of Reduced Diabatic Potential Matrix

In this section we adopt the following notation:  $\mathbf{Z}_N^M$  denotes a *rectangular* matrix,  $\mathbf{Z}$ , with  $M$  columns and  $N$  rows. In other words, the upper index designates number of columns and the lower index, the number of rows.<sup>1</sup> With this notation the diabatic Schrödinger equation in Eq. (2.38) takes the form

$$-\frac{\hbar^2}{2m} \nabla^2 \Phi_N^1 + (\mathbf{W}_N^N - E) \Phi_N^1 = 0 \quad (8.11)$$

where  $\Phi_N^1$  is a column vector that contains  $N$  diabatic (nuclear) wavefunctions and  $\mathbf{W}_N^N$  is the diabatic potential matrix [see Eq. (2.39)]:

$$\mathbf{W}_N^N = \mathbf{A}_N^N \mathbf{u}_N^N \mathbf{A}_N^{\dagger N} \quad (8.12)$$

Next, we recall that the connection between the diabatic wavefunction  $\Phi_N^1$  and the adiabatic one  $\Psi_N^1$  is given as follows [see Eq. (2.35)]

$$\Phi_N^1 = \mathbf{A}_N^N \Psi_N^1 \quad (8.13)$$

where, for convenience, we replaced the  $\mathbf{A}$  in Eq. (2.35) by  $\mathbf{A}^\dagger$ . We continue, assuming that for a given energy  $E$  only  $M$  *adiabatic* states are classically allowed (i.e., classically open). This implies that out of the  $N$  nuclear adiabatic wavefunctions ( $\psi_1, \dots, \psi_N$ ), only the  $M$  lowest ones differ from zero for any practical application. For this reason the row vector  $\Psi^T$  takes the form  $\Psi^T \equiv (\psi_1, \dots, \psi_M, 0, \dots, 0)$  and consequently, Eq. (8.13) can also be written in the following form:

$$\Phi_N^1 = \mathbf{A}_N^M \Psi_M^1 \quad (8.14)$$

Based on this observation, the first  $M$  ( $M < N$ ) diabatic nuclear functions  $\Phi^T \equiv (\phi_1, \dots, \phi_M)$ , are given (without approximation) in the form:

$$\Phi_M^1 = \mathbf{A}_M^M \Psi_M^1 \quad (8.14')$$

In what follows we treat only the first  $M$  equation of Eq. (8.11):

$$-\frac{\hbar^2}{2m} \nabla^2 \Phi_M^1 + (\mathbf{W}_M^N - E) \Phi_N^1 = 0 \quad (8.15)$$

where  $\Phi_N^1$ , in the second term, is still unchanged, but next is replaced employing Eq. (8.14). Consequently, Eq. (8.15) becomes

$$-\frac{\hbar^2}{2m} \nabla^2 \Phi_M^1 + (\mathbf{W}_M^N - E) \mathbf{A}_N^M \Psi_M^1 = 0 \quad (8.16)$$

Recalling Eq. (8.14'),  $\Psi_M^1$  is replaced by a different expression, specifically

$$\Psi_M^1 = (\mathbf{A}_M^M)^{-1} \Phi_M^1 = \mathbf{C}_M^M \Phi_M^1 \quad (8.17)$$

and thus Eq. (8.16) takes the form

$$-\frac{\hbar^2}{2m} \nabla^2 \Phi_M^1 + (\mathbf{W}_M^N - E) \mathbf{B}_N^M \Phi_M^1 = 0 \quad (8.18)$$

where

$$\mathbf{B}_N^M = \mathbf{A}_N^M \mathbf{C}_M^M \quad (8.19)$$

Here  $\mathbf{C}_M^M$  is the inverse of the matrix  $\mathbf{A}_M^M$ :

$$\mathbf{A}_M^M \mathbf{C}_M^M = \mathbf{I} \quad (8.20)$$

Returning to Eq. (8.18), this can be further simplified to become

$$-\frac{\hbar^2}{2m} \nabla^2 \Phi_M^1 + (\tilde{\mathbf{W}}_M^M - E) \Phi_M^1 = 0 \quad (8.21)$$

where the elements of  $\tilde{\mathbf{W}}_M^M$  are

$$(\tilde{\mathbf{W}}_M^M)_{kn} = (\mathbf{W}_M^M)_{kn} + \sum_{j=M+1}^N (\mathbf{W}_M^N)_{kj} (\mathbf{B}_N^M)_{jn} \quad (8.22)$$

Here, both  $k$  and  $n$  are restricted by  $M$ . Thus, although only  $M$  equations are treated (instead of  $N$ ), we still employ all the  $N^2$  elements of  $\mathbf{W}$  (recall that  $\mathbf{W}$  is a symmetric matrix).

To continue the derivation, we examine in more detail the potential matrix elements  $(\tilde{\mathbf{W}}_M^M)_{nk}$  given in Eq. (8.22), which from now on is designated as  $\tilde{\mathbf{W}}_{nk}$  (recalling that

$\tilde{\mathbf{W}} \equiv \tilde{\mathbf{W}}_M^M$ ). For this purpose we consider first the ordinary potential matrix element  $\mathbf{W}_{nk}$ , which is given in the form [see Eq. (8.12)]

$$\mathbf{W}_{nk} = \sum_{j=1}^N A_{nj} u_j (\mathbf{A}^\dagger)_{jk} = \sum_{j=1}^N A_{nj} u_j A_{kj}^* \quad (8.23)$$

where the star designates *complex conjugate*. Along the same line we remember that, due to unitarity, we obtain

$$\sum_{j=1}^N A_{jk}^* A_{jn} = \delta_{kn} \quad (8.24)$$

Returning to Eq. (8.22), we consider the second term on the right-hand side:

$$\begin{aligned} \sum_{j=M+1}^N (\mathbf{W}_M^N)_{kj} (\mathbf{B}_N^M)_{jn} &= \sum_{j=M+1}^N \left[ \sum_{s=1}^N (A_{ks} u_{ss} A_{js}^*) \sum_{t=1}^M (A_{jt} C_{tn}) \right] \\ &= \sum_{s=1}^N \left\{ A_{ks} u_{ss} \sum_{t=1}^M \left[ \sum_{j=M+1}^N (A_{js}^* A_{jt}) C_{tn} \right] \right\} \\ &= \sum_{s=1}^N \left\{ A_{ks} u_{ss} \sum_{t=1}^M \left\{ \left[ \delta_{st} - \sum_{j=1}^M (A_{js}^* A_{jt}) \right] C_{tn} \right\} \right\} \end{aligned}$$

which can be farther simplified as follows:

$$\therefore = \sum_{s=1}^M (A_{ks} u_{ss} C_{sn}) - \sum_{s=1}^N \left\{ A_{ks} u_{ss} \sum_{j=1}^M \left[ A_{js}^* \sum_{t=1}^M (A_{jt} C_{tn}) \right] \right\}$$

From Eq. (8.20), the summation (over  $t$ ) yields the Krönecker  $\delta$  function, that is  $\delta_{jn}$ , so the final form of the preceding above expression is as follows:

$$\begin{aligned} \sum_{j=M+1}^N (\mathbf{W}_M^N)_{kj} (\mathbf{B}_N^M)_{jn} &= \sum_{s=1}^M A_{ks} u_{ss} C_{sn} - \sum_{s=1}^N A_{ks} u_{ss} A_{ns}^* \\ &= \sum_{s=1}^M A_{ks} u_{ss} C_{sn} - (\mathbf{W}_M^M)_{kn} \end{aligned} \quad (8.25)$$

Substituting Eq. (8.25) in Eq. (8.22), we obtain for  $\tilde{\mathbf{W}}_{kn}$  the result

$$\tilde{\mathbf{W}}_{kn} = \sum_{s=1}^M A_{ks} u_{ss} C_{sn} \quad (8.26)$$

where all four matrices are of dimensions  $M \times M$ . Equation (8.26) can also be written as a matrix equation

$$\tilde{\mathbf{W}} = \mathbf{A}\mathbf{u}\mathbf{C} = \mathbf{A}\mathbf{u}\mathbf{A}^{-1} \quad (8.27)$$

which is our final outcome.

The result in Eq. (8.27) is, in fact, somewhat surprising because we managed to show that the modified diabatic potential matrix  $\tilde{\mathbf{W}} (\equiv \tilde{\mathbf{W}}_M^M)$  is similar to the ordinary diabatic potential  $\mathbf{W}$  as given in Eq. (8.12) except that  $\mathbf{A} (\equiv \mathbf{A}_M^M)$  is not the full  $N \times N$  ADT matrix but the reduced one of dimension  $M \times M (M < N)$ . Consequently we do not encounter, in Eq. (8.27), the complex conjugate matrix  $(\mathbf{A}_M^M)^\dagger$  but  $\mathbf{A}^{-1}$ —the inverse matrix of  $\mathbf{A}_M^M$ .

Equation (8.27) yields the (diabatic) potential matrix for the modified (reduced) diabatic framework. At the beginning of our analytical derivation we assumed that the Hilbert subspace is made up of  $N$  states, and therefore one expects a diabatic potential matrix to be of dimension  $N \times N$  and the number of equations to be solved as  $N$ . Following the analytical study presented in the previous section, we reduced this number to  $M$ , which can, in principle, be increased again until convergence is attained ( $M \leq N$ ). This convergence procedure is expected to be energy-dependent.

**Summary** Equation (8.27) clearly exhibits the two aspects that affect most electronic nonadiabatic processes, namely, the topology and the energy. The energy aspect enters through the  $\mathbf{u}$  matrix, which contains the adiabatic surfaces, because the energy controls  $M$ , the number of states to be included in the calculation. The topological aspect enters through the reduced  $\mathbf{A}$  matrix (and its inverse) because its derivation, although it is of dimension  $M \times M$ , involves all the  $N$  states of the Hilbert subspace.

We are aware that since  $\tilde{\mathbf{W}} (\equiv \tilde{\mathbf{W}}_M^M)$  in Eq. (8.27) is not a *symmetric* matrix, the Hamiltonian is not Hermitian (and therefore, e.g., in a scattering calculation the  $\mathbf{S}$  matrix is not guaranteed to be a unitary matrix), but it is our belief that this fact does not necessarily affect the results significantly—at least not those related to the lower states. Non-Hermitian Hamiltonians are frequently applied in molecular dynamics (see, e.g., those that contain optical potential<sup>2–4</sup> or negative imaginary potentials<sup>4–8</sup>); nevertheless, the results are practically correct. In any case the final results, as mentioned earlier, are subject to convergence tests, and therefore in order to achieve convergence, we may need to increase somewhat the dimension  $M$ , just as in any other scattering or spectroscopic cross-sectional calculation.

Having said all that, in the next section we discuss a procedure that overcomes the nonsymmetry *defect* of the potential matrix in a way that differs substantially from the ordinary approaches by employing the special features of the ADT matrix. With this new approach, the user controls the conditions for which (or for which not) to employ this approximation. In fact, it will be shown that even in extreme cases the nonsymmetric potential matrix may yield reliable results simply because of the special features of the ADT matrix employed.<sup>9</sup>

### 8.3.3 Application of Extended Euler Matrix: Introducing the $N$ -State Adiabatic-to-Diabatic Transformation Angle

#### 8.3.3.1 Introductory Comments

In Section 5.5 we suggested using the extended Euler matrix as a way to present an ADT matrix.<sup>10,11</sup> It has been proved that this matrix satisfies the various requirements fulfilled by the ADT matrix. This matrix is now applied to form the ADT angle as derived for an  $N$ -state system. The ADT angle<sup>12</sup> (also known as the *mixing angle*) is characteristic for a two-state system (see Section 3.1.1.1) and can be derived for a two-state Hilbert subspace, but here we show how to derive it for an  $N$ -state Hilbert subspace and then eventually apply it for a two-state system that does not necessarily form a Hilbert subspace. In other words, this angle is applied to construct the  $2 \times 2$  ADT matrix [see, e.g., Eq. (3.4)], which will be used to form the Born–Oppenheimer approximation for an  $N$ -state diabatic system as discussed in Section 8.3.2.

#### 8.3.3.2 Derivation of Adiabatic-to-Diabatic Transformation Angle

Derivation of the ADT angle is done in two steps, first for a three-state system and then for a general  $N$ -state system

The three-state ADT matrix,  $\mathbf{A}^{(3)}$ , is expressed as a product of three *basic* matrices of the type given in Eq. (5.37). Forming the multiplication in Eq. (5.38) yields Eq. (5.39), where the three Euler angles  $\gamma_{12}$ ,  $\gamma_{13}$ , and  $\gamma_{23}$  fulfill the three coupled, first-order, differential equations in Eq. (5.41). A different matrix is obtained by changing the order of the multiplication in Eq. (5.38), namely

$$\mathbf{A}^{(3)} = \mathbf{Q}_{12}^{(3)} \mathbf{Q}_{13}^{(3)} \mathbf{Q}_{23}^{(3)} \quad (8.28)$$

which, on multiplication, yields the following for  $\mathbf{A}^{(3)}$

$$\mathbf{A}^{(3)} = \begin{pmatrix} c_{12}c_{13} & s_{12}c_{23} - c_{12}s_{13}s_{23} & s_{12}s_{23} + c_{12}s_{13}c_{23} \\ -s_{12}c_{13} & c_{12}c_{23} + s_{12}s_{13}s_{23} & c_{12}s_{23} - s_{12}s_{13}c_{23} \\ -s_{13} & -c_{13}s_{23} & c_{13}c_{23} \end{pmatrix} \quad (8.29)$$

where the three angles fulfill a different set of differential equations:

$$\begin{aligned} \nabla \gamma_{12} &= -\tau_{12} - \tan \gamma_{13}(\tau_{23} \cos \gamma_{12} + \tau_{13} \sin \gamma_{12}) \\ \nabla \gamma_{23} &= \tau_{23} \sin \gamma_{12} - \tau_{13} \cos \gamma_{12} \\ \nabla \gamma_{13} &= -(\cos \gamma_{13})^{-1}(\tau_{23} \cos \gamma_{12} + \tau_{13} \sin \gamma_{12}) \end{aligned} \quad (8.30)$$

For the various notations, see Section 5.5.3. In general, the two sets of equations yield different results for the three angles,  $\gamma_{12}$ ,  $\gamma_{13}$ ,  $\gamma_{23}$ ; however, as long as we are interested only in the elements of the  $\mathbf{A}$  matrix, Eqs. (5.39) and (5.41) lead to the same elements as do Eqs. (8.29) and (8.30).<sup>11</sup>

In principle, we may derive other sets of equations, for the other orders of multiplication (to be termed *permutations*) as was discussed in Ref. 11, but here and in

what follows, we are interested only in those permutations where the first matrix on the l.h.s. is  $\mathbf{Q}_{12}^{(3)}(\gamma_{12})$ . This choice guarantees that the angle  $\gamma_{12}$  is *privileged* by a differential equation where its own NACT, namely,  $\tau_{12}$ , is the isolated, free term [see the first equation in Eq. (8.30) and also the first equation in Eq. (5.41)]. In this way, as is shown next,  $\gamma_{12}$  becomes a two-state ADT angle. This fact ensures that whenever the region contains (1,2) *cis*, the corresponding  $\gamma_{12}$  angle has the feature that connects it, in a straightforward way, with  $\tau_{12}$ . This feature is expected when this region is dominated by  $\tau_{12}$ , but, as will be shown here, even in less extreme situations  $\gamma_{12}$ , as derived by Eqs. (5.41) or (8.30), is still dominated by  $\tau_{12}$ .

It is true that  $\gamma_{12}$  can be derived from Eqs. (5.41) or (8.30), but in actual applications the  $\mathbf{A}$  matrix is solved applying the exponentiated line integral [see, e.g., Eq. (2.29)] and not by calculating the individual angles. Consequently  $\gamma_{12}$  is not apparent, and therefore the question is how to extract  $\gamma_{12}$  once  $\mathbf{A}^{(3)}$  is given. A closer look at the analytic expressions of the ADT elements [see, e.g., Eq. (8.29)] reveals that  $\gamma_{12}$  can be obtained from the equation

$$\gamma_{12} = \gamma_{12}^{(1)} = -\tan^{-1}(A_{21}/A_{11}) \quad (8.31a)$$

where  $A_{11}$  and  $A_{21}$  are taken from Eq. (8.29). In the same way we may obtain  $\gamma_{12}$  also from the equation

$$\gamma_{12} = \gamma_{12}^{(2)} = \tan^{-1}(A_{12}/A_{22}) \quad (8.31b)$$

where  $A_{12}$  and  $A_{22}$  are taken from Eq. (5.39).

Since there is no reason to believe that the two expressions yield the same value for  $\gamma_{12}$ , the question is which of the two values should be preferred. This subject is discussed in Ref. 9, and the conclusions are as follows. The two  $\gamma_{12}$  angles apply for two different situations. One of them, obtained from Eq. (8.31a) and designated as  $\gamma_{12}^{(1)}$ , is the ADT angle attached to the lower eigenfunction and therefore should be employed to study  $1 \rightarrow 2$  transitions; the second, obtained from Eq. (8.31b) and designated as  $\gamma_{12}^{(2)}$ , is the ADT angle attached to the upper eigenfunction and therefore should be employed to study  $2 \rightarrow 1$  transition.

[Comment: We remind the reader that in case of a two-state Hilbert space, the ADT angles related to the two eigenfunctions are always *identical*. However, in case of a three-state Hilbert subspace, their values depend on the closed contour traced by the electronic manifold (see also Sections 4.3.2.2 and 5.3.3), and therefore they are not *necessarily identical*.]

The extension to cases where  $N > 3$  was also done in Ref. 9 and will be discussed only briefly. As in the previous three-state case, here, too, we are interested in permutations similar to those given in Eq. (8.28) or (5.38), namely, where the first matrix on the l.h.s. is  $\mathbf{Q}_{12}^{(N)}(\gamma_{12})$ . Therefore, we treat the  $N$ -dimensional case for an ADT matrix given in the form

$$\mathbf{A}^{(N)}(\gamma_{12}, \gamma_{13}, \dots, \gamma_{N-1N}) = \mathbf{Q}_{12}^{(N)}(\gamma_{12}) \tilde{\mathbf{A}}^{(N)}(\gamma_{13}, \dots, \gamma_{N-1N}) \quad (8.32)$$

where we recall that, in general, we have  $N(N - 1)/2$  angles of the type  $\gamma_{kj}; k < j$  as unknowns and that  $\mathbf{Q}_{12}^{(N)}(\gamma_{12})$  is, for instance, for  $N = 5$ , of the following form:

$$\mathbf{Q}_{12}^{(N=5)}(\gamma_{12}) = \begin{pmatrix} \cos(\gamma_{12}) & \sin(\gamma_{12}) & 0 & 0 & 0 \\ -\sin(\gamma_{12}) & \cos(\gamma_{12}) & 0 & 0 & 0 \\ 0 & 0 & 1 & 0 & 0 \\ 0 & 0 & 0 & 1 & 0 \\ 0 & 0 & 0 & 0 & 1 \end{pmatrix} \quad (8.33)$$

Our next task is not to present the first-order differential equations for all the  $N(N - 1)/2$  angles but only to derive the equation for  $\gamma_{12}$ . To achieve that, we substitute Eq. (8.32) in Eq. (1.50) (instead of  $\Omega$ ):

$$\nabla(\mathbf{Q}_{12}^{(N)}(\gamma_{12})\tilde{\mathbf{A}}^{(N)}(\gamma_{13}, \dots, \gamma_{N-1N})) + \tau\mathbf{Q}_{12}^{(N)}(\gamma_{12})\tilde{\mathbf{A}}^{(N)}(\gamma_{13}, \dots, \gamma_{N-1N}) = 0 \quad (8.34)$$

Having obtained Eq. (8.34), it can be shown that the two first-order differential equations for  $\gamma_{12}$  are similar to those in Eqs. (5.41) and (8.30), namely

$$\nabla\gamma_{12}^{(i)} = -\tau_{12} - \sum'_{jk} Z_{jk}^{(i)}\nabla\gamma_{jk}; \quad i = 1, 2 \quad (8.35)$$

where none of the coefficients  $Z_{jk}^{(i)} (\equiv Z_{jk}^{(i)}(\gamma_{13}, \dots, \gamma_{N-1N}))$  depend on  $\gamma_{12}$  and the index  $i$  represents the two possible values of  $\gamma_{12}$ . The prime sign under the summation symbol implies that the summation does not contain the term  $(jk) = (12)$ , because  $Z_{12}^{(i)} \equiv 0$ .

Next, it was shown that Eqs. (8.31) apply also for  $N = 4$  and  $N = 5$  (and probably for any  $N$  value). In other words, using the  $N \times N$  ADT matrix [usually obtained by solving the exponentiated line integral—see, e.g., Eq. (2.29)], we are capable of extracting the two  $\gamma_{12}$  angles. In fact, this procedure can be extended to any two adjacent states  $(j, j + 1)$  and the corresponding two  $\gamma_{jj+1}$  angles, namely, the one responsible for the  $j \rightarrow j + 1$  transition and the other for the  $j + 1 \rightarrow j$  transition.

In Fig. 8.1 are shown results as obtained for the  $\{\text{H}_2, \text{H}\}$  system (see Sections 4.3.1.1 and 4.3.2.1). We present the two  $\gamma_{12}$  angles as calculated once employing Eq. (8.31a) [panels (a), (c), (e), and (g) in Fig. 8.1] and once employing Eq. (8.3b) [panels (b), (d), (f), and (h)] for four different  $N$  values, namely,  $N = 2, 3, 4, 5$ . The results are presented in four columns (of panels)—each column refers to a different circle as shown in the schematic drawings at the top of each column.

Two main features are to be noted:

1. The  $\gamma_{12}$  functions are seen to, approximately, converge as  $N$  increases—a feature to be expected (but that could not be proved analytically at this stage).
2. Fast convergence is achieved in case the contour surrounds only one  $ci$  [see figure panels (a) and (b)]. In all other cases the convergence is slower; in particular, it

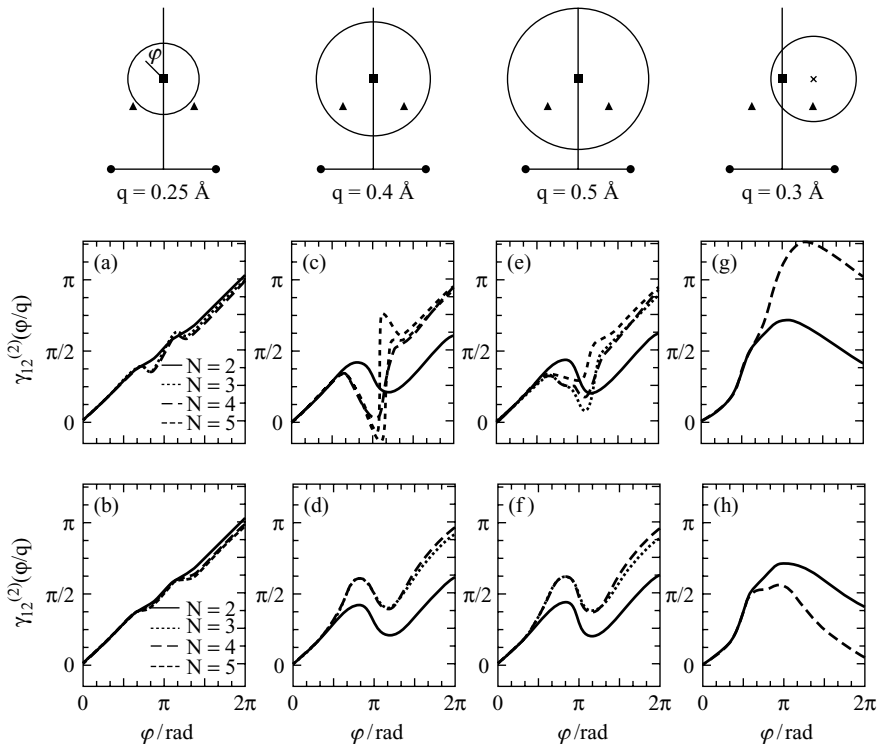


**Figure 8.1** Results as obtained for the  $\{\text{H}_2, \text{H}\}$  system: The two-state ADT angles  $\gamma_{12}^{(1)}$  (upper row of panels) and  $\gamma_{12}^{(2)}$  (lower row of panels) as a function of  $\varphi$  calculated along the closed contours. The different curves in each panel are calculated for different  $N$  values, where  $N$  is the dimension of the subspace (see discussion in Section 8.3.3.2). Results are shown for  $N = 2, 3, 4, 5$ . The main issue here is the large difference between the curves as calculated for  $N = 2$  and those for  $N > 2$ . Also noteworthy is the fast convergence once  $N > 3$ . Interesting results are shown in panels (g) and (h) emphasizing the different characteristics of the two ADT angles,  $\gamma_{12}^{(1)}$  and  $\gamma_{12}^{(2)}$ ; the first ends up with a *topological* phase  $\pi$  and the second, with  $\sim 0$ , as indeed is expected for this particular contour (see discussion in text). As for the notations for the geometry (upper) row: ( $\bullet$ ) denotes positions of the two fixed hydrogens; the single (1,2)  $D_{3h}$  *ci* point is presented in terms of a (full) square and the two (2,3) *ci* points, in terms of (full) triangles. In the first three columns results are presented along circles with their center at the (1,2) *ci* point and in the fourth column along a circle with its center at the *x* point (so that the circle surrounds the (1,2) *ci* and only one (2,3) *ci*).

is observed that the  $\gamma_{12}$  functions for  $N = 2$  are always inadequate, but then, already, for  $N = 3$ , relatively well converged  $\gamma_{12}$  functions are obtained. The only exceptions are  $\gamma_{12}^{(1)}$  functions as calculated for  $q = 0.4, 0.5 \text{ \AA}$  along a short interval around  $\varphi = \pi$ . This slower convergence is due mainly to the strong interaction between  $\tau_{12}$  and  $\tau_{23}$  along that interval. This interaction also affects the convergence for  $\gamma_{12}^{(2)}$  but to a much smaller degree.

### 8.3.4 Two-State Diabatic Potential Energy Matrix

#### 8.3.4.1 Derivation of Diabatic Potential Matrix

In what follows we concentrate on calculating the two-dimensional diabatic matrix according to the prescription given in Eq. (8.27), where the required two-dimensional  $\mathbf{A}$  matrix is obtained from  $\mathbf{A}^{(3)}$  matrices presented in Eqs. (8.29) and (5.39). The decision as to which of the two matrices to apply is, as discussed before, based on which of the two transitions one is interested in studying. If the aim is to study the  $1 \rightarrow 2$  transition, then the  $\mathbf{A}^{(3)}$  given in Eq. (8.29) and the  $\gamma_{12}^{(1)}$  angle given in Eq. (8.31a) should be employed. If the aim is to study the  $2 \rightarrow 1$  transition (viz., the transition from the (first) excited state to the ground state), then the  $\mathbf{A}^{(3)}$  in Eq. (5.39) and the  $\gamma_{12}^{(2)}$  angle, in Eq. (8.31b), have to be used (see discussion in the previous section).

Derivation of  $\tilde{\mathbf{W}}^{(2)}$  for  $\mathbf{A}^{(3)}$  as given in Eq. (8.29) is presented in Problem 8.1. Writing  $\tilde{\mathbf{W}}^{(2)}$  as

$$\tilde{\mathbf{W}}^{(2)} = \mathbf{W}^{(2)} + \Delta\mathbf{W} \quad (8.36)$$

we obtain  $\mathbf{W}^{(2)}$ , the *principal* part of the potential matrix, of the form

$$\mathbf{W}^{(2)} = \begin{pmatrix} c_{12}^2 u_1 + s_{12}^2 u_2 & c_{12}s_{12}(u_2 - u_1) \\ c_{12}s_{12}(u_2 - u_1) & s_{12}^2 u_1 + c_{12}^2 u_2 \end{pmatrix} \quad (8.37)$$

and  $\Delta\mathbf{W}$ , the *correction* term, is given as

$$\Delta\mathbf{W} = \frac{s_{13}s_{23}}{c_{23}} \begin{pmatrix} -c_{12}s_{12} & -c_{12}^2 \\ s_{12}^2 & c_{12}s_{12} \end{pmatrix} (u_2 - u_1) \quad (8.38a)$$

where we recall that  $\mathbf{u}_1(\mathbf{s})$  and  $\mathbf{u}_2(\mathbf{s})$  are the two corresponding adiabatic potentials. Similar expressions are obtained for the second case of  $\mathbf{A}^{(3)}$  given in Eq. (5.39). Here  $\mathbf{W}^{(2)}$  is identical to the one given in Eq. (8.37), but  $\Delta\mathbf{W}$  takes a slightly different form:

$$\Delta\mathbf{W} = \frac{s_{23}s_{13}}{c_{13}} \begin{pmatrix} c_{12}s_{12} & -s_{12}^2 \\ c_{12}^2 & c_{12}s_{12} \end{pmatrix} (u_2 - u_1) \quad (8.38b)$$

**Short Summary** The main outcome of this derivation is that in situations where the elements of  $\Delta\mathbf{W}$  are small, the diabatic potential matrix  $\mathbf{W}$  is of the usual form but expressed in terms of an ADT angle (i.e.,  $\gamma_{12}$ ) that results from a three-state (or  $N$ -state) calculation and therefore is guaranteed to be a multiple of  $\pi$ . This, as is well known, ensures the singlevaluedness of the diabatic potentials. Also, Eq. (8.38a) [Eq. (8.38b)], implies that  $\Delta\mathbf{W}$  can be ignored as long as  $\gamma_{23}$  ( $\gamma_{13}$ ) is small enough. On the other hand, this approximation breaks down when  $\gamma_{23}$  ( $\gamma_{13}$ ) becomes too close to  $\pi/2$ . This, as will be seen next, happens when the contour gets too close to any of the (2,3) *cis*.

### 8.3.4.2 A Numerical Study of $\Delta\mathbf{W}$ Matrix Elements

Usually a numerical study concentrates on comparisons between *accurate* results (when they are available) and *approximate* results. In our study this implies comparing the approximate and the correct diabatic potential matrix elements. However, from the presentation of the approximate diabatic potential matrix [see Eq. (8.27)], it is obvious that the elements of this matrix and the corresponding elements of the so-called *accurate*  $N \times N$  matrix are not necessarily similar. Moreover, going over the derivation, the relevant elements of the two matrices *cannot* be similar because we ignored all those *adiabatic* potentials that, for a given energy  $E$ , are unreachable (or classically *closed*), arguing that doing so does not affect the *solution* of the diabatic (nuclear) Schrödinger equation. No claims were made regarding the resulting *diabatic* potential matrix elements. Therefore, comparing the two kinds of diabatic matrix elements is meaningless.

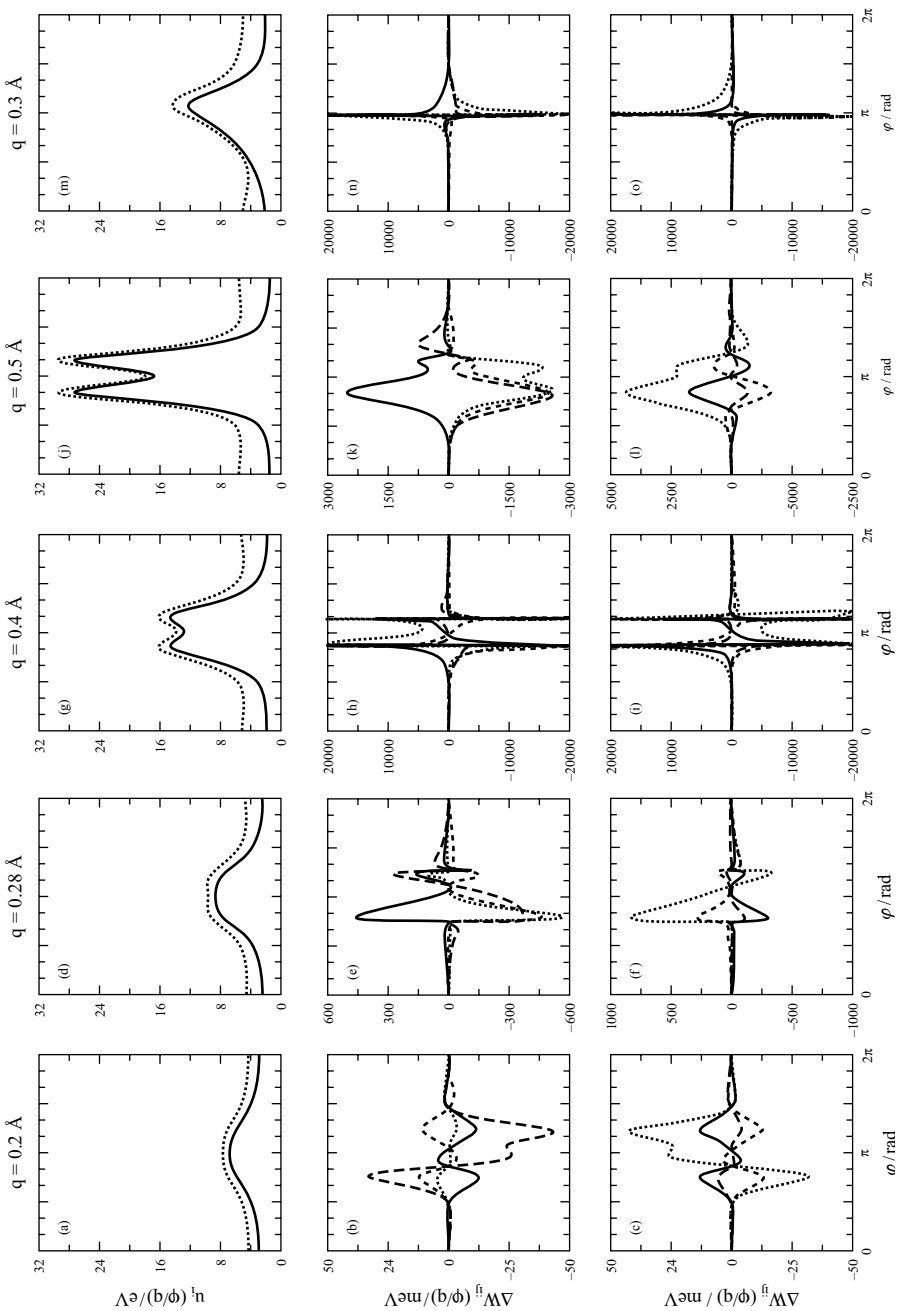
The numerical study in this section concentrates on the two matrices  $\Delta\mathbf{W}$ . The aim is to determine the conditions for which the elements of  $\Delta\mathbf{W}$  remain small enough so that  $\mathbf{W}^{(2)}$  [see Eq. (8.37)] can serve as the relevant  $2 \times 2$  diabatic potential  $\tilde{\mathbf{W}}^{(2)}$ .

To study this issue, we consider Eq. (8.38a) and concentrate mainly on  $c_{23} \equiv \cos \gamma_{23}$  [because  $c_{23}$  appears in the denominator of Eq. (8.38a)]. Since  $(\cos \gamma_{23})^{-1}$  is the only function in Eq. (8.38a) that may attain large values (eventually even infinite values, in case  $\gamma_{23} = \pi/2$ ), we follow what happens to  $\gamma_{23}$  along various contours in configuration space. From the second equation in Eq. (8.30), it is obvious that if  $\tau_{23}$  is small enough along a given contour,  $\gamma_{23}$  is expected to remain small so that it cannot reach  $\pi/2$  [we remind the reader that usually  $|\tau_{13}| \ll |\tau_{23}|$  (see also Chapter 6) so that, in such a situation,  $\tau_{13}$  can be ignored as well]. In other words, we expect  $\gamma_{23}$  to approach  $\pi/2$  only along those contours where  $\tau_{23}$  is large enough, and this can occur only in the vicinity of a (2,3) *ci*. Therefore, as long as the region of interest does not contain any (2,3) *ci*,  $\gamma_{23}$  is not expected to change significantly and therefore  $|\gamma_{23}| \ll \pi/2$ . From Eq. (8.38a) it follows that not only is the denominator finite in such a case but also the numerator  $\rightarrow 0$ . Similar arguments apply for  $\gamma_{13}$ .

The next issue is related to the case when the contour approaches a (2,3) *ci*. The issue is whether we can ignore  $\Delta\mathbf{W}^{(2)}$  even in such a situation. Including the closed vicinity of the (2,3) *ci* usually implies including a region where  $u_2(\mathbf{s})$  is large—at the (2,3) *ci points*, the surface,  $u_2(\mathbf{s})$  most likely reaches its highest (local) values. Consequently, for the case under consideration, these values of  $u_2(\mathbf{s})$  are assumed to be classically closed (if this assumption is not valid, then we have to carry out, instead, a three-state diabatization) and therefore adding the large values of  $\Delta\mathbf{W}$  to the large values of  $\mathbf{W}^{(2)}$  [see Eq. (8.36)] is not expected to affect much the dynamical calculations because the wavefunctions are negligibly small in such a region, with or without  $\Delta\mathbf{W}$ .

The conclusion of this analysis is that in general the elements of  $\Delta\mathbf{W}$  can always be ignored and we are left with the potential matrix  $\mathbf{W}^{(2)}$  dominated by (one) ADT angle.

The results, to be discussed next, are derived for the H+H<sub>2</sub> system (see Section 4.3.2.1) and are presented in a series of panels in Figure 8.2. The upper row of this figure [panels (a), (d), (g), (j), (m)] gives the two lower *adiabatic* potentials of the



$\text{H}+\text{H}_2$  system as calculated along five different circular contours (three of which are shown in Fig. 8.1). In the second and third rows [panels (b), (e), (h), (k), (n) and (c), (f), (i), (l), (o), respectively] the corresponding four elements of the  $\Delta\mathbf{W}^{(2)}$  matrix as calculated along the same contours are presented. The intermediate row [panels (b), (e), (h), (k), (n)] shows the matrix elements as calculated employing  $\gamma_{12}^{(1)}$  (and the corresponding  $\gamma_{23}$  and  $\gamma_{13}$  angles); the lower (third) row [panels (c), (f), (i), (l), (o)] shows those calculated employing  $\gamma_{12}^{(2)}$  (and the corresponding  $\gamma_{23}$  and  $\gamma_{13}$  angles).

The following is to be noted:

1. The first two *columns* [panels (a)–(c) and (d)–(f)] are related to situations where the circular contour [which is centered at the (1,2) *cis*] does not surround any of the (2,3) *cis*. As a result, the elements of  $\Delta\mathbf{W}^{(2)}$  are relatively small—a few millielectronvolts for the inner circle and, at most, a few hundreds of millielectronvolts for the second circle. These values have to be compared with the corresponding values of  $u_1$  and  $u_2$ , calculated along the same *angular* intervals. It is also noteworthy that the values of  $u_1$  and  $u_2$  are between one and two orders of magnitude larger than the corresponding ones of  $\Delta\mathbf{W}^{(2)}$ .

2. The next three columns [panels (g)–(i), (j)–(l), and (m)–(o)] are related to situations where the circular contours surround the two (2,3) *cis*. As is noted, although the values of both those of  $u_1(\mathbf{s})$  and  $u_2(\mathbf{s})$  and those of  $\Delta\mathbf{W}$  are much larger still the values of  $u_1(\mathbf{s})$  and  $u_2(\mathbf{s})$  remain one order of magnitude (or more) larger than those of  $\Delta\mathbf{W}$  [except in those (rare) cases when  $\gamma_{23}$  (or  $\gamma_{13}$ ) becomes (exactly)  $\pi/2$ ]. In fact, this situation is encountered for circles for which the radius  $q = 0.3, 0.4 \text{ \AA}$  (see Fig. 8.1) but no longer along the circle for which  $q = 0.5 \text{ \AA}$ . The reason is that the contour in case of  $q = 0.5 \text{ \AA}$  is located too far away from the (2,3) *cis* so that  $\gamma_{23}$  ( $\gamma_{13}$ ) can no longer become  $\pi/2$ .

**Short Summary** We showed that although the diabatic potential matrix given in Eq. (8.27) is in general nonsymmetric, this nonsymmetry can be easily modified (e.g., by symmetrization of the potential matrix), a correction that causes some damage to the potential, but since it takes place in nonphysical regions, it is not expected to significantly affect the final results.

---

**Figure 8.2** The *adiabatic* potentials  $u_1(\varphi|q)$  and  $u_2(\varphi|q)$  and the elements of the diabatic correction matrix  $\Delta\mathbf{W}(\varphi|q)$  as calculated along various contours. The first two contours surround only the (1,2) *cis*; and the three other contours surround either two or three *cis*, (presented in Fig. 8.1). The first (upper) row in each panel contains, two curves related to the adiabatic potentials,  $u_1(\varphi|q)$  and  $u_2(\varphi|q)$ ; each panel in the next two rows contains four curves describing  $\Delta W_{11}(\varphi|q)$ ,  $\Delta W_{12}(\varphi|q)$ ,  $\Delta W_{21}(\varphi|q)$ , and  $\Delta W_{22}(\varphi|q)$ , respectively. The curves in the intermediate row are calculated, employing Eq. (8.38a), for  $\gamma_{12}^{(1)}$  and the corresponding  $\gamma_{13}$  and  $\gamma_{23}$  angles [obtained from Eq. (8.30)], and the curves in the third row are calculated, employing Eq. (8.38b), for  $\gamma_{12}^{(2)}$  and the respective  $\gamma_{13}$  and  $\gamma_{23}$  angles [obtained from Eq. (5.40)].

### 8.3.4.3 A Different Approach: Helmholtz Decomposition

As a final issue on this subject we briefly refer to another approach that yields two-state ADT angles for a multistate system.<sup>13,14</sup> This approach is based on the Helmholtz theorem,<sup>15</sup> which asserts that each vector  $\tau$  can be decomposed into a longitudinal component  $\tau_\ell$  and a transverse component  $\tau_t$ , where

$$\begin{aligned}\text{Curl } \tau_\ell &= \nabla \times \tau_\ell = 0 \\ \text{Div } \tau_t &= \nabla \cdot \tau_t = 0\end{aligned}\tag{8.39}$$

According to this procedure,<sup>16</sup> the ADT angle  $\beta$  is chosen to be a solution of the following first-order differential equation

$$\nabla \beta = \tau_\ell\tag{8.40a}$$

because this choice guarantees that for any closed contour surrounding the  $ci$ , the angle  $\beta$  becomes a multiple integer of  $\pi$  (cf. discussion in Section 3.1.1). Since  $\tau = \tau_\ell + \tau_t$ , it can be shown that  $\beta$  fulfills the following Poisson equation:

$$\nabla^2 \beta = \nabla \cdot \tau\tag{8.40b}$$

The main advantage of this approach is that in case the two-state system is only slightly affected by higher states, the final equation guarantees a relevant approximate solution. However, in case the higher states significantly affect the two-state system, this approach is not designed to incorporate the effect of the upper states. In other words, the results obtained by this approach depend solely on the two states under consideration.

## 8.4 A NUMERICAL STUDY OF A REACTIVE (EXCHANGE) SCATTERING TWO-COORDINATE MODEL

### 8.4.1 Basic Equations

In this section we present a model that yields deeper insight into the Born–Oppenheimer approximation. We refer to two types of approximation: the ordinary Born–Oppenheimer approximation to be discussed below and the extended Born–Oppenheimer approximation as presented in Eq. (8.9) and governed by the *quantization* condition given in Eq. (8.10). As a *byproduct* we show to what extent the existence of a  $ci$  affects final results, namely, reactive (exchange) *vibrational transitions* for the model to be presented below.

We consider a two-state system described in terms of two coupled adiabatic equations [see Eq. (2.12)]:

$$-\frac{\hbar^2}{2m}(\nabla + \boldsymbol{\tau})^2 \Psi + (\mathbf{u} - E)\Psi = \mathbf{0}\tag{8.41}$$

where  $\Psi$  is a column vector with two elements  $(\psi_1, \psi_2)$ ,  $\mathbf{u}$  is the *adiabatic* (diagonal) potential matrix, and  $\tau$ , the NACM, is given in the following form [see Eq. (2.57)]:

$$\tau = \begin{pmatrix} 0 & \tau_{12} \\ -\tau_{12} & 0 \end{pmatrix} \quad (8.42)$$

Here  $\tau_{12}$  is assumed to fulfill the quantization condition [see Eq. (3.12)]

$$\oint_{\Gamma} \tau_{12} \cdot ds = n\pi \quad (8.43)$$

where  $n$  is an integer.

Next we consider the two Born–Oppenheimer approximations for Eq. (8.39):

1. The ordinary Born–Oppenheimer approximation follows from Eq. (8.39) by assuming that  $\tau_{12} \equiv \mathbf{0}$ . Since  $\tau_{12}$  is the only term that couples the two equations, assuming it to be negligibly small, yields two (approximately) decoupled Born–Oppenheimer equations:

$$-\frac{\hbar^2}{2m} \nabla^2 \psi_j + (u_j - E) \psi_j = 0; \quad j = 1, 2 \quad (8.44a)$$

In what follows we concentrate only on one of them, namely, the equation with  $j = 1$ .

2. The extended Born–Oppenheimer approximation that was derived in Section 6.2.1 and is explicitly given Eqs. (6.6). For completeness, these two equations are presented here as well:

$$\frac{\hbar^2}{2m} (-i \nabla \pm \tau)^2 \psi + (u - E) \psi = 0 \quad (8.44b)$$

In what follows  $u(\mathbf{s})$  is the lowest adiabatic potential [i.e.,  $u(\mathbf{s}) \equiv u_1(\mathbf{s})$ ],  $\tau$  represents  $\tau_{12}$ , and we recall that it fulfills the condition in Eq. (8.43). For this case the solution of Eq. (8.44b) is invariant to the sign in front of  $\tau$ , and therefore we solve, in what follows, only one of the equations.

Before we describe the model, we also present the corresponding two coupled *adiabatic* equations (see Section 2.1.3.2), which are of the form

$$-\frac{\hbar^2}{2m} \nabla^2 \Phi + (\mathbf{W} - E) \Phi = \mathbf{0} \quad (8.44c)$$

where  $\Phi$  is a column vector with two terms  $(\Phi_1, \Phi_2)$  and  $\mathbf{W}$  is the diabatic  $2 \times 2$  matrix with the following elements (see Section 3.1.1.3):

$$\begin{aligned} W_{11}(\mathbf{s}) &= \cos^2 \gamma(\mathbf{s}) u_1 + \sin^2 \gamma(\mathbf{s}) u_2 \\ W_{22}(\mathbf{s}) &= \sin^2 \gamma(\mathbf{s}) u_1 + \cos^2 \gamma(\mathbf{s}) u_2 \\ W_{12}(\mathbf{s}) &= \cos \gamma(\mathbf{s}) \sin \gamma(\mathbf{s}) (u_1 - u_2) \end{aligned} \quad (8.45)$$

Here  $\gamma(\mathbf{s})$  is the ADT angle given in the following form [see Eq. (3.6)]:

$$\gamma(\mathbf{s}|\mathbf{s}_0|\Gamma) = - \int_{\mathbf{s}_0}^{\mathbf{s}} d\mathbf{s} \cdot \boldsymbol{\tau}(\mathbf{s}|\Gamma) \quad (8.46)$$

In the numerical treatment we consider all three Eqs. (8.44). The three types of equations were solved employing a novel efficient approach based on features of the *Toeplitz* matrix to treat the asymptotic regions of each arrangement channel.<sup>1–4</sup> (It can be of interest to know that there also exist a *time-dependent wavepacket* approach based on features of the *Toeplitz* matrix developed by Kouri and colleagues<sup>5</sup>). We do not elaborate on this approach as it is beyond the scope of this book. However, we will say a few words about Eq. (8.44b), which contains singular terms [see Eq. (8.47)]. This equation may pose some difficulties because the relevant boundary conditions have to be treated with care. Because of this sensitivity, the present author, together with Englman, developed a perturbative approach<sup>6</sup> that guarantees the correct treatment of this kind of equation (see also Refs. 7 and 8).

#### 8.4.2 A Two-Coordinate Reactive (Exchange) Model

The model to be applied was described on several occasions<sup>9–14</sup> and was solved by applying several approaches: (1) R. Baer et al. solved Eq. (8.44b), within the time-independent framework, employing the previously mentioned perturbative-Toeplitz-type approach;<sup>9,10</sup> (2) Adhikari and Billing solved this equation within the time-dependent framework,<sup>11</sup> employing two methods, one based on the vector potential and the other based on the application of anti-symmetric basis functions<sup>(12)</sup> (in both cases they applied wave packets and absorbing boundary conditions<sup>(13)</sup>); and (3) finally, Adhikari and colleagues treated this model semiclassically<sup>14,15</sup> employing the quantum-classical approach as developed by Billing and colleagues.<sup>16–18</sup>

It may be important to mention that there also exists a three-state version of this model<sup>19–21</sup> that yields different results, thus showing to what extent the final results depend on the dimension of the Hilbert subspace. This treatment is not discussed here.

We consider a planar system expressed in terms of two Cartesian coordinates ( $R, r$ ) within the range  $-\infty \leq x \leq \infty; x = r, R$ . In this model  $r$  represents a vibrational coordinate and  $R$  is the translational coordinate. The system starts at  $R = -\infty$  and moves toward the origin  $(R, r) = (0, 0)$ . At the origin it encounters a *ci* that is assumed to be of a Jahn-Teller type [see Eq. (3.58)]. Since the numerical treatment is carried out employing Cartesian coordinates, we present the Cartesian components of the corresponding Jahn-Teller NACT:

$$\boldsymbol{\tau}_R = -\frac{1}{2} \frac{r}{r^2 + R^2}; \quad \boldsymbol{\tau}_r = \frac{1}{2} \frac{R}{r^2 + R^2} \quad (8.47)$$

**TABLE 8.1 Adiabatic Potential Energy Parameters Used for Two-State Adiabatic Model Potential<sup>a</sup>**

|            |                                       |
|------------|---------------------------------------|
| $m$        | 0.58 Atomic mass units                |
| $A$        | 3.0 eV                                |
| $D$        | 5.0 eV                                |
| $\sigma$   | 0.30 Å                                |
| $\sigma_0$ | 0.75 Å                                |
| $\omega_0$ | $39.14 \times 10^{13} \text{ s}^{-1}$ |
| $\varpi_0$ | $7.83 \times 10^{13} \text{ s}^{-1}$  |

<sup>a</sup>See Section 8.4.

Next we present the two adiabatic PESs, namely,  $u_j$ ,  $j = 1, 2$ :

$$u_1(R, r) = \frac{1}{2}m(\omega_0 - \omega(R))^2r^2 + Af(R, r) \quad (8.48a)$$

$$u_2(R, r) = \frac{1}{2}m\omega_0^2r^2 - (D - A)f(R, r) \quad (8.48b)$$

Here  $m$ ,  $\omega_0$ ,  $A$ , and  $D$  are parameters (their values are listed in Table 8.1), the function  $f(R, r)$  is chosen to be a two-variable Gaussian that peaks at (0,0), namely

$$f(R, r) = \exp\left(-\frac{R^2 + r^2}{\sigma^2}\right) \quad (8.49)$$

and  $\omega(R)$  is an  $R$ -dependent frequency given in the following form:

$$\omega(R) = \varpi_0 \exp\left(-\frac{R^2}{\sigma_0^2}\right) \quad (8.50)$$

The values of  $\sigma$  and  $\sigma_0$  are also listed in Table 8.1. It is important to emphasize that the adiabatic potentials are of the Renner–Teller type<sup>22–24</sup> (see Section 5.1), although we assumed the NACT to be of the Jahn–Teller type.

In Figure 8.3 we present the corresponding two-coordinate, two adiabatic PESs. It can be seen that these potentials describe a two-arrangement channel system: the reagent arrangement is defined for  $R \rightarrow \infty$  and the product arrangement is defined for  $R \rightarrow -\infty$ .

This completes the derivation of the model.

### 8.4.3 Numerical Results and Discussion

The model is made up of two arrangement channels: an inelastic one, located at the entrance (reagents) arrangement, namely, at  $R \sim -\infty$ ; and one at the exit (products) arrangement, namely, at  $R \sim +\infty$ .

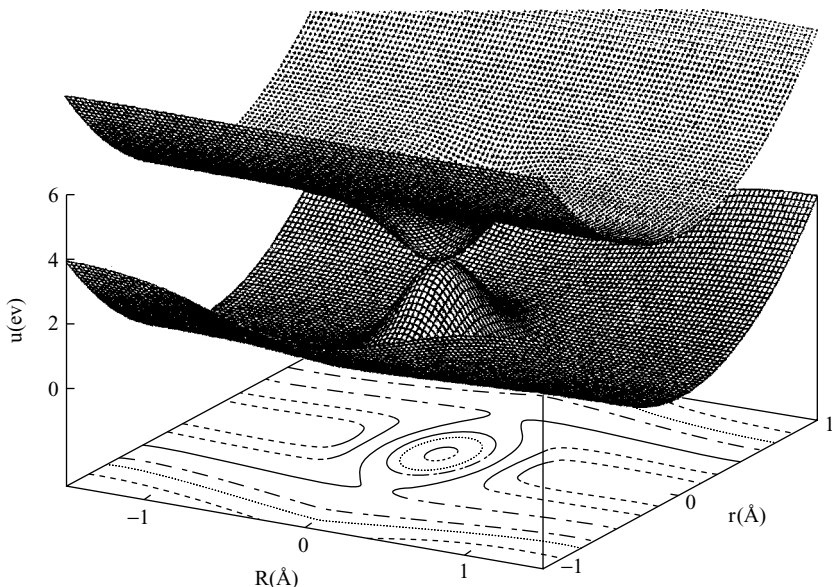


**Figure 8.3** The two reactive adiabatic potential energy surfaces applied in the quasi-Jahn–Teller model. The *ci* point is located at the origin, namely, at ( $r = 0, R = 0$ ), the point where the two adiabatic surfaces approach each other tangentially.

Once all three types of Schrödinger equations are solved, the relevant wavefunctions are analyzed at the two asymptotic regions with the aim of deriving the *nonreactive* and the *reactive* state-to-state S-matrix elements, namely,  $S_{ij}^{N_x}$ ;  $x = R, NR$ , where  $R$  and  $NR$  designate *reactive* and *nonreactive*, respectively, and following that the corresponding state-to-state reactive/nonreactive transition probabilities. The indices  $i$  and  $j$  denote the initial (reagent) state  $i$  and the final states  $j$ , respectively. Table 8.2 lists some of these probabilities as calculated for four energies:  $E = 1.0, 1.5, 2.0$ , and  $2.5$  eV. In this respect we make the following three technical comments:

1. Since the lowest point of the upper surface [located at the *ci* point ( $r = 0, R = 0$ )] is at  $E = 3.0$  eV (see Table 8.1), this implies that for all chosen energies the upper surface is classically forbidden or, in other words, is a closed state throughout configuration space.
2. The threshold energy for the reactive (“exchange”) process is in the vicinity of  $E_k \sim 1.0$  eV.
3. Reactive probabilities will be shown only for the initial state  $v_i = 0$  but for all possible final states. (More results as obtained within this treatment and also within the time-dependent treatment can be found in Refs. 9 and 10, respectively).

Before presenting the results, we elaborate on the potential effect of the nonadiabatic coupling terms. The two adiabatic potentials  $u_1(r, R)$  and  $u_2(r, R)$  in Eqs. (8.48a)

**TABLE 8.2** Reactive State-to-State Transition Probabilities<sup>a</sup>

| $0 \rightarrow 0$     | $0 \rightarrow 1$  | $0 \rightarrow 2$ | $0 \rightarrow 3$ | $0 \rightarrow 4$ | $0 \rightarrow 5$ | $0 \rightarrow 6$ | $0 \rightarrow 7$ | $0 \rightarrow 8$ | $0 \rightarrow 9$ | Total |
|-----------------------|--------------------|-------------------|-------------------|-------------------|-------------------|-------------------|-------------------|-------------------|-------------------|-------|
| $E = 1.00 \text{ eV}$ |                    |                   |                   |                   |                   |                   |                   |                   |                   |       |
| —                     | 0.027 <sup>b</sup> | —                 | 0.010             |                   |                   |                   |                   |                   |                   | 0.037 |
| —                     | 0.030 <sup>c</sup> | —                 | 0.011             |                   |                   |                   |                   |                   |                   | 0.041 |
| 0.011 <sup>d</sup>    | —                  | 0.031             | —                 |                   |                   |                   |                   |                   |                   | 0.042 |
| $E = 1.5 \text{ eV}$  |                    |                   |                   |                   |                   |                   |                   |                   |                   |       |
| —                     | 0.189              | —                 | 0.034             | —                 | 0.071             |                   |                   |                   |                   | 0.295 |
| —                     | 0.189              | —                 | 0.038             | —                 | 0.076             |                   |                   |                   |                   | 0.304 |
| 0.098                 | —                  | 0.090             | —                 | 0.115             | —                 |                   |                   |                   |                   | 0.304 |
| $E = 2.0 \text{ eV}$  |                    |                   |                   |                   |                   |                   |                   |                   |                   |       |
| —                     | 0.068              | —                 | 0.047             | —                 | 0.133             | —                 | 0.203             |                   |                   | 0.451 |
| —                     | 0.063              | —                 | 0.046             | —                 | 0.125             | —                 | 0.215             |                   |                   | 0.454 |
| 0.047                 | —                  | 0.022             | —                 | 0.056             | —                 | 0.371             | —                 |                   |                   | 0.446 |
| $E = 2.5 \text{ eV}$  |                    |                   |                   |                   |                   |                   |                   |                   |                   |       |
| —                     | 0.105              | —                 | 0.032             | —                 | 0.150             | —                 | 0.014             | —                 | 0.319             | 0.621 |
| —                     | 0.110              | —                 | 0.041             | —                 | 0.163             | —                 | 0.013             | —                 | 0.332             | 0.666 |
| 0.147                 | —                  | 0.005             | —                 | 0.010             | —                 | 0.114             | —                 | 0.118             | —                 | 0.393 |

<sup>a</sup> See Section 8.4.<sup>b</sup> Two-surface calculation.<sup>c</sup> Single-surface calculation (including the nonadiabatic coupling term).<sup>d</sup> Single-surface calculation (ordinary Born–Oppenheimer treatment).

and (8.48b) are seen to be constructed from even powers of the vibrational coordinate  $r$  (that is why the model is, in fact, a Renner-Teller model<sup>22</sup>); therefore, as long as the NACTs are ignored, the state-to-state transitions *even*→*even* and *odd*→*odd* transitions are allowed whereas the *even*→*odd* and *odd*→*even* transitions are forbidden. If now, following the inclusion of the NACTs, these *selection* rules are affected to any extent, the deviations are unambiguously attributed to the inclusion of the NACTs, and therefore these deviations are considered as geometric (or topological) effects.

Table 8.2 presents state-to-state “reactive” transition probabilities for the four different energies described above. As mentioned earlier, three types of transition probability are shown: one type, given in the first row, is due to the exact treatment [solving the coupled equations, Eq. (8.44c)]; a second type, presented in the second row, is due to the *extended* Born–Oppenheimer approximation [solving Eq. (8.44b)]; and a third type, presented in the third row, is due to the *ordinary* Born–Oppenheimer approximation [solving Eq. (8.44a)]. We note that the *extended* Born–Oppenheimer treatment reproduces very nicely the exact state-to-state reactive probabilities whereas the *ordinary* Born–Oppenheimer treatment fails to do that. However, the failure is

expressed in producing not only erroneous numbers but also results of the wrong character. The *ordinary* approximation is found to fulfill the *even*→*even* and *odd*→*odd* selection rule, whereas the accurate treatment as well the *extended* approximation obey different selection rules, namely, the *even*→*odd* and the *odd*→*even*<sup>9</sup> selection rule.

## PROBLEM

- 8.1 Given the  $3 \times 3$   $\mathbf{A}$  matrix in Eq. (8.29), derive the relevant  $2 \times 2$  diabatic potential matrix applying Eq. (8.27).

*Solution* In order to apply the  $\mathbf{A}$  matrix in Eq. (8.29) for the reduced  $2 \times 2$  case, we have to extract the  $2 \times 2$  submatrix located at the upper left corner of  $\mathbf{A}$ , namely  $\mathbf{A}^{(2)}$ :

$$\mathbf{A}^{(2)} = \begin{pmatrix} c_{12}c_{13} & s_{12}c_{23} - c_{12}s_{13}s_{23} \\ -s_{12}c_{13} & c_{12}c_{23} + s_{12}s_{13}s_{23} \end{pmatrix} \quad (8.51)$$

Next, according to the theory, we form its inverse:

$$(\mathbf{A}^{(2)})^{-1} = \frac{1}{c_{13}c_{23}} \begin{pmatrix} c_{12}c_{23} + s_{12}s_{13}s_{23} & -s_{12}c_{23} + c_{12}s_{13}s_{23} \\ s_{12}c_{13} & c_{12}c_{13} \end{pmatrix} \quad (8.52)$$

The corresponding  $2 \times 2$  diabatic matrix,  $\tilde{\mathbf{W}}^{(2)}$ , is given in the form

$$\tilde{\mathbf{W}}^{(2)} = \mathbf{A}^{(2)} \begin{pmatrix} u_1 & 0 \\ 0 & u_2 \end{pmatrix} (\mathbf{A}^{(2)})^{-1} \quad (8.53)$$

and we suggest expressing it as follows

$$\tilde{\mathbf{W}}^{(2)} = \mathbf{W}^{(2)} + \Delta\mathbf{W} \quad (8.54)$$

where  $\mathbf{W}^{(2)}$ , the principal term, is given in the form

$$\mathbf{W}^{(2)} = \begin{pmatrix} c_{12}^2u_1 + s_{12}^2u_2 & c_{12}s_{12}(u_2 - u_1) \\ c_{12}s_{12}(u_2 - u_1) & s_{12}^2u_1 + c_{12}^2u_2 \end{pmatrix} \quad (8.55)$$

and  $\Delta\mathbf{W}$ , the correction term, is given in the form

$$\Delta\mathbf{W}^{(2)} = \frac{s_{13}s_{23}}{c_{23}} \begin{pmatrix} -c_{12}s_{12} & -c_{12}^2 \\ s_{12}^2 & c_{12}s_{12} \end{pmatrix} (u_2 - u_1) \quad (8.56)$$

## REFERENCES

### Section 8.1

1. M. Born and J. R. Oppenheimer, *Ann. Phys. (Leipzig)* **84**, 457 (1927).
2. M. Born, *Festschrift Goett. Nach. Math. Phys.* **K1**, 1 (1951).
3. M. Born and K. Huang, *Dynamical Theory of Crystal Lattices*, Oxford Univ. Press, New York, 1954, Chapter 4.
4. E. E. Nikitin, in *Chemische Elementarprozesse*, H. Hartman, ed., Springer-Verlag, Berlin, 1968.
5. B. Lepetit and A. Kuppermann, *Chem. Phys. Lett.* **166**, 581 (1990).
6. Y.-S. M. Wu and A. Kuppermann, *Chem. Phys. Lett.* **235**, 105 (1995).
7. A. Kuppermann, in *Dynamics of Molecules and Chemical Reactions*, R. E. Wyatt and J. Z. H. Zhang, eds., Marcel Dekker, New York, 1996, p. 411.
8. R. Abrol and A. Kuppermann, *Adv. Chem. Phys.* **124**, 283 (2002).
9. X. Wu, R. E. Wyatt, and M. D'mello, *J. Chem. Phys.* **101**, 2953 (1994).
10. R. Baer, D. Charutz, R. Kosloff, and M. Baer, *J. Chem. Phys.* **105**, 9141 (1996).
11. D. Charutz, R. Baer, and M. Baer, *Chem. Phys. Lett.* **265**, 629 (1997).
12. S. Adhikari and G. D. Billing, *J. Chem. Phys.* **111**, 40 (1999).
13. M. Baer, *Chem. Phys.* **259**, 123 (2000).
14. S. Adhikari and G. D. Billing, *Adv. Chem. Phys.* **124**, 143 (2002).
15. M. Baer, S. H. Lin, A. Alijah, S. Adhikari, and G. D. Billing, *Phys. Rev. A* **62**, 032506-1 (2000).
16. S. Adhikari, G. D. Billing, A. Alijah, S. H. Lin, and M. Baer, *Phys. Rev. A* **62**, 032507-1 (2000).
17. M. Baer, T. Vértesi, G. J. Halász, and Á. Vibók, *J. Phys. Chem. A* **108**, 9134 (2004).
18. T. Vértesi, E. Bene, Á. Vibók, G. J. Halász, and M. Baer, *J. Phys. Chem. A* **109**, 3476 (2005).

### Section 8.2

1. M. Baer and A. Alijah, *Chem. Phys. Lett.* **319**, 489 (2000).
2. M. Baer, *J. Phys. Chem.* **104**, 318 (2000).
3. M. Baer, in *Low-Lying Potential Energy Surfaces*, M. R. Hoffmann and K. G. Dyall, eds., ACS Symposium Series 828, Washington, DC, 2002, p. 361.
4. M. Baer, S. H. Lin, A. Alijah, S. Adhikari, and G. D. Billing, *Phys. Rev. A* **62**, 032506-1 (2000).
5. S. Adhikari and G. D. Billing, *Adv. Chem. Phys.* **124**, 143 (2002).

### Section 8.3

1. M. Baer, T. Vértesi, G. J. Halász, and Á. Vibók, *J. Phys. Chem.* **108**, 913 (2004).
2. R. D. Levine, *Quantum Mechanics of Molecular Rate Processes*, Oxford Univ. Press, London, 1969.

3. D. A. Micha, in *Modern Theoretical Chemistry*, W. H. Miller ed., Plenum, New York, 1976, Vol. I.
4. J. G. Muga, J. P. Palao, B. Navaro, and I. L. Egusquiza, *Phys. Rep.* **395**, 357 (2004).
5. D. Neuhauser and M. Baer, *J. Chem. Phys.* **90**, 4351 (1989).
6. I. Last and M. Baer, *Chem. Phys. Lett.* **189**, 84 (1992).
7. Á. Vibók and G. Balint-Kurti, *J. Phys. Chem.* **96**, 8712 (1992).
8. Á. Vibók and G. J. Halász, *Chem. Phys. Lett.* **323**, 287 (2000).
9. T. Vértesi, E. Bene, Á. Vibók, G. J. Halász, and M. Baer, *J. Phys. Chem. A* **109**, 3476 (2005).
10. Z. H. Top and M. Baer, *J. Chem. Phys.* **66**, 1363 (1977).
11. A. Alijah and M. Baer, *J. Phys. Chem. A* **104**, 389 (2000).
12. M. Baer, *Chem. Phys. Lett.* **35**, 112 (1975).
13. R. G. Sadigov and D. R. Yarkony, *J. Chem. Phys.* **109**, 20 (1998).
14. R. Abrol and A. Kuppermann, *Adv. Chem. Phys.* **124**, 283 (2002).
15. P. M. Morse and H. Feshbach, *Methods of Theoretical Physics*, McGraw-Hill, New York, 1953, pp. 52–54.
16. Ref. 14, p. 303.

## Section 8.4

1. M. Gilibert, A. Baram, H. Szychman, and M. Baer, *J. Chem. Phys.* **99**, 3503 (1993).
2. E. Eisenberg, S. Ron, and M. Baer, *J. Chem. Phys.* **101**, 3802 (1994).
3. E. Eisenberg, A. Baram, and M. Baer, *J. Phys. A* **28**, L433 (1995).
4. E. Eisenberg, D. M. Charutz, S. Ron, and M. Baer, *J. Chem. Phys.* **104**, 1886 (1996).
5. Y. Huang, D. J. Kouri, M. Arnold, I. Thomas, L. Marchioro, and D. K. Hoffman, *Comp. Phys. Commun.* **80**, 1 (1994).
6. M. Baer and R. Englman, *Chem. Phys. Lett.* **265**, 105 (1997).
7. M. Baer and H. Nakamura, *J. Chem. Phys.* **96**, 6565 (1992).
8. I. Last, D. Neuhauser, and M. Baer, *J. Chem. Phys.* **96**, 2017 (1992).
9. R. Baer, D. M. Charutz, R. Kosloff, and M. Baer, *J. Chem. Phys.* **105**, 9141 (1996).
10. D. M. Charutz, R. Baer, and M. Baer, *Chem. Phys. Lett.* **265**, 629 (1997).
11. S. Adhikari and G. D. Billing, *J. Chem. Phys.* **111**, 40 (1999).
12. B. Lepetit and A. Kuppermann, *Chem. Phys. Lett.* **166**, 581 (1990).
13. D. Neuhauser and M. Baer, *J. Chem. Phys.* **91**, 4651 (1989).
14. P. Puzari, B. Sarkar, and S. Adhikari, *J. Chem. Phys.* **121**, 707 (2004).
15. B. Barkakaty and S. Adhikari, *J. Chem. Phys.* **118**, 5302 (2003).
16. S. Adhikari and G. D. Billing, *J. Chem. Phys.* **113**, 1409 (2000).
17. C. Coletti and G. D. Billing, *Phys. Chem. Chem. Phys.* **1**, 4141 (1999).
18. G. D. Billing, *The Quantum Classical Theory*, Oxford Univ. Press, New York, 2003.
19. M. Baer, S. H. Lin, A. Alijah, S. Adhikari, and G. D. Billing, *Phys. Rev. A* **62**, 032506-1 (2000).

20. S. Adhikari, G. D. Billing, A. Alijah, S. H. Lin, and M. Baer, *Phys. Rev. A* **62**, 032507-1 (2000).
21. S. Adhikari and G. D. Billing, *Adv. Chem. Phys.* **124**, 143 (2002).
22. E. Renner, *Z. Phys.* **92**, 172 (1934).
23. H. C. Longuet-Higgins, *Adv. Spectrosc.* **2**, 429 (1961).
24. G. Herzberg, *Molecular Spectra and Molecular Structure*, Vol. III Krieger, Malabar, 1991.

# CHAPTER 9

---

## A SUMMARY

---

The features of conical intersection (*cis*) and the physics of their NACTs are discussed in this book. To be more specific, we discuss four issues related to the *ci*/NACT system:

1. One issue, the more analytical one, is related to the physical content of the *ci*/NACT system and is treated mainly in Chapters 2 and 5–7. We start by mentioning that the NACM elements related to a Hilbert subspace are quantized (the matrix as a whole, not every individual element). This quantization leads to the introduction of the topological spin for this group (Chapter 5) and reveals the relations between characteristic magnitudes of the time-independent framework, namely, the ADT matrix elements, and *adiabatic* magnitudes defined within the time-dependent framework (Chapter 7). In particular, we have established the connection between the topological (Berry) phases and the diagonal elements of the topological **D** matrix. Other significant achievements are the Curl–Div equations (Chapter 6), which, once solved, yield the spatial distribution of the various NACTs for a set of *cis* in a given region. This fact leads to the definition of *molecular fields*, namely, fields formed by *cis* in a given region of configuration space. It is important to realize that these fields differ from the ordinary electromagnetic field. In particular, we have shown that they decay, in a close vicinity of any given *ci*, to become identically zero except for the one single field that is formed at that *ci*. It is tempting to define these fields as *weak* electromagnetic fields.

2. One of the more interesting magnitudes that is revealed in the present study is the existence of topological spin (see Section 5.4). Although its introduction seems to be somewhat artificial, it is likely that it creates magnetic dipole interaction—an

interaction of a new kind—whenever the molecular system is exposed to an electromagnetic field<sup>1</sup>.

3. The next issue, the more technical one, is related to the fact that the original nuclear Schrödinger equation, which follows from the Born–Oppenheimer treatment, may contain the singular NACTs and therefore is unfriendly to the interested user. Numerous approaches and approximations were suggested to overcome this difficulty; some of them have been known for quite some time, and some are new. The basic approach, namely, how to form the diabatic framework, is discussed in Chapter 2, but it is recommended to study also Chapter 8, where various approximations are presented to this effect, which can be applied as such or be used for developing new ideas.

4. The fourth issue is related to the distinction between the time-independent and time-dependent frameworks. In Section 2.3.2 we discuss the time-dependent framework, derive the relevant nuclear Schrödinger equation for the general case (which involves time-dependent dressed NACTs), and show how such an equation should be *diabatized* employing contours within *spacetime* configurations. The fact that the Curl condition is now extended to include mixed spacetime derivatives and the fact that the usual spatial contours become spacetime contours cause the present treatment to be reminiscent of the theory of special relativity without explicitly mentioning it.<sup>2</sup>

I want to end this book by quoting Felix Smith,<sup>3</sup> who emphasizes the importance of electronic nonadiabatic transitions in molecular systems:

I believe that calculations based on a single-potential energy surface will be of very limited usefulness in the real world of chemically reacting systems, and that electronic transitions between a multiplicity of states are likely to play a very large role in such events. Even where adiabatic calculations with a single potential surface are valid, it is desirable to demonstrate their validity, and this can only be done in the framework of a theory which takes proper account of all the couplings between states that may exist, so that they can be evaluated and proved to be small. If these couplings are strong, quantum effects associated with such non-adiabatic behavior may prove to be one of the most important features of many chemical reaction processes. Probably such quantum effects will turn out to be more important than the quantum effects associated with barrier leakage and vibrational zero-point energy that are often discussed in connection with the movement of systems over adiabatic surfaces.

## REFERENCES

1. M. V. Berry, *Proc. Roy. Soc. London A*, **392**, 45 (1984).
2. R. Englman and A. Yahalom, *Adv. Chem. Phys.* **124**, 197 (2002).
3. F. Smith, *Phys. Rev.* **179**, 111 (1969).

# INDEX

---

- Abelian Curl equations, 3–6  
Abelian divergence equations, 6–7  
Abelian first-order differential equations, 12–13  
Abelian systems, 154. *See also* Two-state systems  
molecular fields as, 141–151  
Ab initio angular NACTs. *See also* Ab initio  
NACTs; Nonadiabatic coupling terms  
(NACTs)  
in {C<sub>2</sub>,H} system, 99–103  
in {C<sub>2</sub>,H<sub>2</sub>} system, 92–95  
in {H<sub>2</sub>,H} system, 88–90, 96–99  
in {H<sub>2</sub>,O} system, 91–92  
Ab initio molecular systems, 85, 87–103, 155–157  
Berry phase and open phase in, 175–187  
Ab initio NACTs, in {H<sub>2</sub>,H} system, 160, 162. *See also* Nonadiabatic coupling terms (NACTs)  
Ab initio surfaces, 95  
Adiabatic Born–Oppenheimer eigenfunctions, 139  
Adiabatic Born–Oppenheimer equation, 28,  
199–200  
Adiabatic eigenfunctions, sign flips of, 109–122  
Adiabatic eigenstates, xiii  
Adiabatic framework, xiv–xv, 26–28, 224  
Berry phase in, 179–181  
for molecular fields, 141–143  
topological phase in, 191–194  
Adiabatic potential matrix, 35, 179  
Adiabatic Schrödinger equation, 42–43  
complex eigenfunctions with, 39–40  
time-dependent, 46–47, 49–50  
Adiabatic surfaces, 95, 115–117  
Adiabatic-to-diabatic transformation (ADT), xv,  
30–39  
electronic basis sets for, 30–33  
for nuclear wavefunctions, 33–34  
time-dependent, 47–50  
Adiabatic-to-diabatic transformation (ADT)  
angles, 59–60, 68, 69, 81–82, 215–216  
derivation of N-state, 206–209  
in {H<sub>2</sub>,H} system, 88–90  
in triatomic systems, 86–87  
Adiabatic-to-diabatic transformation (ADT)  
matrices, 38, 39, 47–50, 58, 61, 75–82, 134,  
178, 205, 206  
complex, 40–41  
extended Euler matrix as model for, 125–131  
for four-state systems, 64–65  
for three-state systems, 62  
for triatomic systems, 86–87  
for two-state systems, 59–60  
Analytical models, 58–67  
eigenfunction sign flips and, 110  
Analyticity, of differential equation solutions,  
12–14

- Angular component of Poisson equations, 158  
 Angular momentum  
   intrinsic, 122–123  
   ordinary, 123  
 Angular NACTs, 72, 81–82, 85. *See also* Ab initio angular NACTs; Nonadiabatic coupling terms (NACTs)  
 Angular rotation operator, 76  
 Arrangement channels, 217–218  
 Atom–atom systems, xv
- Basis sets, electronic, 30–33, 45  
 Berry phase, 175–195. *See also* Longuet–Higgins/Berry phase  
   defined, 177  
 Bohr–Sommerfeld quantization, 60, 123  
 Born–Oppenheimer adiabatic eigenfunctions, sign flips of, 109–122  
 Born–Oppenheimer approximations, xiii, xiv  
   extended, 197–220  
   with multistate systems, 199–201  
 Born–Oppenheimer coupling terms, 105, 167  
 Born–Oppenheimer eigenfunctions, adiabatic, 139  
 Born–Oppenheimer expansion, 2, 26–27, 41  
 Born–Oppenheimer surfaces, NACTs and, 105–106  
 Born–Oppenheimer systems, 6, 27–28, 85, 86  
   geometric phase in, 176  
 Born–Oppenheimer theory, xiii, xiv–xv, 26–54  
   complex eigenfunctions in, 39–43  
   time-dependent treatment in, 43–51  
   time-independent treatment in, 26–39  
 Boundary conditions, with  $\{\text{H}_2, \text{H}\}$  system, 161–162  
 Bundles, of contours, 125
- $\{\text{C}_2, \text{H}\}$  system  
   Euler matrix for, 128–130  
   multistate quasiquantization of, 99–103  
 $\{\text{C}_2, \text{H}_2\}$  system, two-state quasiquantization of, 92–95  
 Cauchy integral formula, 187  
 Charge transfer, xv  
 $ci$  points, 70. *See also* Conical intersections (*cis*)  
 Circles, conical intersection points in, 79–82,  
   85–92, 94, 95, 98–99, 100. *See also* Circular contours; Semicircles  
 Circular contours, 24, 150–151, 182, 184–186. *See also* Circles  
   for  $\{\text{H}_2, \text{H}\}$  system, 161–162  
 Closed contours, 35–37, 131, 180, 182, 195  
   conical intersections and, 73–75  
   eigenfunction sign flips and, 110–113, 115–119  
   geometric phase and, 175–177  
   for  $\{\text{H}_2, \text{Na}\}$  system, 149–151  
   integral equations along, 16–19, 23, 31–32  
   Stokes theorem and, 144–146  
   topological spin and, 125  
   Wigner rotation matrix and, 77  
 Complete active-space self-consistent field (CASSCF) method, 88, 91, 92, 100  
 Complete Hilbert spaces, 5, 8  
 Complex conjugate, 204  
 Complex eigenfunctions, with adiabatic Schrödinger equation, 39–40  
 Complex functions, 188  
 Conical intersections (*cis*), xiv, 6, 70–71, 168, 225  
   Born–Oppenheimer approximations and, 198  
   in  $\{\text{C}_2, \text{H}\}$  system, 99–103  
   in  $\{\text{C}_2, \text{H}_2\}$  system, 92–95  
   constructing Hilbert subspaces and, 108–109  
   degeneracy points and, 107–108  
   distribution of, 73–75, 79–82  
   eigenfunction sign flips and, 110–112, 114–120  
   equilateral, 183–187  
   in  $\{\text{H}_2, \text{H}\}$  system, 87–90, 96–99, 162  
   in  $\{\text{H}_2, \text{O}\}$  system, 91–92  
   multidegeneracy points and, 120–122  
   with multistate Hilbert subspaces, 167  
   in non-Abelian systems, 154  
   solenoids and, 140  
   Stokes theorem and, 144–147  
   *Strange* matrix and, 159  
   topological spin and, 123–124  
   with two-state Hilbert subspaces, 147–149  
 Continuity, of differential equation solutions, 12  
 Contours, 60–61, 69. *See also* Circular contours;  
   Closed contours; Seams  
   differential vector equations and, 20–22  
   eigenfunction sign flips and, 110–113, 115–119  
   geometric phase and, 175–177  
   for  $\{\text{H}_2, \text{H}\}$  system, 161–162  
   for  $\{\text{H}_2, \text{Na}\}$  system, 149–151  
   integral equations along, 11, 15–19, 23, 30–32  
   spacetime, 225  
   Stokes theorem and, 144–146  
   topological spin and, 125  
   in triatomic systems, 86–87, 96–99, 100–103  
 Coulomb field, 29  
 Coupled Schrödinger equations, 198  
 Covariant derivative, 47, 48  
 Curl-Div (C-D) equations, 7–9, 139–141,  
   154–159, 224  
   with  $\{\text{H}_2, \text{H}\}$  system, 160  
   with multistate Hilbert subspaces,  
     166–167

- Curl equations, 13, 14, 16, 32–33, 69, 70, 84, 157, 159, 169–171  
 Abelian, 3–6  
 extended, 3, 4, 7, 9–11  
 four-component, 48–49  
 multistate extended, 151–154  
 with multistate Hilbert subspaces, 166–167  
 non-Abelian, 3–6, 151–154  
 with pseudomagnetic fields, 168  
 Stokes theorem and, 145  
 with three-state Hilbert subspaces, 155–156  
 two-state, 143–144  
 with two-state Hilbert subspaces, 147–149
- Curl operator, 3, 140
- Decoupled Poisson equations, 158  
 with  $\{\text{H}_2, \text{H}\}$  system, 160–161
- Degeneracy points, xiii–xiv, 105–108. *See also*  
 Multidegeneracy points  
 eigenfunction sign flips and, 110
- Degenerate states, molecular, xiii
- Diabatic framework, xiv–xv, 28–29, 38
- Diabatic potential, 44, 86
- Diabatic potential matrices, 42, 67–75. *See also*  
 Diabatic potential matrix  
 conical intersections and, 73–75, 79–82  
 multidegeneracy points and, 122  
 two-state, 58
- Diabatic potential matrix, 29, 34, 40–41, 61–62, 67–68, 70, 178, 199–200, 220  
 derivation of two-state, 210  
 recovered, 49  
 reducing dimensions of, 201–214  
 singlevaluedness of, 35–37  
 uniqueness of, 37
- Diabatic Schrödinger equation, 28–29, 33–34, 40
- Diabatic wavefunctions, uniqueness of, 38
- Diabatization, xiv, 26–54, 43, 201–202, 225  
 in triatomic systems, 86
- Diagonal matrices, 20–22  
 imaginary, 199
- Differentiability, of differential equation solutions, 12
- Differential equations, 30  
 first-order, 11–14, 23  
 integral equations versus, 14, 23  
 vector, 20–22
- Dirac bracket notation, 2
- Dirac function, xv, 145, 153
- Dirichlet-type boundary conditions, with  $\{\text{H}_2, \text{H}\}$  system, 161–162
- Dispersion relations, 187
- Divergence equations, 9, 11, 154–155, 157, 159
- Abelian and non-Abelian, 6–7  
 for multistate Hilbert subspaces, 166–167  
 for three-state Hilbert subspaces, 155–156
- $\mathbf{d}^i$  matrix, 58, 75–79
- D** matrices, 32, 33, 36, 58, 60–61, 63, 65–67, 153–154, 195, 224  
 Berry phase and, 179–181  
 in  $\{\text{C}_2, \text{H}\}$  system, 101–103  
 eigenfunction sign flips and, 110, 111, 113–114, 117–120  
 in  $\{\text{H}_2, \text{H}\}$  system, 96–99  
 Mathieu equation and, 131  
 multidegeneracy points and, 121–122  
 multidimensional  $\mathbf{A}$  matrix and, 130–131  
 nondiabatic coupling matrix and, 133–134  
 three-dimensional  $\mathbf{A}$  matrix and, 128, 130  
 topological spin and, 123, 125  
 in triatomic systems, 87  
 two-dimensional  $\mathbf{A}$  matrix and, 126–127
- Dressed NACM, 42, 47, 50–52. *See also*  
 Nonadiabatic coupling matrix (NACM)
- Dynamical phase factor, 176
- Eigenfunctions  
 electronic, 45, 197–198  
 Hilbert space of, 1–3  
 of Mathieu matrix, 131–133  
 multivalued, 177–187  
 real, 3, 41–42  
 sign flips of, 109–122  
 singlevalued, 176–177
- Eigenvalues, electronic, 26–27
- Electric potential, 43
- Electromagnetic vector potential, 43
- Electronic basis sets, 45  
 for adiabatic-to-diabatic transformation, 30–33
- Electronic coordinates, 1–3, 197
- Electronic coupling term ( $G$ ), 191
- Electronic eigenfunctions, 45, 197–198  
 sign flips of, 109–122
- Electronic eigenstates, xiii
- Electronic eigenvalues, 26–27
- Electronic Hamiltonian, 1, 26, 43–46, 50, 53–54, 105–107, 134  
 Berry and open phase and, 176–177  
 diabatic potential matrix and, 67–68  
 time-independent, 41–42
- Electronic kinetic energy operator, 29
- Electronic NACTs, Hilbert space of, 1–3. *See also*  
 Nonadiabatic coupling terms (NACTs)
- Electronic potential, 131–132
- Electronic wavefunctions, 197–198
- Electron motions, 26

- Elliptic Jahn–Teller model, 72, 75  
Equation of motion, 38  
Euler matrix, extended, 125–131, 206–209  
Even functions, 189  
Exchange scattering two-coordinate model, 214–220  
Extended Curl equation, 3, 4, 7, 9–11  
multistate, 151–154  
Extended divergence equation, 7  
Extended Euler matrix, 125–131, 206–209  
Extended potential, 42  
Extended Stokes theorem, 144–147  
External cyclic time-dependent fields, phase-modulus relations for, 187–195  
External region, for  $\{\text{H}_2, \text{H}\}$  system, 161–162  
Feshbach projection operators ( $\mathbf{P}_N$ ), 8–9  
Fields, 139  
time-dependent, 187–195  
First-order differential equations, 11–14, 23  
First-order NACTs, 2, 6. *See also* Nonadiabatic coupling terms (NACTs)  
Four-dimensional vectors, 47–49, 225  
Fourier expansion, with  $\{\text{H}_2, \text{H}\}$  system, 160–161  
Fourier series, 132, 160  
Four-state systems, 64–66  
multidegeneracy points and, 121–122  
Wigner rotation matrix with, 78  
Gauge invariance  
for Born–Oppenheimer approximations, 201  
of geometric phase, 176  
Gauge transformations, 41, 43, 157  
*Strange* matrix and, 159  
General Hilbert subspace, eigenfunction sign flips and, 114–120  
Geometric phase, 175–177. *See also* Berry phase  
g matrix, 59–60, 62, 64, 77–79  
G matrices, 60, 62, 64, 142, 199, 200  
eigenfunction sign flips and, 113–114  
multidegeneracy points and, 122  
Grad operator, 2, 53–54, 105–106  
four-component, 48–49  
Gridpoints, 73, 74  
 $\{\text{H}_2, \text{H}\}$  system, 156  
Berry phase in, 183–187  
multistate quasiquantization of, 96–99  
numerical study of, 160–162  
two-state quasiquantization of, 87–90  
 $\{\text{H}_2, \text{Na}\}$  system, 149–151  
 $\{\text{H}_2, \text{O}\}$  system, two-state quasiquantization of, 91–92  
Hamiltonian, 26, 28, 30, 205  
electronic, 1, 26, 41–46, 50, 53–54  
Mathieu equation and, 189–191  
Heaviside function, 146  
Hellman–Feynman theorem, 105  
Helmholtz decomposition, 214  
Hilbert space, 1–7, 27, 28, 30, 45, 50, 58, 139, 151. *See also* Hilbert subspaces  
with Abelian and non-Abelian Curl equations, 3–6  
with Abelian and non-Abelian divergence equations, 6–7  
complete, 8  
constructing subspaces in, 108–109  
of eigenfunctions, 1–3  
Hilbert subspaces, 2, 8–11, 28, 32, 35, 36, 44, 45, 50–51, 84, 92, 99, 102–103, 129, 134, 177, 195, 216, 224  
constructing, 108–109  
eigenfunction sign flips and, 110–120  
multistate, 151–159, 162–167  
three-state, 155–157  
topological spin and, 124  
two-state, 141–144, 147–151  
Hydrogen. *See*  $\{\text{C}_2, \text{H}\}$  system;  $\{\text{C}_2, \text{H}_2\}$  system;  
 $\{\text{H}_2, \text{H}\}$  system;  $\{\text{H}_2, \text{Na}\}$  system;  $\{\text{H}_2, \text{O}\}$  system  
Infinitesimal contours, 19  
Inhomogeneities, 157–159  
with multistate Hilbert subspaces, 166–167  
Inlets, 95  
Integral equations, 11, 14–19, 23, 30–32  
Integration, conical intersections and, 73–75. *See also* Line integrals; Surface integrals  
Internal region, for  $\{\text{H}_2, \text{H}\}$  system, 161–162  
Intrinsic angular momentum, 122–123  
Isolated points, 32  
Jahn–Teller effect  
in  $\{\text{C}_2, \text{H}_2\}$  system, 93  
in  $\{\text{H}_2, \text{H}\}$  system, 88  
in  $\{\text{H}_2, \text{O}\}$  system, 92  
Jahn–Teller model, 70–71, 107, 175, 216–218  
elliptic, 72, 75  
Kinetic energy operator, electronic, 29  
Kinetic operator, 27  
Kramers–Kronig equations, 187, 188  
Krönecker delta function, 2, 204

- Lie algebra, 120, 122  
 Line integrals, 11, 15–19, 31, 80–81, 144, 145, 147, 153  
   eigenfunction sign flips and, 110, 112, 118  
 Longuet–Higgins Berry/phase, xiii, xv. *See also* Berry phase  
 Lorenz force, 143, 144–145
- Magnetic dipole interaction, 224–225  
 Magnetic field (**H**), 140, 143  
   non-Abelian, 168  
 Magnetic monopole, 168  
 Massey parameter, 198  
 Mathieu equation, 131–133, 187, 189–194  
 Matrices  
   unitary, 35–36  
   Wigner rotation, 58, 75–79  
 Mixing angle, 38–39, 68, 69  
 Model systems, 58–82  
   Jahn–Teller, 70–72, 75, 107  
   reactive (exchange) scattering two-coordinate, 214–220  
   Renner–Teller, 85–86, 107  
 Molecular degenerate states, xiii–xiv  
 Molecular fields, xiii, xiv, 139–171, 224  
    $\{\text{H}_2, \text{H}\}$  system, 160–162  
   multistate Hilbert subspaces, 151–159, 162–167  
   pseudomagnetic fields, 167–168  
   seams as solenoids in, 139–141  
   two-state (Abelian) systems, 141–151, 168–171  
 Molecular systems, xiii–xv, 84–103  
   ab initio, 85, 87–103, 155–157, 175–187  
   Berry phase and open phase in, 175–195  
   theoretical background for, 85–87  
   topological effects in, xiv  
 MOLPRO program, 88, 91, 101, 129, 149–150, 156  
 Multidegeneracy points, 120  
 Multistate Hilbert subspaces, 151–159, 162–167  
 Multistate quasiquantization, 96–103  
 Multistate systems, Born–Oppenheimer approximations with, 199–201  
 Multivalued eigenfunctions, Berry and open phase and, 177–187
- NACTs matrix, quantization of, xiv. *See also* Nonadiabatic coupling terms (NACTs)  
 Non-Abelian Curl equations, 3–6, 151–154  
 Non-Abelian divergence equations, 6–7  
 Non-Abelian first-order differential equations, 13–14  
 Non-Abelian magnetic fields, 168  
 Non-Abelian Stokes theorem, 151–154
- Non-Abelian systems, Curl–Div equations for, 154–159  
 Nonadiabatic coupling matrix (NACM), 40, 133–135, 224. *See also* Matrices  
   breakup of, 162–167  
   dressed, 42, 47, 50–52  
   for molecular systems, 84, 86  
   quantization of, 84, 86–103  
   second-order time-independent, 27, 52  
 Nonadiabatic coupling terms (NACTs), xiii–xv, 58, 68–69, 73, 129, 136, 207, 216–217, 224, 225  
   angular, 72, 81–82, 85  
   Born–Oppenheimer approximations and, 198, 202  
   Born–Oppenheimer surfaces and, 105–106  
   in  $\{\text{C}_2, \text{H}\}$  system, 99–103  
   in  $\{\text{C}_2, \text{H}_2\}$  system, 92–95  
   constructing Hilbert subspaces and, 108–109  
   eigenfunction sign flips and, 111–112  
   elliptic Jahn–Teller model and, 72, 75  
   fields of, 139–141  
   in  $\{\text{H}_2, \text{H}\}$  system, 87–90, 96–99, 160, 162  
   in  $\{\text{H}_2, \text{Na}\}$  system, 149–151  
   in  $\{\text{H}_2, \text{O}\}$  system, 91–92  
   Hilbert space of, 1–3  
   Hilbert subspaces and, 8  
   infinitely large, 198  
   Jahn–Teller model and, 70–71, 107  
   for molecular systems, 84–85  
   in non-Abelian systems, 154, 155  
   with pseudomagnetic fields, 168  
   Stokes theorem and, 144  
   topological matrix and, 133  
   topological spin and, 123  
   two-state Hilbert subspaces and, 147–149, 154
- Nonadiabatic framework  
   Berry phase in, 181–183  
   topological phase in, 191–194
- Non-Hermitian Hamiltonians, 205  
 Nonperturbative approach, 45–50  
 Nonreactive **S** matrix elements, 218  
 Nuclear coefficient, 28  
 Nuclear coordinates, 1–4, 197  
 Nuclear-electronic interaction coefficient, 132  
 Nuclear kinetic energy, 26  
 Nuclear kinetic operator, 46  
 Nuclear motions, 26  
 Nuclear Schrödinger equation, 28–29, 33–34  
 Nuclear wavefunctions  
   adiabatic-to-diabatic transformation for, 33–34  
   time-dependent, 43–44, 49, 50

- Open contours, integral equations along, 15–16  
 Open-path phase (OPP), xiii, 181  
 Open phase, 175–195  
     defined, 177  
 Ordinary Born–Oppenheimer approximation, 215, 219–220  
 Ordinary Curl equation, 3  
 Orthogonality, of differential equation solutions, 14  
 Orthogonal matrices, 14, 20, 127, 131  
 Orthogonal transformation, 30  
 Orthonormalization, 42  
 Outlets, 95  
 Overlap matrices, 39
- Parallel planes, in molecular systems, 85  
 Parallel transport law, 3  
 Pathological points, 19, 23  
 Periodic functions, 189  
 Permutations, 206–207  
 Perturbation theory, in triatomic systems, 85–86  
 Perturbative approach, 43–44, 49–50  
 Phase  
     Berry, 175–195  
     geometric, 175–177  
     Longuet–Higgins/Berry, xiii, xv  
     open, 175–195  
     open-path, xiii, 181  
 Phase factors, 31–33, 39–40, 176  
     time-dependent, 41–43  
 Phase-modulus relations, for external cyclic  
     time-dependent field, 187–195  
     wavefunction, 44, 142, 202–203, 215  
     uniqueness of, 38  
 Planes, in molecular systems, 84–85, 107–108  
 Poisson equations, 157–158, 214  
     with {H<sub>2</sub>, H} system, 160–161  
 Polar components, of NACTs, 70–71  
 Poles, xiii, 73, 74, 105  
 Polyatomic systems, NACTs in, xv  
 Potential energy surfaces (PESs), xiii–xiv, 1, 49  
     adiabatic, 217, 218  
 $p$  points, 73–75, 79–82  
 Principal open-path phase (POPP), 181–187, 191–194  
     Mathieu equation and, 189–191  
     topological phase and, 191–194  
 Principal part of **W** matrix, 210  
 Probabilities, reactive state-to-state, 219  
 Problematical points, 32–33
- Propagation, 20–23  
 Pseudomagnetic fields, 167–168  
     column vector, 33, 202, 215  
     wavefunction. *See also* Total wavefunction()  
     time-dependent form of, 43, 44  
     time-dependent phase factors with, 41–43  
     uniqueness of, 37–38
- Quantization, xiii, xiv, 8, 66, 73, 78–79, 106–107, 214. *See also* Quasiquantization  
     Bohr–Sommerfeld, 60, 123  
     of NACMs, 84, 86–103  
     of pseudomagnetic fields, 168  
     Stokes theorem and, 144–146  
     of matrix, 131–134  
     three-state, 86  
     in triatomic systems, 85–87  
     two-state, 86–95  
 Quantum chemistry, 30  
 Quantum effects, 225  
 Quasi-complete Hilbert spaces, 8  
 Quasiquantization  
     multistate, 96–103  
     two-state, 87–95
- Radial component, of Poisson equations, 158  
 Reactive (exchange) scattering two-coordinate model, 214–220  
 Reactive **S** matrix elements, 218  
 Reactive state-to-state probabilities, 219  
 Real eigenfunctions, 3, 41–42  
 Reduced tensorial vector, 10–11  
 Regions, 108, 111–112  
     for {H<sub>2</sub>, H} system, 161–162  
     with Mathieu equation, 131–132  
 Renner–Teller model, 85–86, 107, 217, 219  
 Rotation matrices, 127  
 Rydberg states, 88
- Scalar product, 2  
 Schrödinger equation, xiii, xiv, xv, 225  
     in adiabatic framework, 26–28, 39–40, 42, 141–143  
     adiabatic nuclear, 7  
     adiabatic time-dependent, 46–47, 49–50  
     Born–Oppenheimer approximations and, 198, 202  
     in diabatic framework, 28–29, 33–34, 40  
     nuclear, 28–29, 33–34  
     time-dependent, 41–43, 44, 189–191, 195  
 Seams, 107–108, 139, 140  
     in molecular systems, 85  
     multidegeneracy points and, 120

- quantization of pseudomagnetic fields along, 168  
 solenoids as modeling, 139–141  
 two-state Hilbert subspaces and, 148
- Second-order NACM, 40. *See also* Nonadiabatic coupling matrix (NACM)  
 time-independent, 27, 52
- Second-order NACTs, 6. *See also* Nonadiabatic coupling terms (NACTs)
- Semicircles, with phase-modulus relations, 187–188
- Shift transformations, 168–171
- Sign flips, 175  
 of electronic eigenfunctions, 109–122  
 multidegeneracy points and, 120–122  
 topological spin and, 124–125
- Singlevalued eigenfunctions, Berry and open phase and, 176–177
- Singular NACTs, xv. *See also* Nonadiabatic coupling terms (NACTs)
- S** matrix, 67, 151, 153, 205, 218
- Smoothness of diabatic states, 38
- Solenoids, 139, 140  
 as seam models, 139–141
- Spacetime. *See* Four-dimensional vectors
- Spacetime contours, 225
- Special theory of relativity, xiv
- Spin (**S**), 122–123  
 topological, xiii, 122–125, 224–225
- Spin-orbit coupling, xv
- Spin quantum number ( $S$ ), 124
- Spin transitions, xv
- State-average complete active-space self-consistent field (CASSCF) method, 88, 91, 92, 100
- Stokes theorem, 144–147  
 non-Abelian, 151–154
- Strange* elements, 155, 157, 159  
 with multistate Hilbert subspaces, 166
- Strange* matrix, 155, 157, 159
- Sum rule, 154
- Surface integral, 144, 145, 147, 153
- Tensorial vector, 3–4  
 matrix, 42
- Three-state Hilbert subspace  
 Curl–Div equations for, 155–157  
 eigenfunction sign flips and, 110–114
- Three-state quantization, 86
- Three-state systems, 62–63  
 Berry phase in, 183–187  
 multidegeneracy points and, 121  
 Wigner rotation matrix with, 78
- Time-dependent adiabatic-to-diabatic transformation, 47–50
- Time-dependent fields, external cyclic, 187–195
- Time-dependent framework, 225
- Time-dependent nonperturbative approach, 45–50
- Time-dependent perturbative approach, 43–44, 49–50
- Time-dependent Schrödinger equation, 195  
 adiabatic, 46–47, 49–50  
 Berry and open phase and, 176–180  
 Mathieu equation and, 189–191
- Time-dependent wave packet approach, 216
- Time-independent framework, 225
- Time-independent NACM, 27, 52
- Time-ordering operator, 46
- Toeplitz matrix, 216
- Topological matrix (**D**), 26–54, 58, 60–61, 195, 224  
 Berry phase and, 179–181  
 in  $\{C_2, H\}$  system, 101–103  
 eigenfunction sign flips and, 110, 111, 113–114, 117–120  
 for four-state systems, 65–66  
 in general theory, 66–67  
 in  $\{H_2, H\}$  system, 96–99  
 Mathieu equation and, 131  
 multidimensional **A** matrix and, 130–131  
 matrix and, 133–134  
 for three-state systems, 63  
 topological spin and, 123  
 in triatomic systems, 87
- Topological number ( $K$ ), 115, 119  
 multidimensional **A** matrix and, 130–131  
 topological spin and, 123–125
- Topological phase, numerical study of, 191–194
- Topological spin, xiii, 122–125, 224–225
- Total angular momentum operator (**J**), 76, 78
- Total wavefunction, 142  
 time-dependent form of, 43, 44, 49  
 uniqueness of, 37–38
- Triatomic systems, 84–85  
 quantization in, 85–87
- Trigonometric functions, 190–191
- Twin *cis*, 87–90, 100, 147
- Two-coordinate reactive (exchange) model, 214–220
- Two-state adiabatic-to-diabatic transformation matrices, 59–60
- Two-state conical intersections, Stokes theorem and, 146–147
- Two-state Curl equations, 143–144
- Two-state diabatic potential matrix, 58, 210

- Two-state quantization, 86–95  
 Two-state quasiquantization, 87–95  
 Two-state systems, 5–6, 7  
   with Born–Oppenheimer approximation, 214–220  
   molecular fields as, 141–151  
   Wigner rotation matrix with, 78  
 Two-state matrices, 142  
   eigenfunction sign flips and, 110, 111  
 Unitary matrices, 35–36  
 Unity matrix ( $\mathbf{I}$ ), 1, 3  
 Vector algebra, 160, 168–171  
 Vector equations, differential, 20–22  
 Vectorial first-order differential equations, 11–14  
 Vector-matrices, 11, 13–14  
 Vector potentials ( $\mathbf{A}$ ), 139–141. *See also A*  
   matrices  
   NACTs as, 141–143  
 Vectors, 11–13  
   four-dimensional, 47–49, 225  
   reduced tensorial, 10–11  
 Vibrational transitions, 214  
 Virgin functions/distributions, 146, 149, 150  
 Wavefunctions, electronic, 197–198  
 Wigner rotation matrix ( $\mathbf{d}^j$ ), 58, 75–79  
 Yang–Mills field ( $\mathbf{F}$ ), 4  
 $z$  points, 73–75, 79–82

*Koλχος*

3/29/06